Institute of Experimental and Clinical Pharmacology and Toxicology

Preclinical Center for Molecular Signaling (PZMS)

Faculty of Medicine

Saarland University, Homburg (Saar)

Cell-specific regulation and function of ADAM10 and ADAM17 during *Pseudomonas aeruginosa* infection

Dissertation

Submitted in Fulfilment of the Requirements for the Degree of

Doctor rerum naturalium (Dr. rer. nat.)

of the Medical Faculty of Saarland University

2023

By

Ahmad Aljohmani

born on 01.01.1993 in Syria

Doctoral supervisor: Jun.-Prof. Dr. rer. nat. Daniela Yildiz

Table of Contents

List of Abbreviations

ADAMs	A Disintegrin And Metalloproteinases
AP-BTC	Alkaline Phosphatase-Betacellulin
APP	Amyloid Precursor Protein
AP-TGF-α	Alkaline Phosphatase-Transforming Growth Factor Alpha
BAL	Bronchioalveolar Lavage
BSA	Bovine Serum Albumin
Ca	Calcium Ions
CAP	Community-Acquired Pneumonia
CFU	Colony Forming Unit
DAMP	Damage-Associated Molecular Patterns
DMEM	Dulbecco's Modified Eagle Medium
DMSO	Dimethylsulfoxide
eEF-2	Eukaryotic Elongation Factor-2
EGF	Epidermal Growth Factor
ELISA	The Enzyme-Linked Immunosorbent Assay
ER	Endoplasmic Reticulum
ESE	Early-Sorting Endosome
EVs	Extracellular Vesicles
FACS	Fluorescence-Activated Cell Sorting
Fc receptor	Fragment Crystallizable Receptor
FCS	Fetal Calf Serum
FITC	Fluorescein isothiocyanate
FRET	Fluorescence Resonance Energy Transfer
GAPDH	Glyceraldehyde 3-Phosphate Dehydrogenase
GFP	Green Fluorescent Protein
HAP	Hospital-Acquired Pneumonia
HRP	Horseradish peroxidase
HSAEpC	Human Small Airway Epithelial Cells
ICAM-1	Intercellular Adhesion Molecule 1
ICU	Intensive Care Unit
IgG	Immunoglobulin G
IHC	Immunohistochemistry
IL	Interleukin
JAM-A	Junctional Adhesion Molecule A
KD	Knockdown
kDa	Kilo Dalton
LPS	Lipopolysaccharide
LSE	Late-Sorting Endosome
M-CASS	Mouse Clinical Assessment Score for Sepsis
MCP-1	Monocyte Chemoattractant Protein 1
MCP-1/CCL2	monocyte chemoattractant protein 1
MDR	Multi-drug resistance
MOI	Multiplicity of Infection
MPO	Myeloperoxidase
MVBs	Multivesicular Bodies
NICD	Notch Intracellular Domain
OD	Optical Density
P. aeruginosa	*Pseudomonas aeruginosa*
PAMP	Pathogen-Associated Molecular Pattern
PBS	Phosphate Buffered Saline

PC	Prohormone Convertase
PCR	Polymerase Chain Reaction
PFA	Paraformaldehyde
PMA	Phorbol 12-Myristate 13-Acetat
PRR	Pattern Recognition Receptor
RAGE	Receptor for Advanced Glycation End Products
RIPing	Regulated Intramembrane Proteolysis
ROI	Region of Interest
ROS	Reactive Oxygen Species
Rpm	Round Per Minute
S. aureus	*Staphylococcus aureus*
S. pneumoniae	*Streptococcus pneumoniae*
Scr	Scramble
SDS-PAGE	Sodium Dodecyl-Sulfate Polyacrylamide Gel Electrophoresis
shRNA	Short Hairpin Ribonucleic Acid
T2SS	Type 2 Secretion System
T3SS	Type 3 Secretion System
T-ALL	T Cell Acute Lymphoblastic Leukaemia
TBE	Tris/Borate/EDTA
TBS	Tris-Buffered Saline
TEMED	Tetramethylethylenediamine
TGF-α	Transforming Growth Factor Alpha
THB	Todd Hewitt Broth
TLR	Toll-Like Receptor
TNF-α	Tumor Necrosis Factor Alpha
TRITC	Tetramethylrhodamine
VCAM-1	Vascular Cell Adhesion Molecule 1
WB	Western blot
WT	Wildtype
µg	Microgram
µL	Microliter

List of figures

List of tables

1 Summary

Pneumonia is a serious, life-threatening lung infection often caused by infection with *Streptococcus pneumoniae* and *Pseudomonas aeruginosa* and mainly characterized by an inflammation of the alveoli leading to various pathophysiologies such as respiratory failure, acute respiratory distress syndrome and sepsis. Severe epithelial dysfunction is one major hallmark throughout the pathophysiological progress of bacterial pneumonia. Many of the mediators (e.g., TNF-α, IL-6R) and junction and adhesion molecules (e.g., E-cadherin, JAM-A) orchestrating inflammatory cell recruitment and loss of barrier integrity are proteolytically cleaved through a disintegrin and metalloproteinases (ADAMs), especially ADAM10 and ADAM17. ADAM10 and ADAM17 showed to be essential control elements during several infectious diseases, which make them suitable and promising therapeutic target. However, the cell-specific regulation and function during lung infection is still poorly understood.

Employing western blot, surface expression analysis, and cell-based assays revealed that the protein expression, maturation, and activation of ADAM10 and ADAM17 in epithelial cells are upregulated upon infection with *Pseudomonas aeruginosa* and stimulation with Exotoxin A, without any impact of infection by *Streptococcus pneumoniae*, respectively. Notably, the experiments with heat-inactivated bacteria suggest that the activation of ADAM10 and ADAM17 is attributed to the toxin repertoire rather than the mere interaction with the bacterial particle itself. In addition, pharmacological targeting and gene silencing of ADAM10 and ADAM17 showed that this activation is critical for the cleavage of E-cadherin and junctional adhesion molecule-A and epithelial cell survival, both modulating barrier integrity, as well as epithelial regeneration, leukocyte adhesion and transepithelial migration. Furthermore, *Pseudomonas aeruginosa* induced the release of ADAM10 but not ADAM17 on exosomes, which were able to perform proteolytic cleavage *in trans* (on distinct cells).

The second part of this thesis focused on the role of leukocytic ADAM10 and ADAM17 in pulmonary infection. For these investigations, the analysis of patient samples, an *in vivo Pseudomonas aeruginosa* pneumonia model and detailed *in vitro* mechanistic studies were combined. Patients with bacterial pneumonia and Covid-19 patients showed a severity-dependent activity of ADAM10 and ADAM17 on serum exosomes. Based on the murine pneumonia model and infection of human leukocytes, it could be assumed that the induced release of ADAM10 and ADAM17 carrying exosomes was mainly caused by leukocytes. Furthermore, ADAM10 and ADAM17 distinctively regulated leukocyte recruitment to the alveolar space and the lung tissue, edema formation, cytokine release, macrophage polarization, reactive oxygen formation, bacterial clearance and sepsis severity during *Pseudomonas aeruginosa* infection. Thus, ADAM10 and ADAM17 in epithelial cells and leukocytes are critical regulatory elements of bacterial and viral pneumonia. These results highlight the significance of ADAM10 and ADAM17 as proposals for new prognostic and therapeutic tools that need to be addressed in further preclinical and translational studies.

1 Zusammenfassung

Lungenentzündung ist eine schwere, lebensbedrohliche Lungeninfektion, die häufig durch eine Infektion mit Streptococcus pneumoniae und Pseudomonas aeruginosa verursacht wird und hauptsächlich durch eine Entzündung der Lungenbläschen gekennzeichnet ist, die zu verschiedenen Pathophysiologien wie Atemversagen, akutem Atemnotsyndrom und Sepsis führt. Eine schwere Epitheldysfunktion ist ein Hauptmerkmal des pathophysiologischen Verlaufs der bakteriellen Pneumonie. Viele der Mediatoren (z. B. TNF-□, IL-6R) sowie Verbindungs- und Adhäsionsmoleküle (z. B. E-Cadherin, JAM-A), die für die Rekrutierung von Entzündungszellen und den Verlust der Barriereintegrität verantwortlich sind, werden proteolytisch durch A-Disintegrin- und Metalloproteinasen (ADAMs), insbesondere ADAM10 und ADAM17, gespalten. ADAM10 und ADAM17 haben sich bei verschiedenen Infektionskrankheiten als wesentliche Steuerungselemente erwiesen, was sie zu einem geeigneten und vielversprechenden therapeutischen Ziel macht. Die zellspezifische Regulierung und Funktion während einer Lungeninfektion ist jedoch noch nicht ausreichend geklärt.

Western Blot, Oberflächenexpressionsanalysen und zellbasierte Assays zeigten, dass die Proteinexpression, Reifung und Aktivierung von ADAM10 und ADAM17 in Epithelzellen bei einer Infektion mit Pseudomonas aeruginosa bzw. einer Stimulation mit Exotoxin A hochreguliert werden, ohne dass eine Infektion mit Streptococcus pneumoniae eine Rolle spielt. Insbesondere die Experimente mit hitzeinaktivierten Bakterien deuten darauf hin, dass die Aktivierung von ADAM10 und ADAM17 eher auf das Toxinrepertoire als auf die bloße Interaktion mit dem bakteriellen Partikel selbst zurückzuführen ist. Darüber hinaus zeigten pharmakologisches Targeting und Gen-Silencing von ADAM10 und ADAM17, dass diese Aktivierung für die Spaltung von E-Cadherin und Junctional Adhesion Molecule-A und das Überleben von Epithelzellen entscheidend ist, die beide die Integrität der Barriere sowie die epitheliale Regeneration, die Leukozytenadhäsion und die transepitheliale Migration beeinflussen. Darüber hinaus induzierte Pseudomonas aeruginosa die Freisetzung von ADAM10, aber nicht von ADAM17 auf Exosomen, die in der Lage waren, proteolytische Spaltungen in trans (auf verschiedenen Zellen) durchzuführen.

Der zweite Teil dieser Arbeit befasste sich mit der Rolle von leukozytärem ADAM10 und ADAM17 bei Lungeninfektionen. Für diese Untersuchungen wurden die Analyse von Patientenproben, ein in vivo Pseudomonas aeruginosa-Pneumoniemodell und detaillierte in vitro mechanistische Studien kombiniert. Patienten mit bakterieller Lungenentzündung und Covid-19-Patienten zeigten eine vom Schweregrad abhängige Aktivität von ADAM10 und ADAM17 auf Serumexosomen. Basierend auf dem Mauspneumoniemodell und der Infektion menschlicher Leukozyten konnte angenommen werden, dass die induzierte Freisetzung von ADAM10 und ADAM17 tragenden Exosomen hauptsächlich durch Leukozyten verursacht wurde. Darüber hinaus regulierten ADAM10 und ADAM17 die Rekrutierung von Leukozyten in den Alveolarraum und das Lungengewebe, die Ödembildung, die Freisetzung von

Zytokinen, die Makrophagenpolarisierung, die Bildung von reaktivem Sauerstoff, die bakterielle Clearance und den Schweregrad der Sepsis während einer Infektion mit Pseudomonas aeruginosa in besonderer Weise. Somit sind ADAM10 und ADAM17 in Epithelzellen und Leukozyten entscheidende regulatorische Elemente der bakteriellen und viralen Lungenentzündung. Diese Ergebnisse unterstreichen die Bedeutung von ADAM10 und ADAM17 als Vorschläge für neue prognostische und therapeutische Instrumente, die in weiteren präklinischen und translationalen Studien untersucht werden müssen.

2 Introduction

2.1 Pneumonia

Pneumonia is a pathological condition of the lower respiratory tract that frequently leads to acute lung injury and acute respiratory distress syndrome (ARDS). This respiratory infection typically involves inflammation of the lung parenchyma, which is frequently caused by respiratory viruses, Gram-negative or Gram-positive bacteria, and, on a global scale, mycobacteria. Bacterial pneumonia is classified as either "community-acquired" or "hospital-acquired" pneumonia (CAP or HAP), depending on the context in which the disease was acquired (Aliberti et al., 2021; Long et al., 2022). CAP is an acute lower respiratory tract infection that arises outside the hospital setting, presenting with different degrees of severity, from mild fever and cough to severe pneumonia with sepsis, acute respiratory failure, and ARDS (Aliberti et al., 2021). Excluding Sars-CoV-2, approximately 1.5 million adults in the U.S.A. are hospitalized with CAP annually (Ramirez et al., 2017). A population survey conducted from 2010 to 2012 revealed a yearly incidence of CAP requiring hospitalization of roughly 24.8 cases per 10,000 adults, with 21% of those patients requiring intensive care and an overall mortality rate of 2% (Jain et al., 2015). Aging is a significant risk factor for severe CAP requiring hospitalization, with an incidence of 63 per 10,000 adults in the age of 65-79 years, which increases to 164.3 per 10,000 in those over the age of 80 (Jain et al., 2015). In contrast, HAP and ventilation-associated pneumonia are infections that develop two or more days after hospital admission and mechanical ventilation initiation, respectively (Luyt et al., 2018). The burden of HAP is estimated to affect around 1.5% of all hospital admissions in the U.K., although the global prevalence of HAP remains incompletely understood (Ewan et al., 2017).

Bacterial pathogens are common culprits of both CAP and HAP, with *Streptococcus pneumoniae (S. pneumoniae)* being the most prevalent. To counteract its spread, vaccination strategies have been implemented, leading to a replacement of colonizing serotypes (Lannes-Costa et al., 2021). However, while such prevention measures have had some success, a more significant global issue lies in the evolution of multi-drug resistance (MDR) in bacterial pathogens. Indeed, the emergence of MDR poses increasing clinical challenges, particularly in the context of HAP. While numerous bacterial species have developed MDR, the World Health Organization has identified the ESKAPE pathogens, including *Enterococcus faecium*, *Staphylococcus aureus*, *Klebsiella pneumoniae*, *Acinetobacter baumannii*, *Pseudomonas aeruginosa (P. aeruginosa)*, and *Enterobacter* species, as a top priority for concern (De Oliveira et al., 2020).

2.1.1 *Pseudomonas aeruginosa*

Bacterial pathogens often have multiple virulence factors that enable them to evade or disrupt host defense mechanisms and especially the innate immune system. For instance, *P. aeruginosa* utilizes a single flagellum and type IV pili, which facilitate its motility and attachment to epithelial cells, and

soluble virulence factors released by different secretion systems. *P. aeruginosa* is a Gram-negative bacterium with MDR property that can opportunistically infect immunocompromised patients suffering from, e.g., cancer or chronic obstructive pulmonary disease (Cendra, Torrents, 2021; Rossi et al., 2021). *P. aeruginosa* has been predominantly developed to be an etiological agent of HAP with a 30-40% attributable mortality rate (Ware, Matthay, 2000). The initial immune response is mediated by the interaction with the epithelial toll-like receptors (TLRs), particularly, TLR2, TLR4 and TLR5, through recognition of bacterial flagellin (Feuillet et al., 2006). However, poor prognostic signs and symptoms during *P. aeruginosa* induced pneumonia are mainly linked to cytotoxic effects and destruction of the barrier integrity, finally resulting in sepsis development (Wagener et al., 2021). Paracellular permeability is regulated through tight junction and adherence junction proteins such as junctional adhesion molecule A (JAM-A), claudins, E-cadherin and beta-catenin (Azghani et al., 1993; Cott et al., 2016; Schneeberger, Lynch, 2004; Van Itallie, Anderson, 2004; Vikstrom et al., 2009). Destruction of those junctions permits pathogens and other macromolecules to diffuse between adjacent cells and, therefore, through the epithelium. Due to the thin layer of epithelial cells in the alveoli, the pulmonary system has been shown to be highly vulnerable to *P. aeruginosa* and its released toxins compared to the gut or skin epithelium (Wagener et al., 2021), finally leading to damage of the endothelial layer and sepsis formation.

Virulence factors of *P. aeruginosa* establish contractile forces to disrupt the intercellular connections resulting in gap formation and increased protein permeability. Most *P. aeruginosa* released toxins are derived from type 2 and type 3 secretion systems (T2SS and T3SS) (Filloux, 2011). One major virulence factor released by T2SS is Exotoxin A, which belongs to the mono-ADP-ribosyltransferase family (Liu, 1974). The ADP-ribosylation process inactivates the eukaryotic elongation factor-2 (eEF-2) on the ribosomes leading to apoptotic-induced cell death (Chang, Kwon, 2007). It has been shown that 80% of *P. aeruginosa* isolates produce Exotoxin A, with three times higher mortality rate compared to non-Exotoxin A producing strains (Cross et al., 1980). Cytoskeleton remodeling induced by Exotoxin A impairs wound healing and increases protein permeability (Azghani, 1996; Heggers et al., 1992). Pneumonia induced by a *P. aeruginosa*-Exotoxin A mutant was associated with less bacterial burden in lung tissues and lower cytokines release in the alveolar space relative to wildtype strain (Schultz et al., 2001). Interestingly, the immunization of mice with a DNA vaccine encoding for *P. aeruginosa*-Exotoxin A improved immunity and prevented lethal infection (Shiau et al., 2000). Furthermore, Exotoxin A induces intrinsic and extrinsic programmed cell death (Wood et al., 2023).

P. aeruginosa also possesses a T3SS encoding the effector proteins ExoS, ExoT, ExoY, and ExoU (Hardy et al., 2021). ExoU induces rapid epithelial cytotoxicity, and *P. aeruginosa* strains expressing ExoU have been associated with more severe pneumonia and adverse outcomes (Faure et al., 2014; Hardy et al., 2021). ExoS and ExoT are two of the earliest identified bifunctional T3 effectors found in *P. aeruginosa* that possess both GTPase activating protein and ADP-ribosyltransferase activity. The activities of these effectors trigger a cascade of harmful events in the host cell cytoskeleton, which

ultimately results in cytotoxicity (ExoS) or cytoskeletal rearrangements that limit phagocytosis (ExoT) (Barbieri, Sun, 2004; Hauser, 2009). ExoY, on the other hand, is a promiscuous nucleotidylyl cyclase, which disrupts the inter-endothelial gap junctions that facilitate communication between cells. This disruption promotes hyperphosphorylation and the subsequent release of tau and amyloid-β, two proteins that are implicated in neurodegenerative diseases (Hardy et al., 2021).

Besides the direct cytotoxic effects, TLR signaling and downstream signaling of toxin action induce an inflammatory response of the epithelial layer, resident lung macrophages, and newly recruited leukocytes. The binding of Pathogen-Associated Molecular Patterns (PAMPs) or Damage-Associated Molecular Patterns (DAMPs) to TLRs on the cells activates Nuclear Factor κB signaling. This, in turn, prompts the expression and the release of proinflammatory mediators such as cytokines and chemokines, which is vital for instigating immune and inflammatory responses (Jouault et al., 2022). In addition, the toxins repertoire of *P. aeruginosa* increases the levels of interleukin-1α (IL), IL-1β, IL-6, IL-8 which is important for prompt bacteria killing and eradication of infection (Wood et al., 2023).

2.1.2 Inflammation

Inflammation is a biological response of the body's immune system to an internal or external source of injury or infection. This process involves the activation of various cell types such as epithelial cells, endothelial cells and immune cells to protect the inflamed area and eliminate the causing insult (Chen et al., 2018). The hallmarks of inflammation are redness, warm sensation, edema, and pain which is a consequent of increased blood flow to the site of inflammation. Thereby, more oxygen and nutrients are supplied improving the healing process, and leukocytes migrate and release different cytokines and chemokines to coordinate the immune response (Fioranelli et al., 2021; Hannoodee, Nasuruddin, 2022). However, overshooting inflammation or an ineffective immune response result in damage of the healthy tissue and progression of the diseases (Levi, 2010; Sherwood, Toliver-Kinsky, 2004).

The initial phase of the inflammatory response to an infection is the recognition of the exogenous pathogen by immune cells, mainly through pattern recognition receptors (PRRs) (Gulati et al., 2018; Janeway, 1989). PRRs are present on the surface of immune cells such as macrophages, dendritic cells, and natural killer cells and are responsible for detecting specific molecular patterns that are derived from different pathogens (Mogensen, 2009). These patterns, known as PAMPs, are conserved among pathogens and essential for their survival and replication (Kumar et al., 2011). One of the most well-known PRRs is the TLR family. TLRs are found on the surface of immune cells and recognize a wide range of PAMPs, including lipopolysaccharides (LPS) found in the outer membrane of Gram-negative bacteria, flagellin from bacterial flagella, and double-stranded RNA from viruses (Kumar, 2022; Vijay, 2018). Recognition of a PAMP by a TLR triggers a signaling cascade that leads to the activation of the immune cell and the initiation of an immune response. Moreover, the activation of TLR results in a release of several cytokines and chemokines such as tumor necrosis factor alpha (TNF-α), IL-1, IL-6 or

the monocyte chemoattractant protein 1 (MCP-1/CCL2), which promote signals to attract and activate other immune cells, such as neutrophils and monocytes (Chen et al., 2018; Medzhitov, 2008).

The recruitment of leukocytes during inflammation involves several key steps. Activation of vascular endothelium induces degradation of junctional molecules such as JAM-A, which promotes vascular permeability and facilitates leukocyte extravasation (Leick et al., 2014; Medzhitov, 2010). Subsequently, the leukocytes adhere to the activated endothelium, enhanced by the increased expression of adhesive molecules, such as E-selectin and P-selectin, integrins, intercellular adhesion molecule 1 (ICAM-1) and vascular cell adhesion molecule 1 (VCAM-1) on the cell surface (Muller, 2003, 2011; Nourshargh et al., 2006). Once the leukocytes have adhered to the walls of the blood vessels, they are directed to the site of inflammation through a process known as chemotaxis (Hordijk, 2016). Chemokines, which are secreted by the activated immune cells, epithelial cells and endothelial cells, serve as attractants for leukocytes and direct their migration towards the site of inflammation (Adams, Lloyd, 1997). The next step in the recruitment of leukocytes is their activation and aggregation at the site of inflammation, which initiates the transmigration through the endothelium into the inflamed tissue (Muller, 2013). This allows the leukocytes to phagocytose and eliminate the harmful stimuli, such as bacteria, viruses, or other pathogens (Figure 2.1).

2.1.3 Phagocytosis and reactive oxygen species generation

Phagocytosis is a process by which cells internalize foreign particles or microorganisms, such as bacteria and viruses, for destruction and degradation. Phagocytosis is carried out mainly by macrophages, monocytes and neutrophils (Aderem, 2003; Gordon, 2016; Rosales, Uribe-Querol, 2017). The phagocytosis process begins with the recognition of foreign particles by phagocytes in an opsonin-dependent or independent manner (Gordon, Rice, 1988). Opsonization is the process by which a foreign particle is coated with proteins that enhance its recognition and internalization by phagocytes (Rosales, Uribe-Querol, 2017). These proteins, called opsonins, include immunoglobulins (IgGs), complement components, and collectins. Opsonins bind to specific receptors on the phagocyte, such as Fc (fragment crystallizable) receptors and complement receptors (CR1, CR3, CR4), and facilitate phagocytosis by increasing the specificity and efficiency of the phagocytic process (Jaumouille, Grinstein, 2011; Nimmerjahn, Ravetch, 2011; Uribe-Querol, Rosales, 2020). On the other hand, Opsonin-independent phagocytosis occurs through the recognition of PAMPs on the surface of pathogens, such as LPS on the surface of Gram-negative bacteria and lipoteichoic acids on the surface of Gram-positive bacteria, by phagocytes through PRRs like TLRs (Medzhitov, 2001; Tricker, Cheng, 2008). The specificity of the TLR-PAMP interaction is critical for the proper initiation of phagocytosis. For example, TLR2 recognizes a broad range of PAMPs, including peptidoglycans, lipopeptides, and zymosan, which are all components of the cell walls of various pathogens. In contrast, TLR4 is highly specific for LPS, and its activation by other PAMPs is much weaker (Medzhitov, 2001; Tricker, Cheng, 2008).

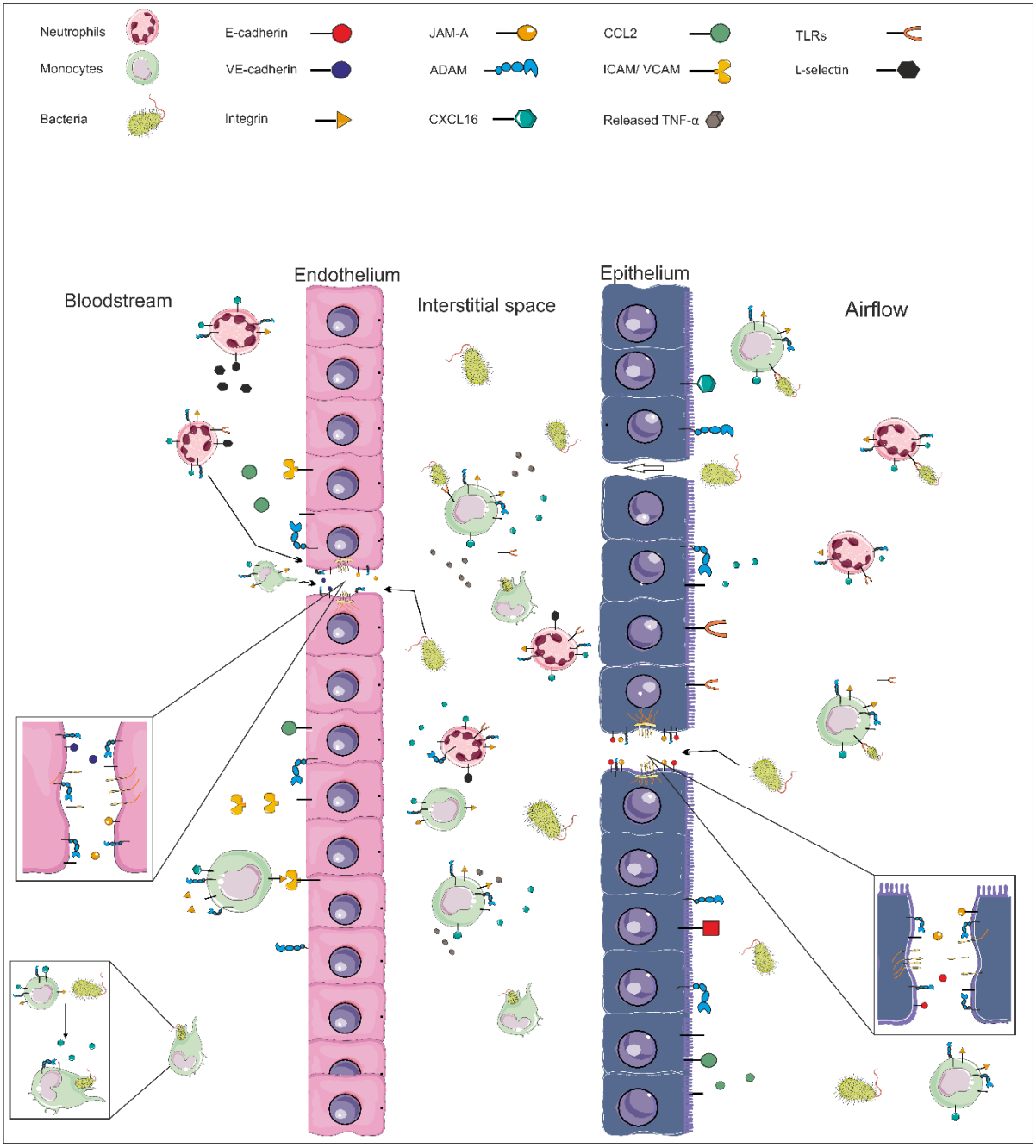

Figure 2. 1: Schematic representation of the inflammatory process.
The invading pathogen enters the body by attaching to the respiratory epithelium stimulating the release of cytokines and chemokines. This results in further recruitment of leukocytes such as neutrophils, monocytes and macrophages from the blood to the site of inflammation. these recruited leukocytes roll, adhere and transmigrate through the vascular endothelium to the site of inflammation.

Upon recognition of the foreign particle, the phagocyte undergoes a series of changes in shape and behavior, resulting in the formation of a phagosome (Aderem, Underhill, 1999). This structure is created by the invagination of the plasma membrane around the particle, enclosing it in a vesicle. The phagosome then moves towards the center of the cell and fuses with lysosomes, which contain hydrolytic enzymes that degrade cellular waste and the invaded pathogen (Lee et al., 2020; Tjelle et al., 2000). The fusion of the phagosome and lysosome forms a phagolysosome, which serves as a site for the

degradation of the engulfed particle (Figure 2.2). The phagolysosome is characterized by various hydrolytic enzymes, such as proteases, lipases, and nucleases, which degrade the foreign particle. In addition, the phagolysosome has a low pH, which creates a hostile environment for microorganisms and helps to inactivate virulence factors (Lee et al., 2020; Pauwels et al., 2017).

The phagolysosome is a highly reactive environment containing reactive oxygen species (ROS) that can destroy the engulfed pathogen (Robinson, 2008). Despite that the specific role of ROS in pathogen killing process is still debated. On the one hand, ROS damage the microbe's membrane and other structures directly. Furthermore, ROS participate in the activation of other antimicrobial mechanisms, such as the secretion of antimicrobial peptides and the recruitment of excessive phagocytic cells to the infection site (Mittal et al., 2014). However, the excessive production of ROS can also decrease the survival of the phagocytic cell, resulting in oxidative stress and damage of the cellular structures (Siraki, 2021). Therefore, ROS generation in response to an infection is tightly regulated to maintain balance between effective antimicrobial activity and cellular protection. Myeloperoxidase (MPO) has been given a prominent role in ROS activity, constituting 5% of the neutrophil's dry mass and mainly located in lysosomal azurophilic granules. MPO catalyzes the reaction of H_2O_2 with chloride ions (Cl^-) to form hypochlorous acid (HOCl), which destroys the microbes within the phagolysosome (Dupre-Crochet et al., 2013). On the tissue level, macrophages and neutrophils generate an increased amount of ROS at the site of inflammation, which participates to endothelial dysfunction and tissue damage (Dupre-Crochet et al., 2013). Thus, ROS serve as a key signaling messenger, mediating a significant influence on the development and progression of the inflammation. Interestingly, most of the mentioned molecules involved in the different stages of the inflammatory process, such as cytokines, chemokines, junction and adhesion molecules, exist as transmembrane protein on the cell surface. A significant number of these molecules can be released from the cell surface by the action of a disintegrin and metalloproteinases (ADAMs) family (Dreymueller et al., 2012b). In addition, members of ADAM proteases contribute to cellular differentiation and immune modulation, such as phagocytosis and ROS generation (Aljohmani, Yildiz, 2020).

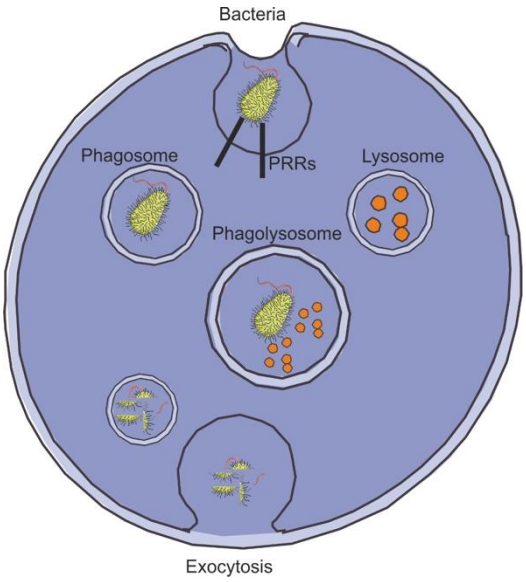

Figure 2. 2: phagocytosis process.
Surface receptors recognize and engulf bacteria in a process called phagocytosis. The phagosome fuses with a lysosome to form a phagolysosome, where the bacteria are broken down by ROS and degradative enzymes. The resulting fragments are then released from the cell via exocytosis.

2.2 ADAMs

ADAMs are type 1 transmembrane proteins characterized by a multidomain structure that includes a removable pro-domain, an N-terminal zinc ion-dependent metalloproteinase domain, followed by a disintegrin-like domain, an epidermal growth factor-like domain, a cysteine-rich domain, a transmembrane domain, and finally a cytoplasmic domain (figure 2.3) (Giebeler, Zigrino, 2016). The metalloproteinase domain contains the metzincin sequence HEXXHXXGXXH, which is required for the catalytic activity upon removal of the pro-domain. The disintegrin-like domain is involved in cell adhesion and interaction with integrins, while the cysteine-rich domain is involved in the characterization of the C-shape of the protease as well as the recognition of substrates and regulation of the proteolytic activity (Edwards et al., 2008; Seegar, Blacklow, 2019). While the epidermal growth factor-like domain has no clear structure and function, the cytoplasmic domain regulates the subcellular localization and maturation of the proteases, cell signaling and the metalloproteinase activity (Seals, Courtneidge, 2003). ADAMs are predominantly synthesized in the rough endoplasmic reticulum (ER) as a proform, where the pro-domain blocks the metalloproteinase domain. Maturation of ADAMs occurs in the late Golgi compartment through the removal of the pro-domain and translocation to the surface to perform the catalytic activity (Hougaard et al., 2000; Lum et al., 1998; Roghani et al., 1999).

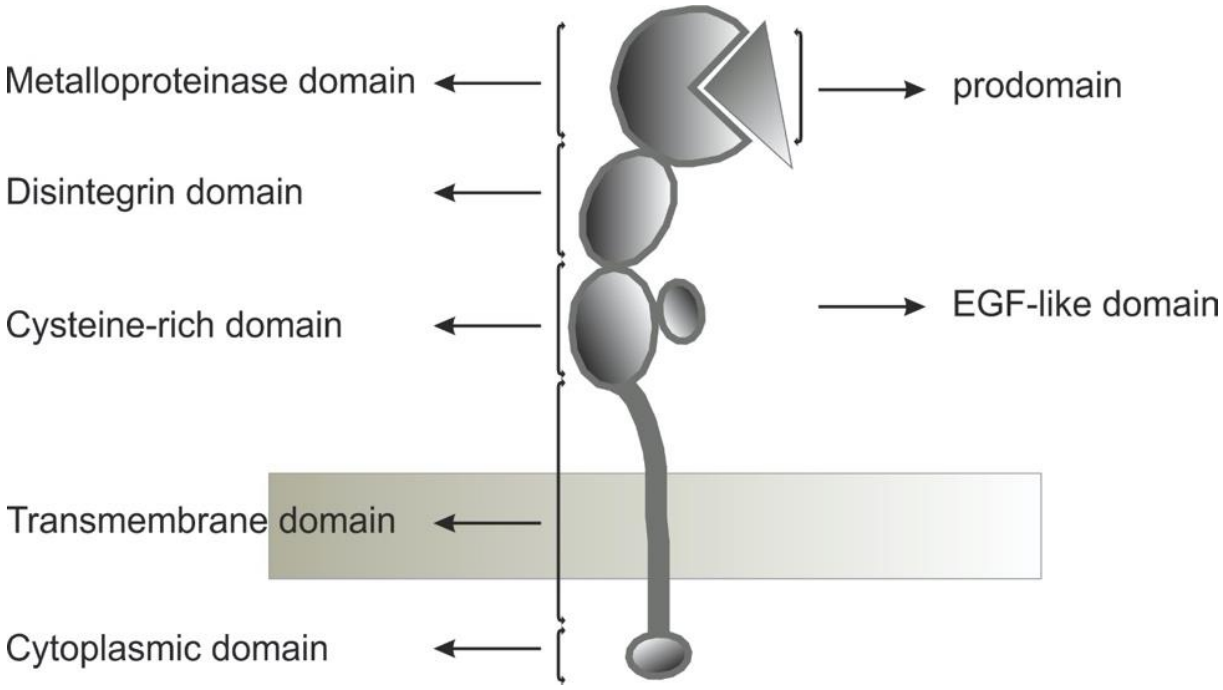

Figure 2. 3: Schematic representation of a disintegrin and metalloproteinase (ADAM) protease.
ADAMs are type 1 transmembrane proteins characterized by a multidomain structure and several functions in cell biogenesis, cell migration and inflammation mediated by the catalytic and noncatalytic activity of the different domains. The metalloproteinase domain is involved in the proteolytic activity and the cleavage of the transmembrane molecules, the disintegrin-like domain is involved in cell adhesion and interaction with integrin, the cysteine-rich domain is involved in the characterization of C-shape of the protease as well as recognition of the substrates and regulation of the proteolytic activity while the EGF-like domain has no clear function (absent in ADAM10 and ADAM17). Finally, the cytoplasmic domain regulates the subcellular localization and maturation of the proteases, cell signaling and the metalloproteinase activity.

ADAMs have shown to play a fundamental role in maintaining body homeostasis through several functions such as proteolysis, cell differentiation and fusion, as well as intracellular signaling (Stone et al., 1999). Among all the functions, the proteolytic activity of ADAMs is highlighted as a predominant process regulating cell migration and proliferation, angiogenesis, tissue inflammation and regeneration and neurodegenerative diseases (Deuss et al., 2008; Edwards et al., 2008). Among 34 *ADAM* genes in various species, 22 are well described in humans. 12 of these ADAMs are proteolytically active (ADAM8, ADAM9, ADAM10, ADAM12, ADAM15, ADAM17, ADAM19, ADAM20, ADAM21, ADAM28, ADAM30, ADAM33) (Andreini et al., 2005; Seals, Courtneidge, 2003). Proteolytically active proteases mediate proteolytic cleavage of other transmembrane proteins in a process called ectodomain shedding (Schlondorff, Blobel, 1999). The proteolytic activity of ADAM proteases mediates the ectodomain shedding of several molecules. For instance, the cleavage of TNF-α by ADAM17 drives the inflammatory surrogate, while the cleavage of TNF-α receptor by the same protease has an antagonistic effect (Hooper et al., 1997). Furthermore, the cleavage of E-cadherin by ADAM10 affects epithelial cell-cell adhesion and migration as well as modulates the β-catenin subcellular localization and downstream signaling (Maretzky et al., 2005). In addition, the shedding of the ectodomain can act as a critical bottleneck for the occurrence of further cleavage events within the

plasma membrane. This process, known as regulated intermembrane proteolysis (RIPing), is well-understood in the context of the proteolytic processing of Notch receptors (Andersson et al., 2011; Kopan, Ilagan, 2009). Overall, the inflammatory process, body homeostasis, tissue regeneration, and cancer development and progression can be influenced by the actions of ADAMs.

2.2.1 ADAM10

ADAM10 is synthesized as an inactive zymogen in the ER and maturates by removal of the inhibitory pro-domain through furin and/or prohormone convertase 7 in Golgi compartment through furin and prohormone convertas7 recognition sequences located between the pro-domain and the metalloproteinase domain (Lichtenthaler, 2011). The importance of ADAM10 is highlighted by the fact that mice with an ADAM10 knockout die within 10 days of embryonic development due to several cardiovascular and neurological complications. ADAM10 cleaves multi-different substrates (Table 2.1), however, cleavage of Notch receptor is one of the most important proteolytic activities of ADAM10. As a sheddase for diverse substrates, ADAM10 considers to be a therapeutic target for several inflammatory diseases, cancer and Alzheimer's disease (Smith et al., 2020; Wetzel et al., 2017). In addition, ADAM10 activity promotes the development and progression of several cancer diseases such as breast cancer, glioblastoma, T cell acute lymphoblastic leukemia and squamous cell carcinoma (Ko et al., 2007; Kohutek et al., 2009; Liu et al., 2006; Tosello, Ferrando, 2013). Cleavage of the Notch1 in T cell acute lymphoblastic leukemia, N-cadherin and L1 in glioblastoma, HER2 and its ligands in breast cancer are all examples of the impact of ADAM10 proteolytic activity on diseases progression (Ko et al., 2007; Kohutek et al., 2009; Liu et al., 2006; Tosello, Ferrando, 2013).

Several inflammatory mediators are well documented substrates for ADAM10, such as the receptor for advanced glycation end products (RAGE), VE- and E-cadherin, CX3CL1 and CXCL16 (Abel et al., 2004; Maretzky et al., 2008; Raucci et al., 2008; Schulz et al., 2008; Shimaoka et al., 2003). ADAM10 catalytic activity on endothelial cells, epithelial cells and leukocytes have been shown to shape and control the inflammatory process during several diseases (Dreymueller et al., 2015). Leukocytic ADAM10 acts pro-inflammatorily through regulation of adhesion and transmigration of leukocytes both *in vivo* and *in vitro* (Pruessmeyer et al., 2014). Endothelial ADAM10 sheds VE-cadherin increasing protein leakage and facilitating leukocyte trans-endothelial migration (Schulz et al., 2008). Moreover, ephrin-A shedding by endothelial ADAM10 prevents the interaction with its ligand and thereby disrupts endothelial cell-cell adhesion and increases protein permeability (Coulthard et al., 2012). In addition, epithelial ADAM10 processing of RAGE mediates acute lung inflammation (Raucci et al., 2008).

ADAM10 fulfils several functions during infectious diseases (see table 1), such as pathogen recognition and entrance, pathogen phagocytosis, leukocyte recruitment and polarization and finally, initiation and resolution of inflammation (Aljohmani, Yildiz, 2020). ADAM10 mediates the release of the soluble form of the scavenger receptor CD163 during *Staphylococcus aureus* (*S. aureus*) infection resulting in

enhanced bacterial clearance (Kneidl et al., 2012). In addition to its role in the initial pathogen recognition, ADAM10 acts as a receptor for *S. aureus* α-hemolysin, increasing the infection severity (Wilke, Bubeck Wardenburg, 2010). Moreover, *S. aureus*, *Helicobacter pylori* and *P. aeruginosa* mediate ADAM10-dependent shedding of E-cadherin, increasing diseases severity (Inoshima et al., 2011; Inoshima et al., 2012; Reboud et al., 2017; Schirrmeister et al., 2009). Thus, ADAM10 displays important functions during several stages of infection.

2.2.2 ADAM17

ADAM17 (TNF-α converting enzyme) is one of the most important proteolytically active members of the ADAM family. Similar to ADAM10, ADAM17 is inactively resident in the ER as proform that needs processing in the Golgi compartment for further maturation and activation (Grotzinger et al., 2017). ADAM17-mediated shedding of TNF-α plays an important role during inflammatory and immune responses such as asthma, chronic obstructive pulmonary disease, rheumatoid arthritis, acute respiratory distress syndrome (Barnes, 2003; Scheller et al., 2011), neurodegenerative diseases such as Alzheimer's disease and cancer (Zunke, Rose-John, 2017). More than 77 shedding substrates have been described to be shed by ADAM17, including, but not limited to, growth factors of the epidermal growth factor (EGF) family, IL-6R, ICAM-1, VCAM-1 and JAM-A (Pruessmeyer, Ludwig, 2009; Scheller et al., 2011). The release of the soluble domain of the growth factors transforming growth factor (TGF)-α, amphiregulin, heparin-binding (HB)-EGF and neuregulin results in binding to their receptors of the ErbB family, a transactivation pathway regulated by ADAM17 activity (Peschon et al., 1998; Rio et al., 2000). Interestingly, mice with full ADAM17 knockout die during embryogenic development or directly after birth due to skin and hair abnormalities, eyelid opening and defect in epithelial tissue of several organs, which is similar to phenotypes observed in mice lacking amphiregulin, EGFR, HB-EGF or TGF-α (Blobel, 2005; Dreymueller et al., 2015; Sahin et al., 2004). In addition, overexpression or upregulation of ADAM17 has been linked to inflammatory diseases such as psoriasis, rheumatoid arthritis or Crohn's disease (Cesaro et al., 2009; Kawaguchi et al., 2005).

Investigations of ADAM17 conditional knockout in several disease models identified ADAM17 as an additional major regulator of inflammatory processes. Those include leukocyte chemo-attraction, firm adhesion and trans-endothelial migration by cleaving CX3CL1, syndecans, VCAM-1 and ICAM-1 and JAM-A as few examples (Garton et al., 2001; Garton et al., 2003; Koenen et al., 2009; Pruessmeyer et al., 2010). Deletion of endothelial ADAM17 in an endotoxin-induced acute lung inflammation model reduced leukocyte recruitment, cytokine release and edema formation (Dreymueller et al., 2012a). Knockout of ADAM17 in myeloid cells reduced the severity of septic shock induced by LPS (Horiuchi et al., 2007). In several *in vitro* studies, epithelial ADAM17 has been shown to be involved in epithelial cell activation by ligands of TLR, IL-8 expression, and thereby to regulate leukocyte chemo-attraction,

protein permeability, and mucus secretion (Finigan et al., 2011; Koff et al., 2008; Kuwahara et al., 2007; Nakanaga et al., 2007).

In addition to sterile inflammation, ADAM17 plays diver roles in infectious diseases (see table 2.1). ADAM17-dependent shedding of TNF-α was shown to regulates bacterial phagocytosis by monocytes in a cell-autonomous manner (Seifert et al., 2020). In addition, ADAM17 dependent shedding of L-selectin enhanced *S. aureus* clearance by neutrophils (Cappenberg et al., 2019). The absence of ADAM17 during polymicrobial sepsis increased leukocyte recruitment and thereby enhanced bacterial clearance and improved cell survival (Long et al., 2012; Mishra et al., 2016). Interestingly, cleavage of SARS-CoV-2 spike protein (S) by ADAM17 mediated viral entry and pathogenesis (Jocher et al., 2022).

2.2.3 Synthetic inhibitors of ADAM10 and ADAM17

ADAM10 and ADAM17 are control elements in sterile inflammation and infectious diseases as well as chronic diseases such as cancer. Thus, the question of potential targeting by drugs as novel treatment options has been raised. Hydroxamate-based small molecules were found to be effective inhibitors, as they bind to the protease via residues of their pseudopeptide backbone and coordinate the zinc ion in the active site of the proteases via their hydroxamate group (Dreymueller, Ludwig, 2017). While TAPI-1 acts as a metalloproteinase inhibitor, blocking ADAM17, GI254023X is a potent and preferential inhibitor of ADAM10-mediated shedding events (Ludwig et al., 2005; Moss, Minond, 2017), blocking shedding of Notch, constitutive and ionomycin-induced shedding of the low-affinity IgE receptor CD23, cadherins (N, E, VE), transmembrane chemokines (CXCL16 and CX3CL1) and growth factors (EGF and betacellulin) (Abel et al., 2004; Hundhausen et al., 2003; Maretzky et al., 2005; Reiss et al., 2005). Batimastat was the first hydroxamate-based inhibitor successfully passing clinical trials. Due to its poor bioavailability, the inhibitor was replaced by Marimastat (Folgueras et al., 2004; Hu et al., 2007). However, the use of these inhibitors resulted in hepatotoxicity and musculoskeletal side effects, which led to the discontinuation of clinical trials in phase I/II (Wetzel et al., 2017). The lack of specificity of these substances, which inhibit various metalloproteinases such as MMP-1, -2, -3, -7, and ADAM17, may have contributed to their failure in clinical trials (Wetzel et al., 2017). The broad inhibition of these metalloproteinases can dysregulate important signaling pathways such as Notch and NF-kB, causing harmful off-target effects. *In vivo* studies have demonstrated that the inhibitor has the potential to hinder the onset of inflammatory processes and the development of fibrosis in the lungs (Inoshima et al., 2011; Powers et al., 2012). However, the long-term treatment effects of these inhibitors on ADAM10 and ADAM17 over a period of several hours or days remain unknown, as most studies have only investigated their effects for a short period of time, which is required for shedding. Based on previous experiences with the clinical use of hydroxamate-based inhibitors, severe side effects can be assumed. Thus, in-depth research on the underlying regulatory mechanisms and novel specific inhibitors is needed.

Table 2. 1: Roles of ADAM10 and ADAM17 in infection.

Step	Protease	Substrate or non-proteolytic function	Effect	Reference
Pattern recognition and entrance	ADAM10	CXCL16	Conversion from membrane attached scavenger receptor to soluble chemoattractant	(Abel et al., 2004; Gough et al., 2004)
		CD46	Potentiate apoptosis	(Hakulinen, Keski-Oja, 2006)
		TLR4	Reduce inflammatory response to LPS	(Yang et al., 2017)
	ADAM17	ACE2	Attenuate SARS-COV entry Severely worsen the outcome symptoms	(Kuba et al., 2005)
		Ebola virus surface glycoprotein	Block the antibodies that are responsible for virus neutralization	(Dolnik et al., 2004)
		glucose regulated protein 96	Protect against Ctr recurrent infection	(Paland et al., 2008)
Toxin handling	ADAM10	receptor alpha-toxin	Receptor for Staphylococcus aureus α-hemolysin potentiating its cytotoxicity even at low concentration	(INOSHIMA et al., 2011)
Phagocytosis	ADAM10	CD163	Amplifies phagocytosis	(Kneidl et al., 2012)
	ADAM17	CD163	Amplifies phagocytosis	(Etzerodt et al., 2010; Kneidl et al., 2012)
Cytokines release	ADAM17	TNF-α Receptor 2	Macrophage and neutrophil infiltration the lethality of lung injury	(Deberge et al., 2013; Deberge et al., 2015)
Tissue damage, repair and regeneration	ADAM10	heparin-binding-epidermal growth factor	Mucin overproduction, obstruction and infection recurrent	(Basbaum et al., 2002)
		E-and VE-cadherin	Disruption of endothelial and epithelial barrier integrity Amplify epidermal pathogenesis	(Inoshima et al., 2011; Inoshima et al., 2012; Powers et al., 2012; Reboud et al., 2017)
			potentiate tumorigenesis	(Schirrmeister et al., 2009)
		Endothelial protein C receptor	Dysregulation of coagulation and finally thrombosis	(Lecuyer et al., 2018)
chronicity/systemic changes	ADAM10	E-cadherin	Endothelial malfunction mediated sepsis	(Powers et al., 2012)

2.3 Exosomes

In addition to the proteolytic activity on the cell surface, the proteases can also be transported from the cell membrane to the extracellular space through the release of membrane vesicles such as exosomes.

2.3.1 Exosome biogenesis and functions

Exosomes are plasma membrane-derived extracellular vesicles (EVs) with 50-160 nm diameter that have gained increasing attention recently. Exosomes were initially proposed as cellular by-products or waste with no significant function. However, recent studies indicate the importance of these EVs as vehicles for wide number of potential cargos such as nucleic acids, lipids and proteins (Simpson et al., 2009; Valadi et al., 2007; Vidal et al., 1989). The biogenesis process of exosomes is initiated by plasma membrane invagination to form a cup-shape that includes the cell surface and cell soluble proteins called early-sorting endosome (ESE) (Kalluri, Lebleu, 2020). The later one can further mature to late-sorting endosomes (LSEs) and finally multivesicular bodies (MVBs), which contain the intraluminal vesicles (future exosomes). The destiny of the MVBs can be either to fuse with lysosomes for degradation or to fuse with the plasma membrane for the exocytotic release of the exosomes (figure 2.4) (Kahlert, Kalluri, 2013).

The exocytosis and endocytosis property of exosomes mediate their crucial roles in intercellular communication, particularly, immune response and cancer (Mathieu et al., 2019). Thus, EVs, particularly exosomes, show a great capacity in modifying the phenotype of the acceptor cells. The size and the surface molecules of the released EVs influence their recognition, capture or even the way of delivery of their cargos (Mathieu et al., 2019). The cellular uptake of exosomes is a very organized process of three steps: targeting the specific acceptor cell, selecting the entry point, and releasing the content. It has been shown that the tetraspanin-integrin complex is involved in targeting and binding of exosomes to their target cells (Nazarenko et al., 2010; Rana et al., 2012). Moreover, ICAM-1 upregulation on the cell surface during inflammation enhances the adhesion of the exosomes (Clayton et al., 2004). Beside the direct fusion with the plasma membrane, exosomes can exert their desired effect by acting on the surface of the targeting cell without releasing their cargos (Raposo et al., 1996).

Exosomes play an important role in manipulating the inflammatory process and cancer progression. Oncogenic proteins transfer between cancerous cells facilitates metastasis, the proliferation of cancer cells, tumor angiogenesis and induces chemoresistance (Corcoran et al., 2012). Exosomes mediate the transfer of membrane EGFR from cancer cell to endothelial cell, supporting tumor angiogenesis via vascular endothelial growth factor/receptor (VEGF/VEGFR-2) pathway (Al-Nedawi et al., 2009). Lung metastases and endothelial permeability show to be enhanced by exosomes derived from melanoma (Peinado et al., 2012).

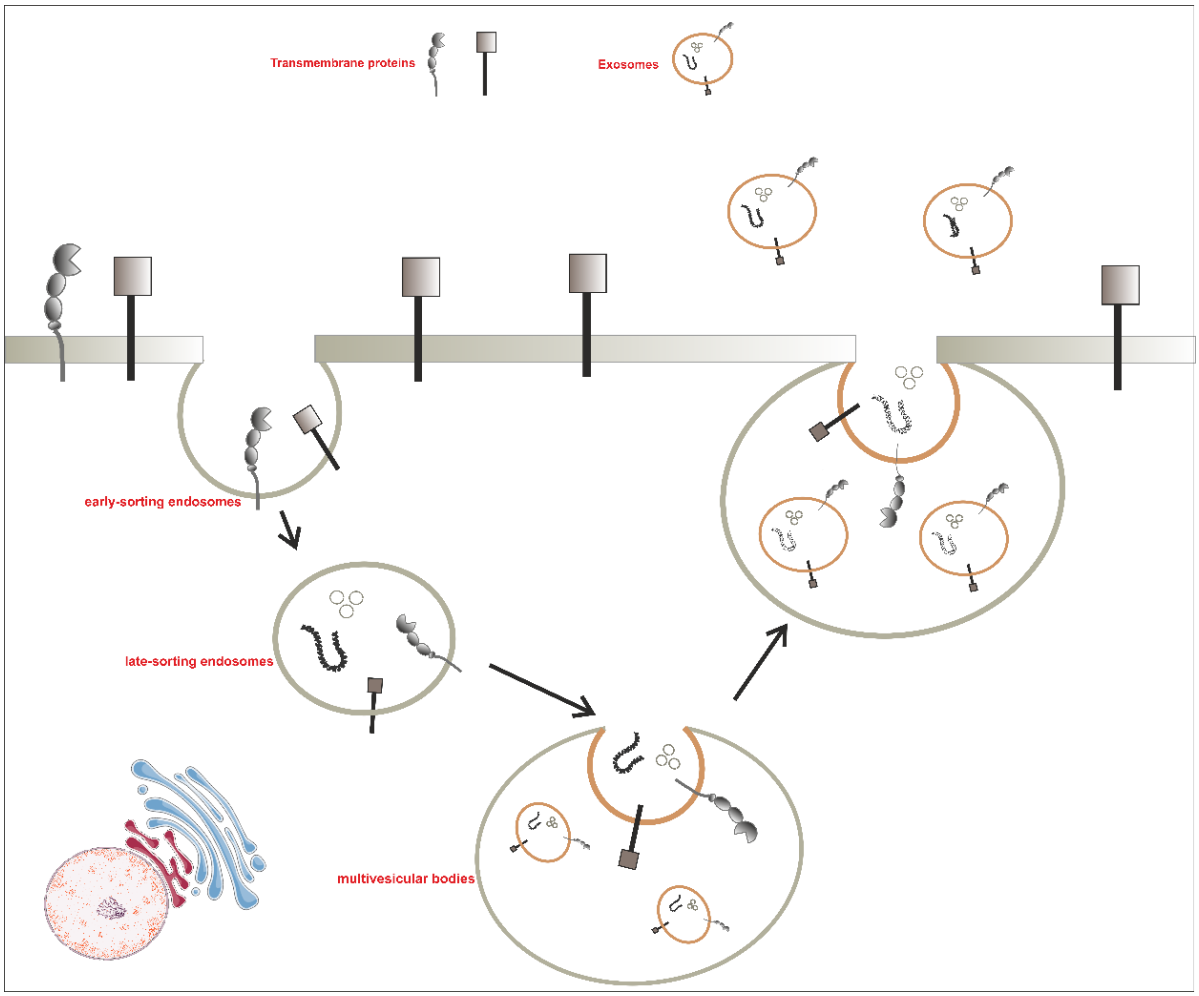

Figure 2. 4: Biogenesis of exosomes.
The biogenesis process of exosomes starts with plasma membrane invagination to form a cup-shape that includes the cell surface and cell soluble proteins called early-sorting endosome (ESE). The ESE further mature to late-sorting endosomes (LSEs) and finally multivesicular bodies (MVBs) which contain the intraluminal vesicles (future exosomes). The MVBs can be either fuse with lysosomes for degradation or fuse with the plasma membrane for exocytotic release of the exosomes.

2.3.2 Exosomes in inflammation

In the context of inflammation, exosomes play an important role in manipulating the immune response and influencing the performance of immune cells. The released exosomes from immune cells can load pro-inflammatory signals and molecules that stimulate immune cell activation and promote the release of cytokines and other signaling molecules involved in the inflammatory process (Li et al., 2022). Additionally, exosomes released from inflamed cells can transport signals to trigger inflammation and recruit immune cells to the site of infection. The cargos of exosomes derived from lung cancer enhance gene silencing of the TLR family in macrophages, and thereby the secretion of pro-inflammatory and pro-metastatic cytokines leading to tumor growth and metastasis (Fabbri et al., 2012). $CD4^+$ T and $CD8^+$ T cell-derived exosomes induce dendritic cell apoptosis (Fabbri et al., 2012). On the other hand, exosomes can also play a role in the resolution of inflammation. Some exosomes carry anti-inflammatory signals that help to suppress the immune response and promote tissue repair (Suh et al., 2021). Exosomes derived from bone marrow-derived mesenchymal stem cell improved oxidative stress and reduced immune response during acute lung injury (Li et al., 2019). Additionally, exosomes released

from immune cells, such as regulatory T cells, can help to modulate the immune response and prevent excessive inflammation (Fang et al., 2020). Thus, the role of exosomes during inflammation is complex and multi-faceted and needs further investigations.

2.4 Aim of the study

In spite of the significant progress in the treatment strategies of infectious diseases, it remains one of the most leading causes of death worldwide. Among these infectious diseases, pneumonia is a particularly severe and life-threatening lung infection that is often caused by *S. pneumoniae* and *P. aeruginosa*. While the inflammatory response is important to eliminate the infections, an excessive and prolonged immune response can lead to chronic inflammation, resulting in tissue damage not only at the site of infection but also in distinct organs. ADAM10 and ADAM17 in epithelial cells and leukocytes fulfil different functions during several infectious and inflammatory diseases ranging from pathogen recognition to resolution of the concurrent inflammation and the development of systemic effects. Thereby, both proteases are essential control elements of infectious diseases making them a suitable therapeutic target to overcome the unmet medical need. Based on the divergent roles in disease and homeostasis, specific targeted approaches are required. This requires in-depth knowledge of the cell-specific regulation and function during lung infection. Thus, the present thesis aimed to evaluate the regulation and function of ADAM10 and ADAM17 in epithelial cells and leukocytes during infection with *P. aeruginosa.*

Part 1: Epithelial ADAM10 and ADAM17 showed to contribute to different aspect during sterile inflammation, however, the cell specific-pathogen specific role of both proteases on epithelial cells during lung infection still unclear. Therefore, the aim of this part of the thesis was to investigate the specific regulation and function of ADAM10 and ADAM17 during the infection of lung epithelial cells with different infectious pathogens. To approach this question, a cell-based assays were used to analyze the regulation of both proteases in alveolar epithelial cell line and human small airway epithelial cells during infection with *P. aeruginosa* and *S. pneumoniae*. In addition, the function of ADAM10 and ADAM17 during different steps of inflammation (ex., protein permeability, epithelial cells regeneration, leukocyte transepithelial migration and adhesion as well as cell survival) was investigated using the synthetic inhibitors (GI254023X and TAPI-1) and shRNA mediated gene silencing.

Part 2: Similar to epithelial cell, several studies described the role leukocytic ADAM10 and ADAM17 during acute lung inflammation. However, a comprehensive study describing the specific role of both proteases during acute lung pneumonia and the mediated mechanism is still missing. Thus, the aim of this part is to investigate the contribution of leukocytic ADAM10 and ADAM17 during acute lung pneumonia. Therefore, I analyzed the exosomal release of both proteases in the serum of pneumonia patients and in *P. aeruginosa*-induced lung pneumonia model of mice lacking either ADAM10 or ADAM17 in all hematopoietic cells. Furthermore, the effect of both proteases on the local lung environment, cytokines release, ROS generation, cell survival and phagocytosis and the polarization of macrophages using the synthetic inhibitors (GI254023X and TAPI-1).

3 Materials and Methods

3.1 Materials

3.1.1 Devices and Software

Used devices and softwares are listed in tables 3.1 and 3.2.

Table 3. 1: Used equipment

Name	Company
Beckman rotor Type Ti50.2	Beckman Coulter GmbH, Krefeld, Germany.
Beckman TLA-55 rotor	Beckman Coulter GmbH, Krefeld, Germany.
BioTec autoscratch	BioTek, Highland Park, Winooski, VT, USA.
Buffer Tank	Bio-Rad Laboratories, Inc., Hercules, USA.
Cell culture incubator CB170-E7	Binder GmbH, Tuttlingen, Germany.
Centrifugation device 5418 R	Eppendorf AG, Hamburg, Germany.
Cooled charge-coupled device (CCD) camera	Imago, TILL Photonics.
Genios fluorescence reader	Tecan, Grödig, Austria.
Hemocytometer	Invitrogen, Frankfurt, Germany.
HLC Heating-ThermoMixer TH 21	DITABIS AG, Pforzheim, Germany.
Inverted microscope	Axiovert S100, Carl Zeiss, Jena, Germany.
Invitrogen™ Minigel Tank and Blot Module Set	Fisher Scientific GmbH, Schwerte, Germany.
LAS3000	Fujifilm, Tokyo, Japan.
Lionheart (FX) Automated Microscope system	BioTec, Highland Park, IL, USA.
Mini-PROTEAN® Casting Frame	Bio-Rad Laboratories, Inc., Hercules, USA.
Mini-PROTEAN® Casting Stand	Bio-Rad Laboratories, Inc., Hercules, USA.
Mini-PROTEAN® Tetra Electrode Assembly	Bio-Rad Laboratories, Inc., Hercules, USA.
PowerPac™ HC High-Current Power Supply	Bio-Rad Laboratories, Inc., Hercules, USA.
Sony SH800	Sony, Berlin Germany.
The NucleoCounter® NC-200™	ChemoMetec GmbH, Allerod, Denmark.
Ultrospec 10, cell density meter	Biochrom Ltd, Cambridge, United Kingdom.

3.1.2 Softwares

Table 3. 2: used softwares

Name	Company
AIDA Image Analysis software 4.27.039	Elysia-raytest, Straubenhardt, Germany
CorelDRAW x7 19.0.0.491	Corel Corporation, Alludo, Ottawa, Canada
FlowJo 10.6.2 software	Tree Star, Inc., Ashland, OR, USA
Gen5 software version 3.05.11	BioTek, Highland Park, Winooski, VT, USA
GraphPad PRISM 9.0	GraphPad Software, La Jollla, CA, USA
TillvisION software 2.7.0.16	TILL Photonics, Kaufbeuren, Germany
ZEN 2.3 blue edition	Carl Zeiss Microscopy GmbH, Oberkochen, Germany

3.1.3 Consumable materials

Special consumables used throughout the study are listed in table 3.3.

Table 3. 3: Consumable materials

Name	Company
Bolt™ 4-12% Bis-Tris 1.0mm Mini Protein Gel	Invitrogen, Frankfurt, Germany.
Columbia blood agar with sheep blood medium	Thermo Fisher, Karlsruhe, Germany.
Conical bottom polypropylene tube, 15, 50 ml.	Greiner Bio-One GmbH, Frickenhausen, Germany.
Disposable syringes, 5, 10, 20 ml	B. Braun Melsungen AG, Melsungen, Gemany.
DULBECCO'S PHOSPHATE BUFFERED SALINE	Sigma-Aldrich, Taufkirchen, Germany.
Filtered pipettes tips, 10, 20, 200, 1000 µl.	Thermo Fisher, Karlsruhe, Germany.
Isotonic Saline Solution 0.9%	Fresenius Kabi, Bad Homburg, Germany.
Micro Tube 1.3 ml K3E, 1.6 mg EDTA/ml	SARSTEDT AG & Co. KG, Nümbrecht, Germany.
Microplate, 96 wells, flat bottom.	SARSTEDT AG & Co. KG, Nümbrecht, Germany.
Microtube, 1.5 ml.	SARSTEDT AG & Co. KG, Nümbrecht, Germany.
Nitrocellulose membrane, 0.2 µm.	Bio-Rad Laboratories, Inc., Hercules, USA.
Omnican®-F, Fine dosing syringe, 1 ml	B. Braun Melsungen AG, Melsungen, Gemany.
Pipettes, 2.5, 10, 20, 200, 1000 µl.	BrandTech Scientific, Inc., NY, USA.
Polystyrene round-bottom tube (FACS), 5ml.	FALCON, corning incorporated, NY, USA.
Polystyrol cuvette 10*4*45 mm	SARSTEDT AG & Co. KG, Nümbrecht, Germany.
Serological pipettes, 2, 5, 10, 25 ml.	SARSTEDT AG & Co. KG, Nümbrecht, Germany.
Tissue culture plate, 12 wells, flat bottom.	SARSTEDT AG & Co. KG, Nümbrecht, Germany.
Tissue culture plate, 6 wells, flat bottom.	FALCON, corning incorporated, NY, USA.
Tissue culture plate, 96 wells, flat bottom.	SARSTEDT AG & Co. KG, Nümbrecht, Germany.
Trans-well insert 5 µm.	Corning, Amsterdam, The Netherlands.
Ultracentrifuge Microtube, 1.5 ml.	Laborgeräte Beranek GmbH, Weinheim, Germany.
Ultracentrifuge polycarbonate tube, 25 ml.	Beckman Coulter GmbH, Krefeld, Germany.
Via1-Cassette™	ChemoMetec GmbH, Allerod, Denmark.

3.1.4 Chemicals

All chemicals used in this work have a certified degree of purity *pro analysis (p.a).* All common chemicals were ordered from Carl Roth and Thermo Fisher. Special chemicals and reagents are listed in table 3.4.

Table 3. 4: Chemicals, reagents and recombinant proteins.

Name	Company
4-Nitrophenyp phosphate disodium salt hexahydrate tablet	Sigma-Aldrich, Taufkirchen, Germany.
70-kDa Tetramethylrhodamine (TRITC)-dextran	Sigma-Aldrich Chemie GmbH, Taufkirchen, Germany.
Accutase solution	Sigma-Aldrich, Taufkirchen, Germany.
Agaros	Carl Roth GmbH, Karlsruhe, Germany
Amersham ECL prime Western blotting reagent	PerkinElmer, Waltham, MA, USA.
Bis-acrylamide 29:1 40 %	Thermo Fisher, Karlsruhe, Germany.
BM blue, POD Substrata	Roche Diagnostics Deutschland GmbH, Mannheim, Germany.
Calcein-AM	Merck Millipore, Darmstadt, Germany.
Collagen G	Biochrom GmbH, Berlin, Germany.
Complete protease Inhibitor cocktail tablet	Roche Diagnostics Deutschland GmbH, Mannheim, Germany.
DNA Molecular Weight Marker XIV	Thermo Fisher, Karlsruhe, Germany.
FCS (fetal calf serum)	Corning, New York, USA
Fisher BioReagents™ EZ-Run™ Prestained Rec Protein Ladder	Thermo Fisher, Karlsruhe, Germany.
Fluorescein isothiocyanate (FITC)-albumin	Sigma-Aldrich Chemie GmbH, Taufkirchen, Germany.
Fura-2 AM	Invitrogen by ThermoFischer Scientific, Eugene, OR, USA.
Gibco™ Opti-MEM™ I Serum Reduced Medium	Thermo Fisher, Karlsruhe, Germany.
jetPEI®	Poly Plus Transfections, Illkirch, France
KAPA2G Fast HotStart Genotyping Mix	Sigma-Aldrich, Taufkirchen, Germany.
Ketamin	
Lipofectamine™ 3000	Thermo Fisher, Karlsruhe, Germany.
Mitomycin	Abcam, Cambridge, United Kingdom.
NucRed™ Live 647	Thermo Fisher, Karlsruhe, Germany.
Paraformaldehyde	Carl Roth, Karlsruhe, Germany
Pancoll human, Density: 1.077 g/ml	PAN-Biotech GmbH, Aidenbach, Germany.
Polybrene	Sigma Aldrich, Steinheim, Germany
Poly-L-lysine	Sigma, Steinheim, Germany.
SYTOX™ green	Thermo Fisher, Karlsruhe, Germany.
Todd–Hewitt–Bouillon (THB)	Thermo Fisher, Karlsruhe, Germany.
Trypsin Neutralizing Solution	PromoCell, Heidelberg, Germany.
Xylazine	
β-glucuronidase	Santa Cruz Biotech, Dallas, TX, USA.

3.1.5 Kits

All kits were used according to the manufacturers' protocols and recommendations.

Table 3. 5: Kits

Name	Company
ADAM10 Selective Substrate II (Fluorogenic) – PEPDAB063A	Biozym Scientific GmbH, Hessisch Oldendorf, Germany.
ADAM17 Selective Substrate (Fluorogenic) – PEPDAB064	Biozym Scientific GmbH, Hessisch Oldendorf, Germany.
bicinchoninic acid assay (BCA)	Thermo Fisher, Karlsruhe, Germany.
Mouse CXCL1/KC DuoSet Enzyme-linked immunosorbent assay (ELISA)	R&D System, Wiesbaden, Germany.
Mouse IL-6 DuoSet Enzyme-linked immunosorbent assay (ELISA)	R&D System, Wiesbaden, Germany.
Mouse IL-6Ra DuoSet Enzyme-linked immunosorbent assay (ELISA)	R&D System, Wiesbaden, Germany.
Mouse Myeloperoxidase DuoSet Enzyme-linked immunosorbent assay (ELISA)	R&D System, Wiesbaden, Germany.

3.1.6 Stimulants and Inhibitors

Stimulants and inhibitors used in this thesis are mentioned in table 3.6. Detailed information's are given in the methods section and the figure legends.

Table 3. 6: Stimulants and inhibitors

Name	Company	Working concentration
Exotoxin A	Sigma-Aldrich, Taufkirchen, Germany.	100 ng/ml
GI254023X	Merck Millipore, Darmstadt, Germany.	10 µM
Human CCL2 (monocyte chemoattractant protein 1)	Peprotech, Rocky Hill, NJ, USA.	3 nM
Ionomycin	Merck Millipore, Darmstadt, Germany.	1 µM
P38/SAPK2 Inhibitor (SB 203580)	Cell signaling (Danvers, Massachusetts, United States)	10 µM
Phorbol 12-Myristate 13-Acetat (PMA)	Merck Millipore (Darmstadt, Germany)	1 µM
SARK inhibitor (PP2)	Merck Millipore (Darmstadt, Germany)	10 µM
TAPI-1	Merck Millipore, Darmstadt, Germany.	10 µM

3.1.7 Antibodies

In Table 3.7, primary and secondary antibodies used for Western blot (WB), fluorescence activate cell sorting (FACS) analysis and Immunohistochemistry (IHC) are listed.

Table 3. 7: Primary and secondary antibodies
In case, that no information on the stock concentration were given by the supplier, used dilutions are stated.

Name	Company	Working concentration	Application
Allophycocyanin (APC)-conjugated Mouse Ly6G	Invitrogen (Frankfurt, Germany)	1:40	FACS
eFluor450-conjugated Mouse Cluster of differentiation (CD)11c	Invitrogen (Frankfurt, Germany)	1:40	FACS
Fluorescein isothiocyanate (FITC)-conjugated Mouse CD11b	Invitrogen (Frankfurt, Germany)	1:40	FACS
Goat anti-rabbit IgG secondary antibody	Abcam, Cambridge, UK		IHC
Goat polyclonal anti-Mouse IgG (H + L) secondary antibody (Alexa Fluor® 647)	R&D System, Wiesbaden, Germany.	5 µg/mL	FACS
Mouse monoclonal antibody against flotillin-1 (Clon 18)	BD Biosciences, Heidelberg, Germany.	0.25 µg/mL	WB
Mouse monoclonal antibody against human ADAM10 ectodomain (clone 163003)	R&D System, Wiesbaden, Germany.	1 µg/mL	FACS
Mouse monoclonal antibody against human CD9 (MM2/57)	Invitrogen, Frankfurt, Germany.	1 µg/mL	WB
Mouse monoclonal antibody against human E-cadherin C-terminus	BD Biosciences, Heidelberg, Germany.		WB
Mouse monoclonal antibody against Junctional adhesion molecule A (JAM-A) N-terminus	BD Biosciences, Heidelberg, Germany.	0.25 µg/mL	WB
Mouse monoclonal anti-Phospho P38	Cell signaling (Danvers, Massachusetts, United States)	1:2000	WB
Mouse monoclonal IgG2B isotype control (Clone 20116)	R&D System, Wiesbaden, Germany.	1 µg/mL	WB
PE-Cy7-conjugated Mouse F4/80	Invitrogen (Frankfurt, Germany)	1:40	FACS
PerCP-Cy5.5-conjugated Mouse CD45	Invitrogen (Frankfurt, Germany)	1:150	FACS
Peroxidase-conjugated anti-mouse IgG	GE Healthcare, Chicago, IL, USA.	1:20,000	WB
Peroxidase-conjugated anti-rabbit IgG	GE Healthcare, Chicago, IL, USA.	1:40,000	WB

Rabbit polyclonal anti CD163	Abcam, Cambridge, UK	1:200	IHC
Rabbit polyclonal anti CD68	Abcam, Cambridge, UK	1:300	IHC
Rabbit polyclonal anti CD86	New England Biolabs, Ipswich, Massachusetts, USA	1:100	IHC
Rabbit polyclonal antibody against beta actin	Abcam, Cambridge, UK.	0.1 µg/ml	WB
Rabbit polyclonal antibody against human ADAM10 C-terminus	Invitrogen, Frankfurt, Germany.	0.1 µg/mL	WB
Rabbit polyclonal antibody against human ADAM17 C-terminus	Invitrogen, Frankfurt, Germany.	0.1 µg/mL	WB
Rabbit polyclonal antibody against human Glyceraldehyde 3-phosphate dehydrogenase (GAPDH)	Santa Cruz Biotech, Dallas, TX, USA.	0.4 µg/mL	WB
Rabbit polyclonal anti-P38α	Cell signaling (Danvers, Massachusetts, United States)	0.071 µg/ml	WB
Streptavidin horseradish peroxidase (HRP)	Abcam, Cambridge, UK	1:50	IHC

3.1.8 Cells

Table 3. 8: Primary cells and cell lines

Name	Properties	Medium
A549	Adenocarcinoma human alveolar basal epithelial cells, adherent cell line.	DMEM
HSAEpC	Human small airway epithelial cells, adherent primary cells.	MV2 medium
HEK293T	Human cell line expresses a mutant version of the SV40 large T antigen, adherent cell line.	DMEM
Primary neutrophils	Neutrophils isolated from human blood, suspension primary cells.	RPMI 1640
THP-1	Human monocytic cell line from acute monocytic leukemia patient, suspension cell line.	RPMI 1640

3.1.9 Plasmids

Table 3. 9: Plasmids (for vectors map, see appendix).

Name	Properties
pLVTHM	lentiviral backbone vector expressing shRNA from H1 promoter and green fluorescence protein (GFP)
pMD2.G	VSV-G envelope expressing plasmid
psPAX2	Lentiviral packaging plasmid
AP-BTC (Rc/CMV backbone)	Alkaline Phosphatase-Betacellulin Fusion Vector
AP-TGF-α (Rc/CMV backbone)	Alkaline Phosphatase- transforming growth factor alpha Fusion Vector

3.1.10 Buffers and solutions

In table 3.10, the buffers and solution used for western blot, activity measurements, FACS measurement, polymerase chain reaction (PCR) and bacteria preparation are listed.

Table 3. 10: Buffers and solutions

Name	Composition
10x PCR buffer	100mM Tris pH 8,4 500mM KCl 15mM MgCl2
10x PCR loading dye	3.9 mL Glycerol 0.5 mL 10% SDS 0.2 mL 0.5M EDTA 25 mg Bromophenol Blue 25 mg Xylene Cyanol Until 10 ml H2O sterile
10x Tris/Borate/EDTA (TBE) buffer	108 g Tris 55 g Boric acid 9.3 g Na_2EDTA In 1 L H2O PH:8
ADAM lysis buffer 1	5mM Tris Hcl 1 mM EGTA 250 mM sucrose 0.1% SDS 1% Tritonx-100 1x protease inhibitor 1 mM Na3Vo4 1 mM PMSF 10 mM 1,10 phenanthroline monohydrate
ADAM lysis buffer 2	20mM TrisHcl 150mM NaCl 5mM EDTA 30mM Na3Vo4 5mM DTT 1mM PMSF 10mM pNPP 1mM benzamidine 10mM glycerophosphate 1mM Na3PO4 1% Triton X-100

Alkaline Phosphatase (AP)-lysis buffer	1% Tritonx in TBS Add complete X fresh (1:50)
Alkaline Phosphatase (AP)-solution	40 mM Tris-HCl 40 mM NaCl 10 mM MgCl2 PH: 9.5 Add 1 tab of pNPP freshly to each 5 ml
Blood FACS buffer	PBS 5 µM EDTA
Enzyme-linked immunosorbent assay (ELISA) blocking buffer	PBS 1 % BSA 0.05 % Tween 20
Enzyme-linked immunosorbent assay (ELISA) dilution buffer	PBS 0.1 % BSA 0.05 % Tween 20
Erythrocyte lysis buffer	10 mM NaHCO3 155 mM NH4Cl 5mM EDTA pH 7.4
Enzyme-linked immunosorbent assay (ELISA) wash buffer	PBS 0.05 % Tween 20
FACS buffer 1	PBS 0.2% BSA
FACS buffer 2	PBS 5 mM EDTA 1% FCS
Fluorescence resonance energy transfer (FRET) activity buffer	20 mM Tris, 0.0006% Brij-35; pH 8
Lysogeny broth (LB) solid medium	10 g NaCl 10 g pepton 20 g agar 5 g yeast extract 1 L sterile H2O
Phosphate buffered saline (PBS)	136 mM NaCl 2,7 mM KCl 1,47 mM KH2PO4 8 mM Na2HPO4 pH 7,4
Sodium dodecyl sulphate (SDS) buffer (5x)	0.5M Tris (PH: 6.8) 45% Glycerol 5% SDS 0,25% Bromophenol blue 12.5% B-mercaptoethanol
SDS-PAGE separation buffer	1,5M TrisHCl 0,4% SDS
SDS-PAGE stacking buffer	0,5M TrisHCl 0,4% SDS
Stripping buffer	0,2 M Glycin 0,1 % SDS pH 2,2
Tris buffered saline/Tween (TBST)	TBS 1 % Tween 20
Todd–Hewitt–Bouillon (THB) medium	30 g Todd-Hewitt-Bouillion 5 g of Yeast Extract 1 L sterile H2O

Tris buffered saline (TBS)	500 mM TRIS·HCL 1,5 M NaCl pH 7,5
Tyrode's solution	140 mM NaCl 4 mM KCl 1 mM MgCl2 10 mM HEPES 10 mM D-Glucose +/− 2 mM CaCl2 pH 7.4 adjusted with NaOH

3.2 Methodology

3.2.1 Cell culture and *in vitro* investigations

3.2.1.1 Cell propagation

A549 cells, HEK293T, THP-1 cells and HSAEpC were cultured in DMEM (+10% FCS), DMEM (+10% heat-inactivated FCS (56 °C, 20 min), 10% Glutamax), RPMI1640 (+10% FCS) and MV2 medium, respectively. The cells were maintained in a humidified atmosphere with 5% CO_2 at 37°C. Upon reaching 80% confluence, adherent cells were sub-cultured using trypsin/EDTA and resuspended in a standard medium before being seeded at the desired density in new culture dishes. For suspension cells, T25 or T75 cell culture flasks were used at a density of 0.2 to 1 x 10^6 cells per ml.

Approval for the use of human samples was granted by the ethics committee of the Landesärztekammer des Saarlandes (172/18 by Daniela Yildiz) and the study was conducted in compliance with the Declaration of Helsinki. All individuals provided informed consent. Citrated peripheral blood from healthy volunteers was sedimented slowly on Pancoll Human and the fractions were generated by centrifugation for 30 min without a break. The erythrocyte-neutrophil fraction was directly subjected to erythrocyte lysis for 5-10 min at room temperature as described in (Koenen et al., 2009). For experiments requiring inhibitor treatment, the cells were pre-incubated with 10 µM GI254023X (ADAM10 inhibitor), TAPI-1 (ADAM17 inhibitor), SB 203580 (p38/SAPK2 Inhibitor), PP2 (SARC inhibitor) or 0.1% DMSO (vehicle control) for 30 min.

3.2.1.2 Cell counting

To determine the number of viable cells, live/dead staining with trypan blue dye was performed using a hemocytometer. The cell suspension was mixed with a 0.4% trypan blue solution in a 1:1 ratio, and 10 µl of the resulting cell dilution was added to the hemocytometer. The cells were then counted under a microscope, with blue-stained cells indicating those that were dead and excluded from the analysis. Total cell numbers in blood and BAL were measured using The NucleoCounter® NC-200™ following the manufacturer's protocol

3.2.1.3 Preparation of lenitival particles and lentiviral transduction

Short hairpin RNA (shRNA) of ADAM10 or ADAM17 was inserted into the lentiviral expression vector pLVTHM (Addgene plasmid 12247) to target ADAM10 or ADAM17 mRNA sequences. Targeted sequences are indicated in table 3.11 (Pruessmeyer et al., 2010). Production of lentiviral particles was performed by co-transfection of HEK293T cells with the desired pLVTHM-plasmid, psPAX2 (plasmid 12260, Addgene) and pMD2.G (plasmid 12259, Addgene) in the presence of jetPEI as transfection reagent (see table 3.12). HEK293T cells were grown until 70 % of confluence and transfected with the

respective plasmid. The medium was changed after 6 h, the supernatant collected after 72 h, and centrifuged at 26,000xg for 2.5 h. The pellet containing the lentiviral particles was resuspended in sterile PBS, aliquoted and stored at -80°C.

For transduction of A549 cells, 10^5 cells were seeded on a 6-well plate, grown until 70% confluence and transduced with the desired lentiviral particles in the presence of polybrene (4 µg/ml). The medium was changed after 24 h. The efficiency of the transduction was evaluated by counting the number of GFP-expressing cells using a fluorescence microscope, and the efficiency of the knockdown was evaluated by Western blot.

Table 3. 11: shRNA targeted sequences to induce ADAM proteases knockdown (KD).

Targeted gene	shRNA Sequence
Human ADAM10-650 (ADAM10-KD1)	CGCGTCCCCGACATTTCAACCTACGAATTTCAAGAGA ATTCGTAGGTTGAAATGTCTTTTTGGAAAT
Human ADAM10- 1947 (ADAM10-KD2)	CGCGTCCCCACAGTGCAGTCCAAGTCAATTCAAGAGA TTGACTTGGACTGCACTGTTTTTTGGAAAT
Human ADAM17-2061 (ADAM17-KD1)	CGCGTCCCCAGGAAAGCCCTGTACAGTATTCAAGAGA TACTGTACAGGGCTTTCCTTTTTTGGAAAT
Human ADAM17-2846 (ADAM17-KD2)	CGCGTCCCCGAAGGTGAATCTAGCTTATTTCAAGAGA ATAAGCTAGATTCACCTTCTTTTTGGAAAT
Scramble	CGCGTCCCCCCGTCACATCAATTGCCGTTTCAAGAGA ACGGCAATTGATGTGACGGTTTTTGGAAAT

Table 3. 12: jetPEI® based transfection protocol

Plasmid solution	Transfection-reagent solution
pLVTHM (desired shRNA) (12,5 µg)	250 µl jetPEI® (PolyPlus Transfections, Illkirch, France)
PsPAX2 (8,13 µg)	625 µl 150 mM NaCl solution
PMD2.G (4,37 µg)	
250 µl 150 mM NaCl solution	
mixed and incubated for 15 min	mixed and incubated for 15 min
mix together for 15 min	
added dropwise to the cells	

3.2.1.4 Exosome preparation

Approval for the use of human samples was granted by the ethics committee of the Landesärztekammer des Saarlandes (62/80 by Robert Bals, department for Internal Medicine V – Pulmonology, Allergology, Intensive Care Medicine. Saarland University, Homburg, Germany). 2×10^7 of A549 cells, THP-1 cells or human neutrophils were cultured in serum free medium and stimulated as indicated in each respective figure legend. After stimulation, the cells were lysed and analyzed by Western blot (see 3.2.2.1). The serum of Vav-*Adam10*$^{-/-}$ and Vav-*Adam17*$^{-/-}$ mice and the serum of healthy volunteers, pneumonia or COVID-19 patients, respectively, were diluted in Hanks' Balanced Salt Solution (1:3). The medium of the cells or the diluted serum were differentially centrifuged at 300xg for 10 min, 1000xg for 20 min, 10,000xg for 30 min at 4 °C. The pellet from each centrifugation step was directly lysed with 50 µl of SDS buffer for Western blot analysis while the supernatant was assigned for the next centrifugation step. The last supernatant was sterile filtered using 0.22 µm membrane filters and centrifuged at 100,000xg for 1 h at 4 °C to collect the extracellular vesicles using a Beckman rotor Type Ti50.2. The extracellular vesicles were washed with a high volume of ice-cold sterile PBS and sedimented again at 100,000xg and lysed with 50 µL of SDS buffer for Western blot analysis or collected by 100 µL of sterile PBS for sub-fractionation. The collected extracellular vesicles were loaded to a sucrose gradient comprising layers (2, 1.3, 1.16, 0.8, 0.5 and 0.25 M) and centrifuged at 4 °C for 16 h. Subsequently, the density of each of the gradient layers was measured and 1 ml of each gradient was centrifuged at 150,000xg at 4 °C for 4 h using Beckman TLA-55 rotor. The pellet was resuspended in SDS buffer for Western blot analysis, in 100 µL sterile PBS for AP-assay or in 100 µl DMEM medium (phenol red free) for FRET-based activity measurements (see figure 7.6).

3.2.1.5 Calcium imaging

Glass coverslips were coated with poly-L-lysine for 24 h and 2×10^5 of A549 cells were seeded, reaching 70% confluence overnight. The cells were pre-incubated with serum free medium for 2 h, washed two times with sterile PBS, incubated with Tyrode's solution (+/- $CaCl_2$ as indicated in the figure legend) and stimulated with Exotoxin A (100 ng/ml) or sterile PBS as vehicle control for 4 h. Subsequently, the cells were incubated with 5 µM Fura-2 AM for 45 min at 37 °C, washed two times with Tyrode's solution and the coverslips held in a tight open bottom chamber in the presence of 300 µL Tyrode's solution (+/- CaCl2). The chamber was staged to an inverted microscope equipped with monochromator at 21 °C. Fura-2 was excited every 2 s for 20 ms at 340 and 380 nm and the fluorescence was recorded with a cooled charge-coupled device (CCD) camera (Imago, TILL Photonics). Ratio changes (F240/380) of each single cell were plotted versus time. The same cell number for each sample (minimum 20 cells) was labelled as regions of interest (ROI). Monochromator, camera acquisition, and analysis were controlled by TillvisION software 2.7.0.16.

3.2.1.6 Cell survival assay

12-well plates were coated with collagen G (40 µg/mL) for 24 h and 2×10^5 of A549 cells were seeded and grown in DMEM (+10 % FCS) for 48 h until confluence. Subsequently, the cells were stained with NucRed™ Live 647 (plasma membrane permeable nuclear stain) for 15 min. The cells were washed three times with sterile PBS, stained with SYTOX™ green (plasma membrane impermeable nuclear stain, 200 nM), and infected in parallel with *P. aeruginosa* for 4 h. The fluorescence of SYTOX™ green and NucRed™ Live 647 was analyzed every 30 min at excitation/ emission of 480/520 nm and 638/686 nm, respectively, using the Lionheart (FX) Automated Microscope system. A primary mask counting the green labeled cells over time was applied using Gen5 software version 3.05.11.

For THP-1 or human neutrophil survival assay, the cells were infected with GFP-labelled *P. aeruginosa* (PA01) for 2 h and collected by centrifugation at 300xg for 5 min at 4 °C. The GFP signals of the non-phagocytosed *P. aeruginosa* were quenched by resuspending the cells in 200 µl Trypan blue. Cellular survival was analyzed by measuring the median of APC signal of Trypan blue relative to the signal of the non-infected cells by flow cytometry.

3.2.2 Bacteria preparation and counting

3.2.2.1 *P. aeruginosa* preparation

P. aeruginosa (PA103 strain (provided by Prof Bastian Opitz, Department of Infectious Diseases and Respiratory Medicine, Charité–Universitätsmedizin Berlin, Corporate Member of Freie Universität Berlin and Humboldt-Universität zu Berlin, Berlin, Germany) or GFP labeled PA01 (provided by Prof Claus-Michael Lehr, Helmholtz Institute for Pharmaceutical Research Saarland, Helmholtz Centre for Infection Research, Saarland University Campus, Saarbrücken, Germany)) were kept in frozen stocks of 20% glycerol in THB medium at −80 °C. Frozen *P. aeruginosa* was streaked out on blood sheep agar plates, followed by overnight incubation at 37 °C and 0% CO_2. In the following day, a single colony was used to start a liquid culture in THB medium at 37 °C and 150 rpm overnight. The next day, a new culture was established from the previous culture at a starting optical density at 600 nm (OD_{600}) of 0.05 and cultured for 3 h until the bacteria reached the exponential phase. Consequently, the bacteria were centrifuged for 5 min at 6000xg, resuspended in PBS and adjusted to OD_{600} of 1 (10^8 colonies forming unit (cfu)/ml).

P. aeruginosa strains were used to infect the cells with a multiplicity of infection (MOI) of 5, or PA103 was used to induce lung pneumonia by intranasal instillation of 10^5 CFU. For heat-inactivation, the bacteria were incubated in the heat-block at 70 °C for 40 min as described in (Aljohmani et al., 2022b).

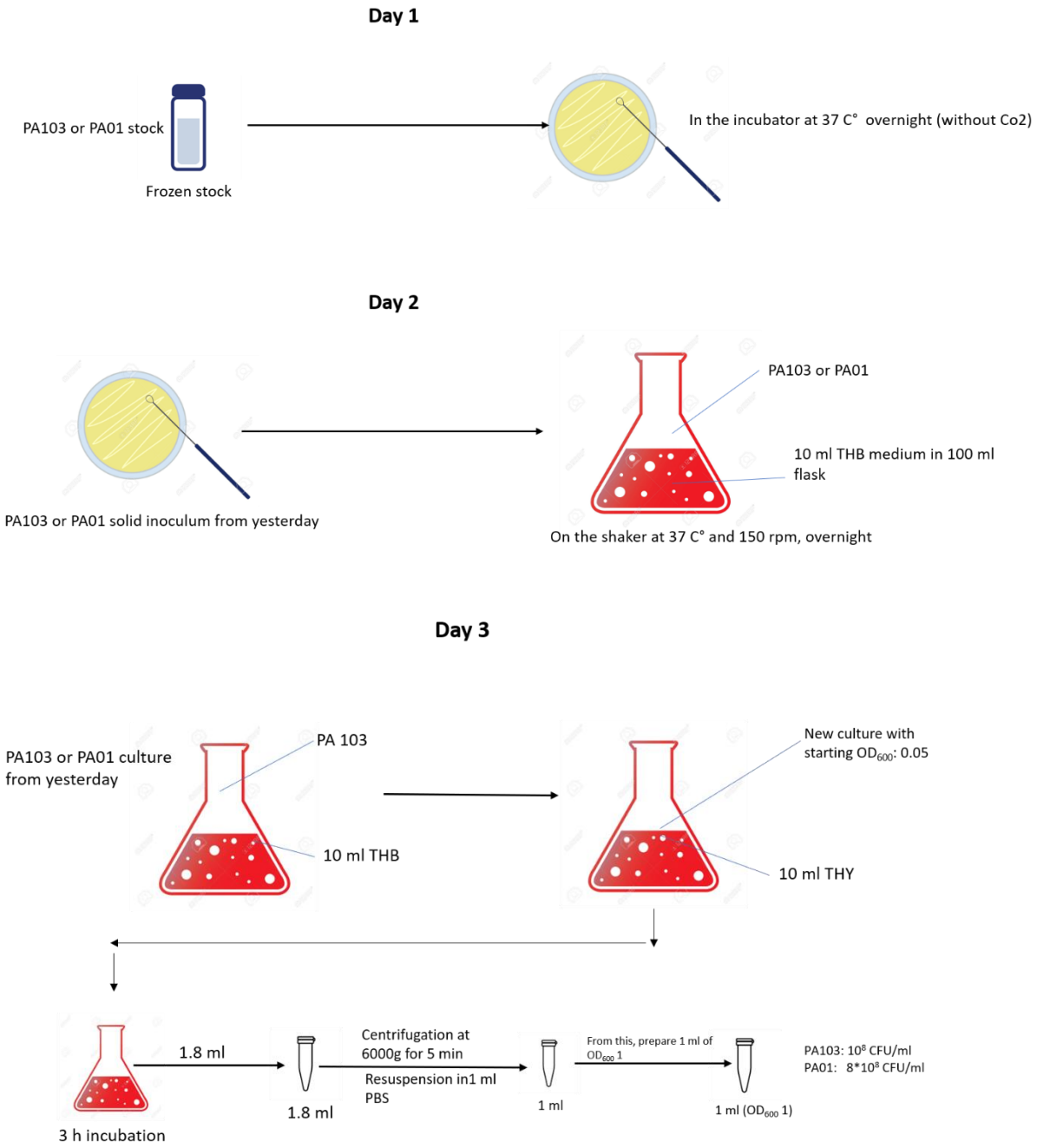

Figure 3. 1: Preparation of *P. aeruginosa* (PA103 strain or GFP labeled PA01)
PA103 or GFP labelled PA01 were streaked out on agar plates and incubated overnight at 37 °C and 0% CO_2. Subsequently, a single colony was added to 10 ml of THB medium and incubated overnight at 37 °C and 150 rpm. At day 3, a new culture of OD_{600} 0.05 was started for 3 h. Consequently, the bacteria were centrifuged for 5 min at 6000 g, resuspended in PBS, and adjusted to OD_{600} of 1 (10^8 cfu/ml).

3.2.2.2 *S. pneumoniae* preparation

S. pneumoniae (R6 strain) were kept in frozen stocks of 20% glycerol in THB medium at −80 °C. Liquid culture in THB medium was started directly from the frozen stock with a starting OD_{600} of 0.05 and culture for 4 h at 37 °C and 5% CO_2. Subsequently, *S. pneumoniae* were centrifuged for 10 min at 4000xg, resuspended in PBS and adjusted to OD_{600} of 1 ($4.7*10^8$ cfu/ml). *S. pneumoniae* were used to infect the cells with MOI of 5.

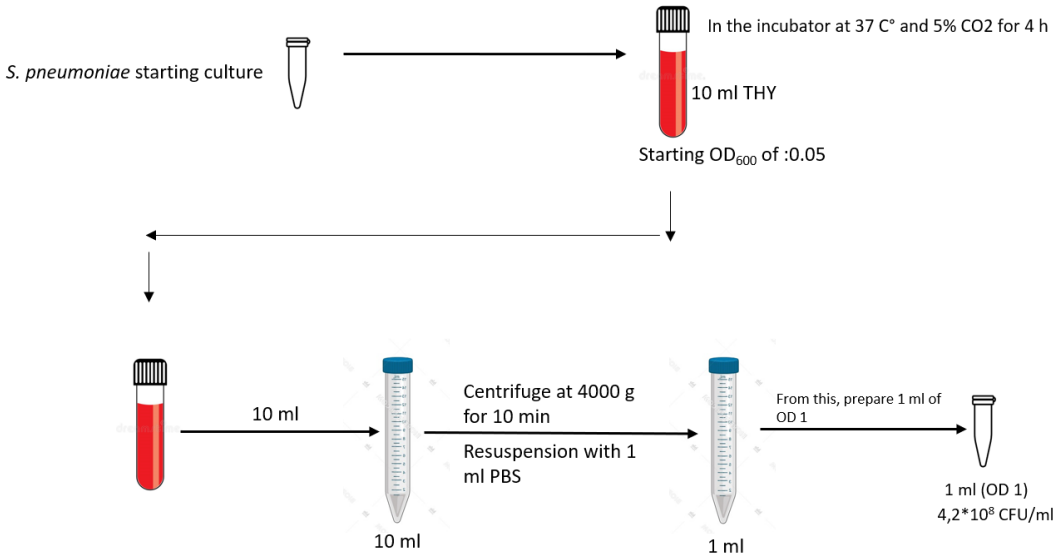

Figure 3. 2: Preparation of *S. pneumoniae* (R6 strain).
S. pneumoniae (R6 strain) liquid culture in THB medium was started directly from the frozen stock with a starting OD_{600} of 0.05 and culture for 4 h at 37°C and 5% CO_2. Subsequently, *S. pneumoniae* cultures were centrifuged for 10 min at 4000xg, resuspended in PBS and adjusted to OD_{600} of 1 ($4.7*10^8$ cfu/ml).

3.2.2.3 CFU determination

Lung tissues (homogenized in 10 ml PBS using a cell strainer), citrated blood or BAL fluid were serially diluted in sterile PBS and streaked out on LB agar plates followed by overnight incubation at 37 °C. *P. aeruginosa* CFUs were counted and multiplied by the dilution factor to get the number of CFU per organ.

3.2.3 Biochemical methods

3.2.2.1 SDS-PAGE and Western blot

A549 cells and HSAEpC were cultured on 6-well plates and lysed with ADAM lysis buffer 1. THP-1 cells and human neutrophils were cultured in 12-well plates and lysed with ADAM lysis buffer 2 (see table 3.10). 10^6 cells were incubated with 200 µL of the respective lysis buffer supplemented with 1× Complete Inhibitor for 10 min on ice. Subsequently, cell debris were pelleted by centrifugation for 10 min at 16,000xg and the supernatant containing the proteins was subjected to protein concentration measurements using the Bicinchoninic acid assay (BCA) kit. Samples were mixed with SDS buffer and denaturized in a heat block at 60 °C for 30 min. The proteins of each sample were separated according to the molecular weight by SDS-polyacrylamide gel electrophoresis (SDS-PAGE) using 10 % (1.5 mm) self-made gels (see table 3.13) or ready-to-use Bolt™ 4-12% Bis-Tris 1.0 mm Mini Protein Gels (Invitrogen, Frankfurt, Germany). Dependent on the gel format, the Mini-PROTEAN gel electrophoresis chamber (BIO-RAD, Hercules, USA) or the Invitrogen™ Minigel Tank (Fisher Scientific GmbH,

Schwerte, Germany) was used. The electrophoresis was run for 90-100 min (at constant 80 V for 20 min, followed by 160 V for 80 min) or for 40-50 min (at a constant 200 V) in SDS-PAGE running buffer at room temperature. For comparison of the molecular weight, 5 µl Fisher BioReagents™ EZ-Run™ Prestained Rec Protein Ladder (Thermo Fisher, Karlsruhe, Germany) was run on each gel, further allowing for separation and transfer control.

Subsequently, the proteins were blotted onto nitrocellulose membrane (0.45 µm), and the membrane was blocked with 5% non-fatty milk to prevent any non-specific antibody binding and incubated overnight at 4 °C with the desired primary antibody. Next day, the membrane was incubated with the desired secondary antibody in 5% non-fatty milk for 1 h followed d by chemiluminescence substrates for 1 min, and the signals were detected using luminescent image analyzer LAS3000. Band intensity was quantified by densitometry after subtracting the background using AIDA Image Analysis software 4.27.039.

Table 3. 13: Composition of separation and stacking gel

Name	Stacking gel 4%	Separating gel 10 %
Bis-acrylamide 29:1 40 %	0.5 ml	2.5 ml
SDS-PAGE separation buffer	-	2.5 ml
SDS-PAGE stacking buffer	1.25 ml	-
ddH2O	3.21 ml	4.91 ml
10 % APS (in ddH2O)	37.5 µl	75 µl
Tetramethylethylenediamine (TEMED)	7.5 µl	15 µl

3.2.3.2 Fluorescence-activated cell sorting

All steps were done on ice at 4 °C. A549 cells or HSAEPC were collected by accutase detachment and resuspended in FACS buffer 1 (table 3.10). The cells were incubated with mouse monoclonal antibodies against human ADAM10 N-terminal domain (1 µg/mL) or isotype control (1 µg/mL) for 1 h. Subsequently, the cells were washed two times with FACS buffer 1 and incubated with APC-conjugated anti-mouse antibody (5 µg/mL) for 45 min. The cells were washed again with FACS buffer 1, fixed with 1% PFA, and the surface expression of ADAM10 was evaluated by measuring the fluorescence signals by FACS analysis and analyzed with FlowJo 10.6.2 software. For each sample, the same cell numbers and populations were used to quantify the mean fluorescence before subtraction of the signals of the isotype controls.

FACS analyses of murine primary samples were performed for bronchoalveolar lavage (BAL) cells and blood leukocytes. BAL cells were collected by centrifugation for 5 min at 300xg, fixed with 1% PFA, washed two times with FACS buffer 2 and finally resuspended in PBS for flow cytometry analysis. Blood was subjected to erythrocytes lysis for 5 min, and the collected leukocytes were fixated with 1%

PFA, washed two times with FACS buffer 2 and finally resuspended in PBS for flow cytometry analysis. Collected BAL or blood cells were stained with FITC-conjugated monoclonal anti-mouse CD11b, eFluor450-conjugated monoclonal anti-mouse CD11c, PerCP-Cy5.5-conjugated monoclonal anti-mouse CD45, APC-conjugated monoclonal anti-mouse Ly6G and PE-Cy7-conjugated monoclonal anti-mouse F4/80 for 1 h at 4 °C (see table 3.17, for gating strategy see Figure 3.3). Flow cytometry analysis was performed using the Sony SH800 and analyzed with FlowJo 10.6.1 software.

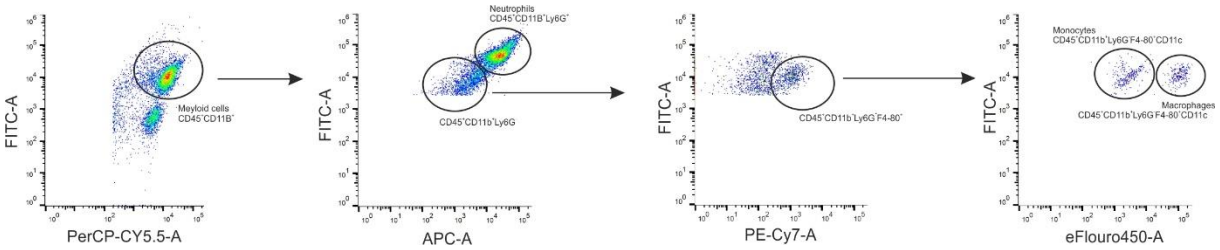

Figure 3. 3: Gating strategy for blood and BAL leukocytes analyzed by flow cytometry.
Collected BAL or blood cells were stained with FITC-conjugated monoclonal anti-mouse CD11b, eFluor450-conjugated monoclonal anti-mouse CD11c, PerCP-Cy5.5-conjugated monoclonal anti-mouse CD45, APC-conjugated monoclonal anti-mouse Ly6G and PE-Cy7-conjugated monoclonal anti-mouse F4/80 for 1 h at 4 °C, and the fluorescence signals were evaluated by flow cytometry. CD45 served as a general leukocyte marker, CD11b to further specify the myeloid cells, while Ly6G was used to distinguish neutrophils from other myeloid cells. F4/80 was used to further distinguish the Ly6G negative cells into monocytes and macrophages.

3.2.3.3 Histochemistry and Immunohistochemistry (IHC)

Lung left lobs were fixated with Roti-Fix® for 48 h, embedded in paraffin and sliced by microtome into 5 µm sections. Deparaffinization of the sections was done by incubation with xylene (2x for 10 min), rehydration by incubation with descending ethanol concentrations (2x for 5 min, 100% EtHO; 2x for 5 min, 96% EtHO; 2x for 5 min, 70% EtHO). Sections were washed with distilled water (1x for 5 min) and 2 times with sterile PBS, followed by antigen retrieval by boiling in citrate buffer (10 mM Citric Acid, 0.05% Tween 20, pH 6.0). The sections were blocked by 1% hydrogen peroxide for 30 min to block the endogenous peroxidases activity and stained with hematoxylin-eosin according to the standard protocol (Cardiff et al., 2014). Slices preparation and hematoxylin-eosin staining were performed by the group's technician Maria Rieseweber.

To evaluate polarization of the macrophages, sections were stained with primary rabbit anti-mouse CD68 (general macrophages), anti-mouse CD86 (M1) or anti-mouse CD163 (M2) overnight at room temperature. Next day, sections were labelled with biotin-tagged goat anti-rabbit IgG secondary antibody for 45 min. Subsequently, the sections were incubated with peroxidase labeled streptavidin for 45 min to capture the biotinylated antibodies.

Images were taken by Axio scan Z1 slide scanner. The thickness of interalveolar septa was blindly analyzed by randomly choosing 10 regions for each section of each mouse using ZEN 2.3 blue edition.

General macrophages, M1 and M2 macrophages were counted manually and blindly in each section and presented as number per mm^2 using ZEN 2.3 blue edition.

3.2.3.4 Enzyme-linked immunosorbent assay (ELISA)

BAL was centrifuged at 16,000xg for 15 min and 4 °C, and the supernatant was used to analyze the BAL content of mTNF-α (1:5), mCXCL1 (KC) (1:5), mIL-6 (1:5) and Myeloperoxidase (MPO) (1:100) using commercial ELISA kits following the manufacturers' protocol (R&D Systems, DuoSet).

3.2.4 Functional assay

3.2.4.1 Alkaline phosphatase assay

Plasmid encoding either betacellulin or TGF-α tagged with alkaline phosphatase (AP) on the N-terminal domain was used to transfect A549 cells in the presence of Lipofectamine™ 3000 as transfection reagent for 24 h (see table 3.14). The next day, 3×10^5 cells were seeded on 12-well plate for 24 h followed by incubation in serum free DMEM medium for 2 h. subsequently, the cells were stimulated as indicated in each figure legend, the supernatants were collected, and the cells were lysed with 500 µl of AP-lysis buffer supplemented with 1x Complete Inhibitor. The supernatant and the cell lysate were centrifuged at 16,000xg for 10 min, and 100 µl of each was transferred to 96-well plates followed by supplementation with 100 µL of alkaline phosphatase substrate 4-nitrophenyl phosphate (a 2 mg/mL) dissolved in AP-solution (see figure 7.7). The activity of AP was analyzed by measuring the absorption at 405 nm for both the supernatant and cell lysate every 1.5 min for 4 h at 37 °C using Genios fluorescence reader (Sahin et al., 2004). Data are shown as a ratio of AP activity in the supernatant to the total activity (lysate and supernatant).

Table 3. 14: AP-Assay transfection protocol

Plasmid solution	Transfection-reagent solution
1 ml Optimem	125 µl Optimem
32 µl Lipofectamine 3000	4 µl P3000 Reagent
	2,5 µg plasmid AP-BTC or AP-TGF-α
mix	Mix
Mix together for 5 min at room temperature	
Add in a dropwise to the cells	

3.2.4.2 Protein permeability assay

2*10^5 A549 cells were seeded on 5 µm polycarbonate trans-well filters coated with collagen G (40 µg/mL) for 48-72 h until forming a monolayer. At confluence, the cells were incubated with serum free medium for 2 h and stimulated as indicated in each respective figure legend. Subsequently, the medium in the upper chamber was replaced by 100 µl of suspension of 70 kDa TRITC-dextran (1 mg/ml) and FITC-albumin (0.25 mg/ml) in PBS supplemented with 0.2 % BSA for 90 min at 37 °C. Total and paracellular permeability were measured by detecting the fluorescence intensity of FITC Albumin (total) and TRITC-dextran (paracellular) in the lower chamber at excitation/ emission of 485/535 nm and 535/595 nm, respectively, using the Genios fluorescence reader. The results are shown as a percentage of the FITC Albumin and TRITC-dextran intensity in the lower chamber relative to an empty insert (see figure 3.4).

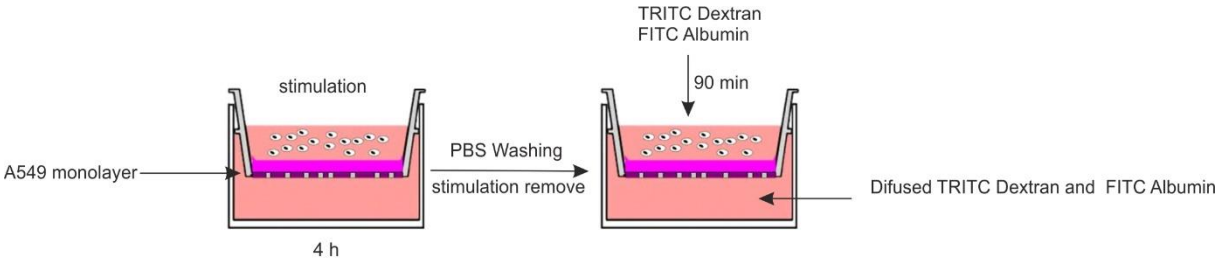

Figure 3. 4: Method description for protein permeability assay.
A549 cells were seeded on 5 µm polycarbonate trans-well filters coated with collagen G until forming a monolayer. Subsequently, the cells were stimulated as indicated in each respective figure legend and the medium in the upper chamber was replaced by 70 kDa TRITC-dextran and FITC-albumin for 90 min. Total and paracellular permeability were measured by detecting the florescence intensity of FITC Albumin (total) and TRITC-dextran (paracellular) in the lower chamber.

3.2.4.3 Transepithelial migration

2*10^5 A549 cells were seeded on 5 µm polycarbonate trans-well filters coated with collagen G (40 µg/mL) for 48-72 h until forming a monolayer (the same number of the cells were seeded on 96-well plate to monitor the confluency). At confluence, the cells were incubated with serum free medium for 2 h and stimulated as indicated in each respective figure legend. After stimulation, the cells were washed two times with sterile PBS, the lower chamber filled with 600 µL RPMI/0.2% BSA in the presence or absence of human CCL-2 (3 nM) followed by the addition of 2 × 10^5 THP-1 cells in 100 µL of RPMI/0.2% BSA to the upper chamber. After 90 min, the trans-wells were removed, and the transmigration of THP-1 cells from the upper chamber to the lower chamber was evaluated by lysing the cells (addition of 0.1% Triton-X100) and measurement of endogenous β-glucuronidase activity (Andrzejewski et al., 2010). To quantify the transmigrated cells, 100 µL of the lysed THP-1 cells were transferred to a 96-well plate and supplemented with 100 µL of the substrate solution (0.032 g of p-nitrophenyl-B-D-glucuronide in 10 ml acetate buffer (0.1 M sodium acetate, PH 4)) and incubated overnight at 37 °C. The reaction was stopped by the addition of 100 µL of stop solution (0.4 M Glycine, PH 10.3), and the absorption was measured at 405 nm using Genios fluorescence reader. In

parallel, a defined number of THP-1 cells were serially diluted and used as a standard to count the transmigrated cells. The results are shown as a percentage of the transmigrated cells relative to empty insert without cells (see figure 3.5).

3.2.4.4 Wound closure assay – Scratch assay

96-well plates were coated with collagen G (40 µg/mL) for 2 h, and 2×10^4 of A549 cells were seeded and grown in DMEM (+10 % FCS) for 48-72 h until the formation of a uniform monolayer. To ensure wound closure by solely migration, the cells were incubated with mitomycin (5 µg/ml) for 2 h for inhibition of proliferation, followed by washing with sterile PBS for 3 times and stimulation as indicated in each respective figure legend. Subsequently, a defined scratch of 1.2 cm^2 was performed using the certified BioTec autoscratch, the cells were washed three times with sterile PBS, and 100 µL of fresh medium were added. Wound closure was monitored by live cell imaging every 2 h for 24 h using the Lionheart (FX) Automated Microscope system. To analyze wound closure, a primary mask tracking the cells over time was applied using Gen5 software version 3.05.11. The data are shown as a percentage of a fully closed wound (see figure 7.8).

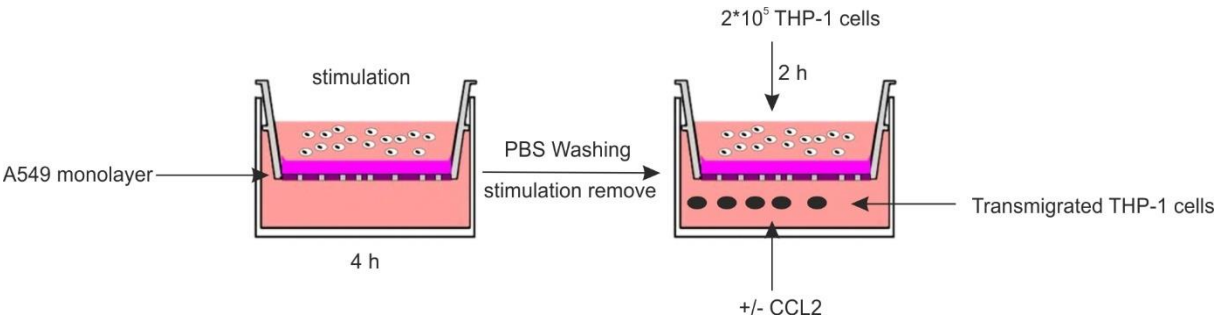

Figure 3. 5: Method description for THP-1 cells trans-epithelial migration assay
A549 cells were seeded on 5 µm polycarbonate trans-well filters coated with collagen G until forming a monolayer. Subsequently, the cells were stimulated as indicated in each respective figure legend and the lower chamber was filled with RPMI/0.2% BSA in the presence or absence of human CCL-2 (3 nM) followed by the addition of 2×10^5 THP-1 cells in 100 µL of RPMI/0.2% BSA to the upper chamber. After 90 min, the transmigration of THP-1 cells from the upper chamber to the lower chamber was evaluated by measurement of endogenous β-glucuronidase.

3.2.4.5 Adhesion assay

A 24-well plate was coated with collagen G (40 µg/mL) for 2 h and 1×10^5 of A549 cells were seeded and grown in DMEM (+10 % FCS) until confluence and infected with *P. aeruginosa* (PA103, MOI 5). THP-1 cells were labeled with 1 mM Calcein-AM in RPMI1640 serum free medium for 30 min, washed with warm sterile PBS, and 5×10^5 cells were added to the infected A549 cell monolayer. The plate was directly centrifuged at 300 g for 3 min, each well washed three times with warm sterile PBS, and finally the fluorescence of the adhered THP-1 cells was measured at excitation/emission of 480/520 nm using the Lionheart (FX) Automated Microscope system. To analyze the adhesion, a primary mask tracking the adhered cells to quantify the GFP signals was applied using Gen5 software version 3.05.11.

3.2.4.6 Phagocytosis assay

The cells were infected with GFP-labelled *P. aeruginosa* (PA01) for 2 h and collected by centrifugation at 300xg for 5 min at 4 °C. The GFP signals of the non-phagocytosed *P. aeruginosa* were quenched by resuspending the cells in 200 µl Trypan blue. The phagocytosis of *P. aeruginosa* was analyzed by measuring the median of GFP signal relative to the signal of the non-infected cells by flow cytometry.

3.2.4.7 Reactive oxygen species (ROS) generation

Flat bottom, black 96-well plate was coated with collage G (40 µg/mL) for 24 h. 10^5 of THP-1 or human neutrophils were stained with ROS red dye (Cellular ROS detection kit) for 30 min in RPMI140 serum free medium, pre-incubated with GI254023X (10 µM), TAPI-1 (10 µM) or 0.1% DMSO for 30 min and finally infected with *P. aeruginosa* (PA103, MOI 5) for 2 h. The generation of ROS was evaluated by detecting the fluorescence signals after subtraction of the background at excitation/emission of 520/605 nm using Genios fluorescence reader.

3.2.4.8 FRET-based activity measurements

Assessment of ADAM10 or ADAM17 exosomal activity was performed by using polypeptides with highly specific substrate cleavage sites. The FRET linked fluorophores can undergo a fluorescence induction upon cleavage of the substrate´s peptide. The charged tail of these peptides assures measurement of only the surface activity and prevents the plasma membrane entry. Exosomes were resuspended in DMEM phenol red free and pre-incubated with GI254023X (10 µM), TAPI-1 (10 µM) or 0.1% DMSO for 30 min. Subsequently, 50 µl of exosomes were transferred to 96-well plate followed by the addition of 50 µl of 10 µM ADAM10 (PEPDAB063A, Acetyl-dArg(3)-dGlu(3)-hexaminoyl-K(Dabcyl)-PRYEAYKMGK(5FAM)-NH2) or ADAM17 (PEPDAB064, Dabcyl-PRAAAHomopheTSPK(5FAM)-NH2) FRET substrate (Biozym Scientific GmbH, Hessisch Oldendorf, Germany) in FRET activity buffer (20 mM Tris, 0.0006% Brij-35; pH 8). ADAM10 or ADAM17 activity in exosomes was determined by analyzing the absorption at 405 nm at 37 °C every 2.5 min for 240 min using Genios fluorescence reader (Tecan, Grödig, Austria).

3.2.5 *In vivo* investigations

3.2.5.1 Mice

The Saarland animal welfare and ethics committee granted permission for animal experimentation (project identification number 2.4.2.2-42/2018 by Daniela Yildiz). Throughout animal experiments, 6 to 8 weeks old Vav-*Adam10*$^{-/-}$ and Vav-*Adam17*$^{-/-}$ mice with C57BL/6 background were used. These mice expressed Cre recombinase under control of the Vav-promotor and were homozygous of floxed

Adam10 or floxed *Adam17* allele resulting in leukocyte-specific knockout mice (Horiuchi et al., 2007; Jorissen et al., 2010). Littermate controls were from the same mouse lines expressing Cre recombinase and the wildtype alleles of Adam10 and Adam17.

3.2.5.2 Genotyping of transgenic mice

DNA isolation, PCR and separation of DNA with agarose gel were performed by the group's technician Nina Schnellbach. Mastermix of Vav-cre, *Adam10* and *Adam17* genotypes were prepared under the sterile hood as described in table 3.16, 3.19 and 3.22 followed by the ddition of 2 µl, 0.8 µl and 0.5 µl of sample DNA of Vav-cre, *Adam10* and *Adam17*, respectively. PCR reactions were run as described in tables 3.17, 3.20 and 3.23.

The DNA fragments were separated by size using agarose gel electrophoresis, with 1% and 2% agarose gels being utilized due to the anticipated size of the amplified DNA fragments being between 200-400 and 700-1000 base pairs, respectively. The preparation of the agarose gel involved dissolving agarose standard (CarlRoth) in 1x TBE buffer and boiling it for 2 to 3 minutes in a microwave. Ethidium bromide (0.5 µg/ml) was added after cooling, and the agarose was loaded onto the gel tray. Samples were then applied to the gel wells using loading dye (10X) before being run at 100 V for 30 min (Consort EV 261 Sigma-Aldrich). The resulting bands were visualized using UV light (312 nm) (Herolab B1228-U5), and photos were captured using an attached camera (HeroLab UVT-28 ME-HC). Figure 3.6 shows exemplary images of the genotyping for each gene.

Table 3. 15: Primers used for Vav-cre, *Adam10* and *Adam17* genotyping.

Name	Sequence
Vav-cre primer forward	AGA TGC CAG GAC ATC AGG AAC CTG
Vav-cre primer reverse	ATC AGC CAC ACC AGA CAC AGA GAT C
Adam10 primer forward	5’ ATG GAT TGC CCT TTT ATG TAT TTA
Adam10 primer reverse	5’ GCC GAT GTG CCA GAT GAG TG
Adam17 primer forward	AC TGG TGG GGA GGG GGA GAG ATT ACG AAG GC
Adam17 primer reverse flox	TAC TGC CGG GCC TCT TGC GGG G
Adam17 primer reverse KO	ATG TTC CCC CAG CTA GAT TGT TTG CC

Table 3. 16: Composition of master mix used for Vav-cre genotyping.

Component	1x Reaction
10x PCR buffer	1,2 µL
Vav_for 10µM	0,6 µL
Vav_rev 10µM	0,6 µL
MgCl 20µM	0,96 µL
dNTPs 10mM each	0,96 µL
Taq Polymerase 1:25	0,2 µL
H_2O sterile	5,48 µL
Total	10

Table 3. 17: PCR protocol for Vav-cre genotyping.

Temperature	Time	
94°	90 sec	
94°	30 sec	
64°	45 sec	30x
72°	45 sec	
72°	120 cec	
10°	∞	

Table 3. 18: Composition of master mix used for *Adam10* genotyping.

Component	1x Reaction
10x PCR buffer	2 µL
SW17 (10µM)	1 µL
SW18 (10µM)	1 µL
dNTPs (10mM)	0,4 µL
Taq Polymerase 1:25	0,4 µL
H_2O sterile	14,4 µl
Total	19,2

Table 3. 19: PCR protocol for *Adam10* genotyping.

Temperature	Time	
95°	5 min	
95°	30 sec	
56°	30 sec	30x
72°	30 sec	
72°	10 min	
10°	∞	

Table 3. 20: Composition of master mix used for *Adam17* genotyping.

Component	1x Reaction	Component	1x Reaction
KAPA2G Fast HotStart Genotyping Mix	6,25 µL	KAPA2G Fast HotStart Genotyping Mix	6,25 µL
Primer forward	0,625 µL	Primer forward	0,625 µL
Primer reverse flox	0,625 µL	Primer reverse KO	0,625 µL
H2O sterile	4,5 µL	H2O sterile	4,5 µL
Total	12	Total	12

Table 3. 21: PCR protocol for *Adam17* genotyping.

Temperature	Time
95°	3 min
95°	15 sec 30x
62°	15 sec 30x
72°	15 sec 30x
72°	7 min
10°	∞

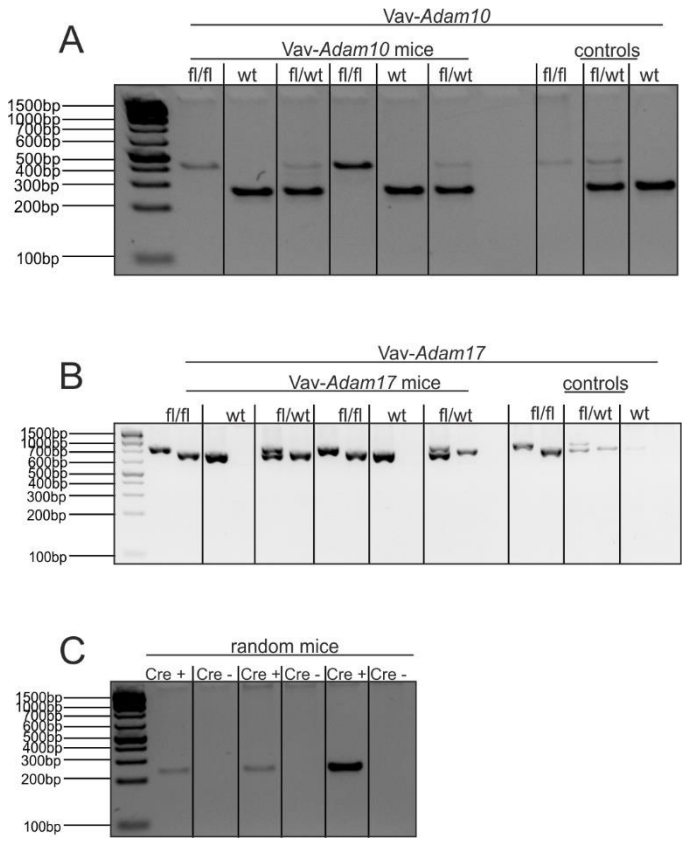

Figure 3. 6: Examples of Vav-cre, Adam10 and Adam17 genotypes. Genotyping was done by Nina Schnellbach. Mastermix of vav-cre, *Adam10* and *Adam17* genotypes were prepared as described in table 3.16, 3.18 and 3.20 followed by the addition of 2 µl, 0.8 µl and 0.5 µl of sample DNA of vav-cre, *Adam10* and *Adam17*, respectively. The DNA fragments were separated by size using agarose gel electrophoresis. The resulting bands were visualized using UV light transilluminator (HeroLab UVT-28 ME-HC).

3.2.5.3 *P. aeruginosa*-induced lung pneumonia model

Ketamine (100 mg/kg)/xylazine (25 mg/kg) were used to anesthetize the mice by intraperitoneal injection (250 µl), followed by intranasal instillation of *P. aeruginosa* (10^5 CFU in 20 µl PBS) or PBS as a control (see figure 3.7). After 12 h of lung infection, the severity of pneumonia and the development of hypothermia were evaluated using the Gesellschaft für Versuchstierkunde/Society of Laboratory Animal Science welfare (GV-Solas) scoring and Mouse Clinical Assessment Scoring System for Sepsis (M-CASS) (See table 3.24 for details, (Conrad et al., 2022; Huet et al., 2013)). Subsequently, the mice were sacrificed by intraperitoneal injection of 500 µl of ketamine (500 mg/kg)/xylazine (50 mg/kg) and were fixed on a dissection board in a supine position. Blood was directly collected from the inferior vena cava for serum isolation, total cell count and CFU determination (100 µl citrated with sodium citrate) as well as for flow cytometry analysis of the leukocyte content (100 µl in 1 ml of blood FACS buffer).

The right auxiliary lobe of the lung was pinched off before lavage and incubated at 60 °C for 72 h to determine lung wet-dry ratio. To collect bronchoalveolar lavage fluid (BAL), the nick skin was

disinfected by 70% ethanol and removed by anatomical scissors to carefully expose the trachea. A 1-ml syringe filled with ice-cold sterile PBS was inserted in the trachea to form a straight line in order to avoid bleeding or esophagus injury, and the lung was lavaged 2-3 times. The collected BAL was used for total cell count, CFU determination, cytokines release evaluation and flow cytometry analysis of the leukocytes content. Total cell numbers in blood and BAL were measured using the NucleoCounter® NC-200™ following the manufacturer's protocol. The left lobe of the lung was perfused 2-3 times with sterile PBS, filled with Roti-Fix®, ligated and immersed in Roti-Fix® for 48 h for (immuno)histochemistry analysis.

Figure 3. 7: Method description for *P. aeruginosa*-induced lung pneumonia model.

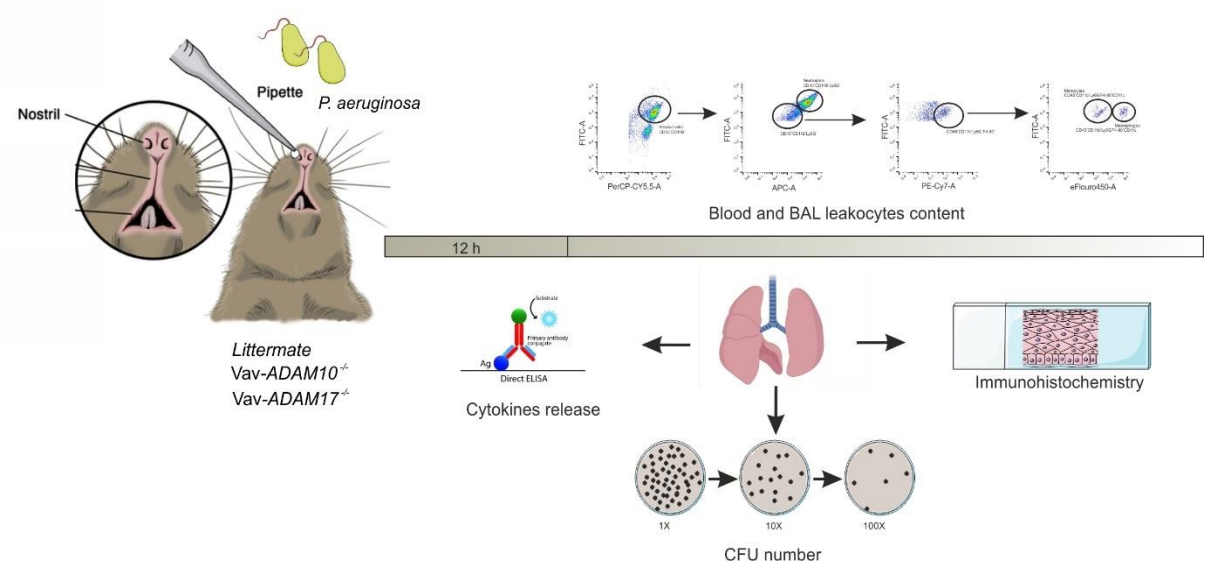

Littermates, Vav-*Adam10*$^{-/-}$ or Vav-*Adam17*$^{-/-}$ mice were infected with *P. aeruginosa* or PBS as a control by intranasal instillation for 12 h. Subsequently, blood and BAL leukocyte content were evaluated by flow cytometry and cytokine release by ELISA. Lung right auxiliary lobe was used to determine lung wet-dry ratio and left lobe for immunohistochemical analysis and macrophages polarization analysis.

Table 3. 22: Scoring system for evaluating pneumonia severity in mice. Mouse Clinical Assessment Score for Sepsis (M-CASS). Adapted from (Conrad et al., 2022).

Mouse Clinical Assessment Score for Sepsis (M-CASS)				
Score	**1**	**2**	**3**	**4**
Fur Aspect	Normal fur	Slightly ruffled fur	Ruffled fur	Ruffled fur and piloerection
Activity	Normal	Reduced	Only when provoked	Little or none with provocation
Posture	Normal	Hunched, moving freely	Hunched, strained or stiff movement	Hunched, little or no movement
Behavior	Normal	Slow	Abnormal when disturbed or provoked	Abnormal, no relocation
Chest Movements	Normal	Mild dyspnea	Moderate dyspnea	Severe dyspnea
Eyelids	Normal, open	Opened when disturbed	Partially closed, even when disturbed	Mostly or completely closed, even when provoked

3.2.6 Statistical methods

Data were analyzed using GraphPad PRISM 9.0 (GraphPad Software, La Jollla, CA, USA). Data are shown as mean ± SD. Differences were considered significant with a p-value < 0.05. Statistical analysis tests used in this thesis and the p-values are indicated in each figure legend.

4 Results

The lung-blood barrier belongs to the first line of defense against exogenous insults such as bacterial pathogens. Pneumonia may cause the disruption of this barrier resulting in pulmonary damage. To investigate the role of ADAM10 and ADAM17 in lung infection in more detail, a cell- and pathogen-specific analysis was performed.

4.1 Functional implications of ADAM10 during lung infection *in vitro*

4.1.1 Pathogen-specific regulation of ADAM10 in lung epithelial cell infection

A549 cells and HSAEpC served as model cells and were subjected to sterile inflammation caused by bacterial toxins or bacterial infection itself. The cell-associated expression was analyzed by Western blot, and the surface expression was detected by immunostaining and subsequent flow cytometric analysis. Infection of A549 cells with the Gram-negative bacterium *P. aeruginosa* (MOI 5) induced maturation of ADAM10, defined by an increase in the mature form (70 kDa) and a decrease in the proform (100 kDa) after 1 and 4 h of infection (figure 4.1 A). Interestingly, after 2 h of infection, the mature form of ADAM10 significantly dropped compared to non-infected control cells (Figure 4.1 A). The time-dependence of ADAM10 maturation was further observed by an increase in the surface expression of intact cells (figure 4.1 B), with a similar drop after 2 h of infection.

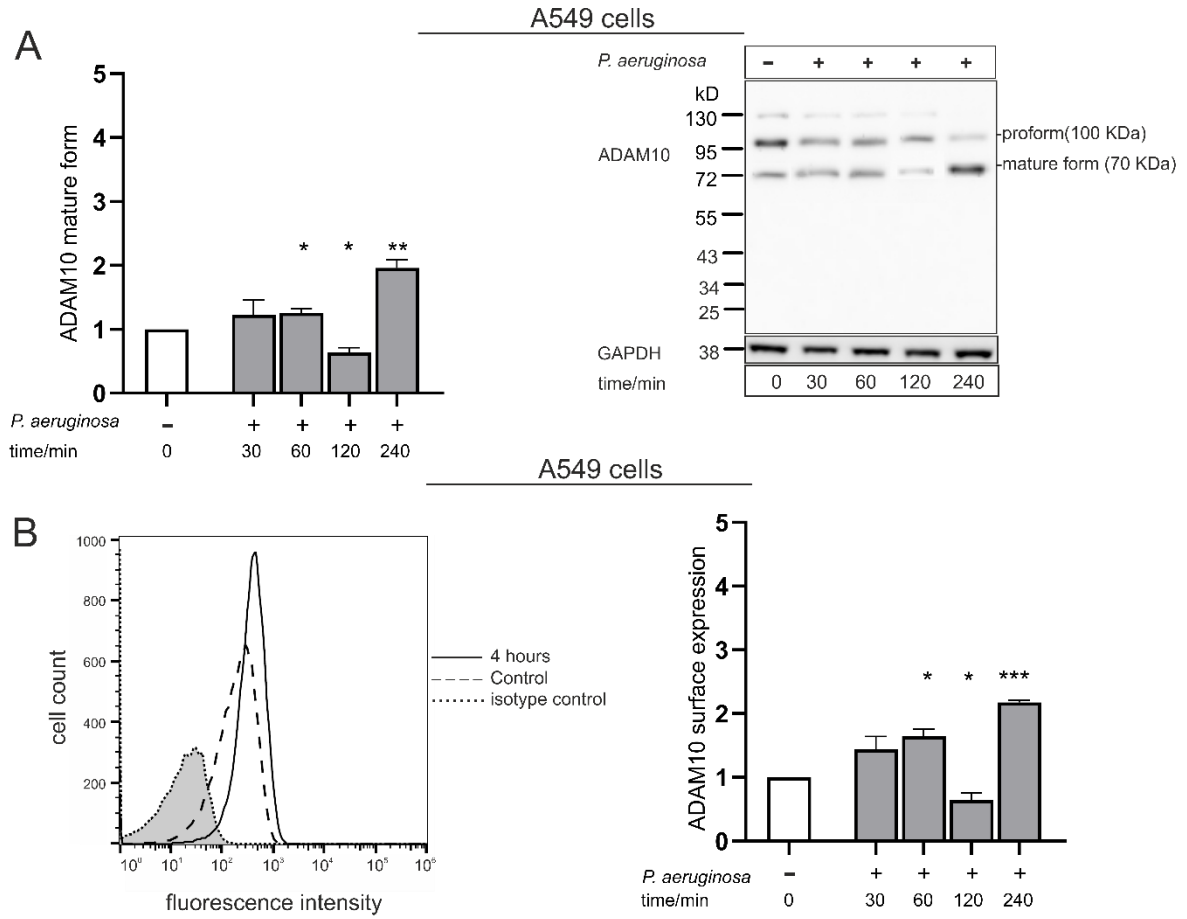

Figure 4. 1: Regulation of ADAM10 in A549 cells during infection with *P. aeruginosa*.
(A-B) A549 cells were grown in standard medium and infected with *P. aeruginosa* (MOI 5) for 30, 60, 120 and 240 min. (A) ADAM10 maturation was analyzed in the cell lysate by Western blot using an antibody against the C-terminal domain. GAPDH served as loading control. Band intensity was quantified by densitometry relative to non-infected cells. (B) The surface expression of ADAM10 was analyzed using a primary antibody against the N-terminal domain, followed by incubation with an APC-labeled secondary antibody and subsequent flow cytometric analysis. Data are shown after subtraction of the mean fluorescence intensity of the isotype control and in relation to non-infected cells. Quantitative data are presented as means + SD of three independent experiments. Asterisks reveal significance difference relative to the control analyzed using two tailed two samples t-test (* $p < 0.05$, ** $p < 0.01$, *** $p < 0.001$).

In contrast to *P. aeruginosa*, infection of A549 cells with the Gram-positive bacterium *S. pneumoniae* (MOI 5) induced no change of ADAM10 expression on the cell-associated protein expression level (Figure 4.2 A) or the surface expression level (Figure 4.2 B).

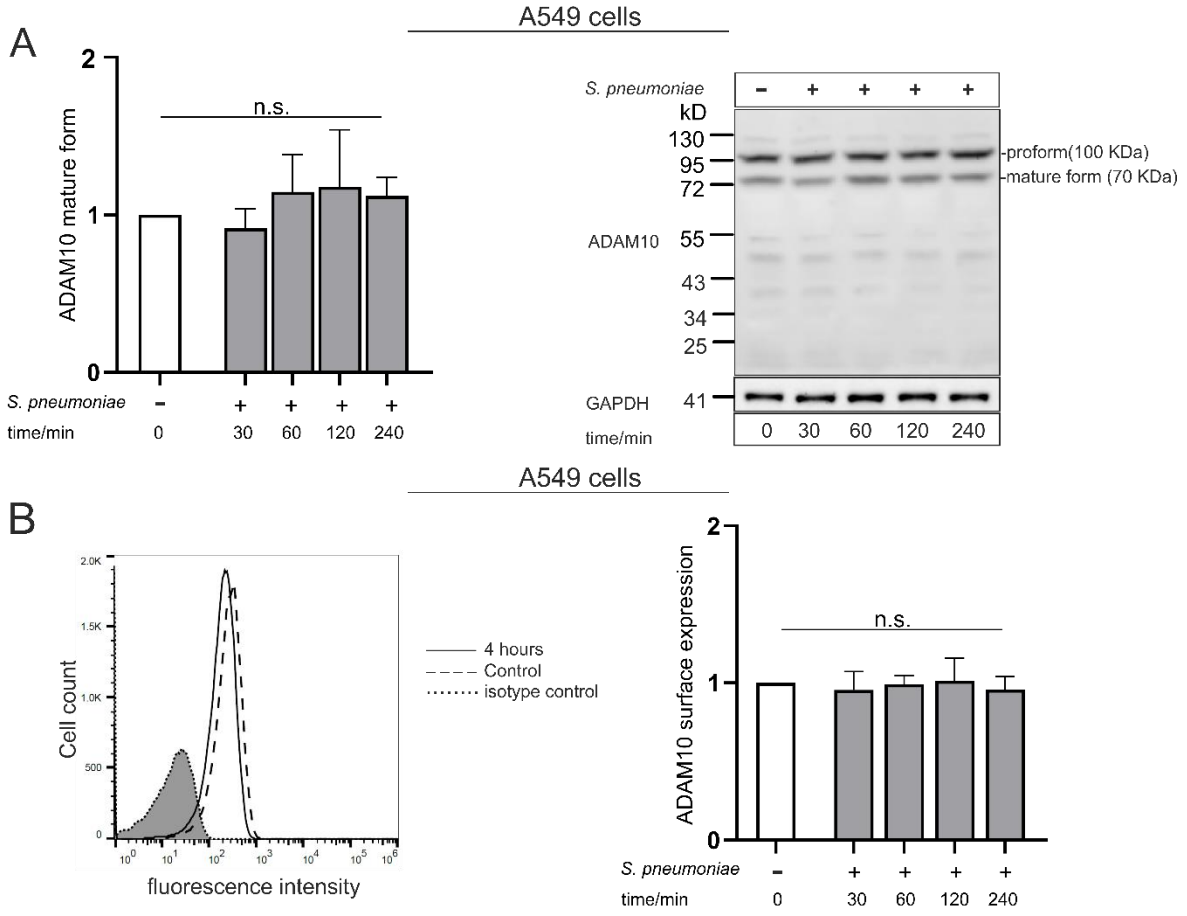

Figure 4. 2: Regulation of ADAM10 in A549 cells during infection with *S. pneumoniae.*
(A-B) A549 cells were grown in standard medium and infected with *S. pneumoniae* (MOI 5) for 30, 60, 120 and 240 min. (A) ADAM10 maturation was analyzed in the cell lysate by Western blot using an antibody against the C-terminal domain. GAPDH served as loading control. Band intensity was quantified by densitometry relative to non-infected cells. (B) The surface expression of ADAM10 was analyzed using a primary antibody against the N-terminal domain, followed by incubation with an APC-labeled secondary antibody and subsequent flow cytometric analysis. Data are shown after subtraction of the mean fluorescence intensity of the isotype control and in relation to non-infected cells. Quantitative data are presented as means + SD of three independent experiments. Asterisks reveal significance difference relative to the control analyzed using two tailed two samples t-test. No significant difference was observed.

Several cellular reactions can not only be induced by the direct cell-pathogen interaction, but also by the virulence factors and the toxins released by the bacteria. To mimic this, Exotoxin A was chosen as one of the most virulent toxins secreted by *P. aeruginosa* (Michalska, Wolf, 2015). Stimulation with Exotoxin A (4 h, 100 ng/ml) increased maturation and surface expression of ADAM10 compared to the non-stimulated control (Figure 4.3 A and B).

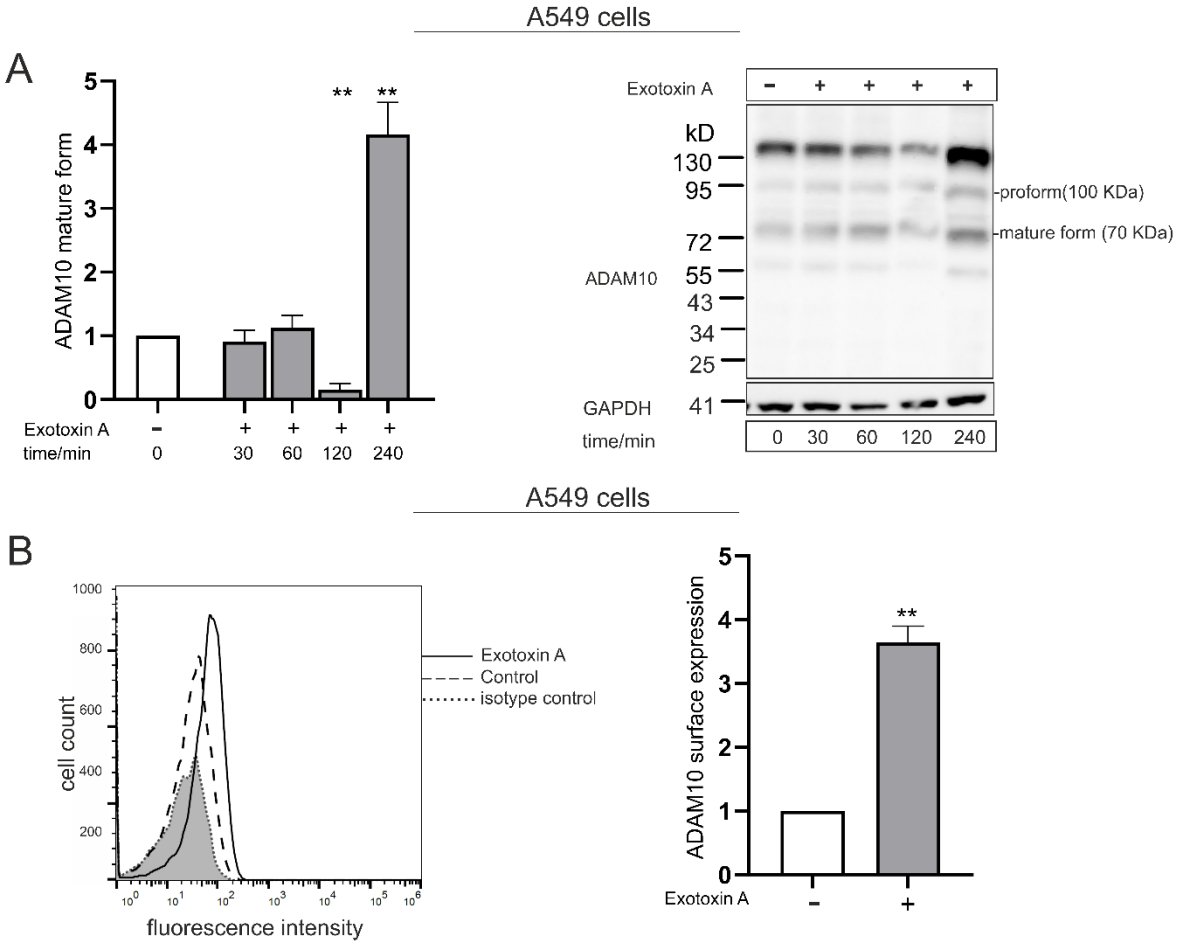

Figure 4. 3: Regulation of ADAM10 in A549 cells during stimulation with Exotoxin A.
(A-B) A549 cells were grown in standard medium and stimulated with 100 ng/ml Exotoxin A for 4 h. (A) ADAM10 maturation was analyzed in the cell lysate by Western blot using an antibody against the C-terminal domain. GAPDH served as loading control. Band intensity was quantified by densitometry relative to non-stimulated cells. (B) The surface expression of ADAM10 was analyzed using a primary antibody against the N-terminal domain, followed by incubation with an APC-labeled secondary antibody and subsequent flow cytometric analysis. Data are shown after subtraction of the mean fluorescence intensity of the isotype control and in relation to non-stimulated cells. Quantitative data are presented as means + SD of three independent experiments. Asterisks reveal significance difference relative to the control analyzed using two tailed two samples t-test (** $p < 0.01$, *** $p < 0.001$).

To confirm these findings in primary cells, the experiments were repeated with HSAEpC. In general, these cells showed a weaker expression of ADAM10 in comparison to A549 cells. Again, *P. aeruginosa* and Exotoxin A induced an upregulation of ADAM10 surface expression, following the same pattern of regulation observed in A549 cells (figure 4.4 A and B). In addition, *S. pneumoniae* had no impact on the regulation of ADAM10 (figure 4.4 C).

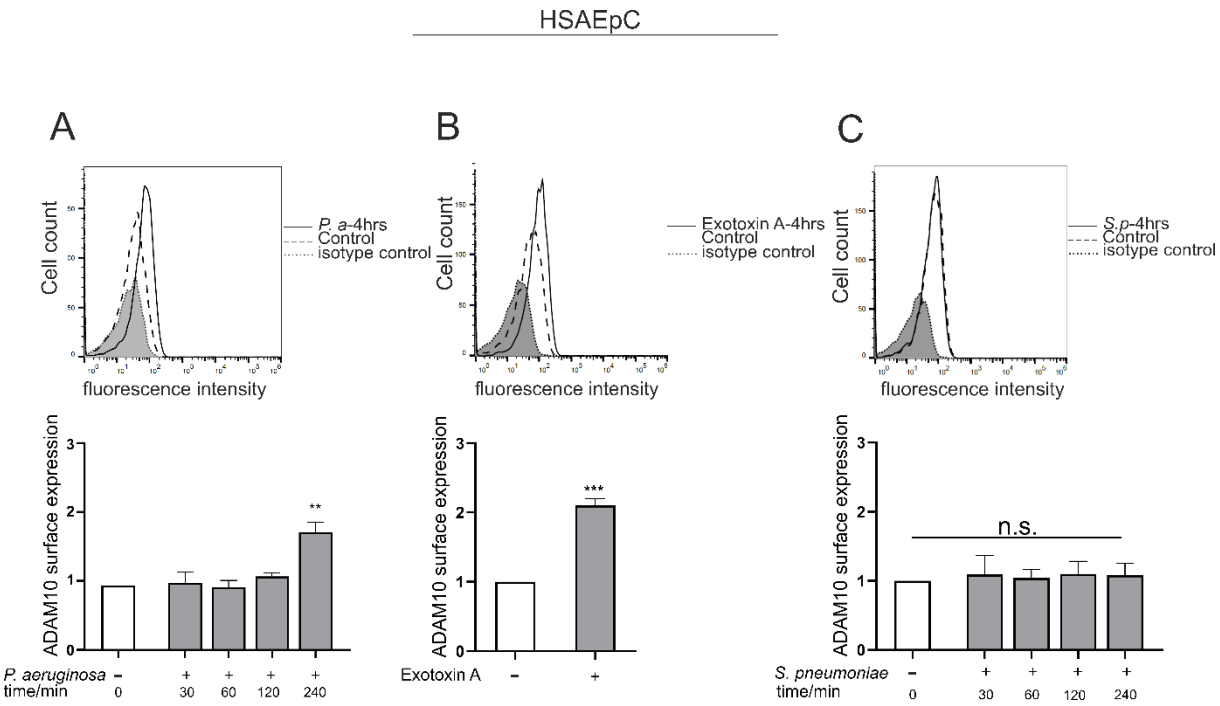

Figure 4. 4: Regulation of ADAM10 in HSAEPC during infection with *P. aeruginosa, S. pneumonia* or stimulation with Exotoxin A.
(A-C) HSAEPC cells were grown in MV2 medium and infected with *P. aeruginosa* or *S. pneumoniae* (MOI 5) for 30, 60, 120 and 240 min or stimulated with 100 ng/ml Exotoxin A for 4 h. (A-C) The surface expression of ADAM10 was analyzed using an antibody against the N-terminal domain, followed by incubation with an APC-labeled secondary antibody and subsequent flow cytometric analysis. Data are shown after subtraction of the mean fluorescence intensity of the isotype control and in relation to non-stimulated cells. Asterisks reveal significance difference relative to the control analyzed using two tailed two samples t-test (** $p < 0.01$, *** $p < 0.001$).

4.1.2 *P. aeruginosa* and Exotoxin A induce ADAM10 shedding activity

To investigate whether the changes in ADAM10 surface expression have functional implications, the shedding activity in response to *P. aeruginosa* and Exotoxin A was tested after 2 h and 4 h. These time points were chosen in correlation to the obtained changes in ADAM10 maturation. The catalytic activity of ADAM10 was investigated by the cleavage of alkaline phosphatase-tagged betacellulin (AP-BTC) (Inoue et al., 2012) and E-cadherin (an endogenous substrate), as both have been described to be specific substrates of ADAM10 (Maretzky et al., 2005; Sahin et al., 2004). Infection with *P. aeruginosa* (2 or 4 h, MOI 5) or stimulation with Exotoxin A (4 h, 100 ng/ml) significantly increased AP release to the supernatant in comparison to the non-infected or non-stimulated control (Figure 4.5 A and B). Pre-treatment with GI254023X as a specific inhibitor of ADAM10 reduced this release significantly (Figure 4.5 A and B). This strong increase in AP-BTC was comparable to the release mediated by ionomycin which is considered one of the strongest activators of ADAM10 (Figure 4.5 C). Although the infection with *S. pneumoniae* did not induce any change in the protein expression or maturation, posttranslational modification could result in changes of activation. However, infection with *S. pneumoniae* had no effect on ADAM10 activity, again with a reduction of the basal activity by the inhibitor pre-treatment (Figure 4.5 D).

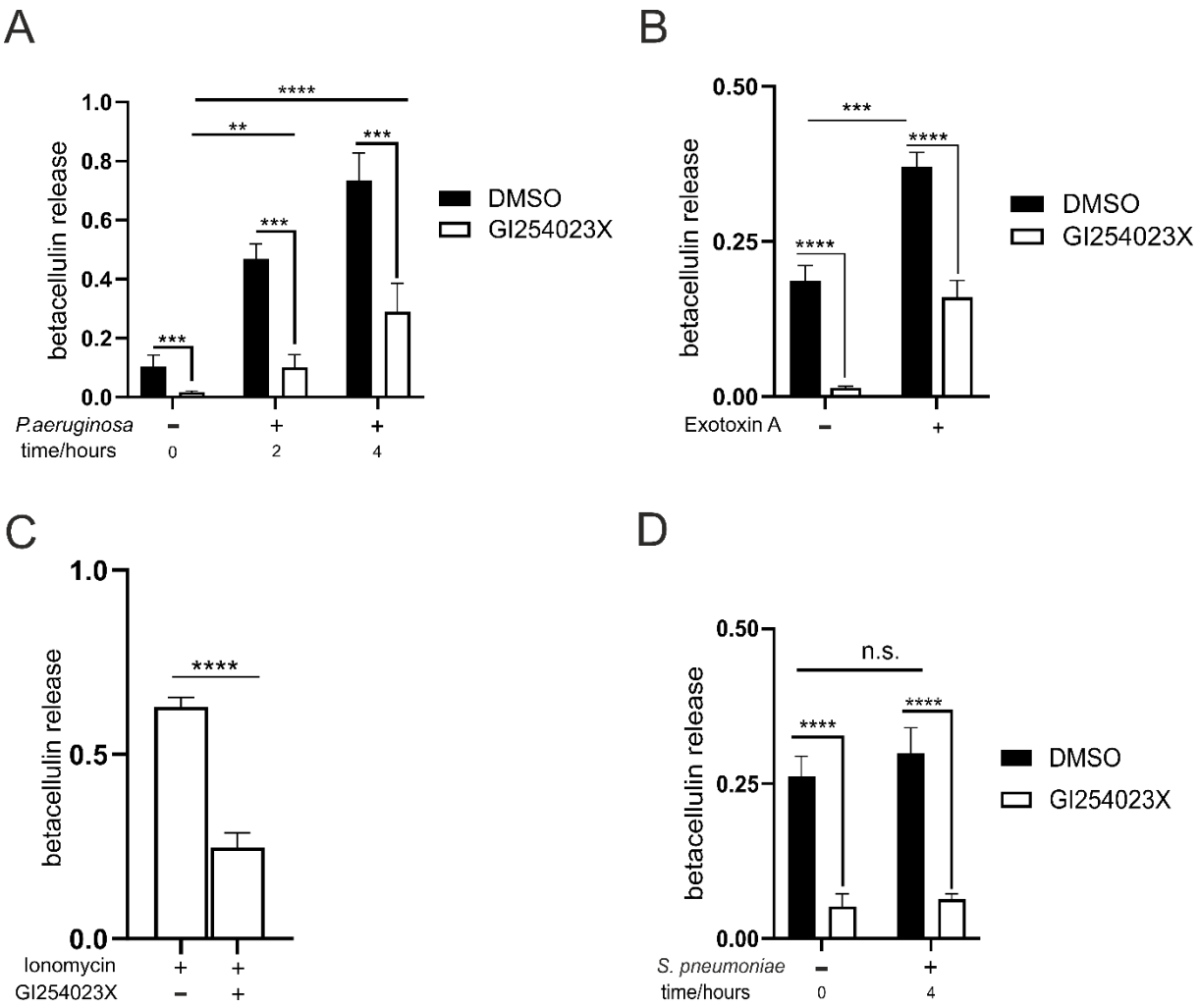

Figure 4. 5: *P. aeruginosa* and Exotoxin A induce activation of ADAM10.
(A-D) A549 cells were transfected with AP-BTC. The cells were incubated with 0.1% DMSO or 10 µM GI254023X for 30 min, followed by (A) infection with *P. aeruginosa* a (2 and 4 h, MOI 5), (B) stimulation with Exotoxin A (4 h, 100 ng/ml), (C) stimulation with ionomycin (1 h, 1 µM) or (D) infection with *S. pneumoniae* (4 h, MOI 5). The activity of AP was determined in both the cell lysate and the supernatant and shown as a ratio of the slope of AP activity in the supernatant to the total activity (lysate and supernatant). (A–D) Data are presented as means + SD of three independent experiments. Asterisks reveal significance among groups analyzed by two-way ANOVA and Tukey post-test (** $p < 0.01$, *** $p < 0.001$, **** $p < 0.0001$, n.s. not significant).

Similar to betacellulin, both *P. aeruginosa* and Exotoxin A induced the cleavage of E-cadherin as shown by a decrease in the full-length band (128 kDa) and an increase in the C-terminal fragment (38 kDa) (Figure 4.6 A and B). This cleavage was blocked by the inhibitor pre-treatment, while the inhibition was more prominent two hours after infection.

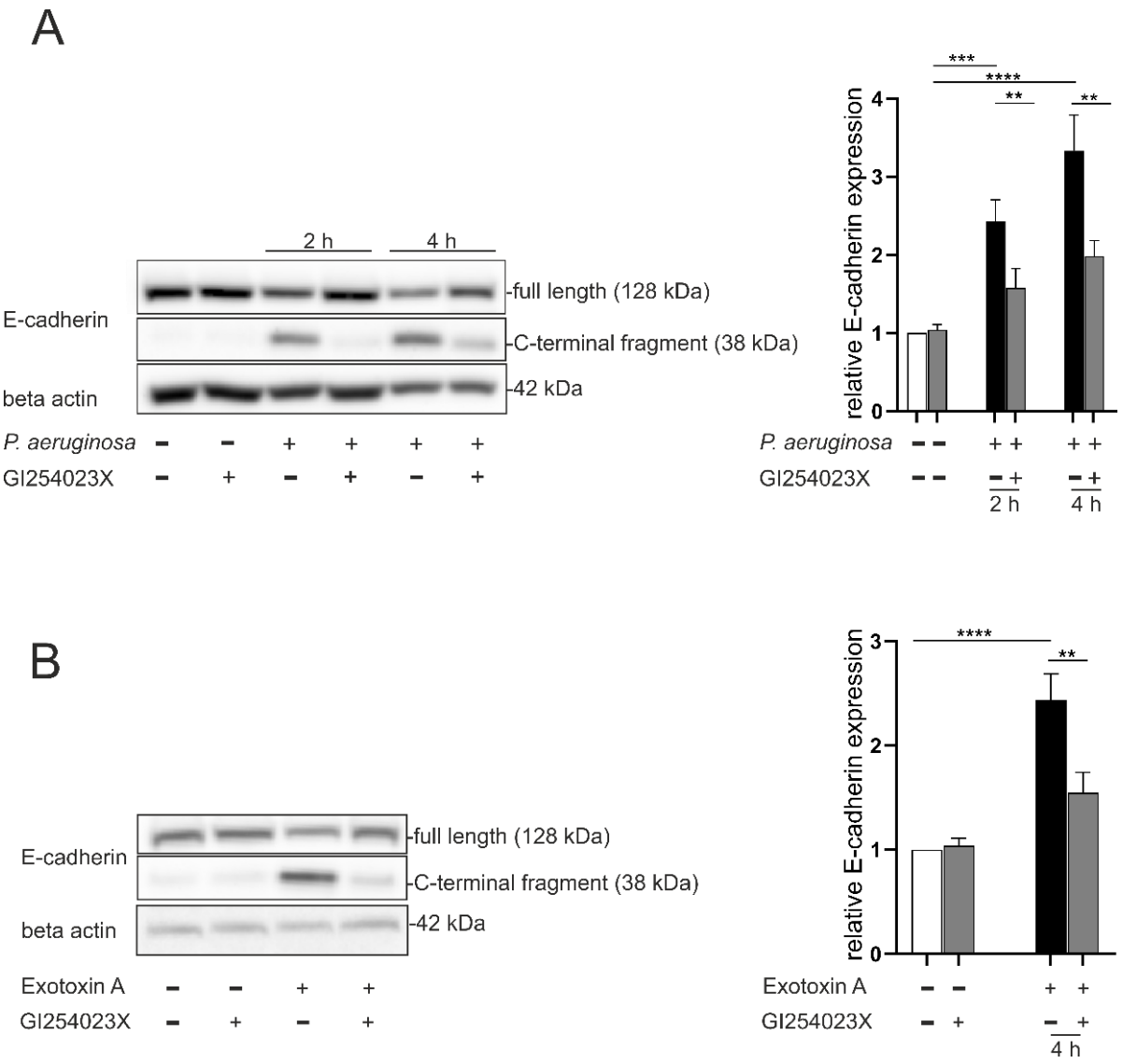

Figure 4. 6*: P. aeruginosa* and Exotoxin A induce activation of ADAM10 mediating E-cadherin cleavage.
(A-B) A549 cells were incubated with 0.1% DMSO or 10 µM GI254023X for 30 min followed by (A) infection with *P. aeruginosa* (2 and 4 h, MOI 5) or (B) stimulation Exotoxin A (4 h, 100 ng/ml). E-cadherin expression was analyzed in the cell lysate by western blot using an antibody against the C-terminal domain. Beta actin served as loading control. Representative blots of three independent experiments are shown. Data are presented as means + SD of three independent experiments. Asterisks reveal significance among groups analyzed by one-way ANOVA and Tukey post-test (** $p < 0.01$, *** $p < 0.001$, **** $p < 0.0001$)

4.1.3 *P. aeruginosa* and Exotoxin A induce epithelial permeability mediated by ADAM10

Edema formation and an increase in protein permeability are important manifestations of pneumonia mediated by disruption of the barrier integrity, which is controlled by junction and adhesion molecules such as E-cadherin. Thus, A549 cells were grown on a trans-well system until forming a monolayer and, subsequently, the total and paracellular permeability were evaluated by FITC-albumin and TRITC-dextran diffusion, respectively, upon infection with *P. aeruginosa* (4 h, MOI 5) or stimulation with Exotoxin A (4 h, 100 ng/ml). Both stimuli led to a strong induction of both total and paracellular permeability, which was inhibited by either ADAM10 gene silencing/knockdown (knockdown efficiency controlled by western blot (figure 4.7 A)) or pharmacological inhibition (figure 4.7 B-E).

With respect to the paracellular permeability, the induction by *P. aeruginosa* was higher than observed after Exotoxin A stimulation.

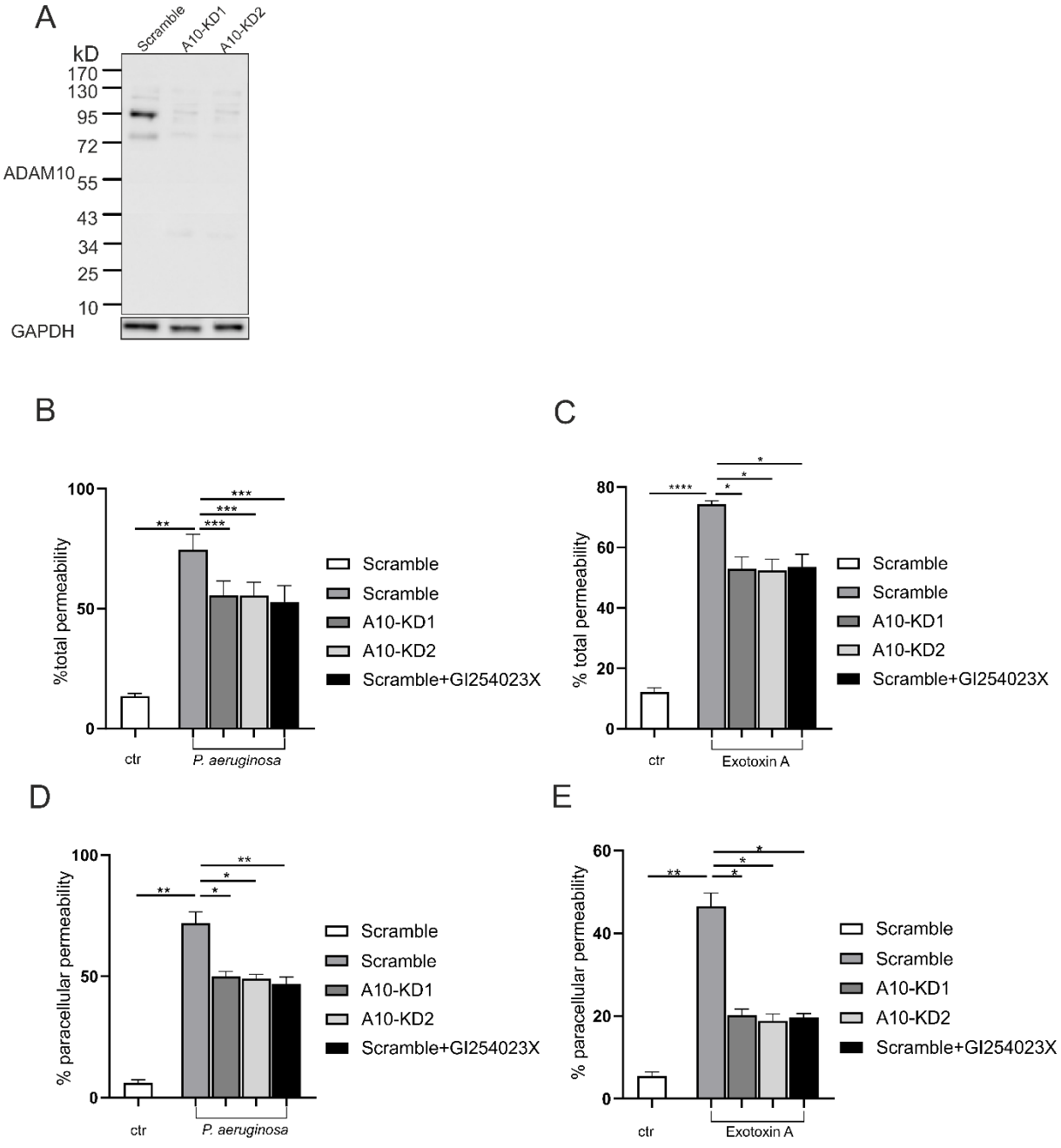

Figure 4. 7: *P. aeruginosa* and Exotoxin A induce epithelial permeability mediated by ADAM10.
(A-E) A549 cells were transduced with lentiviral particles for delivery of shRNA-carrying vectors for gene silencing of ADAM10 (A10-KD1 and A10-KD2). An unspecific shRNA (scramble) served as control. (A) ADAM10 expression was analyzed in the cell lysate by Western blot to confirm the knockdown using an antibody against the C-terminal domain. GAPDH served as loading control. (B-E) A549 cells were grown on a trans-well system until forming a monolayer, incubated with 0.1% DMSO or 10 µM GI254023X for 30 min, followed by infection with *P. aeruginosa* (B/D, 4 h, MOI 5), or stimulation with Exotoxin A (C/E,4 h, 100 ng/ml). Subsequently, the medium in the upper chamber was replaced by a suspension of both 70 kDa TRITC-dextran (1 mg/ml) and FITC-albumin (0.25 mg/ml). After 90 min, paracellular and total permeability were determined. Data are presented as means + SD of three independent experiments. Asterisks reveal significance among groups analyzed by two-way ANOVA and Tukey post-test (* $p < 0.05$, **$p < 0.01$, *** $p < 0.001$, **** $p < 0.0001$).

Leukocyte transmigration is an important step during the elimination of an infection. However, excessive recruitment, fostered by loss of barrier integrity, leads to increased organ dysfunction. Therefore, the influence of ADAM10 activity on monocyte transepithelial migration during infection with *P. aeruginosa* was investigated using a trans-well assay. For higher reproducibility and the possibility of genetic targeting, the well-established monocytic cell line THP-1 was used. The transepithelial migration of THP-1 cells was significantly increased during infection with *P. aeruginosa* (4 h, MOI 5) in the presence (14x) or absence (10x) of the monocytes chemoattractant CCL2 (figure 4.8 A). Targeting ADAM10 by gene silencing or pharmacological inhibition solely reduced the transepithelial migration of THP-1 cells (Figure 4.8 A). However, stimulation with Exotoxin A (4 h, 100 ng/ml) induced much weaker transmigration compared to infection in the presence (2x) or absence (4x) of CCL2, with no observed effect of ADAM10 knockdown or inhibition (Figure 4.8 B). In conclusion, ADAM10 activation mediated by *P. aeruginosa* led to partly barrier disruption with increased protein and cellular permeability.

4.1.4 ADAM10 inhibition improves epithelial wound healing

Resolution of barrier disruption and regeneration is strongly dependent on the wound healing capacity of the epithelial layer. Epithelial wound closure was investigated using an automated scratch assay after stimulation with Exotoxin A (4 h, 100 ng/ml). Treatment with Exotoxin A reduced wound closure by 20 % in comparison to the non-stimulated control, while inhibition of ADAM10 decreased the closure of the wound by about 10% (Figure 4.9 A and B). One could assume that a combined treatment would synergistically reduce the wound closure. However, gene silencing or pharmacological inhibition of ADAM10 did not synergistically reduce the closure but significantly improved the wound closure (Figure 4.9 A and B). These results suggest an ADAM10-dependent cell damage mediated by Exotoxin A. To address this hypothesis, the experiment was repeated in the absence of GI254023X pre-incubation but with the addition of GI254023X after Exotoxin A stimulation (during the wound closure phase). ADAM10 inhibition at this stage did not change the epithelial cell migration upon stimulation with Exotoxin A, leading to the hypothesis of a high relevance of ADAM10 in the initial phase of cellular damage (Figure 4.9 C and D).

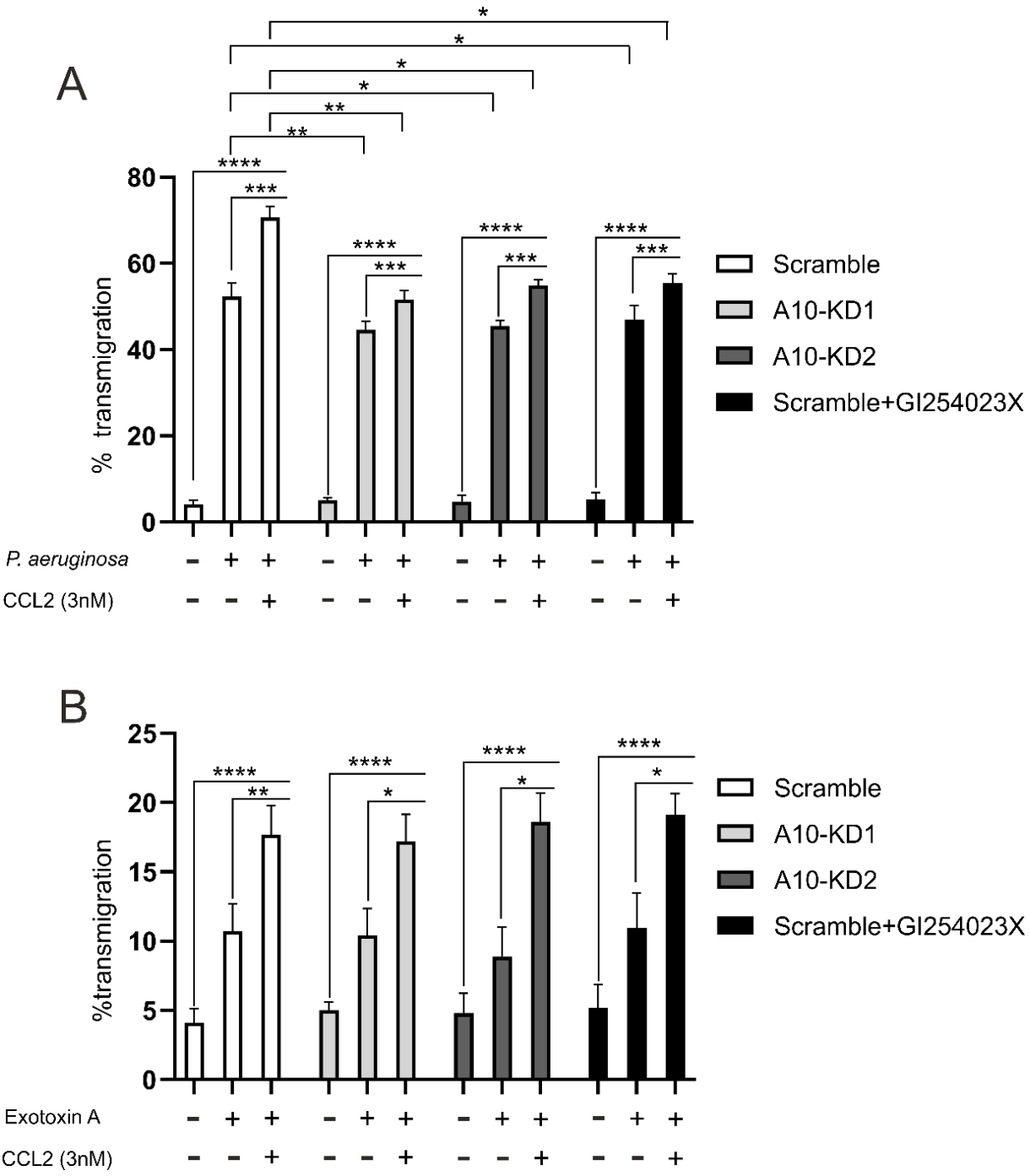

Figure 4. 8: *P. aeruginosa* and Exotoxin A induce THP-1 transepithelial migration mediated by ADAM10.
(A-B) A549 cells were transduced with lentiviral particles for delivery of shRNA-carrying vectors for gene silencing of ADAM10 (A10-KD1 and A10-KD2). An unspecific shRNA (scramble) served as control. The cells were grown on a trans-well system until forming a monolayer, incubated with 0.1% DMSO or 10 µM GI254023X for 30 min, followed by infection with *P. aeruginosa* (A, 4 h, MOI 5) or stimulation with Exotoxin A (B, 4 h, 100 ng/ml). Subsequently, THP-1 cells were added to the upper chamber, and the transmigration was analyzed by measurement of endogenous β-glucuronidase activity. Data are presented as means + SD of three independent experiments. Asterisks reveal significance among groups analyzed by two-way ANOVA and Tukey post-test (* $p < 0.05$, ** $p < 0.01$, *** $p < 0.001$, **** $p < 0.0001$).

4.1.5 *P. aeruginosa* induces the release of ADAM10 in exosomes

ADAM10 has been shown to be vigorously found in exosome like EVs (Stoeck et al., 2006; Tosetti et al., 2018). As mentioned earlier, 2 h of *P. aeruginosa* infection was associated with a significant increase in ADAM10 activity, while the mature form on the cell surface as well as within the cell lysate was reduced (Figure 4.1 A and B). One possible explanation could be that *P. aeruginosa* induces a transit exocytotic release of ADAM10 to the extracellular environment. Therefore, EVs were isolated from infected cells and non-infected cells and further purified for exosome preparation. Mature ADAM10 could only be detected in the vesicle fraction purified from 100,000xg after infection with *P. aeruginosa* while it was totally absent in the non-infected cells (Figure 4.10 A). These vesicle fractions were further characterized as flotillin-1 and CD9 positive, indicating an increase in EVs release upon by *P. aeruginosa* infection (Figure 4.10 A). Sucrose density gradient centrifugation for fractionation of the EVs revealed that the ADAM10, flotillin-1 and CD9 positive EVs were collected at a density of 1.11 and 1.16 g/ml which represent the typical density of exosomes (figure 4.10 B).

4.1.6 Exosomal ADAM10 is proteolytically active and mediates shedding on the cell surface *in trans*

Infection with *P. aeruginosa* led to an increase of the shedding activity of ADAM10, although the surface expression was reduced. This led to the hypothesis that the measured activity could be derived from the exosomal ADAM10. Therefore, an *in vitro* transfer experiment was performed. Exosomes derived from non-infected and *P. aeruginosa* infected cells (without AP-BTC), respectively, was transferred to cells expressing AP-BTC. Interestingly, only exosomes derived from *P. aeruginosa* infected cells could enhance the release of betacellulin to the supernatant, while this process was blocked by pharmacological inhibition of ADAM10 by GI254023X (figure 4.11 A). Thus, ADAM10 released on exosomes upon *P. aeruginosa* infection is active and mediates the ectodomain shedding of betacellulin on distinct cells *in trans*.

To exclude the effect of the surface ADAM10 on the cells themself and to confirm that ADAM10 activity was exosomal based, exosomes were purified from ADAM10 wildtype and knockdown cells, respectively, with and without *P. aeruginosa* infection. These exosomes were used for stimulation of AP-BTC expressing wildtype and ADAM10 knockdown cells, respectively. Exosomes purified from ADAM10 expressing cells increased the cleavage of AP-BTC on both wildtype and ADAM10 knockdown cells (figure 4.11 B). However, exosomes purified from ADAM10 knockdown cells did not change AP-BTC release in both cell types (figure 4.11 B and C).

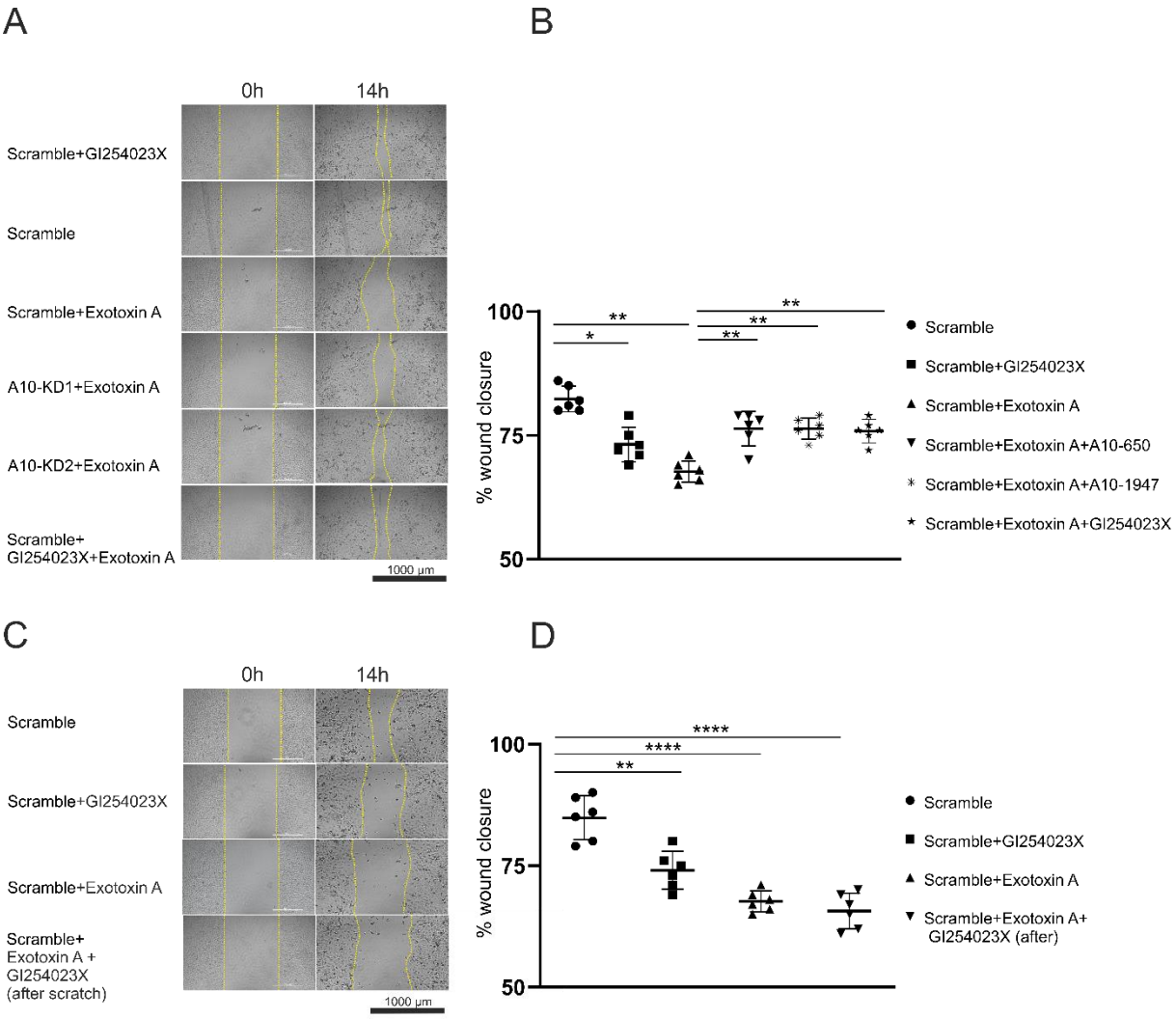

Figure 4. 9: Role of ADAM10 in epithelium regeneration upon damage by Exotoxin A.
(A-D) A549 cells were transduced with lentiviral particles for delivery of shRNA-carrying vectors for gene silencing of ADAM10 (A10-KD1 and A10-KD2). An unspecific shRNA (scramble) served as control. (A-D) the cells were incubated with mitomycin for 2 h and (A-B) 0.1% DMSO or 10 µM GI254023X for 30 min, followed by stimulation with Exotoxin A (4 h, 100 ng/ml) or (C-D) stimulated with Exotoxin A (4 h, 100 ng/ml), followed by treatment with 10 µM GI254023X during the migration phase. Wound closure was monitored automatically over 14 h. (A,C) Representative images are shown. (B,D. Data are presented as means +/- SD of six independent experiments. Asterisks indicate significance between groups analyzed by one-way ANOVA and Tukey post-test (*$p < 0.05$, **$p < 0.01$**** $p < 0.0001$).

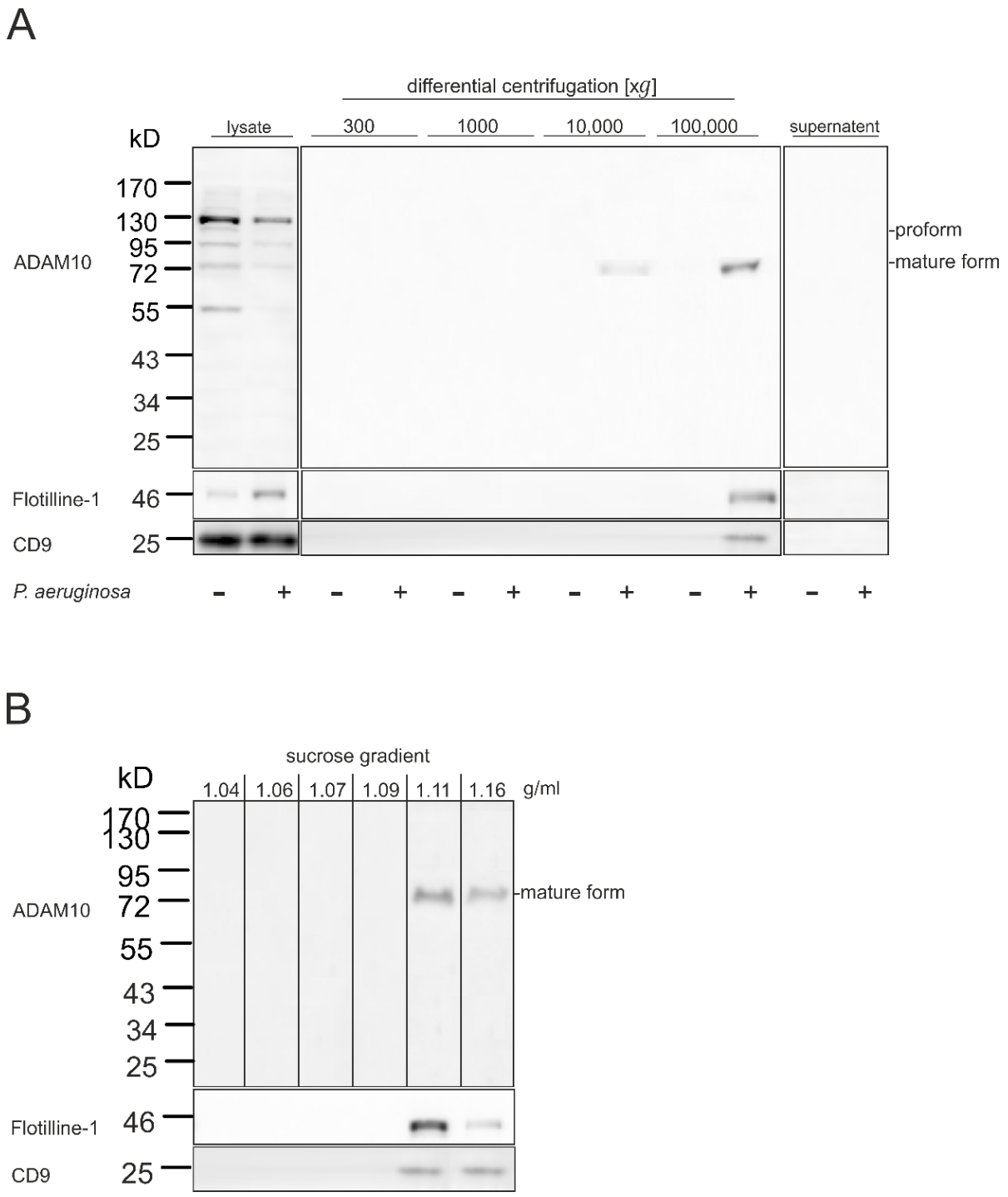

Figure 4. 10: *P. aeruginosa* induces the release of ADAM10 in exosomes.
2×10^7 of A549 cells were grown in serum free medium and infected with *P. aeruginosa* (2 h, MOI 5). Subsequently, the cells were lysed, and the medium was assigned for different centrifugation steps as indicated. (A) The pellet of each centrifugation step was lysed with SDS buffer, and the expression of ADAM10 (antibody against the C-terminal domain), Flottilin-1 and CD9 were analyzed by Western blot. (B) The extracellular vesicles (100,000xg) were collected by sterile PBS and loaded to a sucrose gradient comprising layers to be separated according to the density. The expression of ADAM10 (antibody against the C-terminal domain), Flottilin-1 and CD9 in each layer were analyzed by Western blot. Representative blots of three independent experiments are shown.

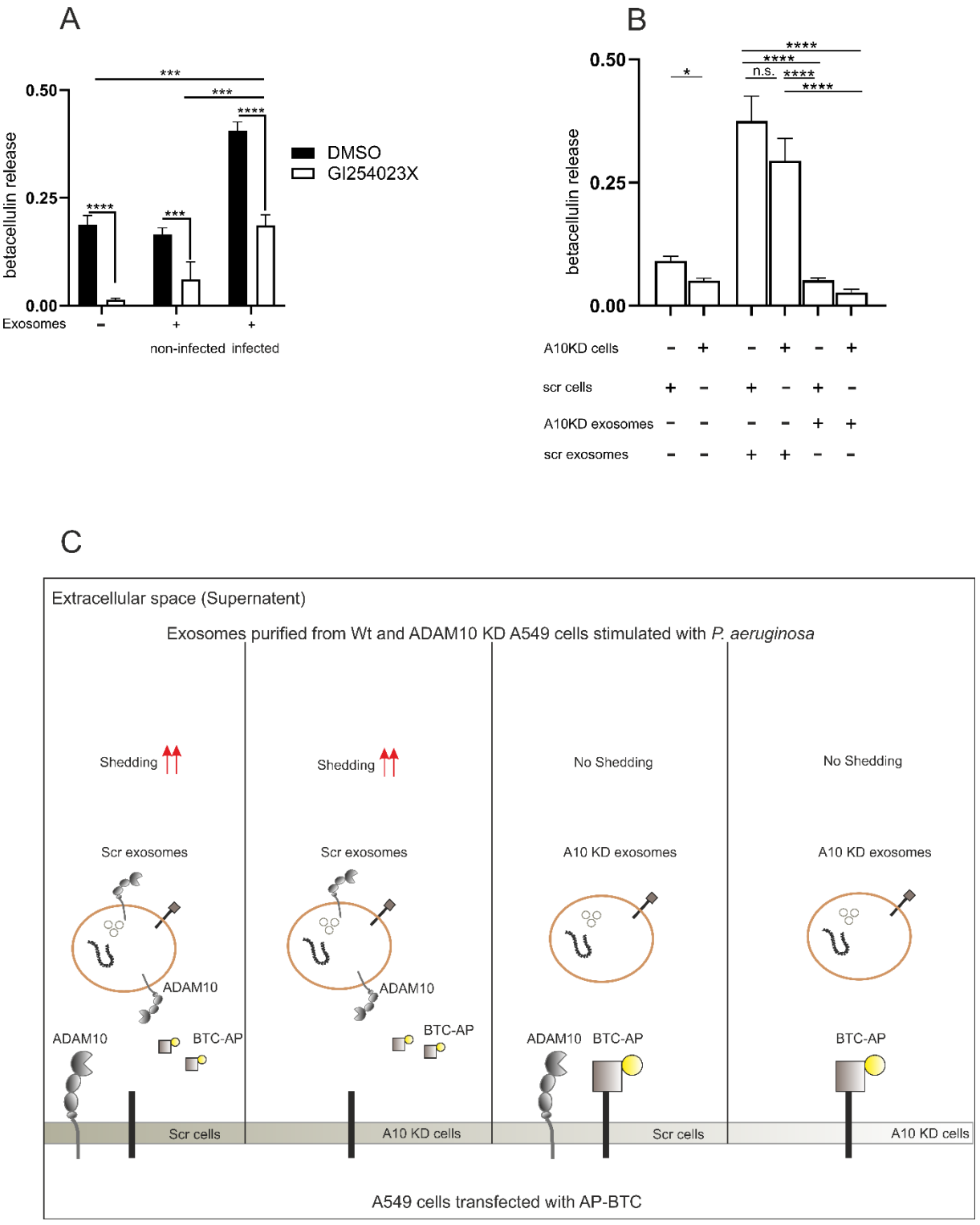

Figure 4. 11: ADAM10 in exosomes is active and mediates shedding activity.
(A) A549 cells were transfected with AP-BTC. The cells were pre-incubated with 0.1% DMSO or 10 µM GI254023X for 30 min, followed by stimulation with exosomes purified from non-infected or *P. aeruginosa* (2 h, MOI 5) infected A549 cells. The activity of AP was determined in both cell lysate and supernatant. (B) A549 cells were transduced with lentiviral particles for delivery of shRNA-carrying vectors for gene silencing of ADAM10 (A10-KD1 and A10-KD2) and an unspecific shRNA (scramble) served as control. The cells were infected with *P. aeruginosa* a (2 h, MOI 5) to purify exosomes. For ADAM10 activity measurement, A549 cells were transfected with AP-BTC as described earlier and stimulated with exosomes (without AP-BTC) derived from scramble or A10-KD cells which were either infected with *P. aeruginosa* (2 h, MOI 5) or left un-infected. (C) Schematic description for the experiment in (B). Data are shown as means + SD of three independent experiments. Asterisks reveal significance among groups analyzed by two-way ANOVA and Tukey post-test in A and one-way ANOVA and Tukey post-test in B (* $p < 0.05$, *** $p < 0.001$, **** $p < 0.0001$).

4.1.7 ADAM10 activation mediated by *P. aeruginosa* infection depends on the released toxins and is calcium-dependent

To investigate whether the activation of ADAM10 is due to the interaction with *P. aeruginosa* itself or due to the released toxins, *P. aeruginosa* was subjected to heat-inactivation under mild and optimal conditions (70 C° for 40 min) to ensure bacterial death without affecting the released toxins (Rabiei et al., 2019). In contrast to living bacteria, infection of A549 cells with heat inactivated *P. aeruginosa* had no impact on the expression/maturation of ADAM10 (figure 4.12 A and B).

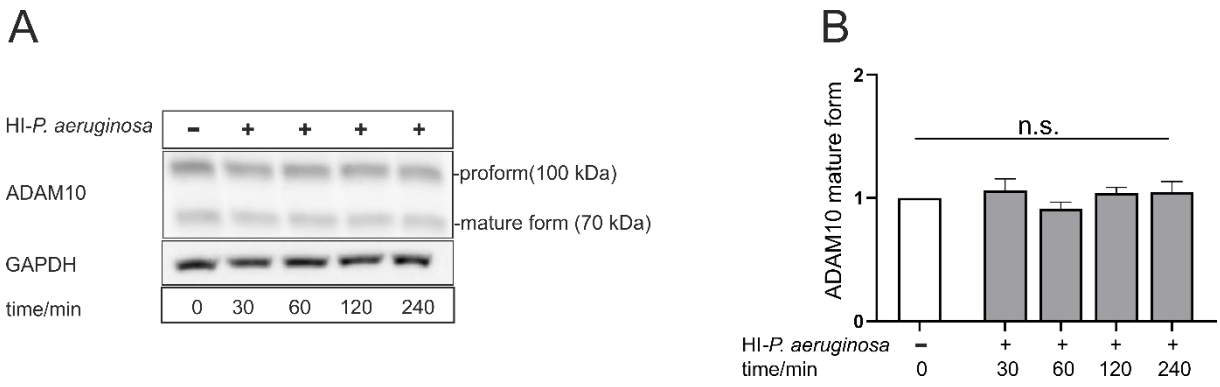

Figure 4. 12: Regulation of ADAM10 in A549 cells during infection with heat-inactivated *P. aeruginosa*.
(A-B) A549 cells were grown in standard medium and infected with heat-inactivated *P. aeruginosa* (MOI 5) for 30, 60, 120 and 240 min. (A) ADAM10 maturation was analyzed in the cell lysate by Western blot using an antibody against the C-terminal domain. GAPDH served as loading control. (B) Band intensity was quantified by densitometry relative to non-infected cells. Quantitative data are presented as means + SD of three independent experiments. Asterisks reveal significance difference relative to the control analyzed using two tailed two samples t-test. No significant difference was observed.

ADAM10 activation is known to be correlated with an increased cytosolic calcium level $[Ca2^+]_i$. As Exotoxin A inhibits e-EF2 (Zdanovsky et al., 1993), the dependence of ADAM10 activation by Exotoxin A on calcium signaling was investigated. Indeed, Exotoxin A stimulation significantly increased $[Ca2^+]_i$ (figure 4.13 A). To address whether the source of intracellular calcium for the described activation would be the release from internal stores (e.g., ER) or the extracellular environment, the experiment was repeated in the presence and absence of calcium in the extracellular environment, respectively. Exotoxin A stimulation did not increase $[Ca2^+]_i$ in the absence of calcium in the extracellular environment (figure 4.13 B). In contrast, a peaked increase in $[Ca2^+]_i$ was detected upon addition of calcium to the extracellular environment (figure 4.13 C). Thus, the *P. aeruginosa*-specific activation of ADAM10 is dependent on the released toxins rather than the particle itself triggered by calcium influx.

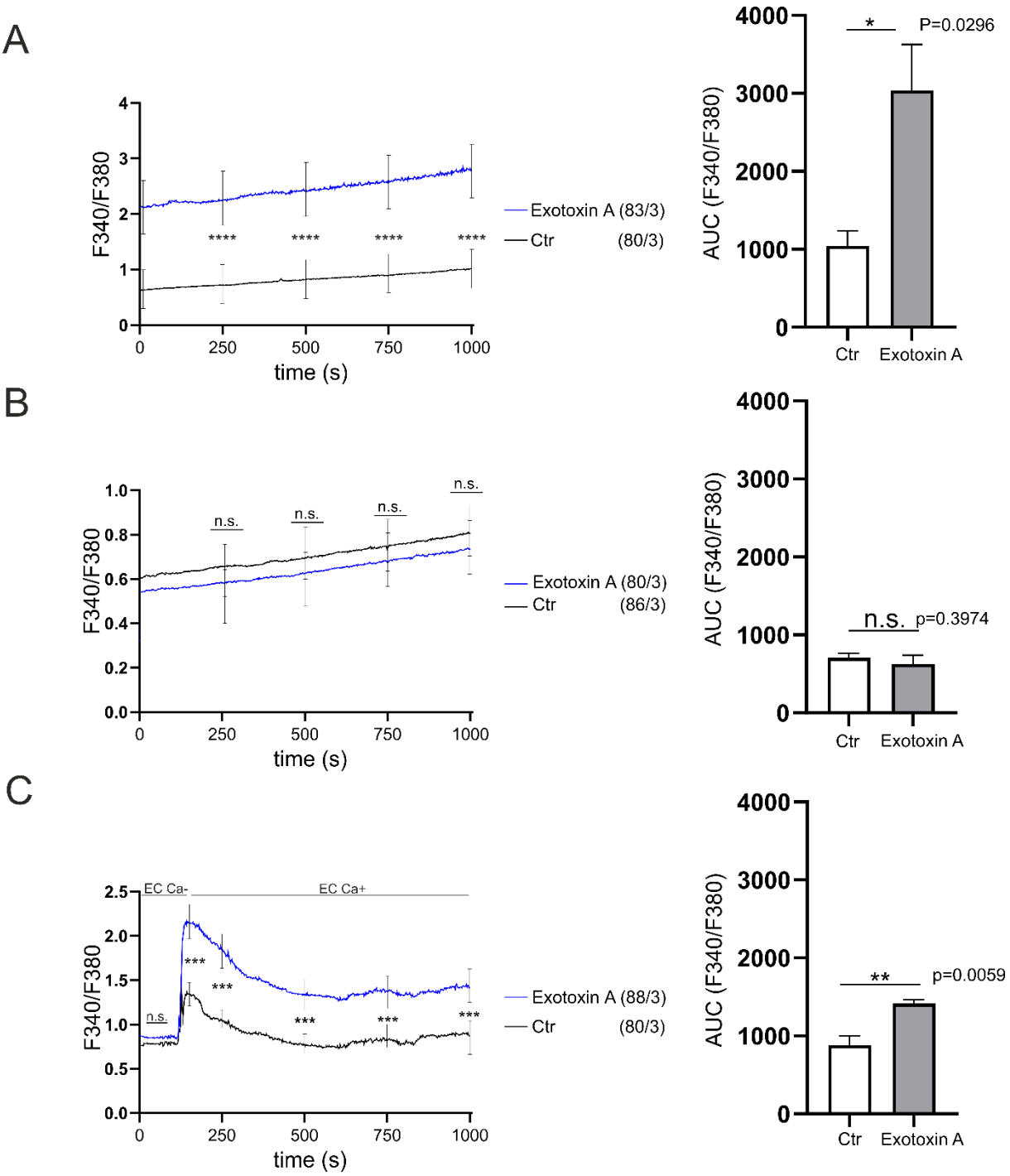

Figure 4. 13: Exotoxin A induces calcium influx from extracellular environment
(A-C) A549 cells were grown on a poly-L-lysine coated glass coverslips until 70% confluence and stimulated with Exotoxin A (4 h, 100 ng/ml) in (A) Tyrode's solution (+ $CaCl_2$) or (B,C) Tyrode's solution (- $CaCl_2$). Subsequently, the cells were incubated with 5 µM Fura-2 AM for 45 min and recorded for calcium signaling in (A) Tyrode's solution with $CaCl_2$, (B) Tyrode's solution without $CaCl_2$ or (C) Tyrode's solution without $CaCl_2$, followed by an addition of 2 mM $CaCl_2$ after 2 min of recording. Quantitative data are presented as means +/- SD for F340/380 ratio and mean + SD for the area under the curve of three independent experiments. Asterisks reveal significance difference among groups at the shown time points analyzed using two-way ANOVA and Bonferroni post-test for F340/380 ratio and one-way ANOVA and Tukey post-test for area under the curve (* $p < 0.05$, ** $p < 0.001$, *** $p < 0.001$, **** $p < 0.0001$, n.s. not significant).

4.2 Functional implication of ADAM17 in lung infection *in vitro*

4.2.1 Pathogen-specific regulation of ADAM17 during infection of lung epithelial cells

As mentioned earlier, lung epithelium is one of the first line defenses against the exogenous pathogens, and disturbances in alveolar epithelium integrity can result in organ damage and systemic effects. Again, we evaluated the pathogen-specific regulation of ADAM17 in both A549 cells and HSAEpC.

Infection of A549 cells with the Gram-negative bacterium *P. aeruginosa* (4 h, MOI 5) induced expression and maturation of ADAM17, defined by an increase in both mature form (100 kDa) and proform (130 kDa) (figure 4.14 A). In contrast to *P. aeruginosa*, infection of A549 cells with the Gram-positive bacterium *S. pneumoniae* (4 h, MOI 5) induced no change in expression or maturation of ADAM17 (Figure 4.14 B). As it was observed earlier that bacterial released toxins participate in the regulation of proteases expression and activation, the regulation of ADAM17 during sterile inflammation mediated by Exotoxin A was investigated. Stimulation with Exotoxin A (4 h, 100 ng/ml) induced expression and maturation of ADAM17 in comparison to the non-stimulated control (Figure 4.14 C).

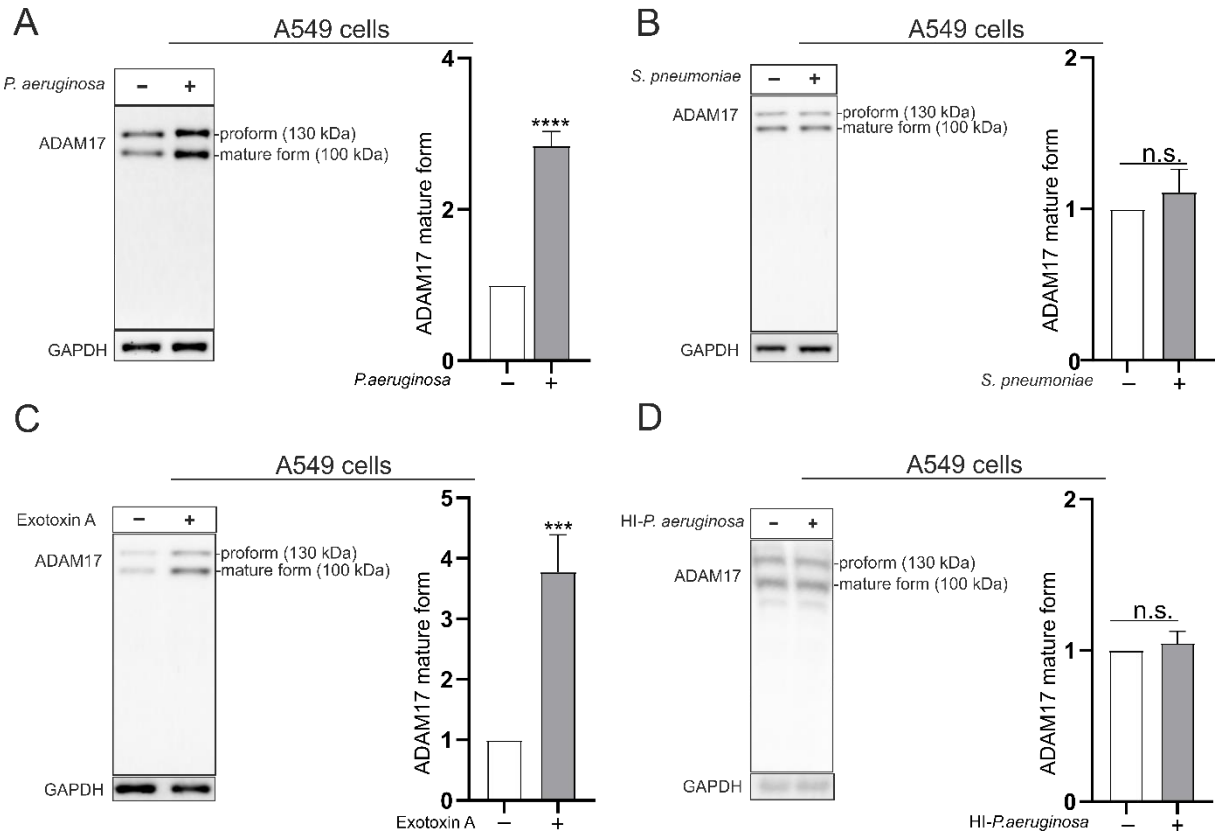

Figure 4. 14: Pathogen-specific regulation of ADAM17 in A549 cells during infection.
(A-D) A549 cells were grown in standard medium and infected with (A) *P. aeruginosa* (4 h, MOI 5), (B) *S. pneumoniae* (4 h, MOI 5), (C) stimulated with Exotoxin A (4 h, 100 ng/ml) or (D) infected with heat-inactivated *P. aeruginosa* (4 h, MOI 5). (A-D) ADAM17 expression and maturation was analyzed in the cell lysate by Western blot using an antibody against the C-terminal domain. GAPDH served as loading control. Band intensity was quantified by densitometry relative to non-infected/non-stimulated cells. Quantitative data are presented as means + SD of three independent experiments. Asterisks reveal significance difference relative to the control analyzed using two tailed two samples t-test (*** $p < 0.001$, **** $p < 0.0001$, n.s. not significant).

To investigate the role of *P. aeruginosa* particle itself in regulating the expression and maturation of ADAM17, *P. aeruginosa* was subjected to heat-inactivation under mild and optimal conditions (70 °C for 40 min) to ensure bacterial death without affecting the released toxins (Rabiei et al., 2019). Infection of A549 cells with heat-inactivated *P. aeruginosa* had no impact on the expression/maturation of ADAM17 (figure 4.14 D). In HSAEPC as primary cells, the same pattern of regulation was observed (figure 4.15 A, B and C).

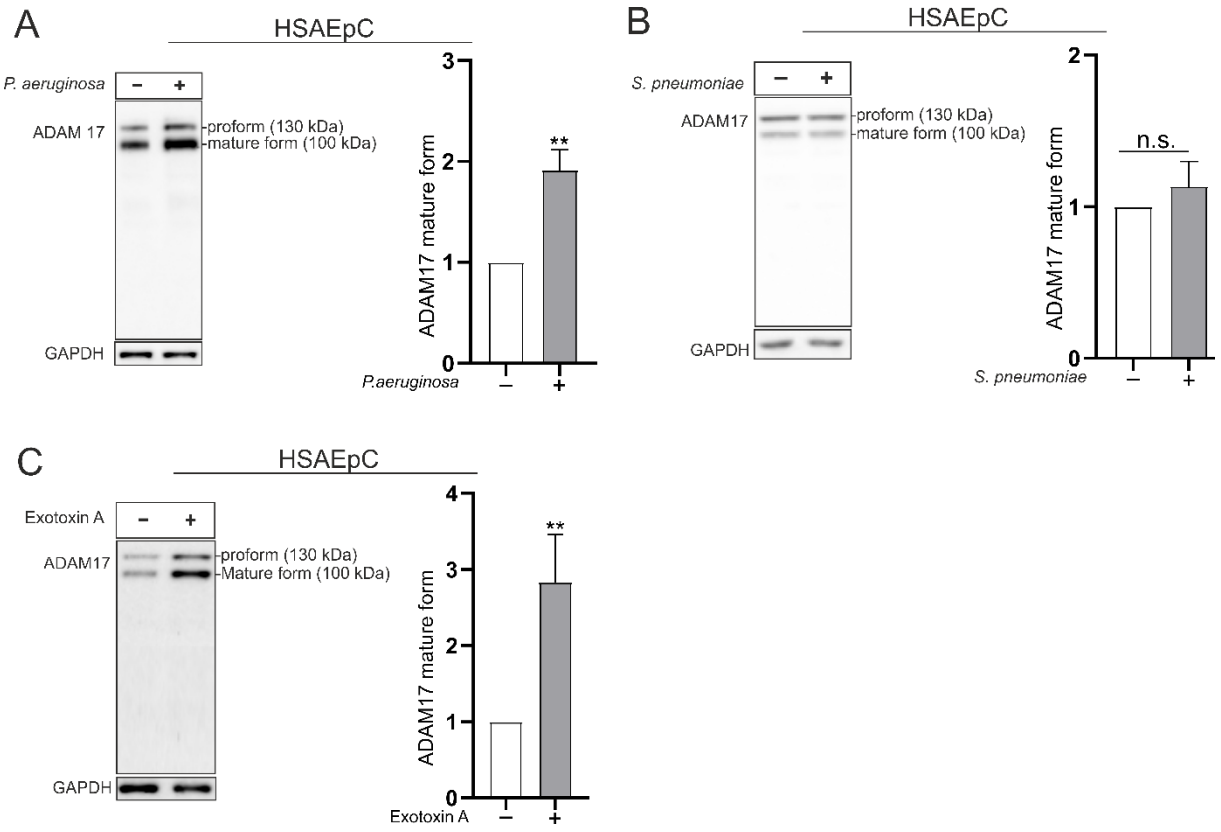

Figure 4. 15: Pathogen-specific regulation of ADAM17 in HSAEpC cells during infection.
(A-C) HSAEpC were grown in MV2 medium and infected with (A) *P. aeruginosa* (4 h, MOI 5), (B) *S. pneumoniae* (4 h, MOI 5) or (C) stimulated with Exotoxin A (4 h, 100 ng/ml). (A-C) ADAM17 expression and maturation was analyzed in the cell lysate by Western blot using an antibody against the C-terminal domain. GAPDH served as loading control. Band intensity was quantified by densitometry relative to non-infected/non-stimulated cells. Quantitative data are presented as means + SD of three independent experiments. Asterisks reveal significance difference relative to the control analyzed using two tailed two samples t-test (** $p < 0.01$, n.s. not significant).

4.2.2 *P. aeruginosa* and Exotoxin A induce ADAM17 shedding activity

To investigate the functional implications on the ADAM17 activity level, the ADAM17-mediated ectodomain shedding was investigated in response to *P. aeruginosa* and Exotoxin A at the time points that were correlated with the change in expression and maturation. The catalytic activity of ADAM17 was investigated by the cleavage of alkaline phosphatase tagged transforming growth factor-alpha (AP-TGF-α) (Inoue et al., 2012). Infection with *P. aeruginosa* (4 h, MOI 5) or stimulation with Exotoxin A (4 h, 100 ng/ml) significantly increased AP-TGF-α release to the supernatant compared to non-

infected/non-stimulated control (Figure 4.16 A and B). Pre-treatment with TAPI-1 as a specific inhibitor of ADAM17 significantly reduced this release (Figure 4.16 A and B). Although the increase in AP-TGF-α cleavage during Exotoxin A stimulation was lower, the levels were comparable to the release mediated by PMA, which is considered one of the strongest activators of ADAM17 (Figure 4.16 C). Infection with *S. pneumoniae* had no effect on ADAM17 activity (Figure 4.16 D). Thus, *P. aeruginosa* and its released toxin Exotoxin A increase ADAM17 catalytic activity in lung epithelial cells.

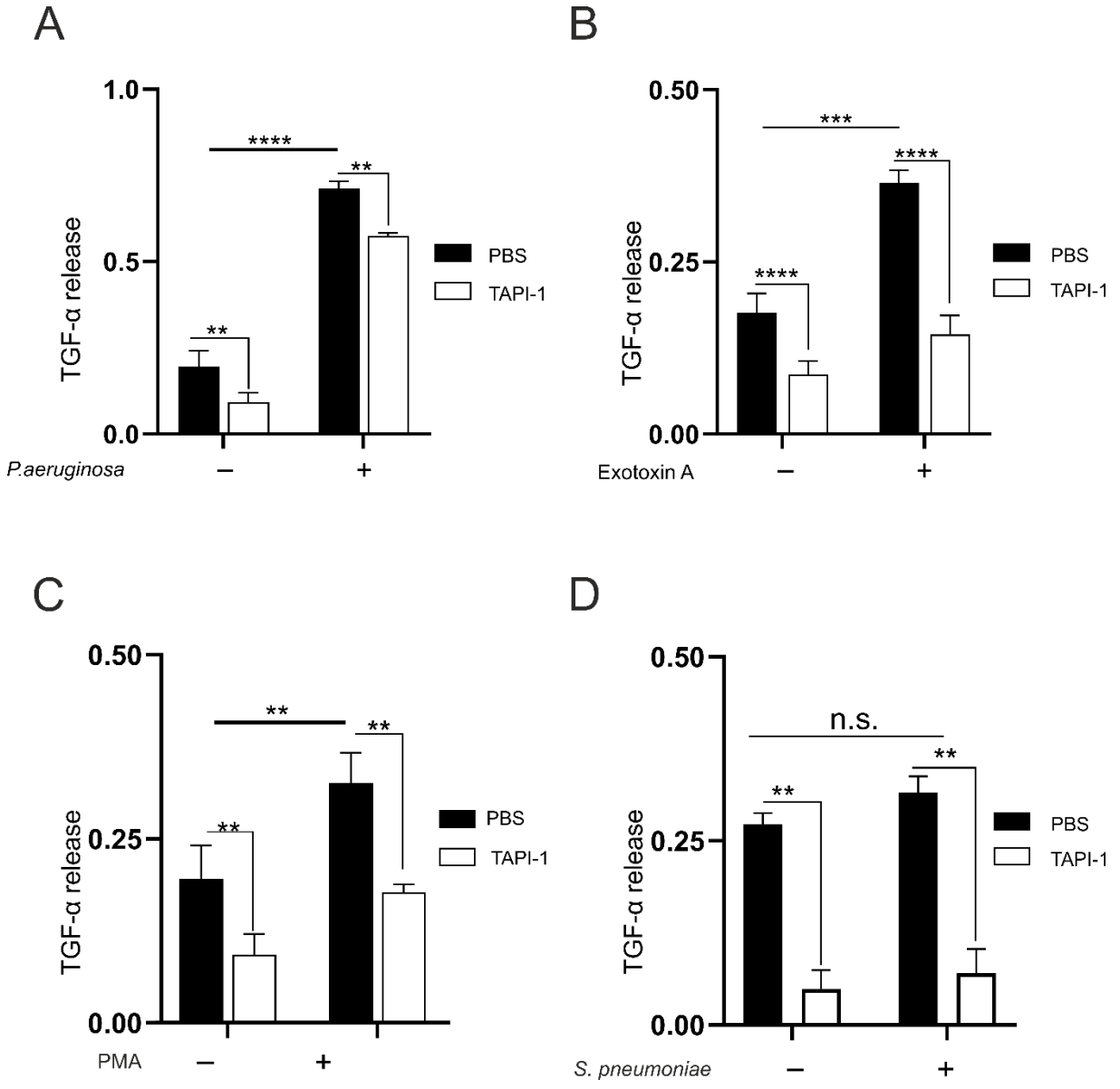

Figure 4. 16: *P. aeruginosa* and Exotoxin A induce activation of ADAM17.
(A-D) A549 cells were transfected with AP-TGF-α. The cells were incubated with 0.1% DMSO or 10 µM TAPI-1 for 30 min followed by infection with (A) *P. aeruginosa* a (4 h, MOI 5), (B) stimulation Exotoxin A (4 h, 100 ng/ml), (C) stimulation with PMA (1 h, 1 µM) or (D) infection with *S. pneumoniae* (4 h, MOI 5). The activity of AP was determined in both cell lysate and supernatant and shown as a ratio of the slope of AP activity in the supernatant to the total activity (lysate and supernatant). (A–D) Data are presented as means + SD of three independent experiments. Asterisks reveal significance among groups analyzed by two-way ANOVA and Tukey post-test (** $p < 0.01$, *** $p < 0.001$, **** $p < 0.0001$, n.s. not significant).

4.2.3 *P. aeruginosa* induces no exocytic release of ADAM17

I have reported earlier in this thesis that *P. aeruginosa* induced an exocytic release of active ADAM10 in exosomes (Aljohmani et al., 2022b). To test if this also holds true for ADAM17, the expression of ADAM17 in EVs and in further purified exosomes from infected and non-infected A549 cells was probed. In contrast to ADAM10, neither the mature form nor the proform of ADAM17 could be detected in extracellular vesicles or in exosomes (Figure 4.17 A and B).

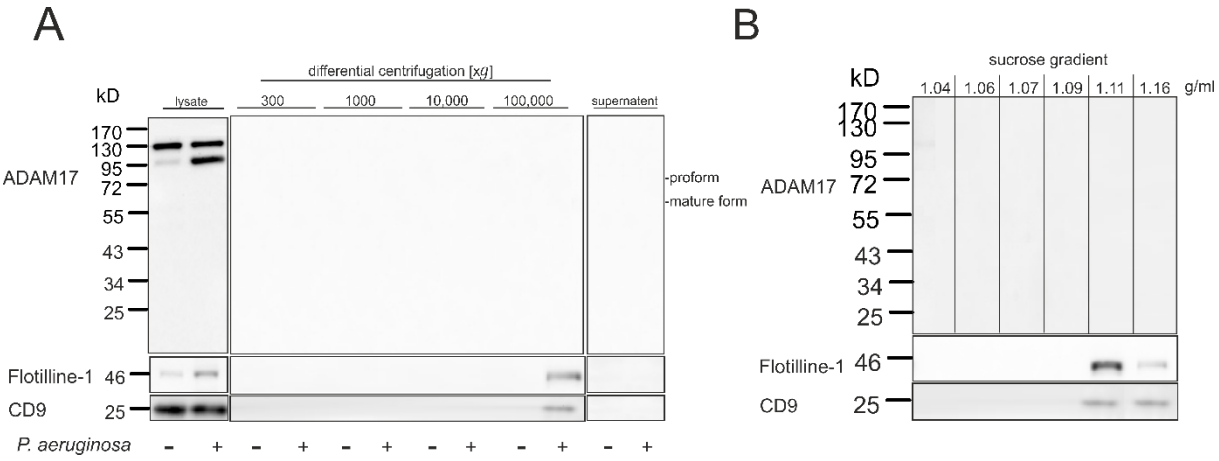

Figure 4. 17: *P. aeruginosa* induces no release of ADAM17 in extracellular vesicles or exosomes.
2×10^7 of A549 cells were grown in serum free medium and infected with *P. aeruginosa* (2 h, MOI 5). Subsequently, the cells were lysed, and the medium was assigned for different centrifugation steps as indicated. (A) The pellet of each centrifugation step was lysed with SDS buffer, and the expression of ADAM17 (antibody against the C-terminal domain), Flottilin-1 and CD9 were analyzed by Western blot. (B) The extracellular vesicles (100,000xg) were collected by sterile PBS and loaded to a sucrose gradient comprising layers to be separated according to the density. The expression of ADAM17 (C-terminal domain), Flottilin-1 and CD9 in each layer were analyzed by western blot. Representative blot of three independent experiments are shown.

4.2.4 *P. aeruginosa* and Exotoxin A induce epithelial permeability mediated by ADAM17

To test the role of epithelial ADAM17 in modulating protein permeability during *P. aeruginosa* infection, A549 cells were grown on trans-well system until forming a monolayer and infected with *P. aeruginosa* (4 h, MOI 5) or stimulated with Exotoxin A (4 h, 100 ng/ml). Total and paracellular permeability were evaluated by the diffusion of FITC-albumin and TRITC-dextran, respectively. ADAM17 gene silencing/knockdown (knockdown efficiency controlled by Western blot (figure 4.18 A)) or pharmacological inhibition suppressed the increase in total and paracellular permeability mediated by *P. aeruginosa* or Exotoxin A (figure 4.18 B-E).

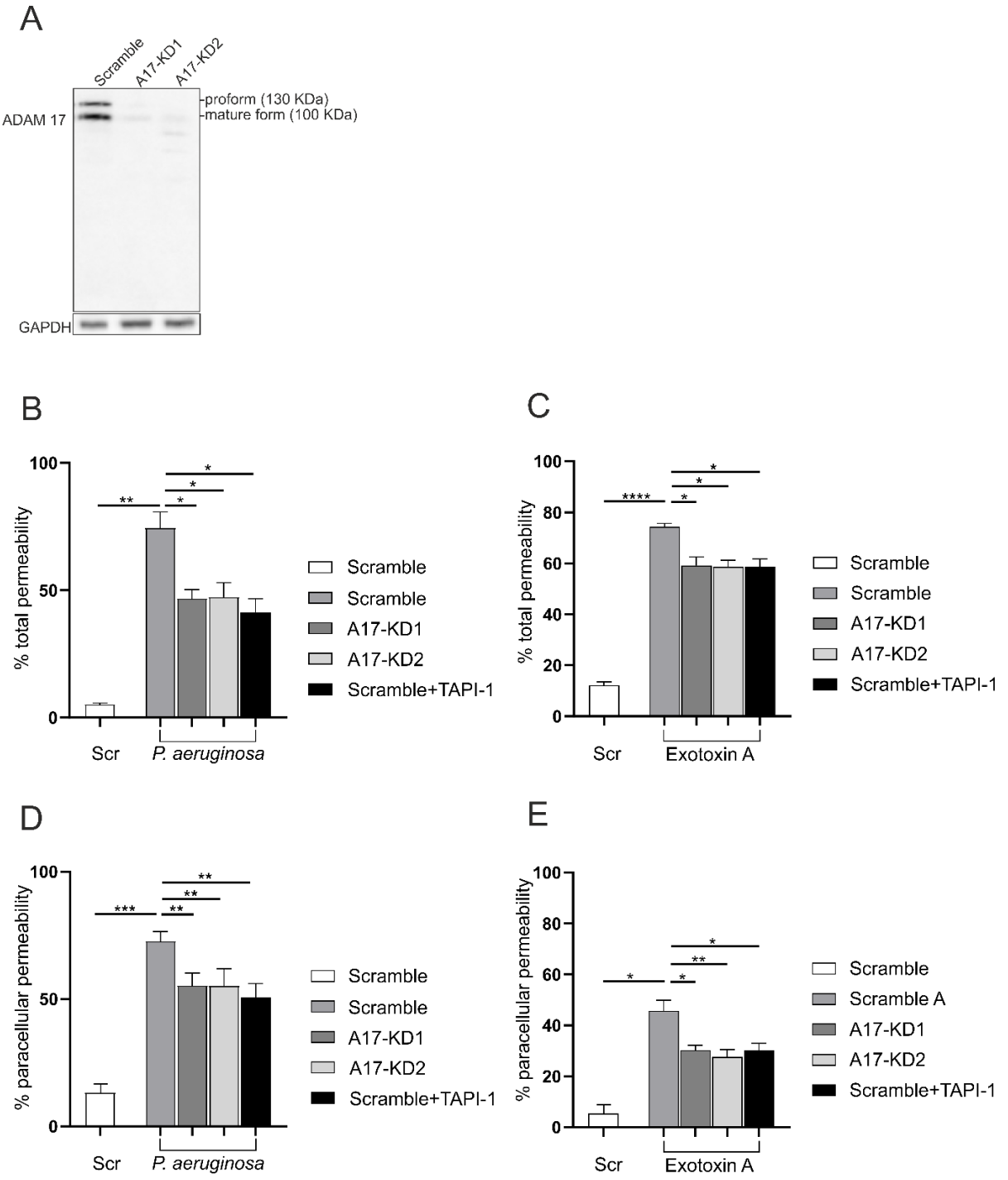

Figure 4. 18: *P. aeruginosa* and Exotoxin A induce epithelial permeability mediated by ADAM17.
(A-E) A549 cells were transduced with lentiviral particles for delivery of shRNA-carrying vectors for gene silencing of ADAM17 (A17-KD1 and A17-KD2). An unspecific shRNA (scramble) served as control. (A) ADAM17 expression was analyzed in the cell lysate by Western blot to confirm the knockdown using an antibody against the C-terminal domain. GAPDH served as loading control. (B-E) A549 cells were grown on a trans-well system until forming a monolayer, incubated with 0.1% DMSO or 10 µM TAPI-1 for 30 min, followed by infection with *P. aeruginosa* (B/D, 4 h, MOI 5), or stimulation with Exotoxin A (C/E,4 h, 100 ng/ml). Subsequently, the medium in the upper chamber was replaced by a suspension of both 70 kDa TRITC-dextran (1 mg/ml) and FITC-albumin (0.25 mg/ml). After 90 min, paracellular and total permeability were determined. Data are presented as means + SD of three independent experiments. Asterisks reveal significance among groups analyzed by two-way ANOVA and Tukey post-test (* $p < 0.05$, **$p < 0.01$, *** $p < 0.001$, **** $p < 0.0001$).

4.2.5 ADAM17 mediates ectodomain shedding of junctional molecules regulating epithelium wound healing

Severe pneumonia can end up in epithelial tissue damage. Stimulation with Exotoxin A decreased the closure of the wounded scratch area by about 45% (Figure 4.19 A and B) in comparison to the non-stimulated control. Interestingly, gene silencing or pharmacological inhibition of ADAM17 significantly improved the wound closure by almost 25% (Figure 4.19 A and B).

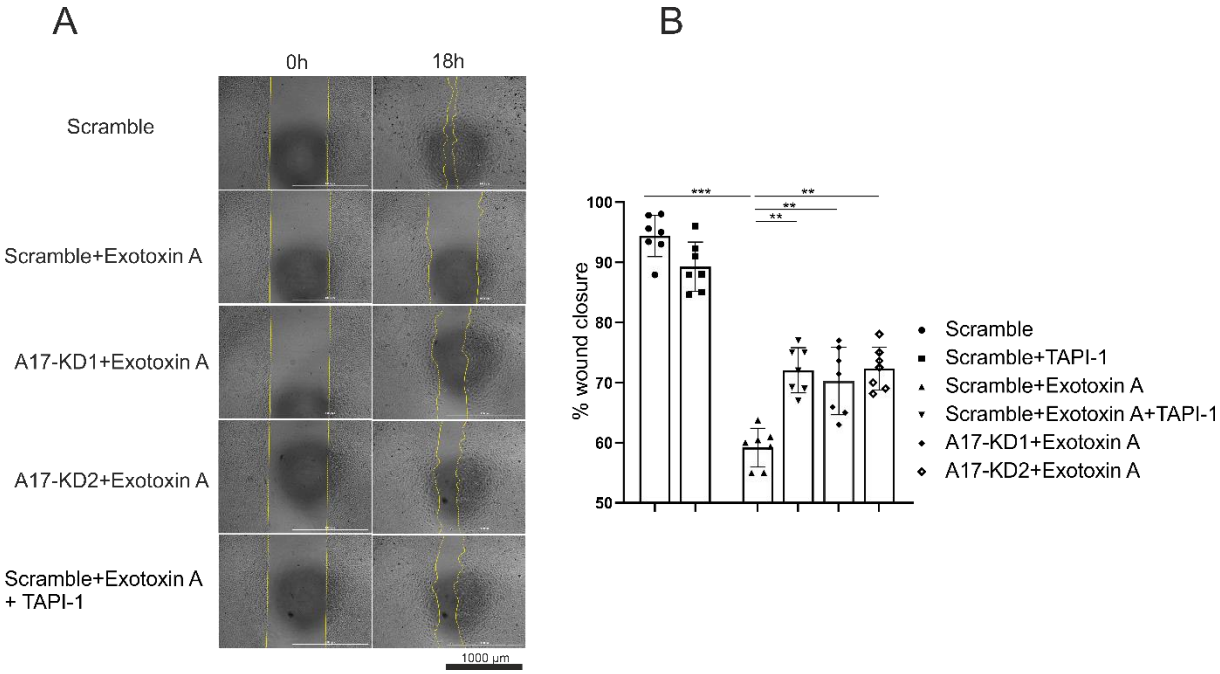

Figure 4. 19: Role of ADAM17 in epithelium regeneration.
(A-B) A549 cells were transduced with lentiviral particles for delivery of shRNA-carrying vectors for gene silencing of ADAM17 (A17-KD1 and A17-KD2). An unspecific shRNA (scramble) served as control. The cells were incubated with mitomycin for 2 and 0.1% DMSO or 10 µM GI254023X for 30 min, followed by stimulation with Exotoxin A (4 h, 100 ng/ml). (A) Representative images are shown. (B) Data are presented as means +/- SD of six independent experiments. Asterisks indicate significance between groups analyzed by one-way ANOVA and Tukey post-test (**p < 0.01*** p < 0.001).

Junctional and adhesion molecules maintain the integrity of the barrier through a tight cell-cell interaction (Tsukita et al., 2001). Ectodomain shedding of junctional molecules during infection can result in impairment of cellular interaction and consequently tissue uniformity. Therefore, the shedding activity of ADAM17 on JAM-A was investigated. Both *P. aeruginosa* (4 h, MOI 5) and Exotoxin A (4 h, 100 ng/ml) induced the cleavage of JAM-A as demonstrated by a decrease in the full-length form (44 kDa) (Figure 4.20 A-D). The decrease in the full-length protein was completely blocked by either gene silencing or pharmacological inhibition of ADAM17 (Figure 4.20 A-D).

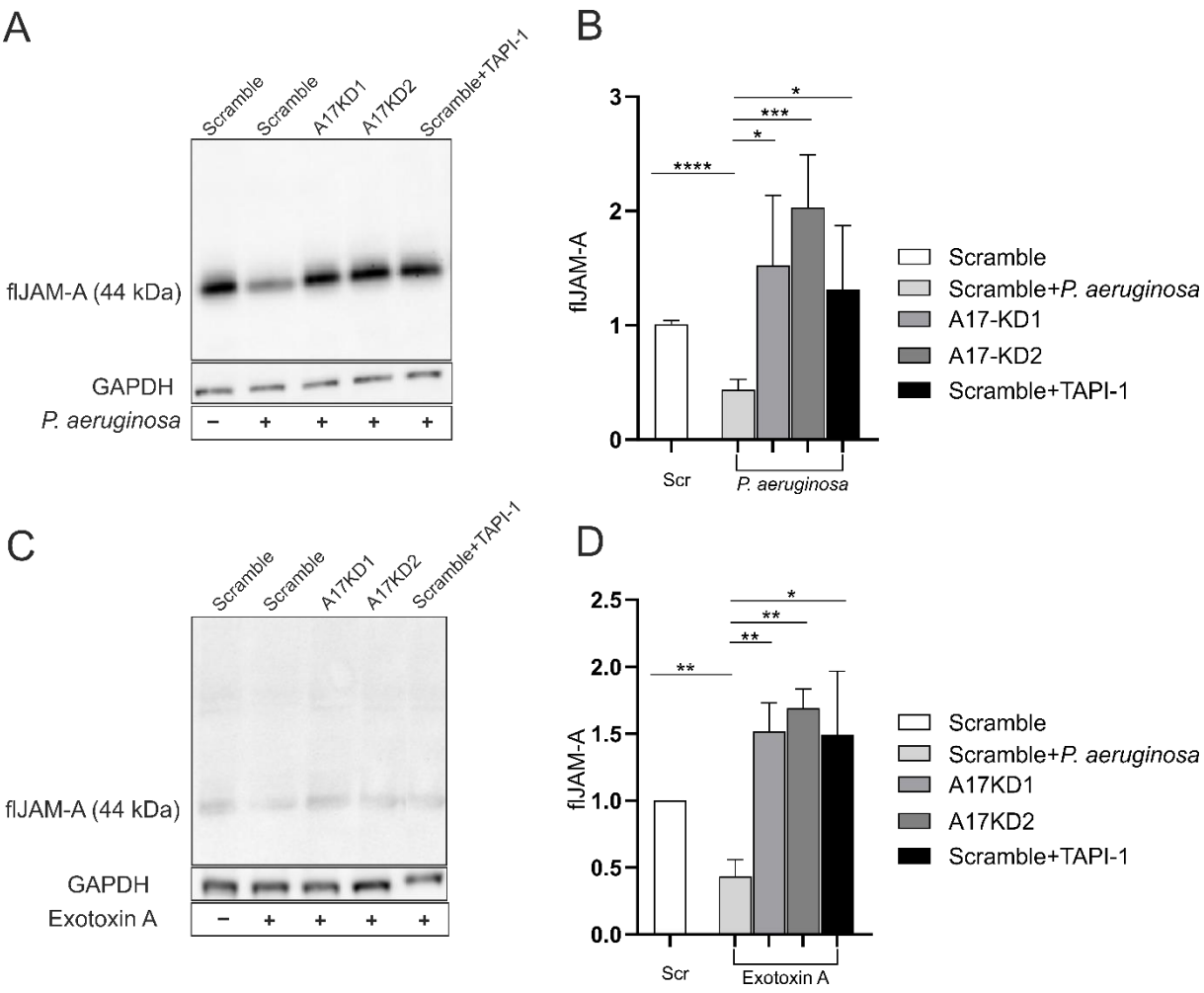

Figure 4. 20: *P. aeruginosa* and Exotoxin A induce activation of ADAM107 mediating JAM-A cleavage.
(A-D) A549 cells were transduced with lentiviral particles for delivery of shRNA-carrying vectors for gene silencing of ADAM17 (A17-KD1 and A17-KD2). An unspecific shRNA (scramble) served as control. The cells were incubated with 0.1% DMSO or 10 µM TAPI-1 for 30 min followed by (A,B) infection with *P. aeruginosa* (4 h, MOI 5) or (C,D) stimulation Exotoxin A (4 h, 100 ng/ml). JAM-A expression was analyzed in the cell lysate by Western blot using an antibody against the N-terminal domain. GAPDH served as loading control. (A,C) Representative blots are shown. Quantitative data are presented as means + SD of three independent experiments. Asterisks reveal significance difference relative to the control analyzed using two tailed two samples t-test (* $p < 0.05$, **$p < 0.01$, *** $p < 0.001$, **** $p < 0.0001$).

4.2.6 ADAM17 mediates transepithelial migration through enhanced leukocyte adhesion and improvement of epithelial survival

ADAM17 is known to regulate most of the leukocyte recruitment steps during inflammation (Dreymueller et al., 2012b). Also, in the present thesis, the transepithelial migration of THP-1 cells was significantly increased during infection with *P. aeruginosa* (4 h, MOI 5) in the presence (7x) or absence (5x) of the monocytes chemoattractant CCL2 (figure 4.21 A). Targeting ADAM17 by gene silencing or pharmacological inhibition significantly increased both random and CCL2-induced transepithelial migration of THP-1 cells (Figure 4.21 A). In contrast, stimulation with Exotoxin A (4 h, 100 ng/ml) induced weaker transmigration (2-4x) in comparison to infection. Further, no effect of ADAM17 knockdown or inhibition was observed (Figure 4.21 B).

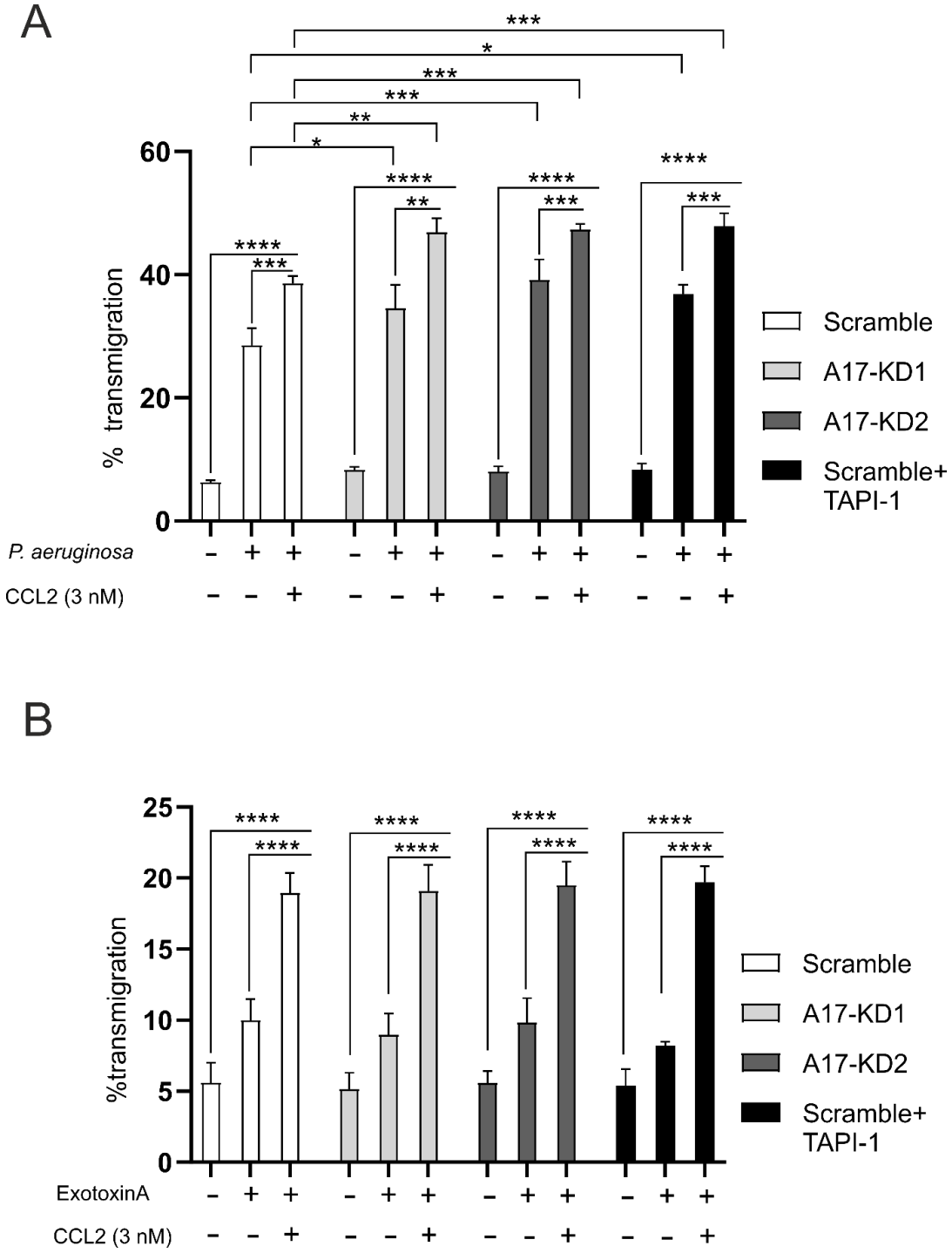

Figure 4. 21: *P. aeruginosa* induces THP-1 transepithelial migration mediated by ADAM17.
(A-B) A549 cells were transduced with lentiviral particles for delivery of shRNA-carrying vectors for gene silencing of ADAM17 (A17-KD1 and A17-KD2). An unspecific shRNA (scramble) served as control. The cells were grown on a trans-well system until forming a monolayer, incubated with 0.1% DMSO or 10 µM TAPI-1 for 30 min, followed by infection with *P. aeruginosa* (A, 4 h, MOI 5), or stimulation with Exotoxin A (B, 4 h, 100 ng/ml). Subsequently, THP-1 cells were added to the upper chamber and the transmigration was analyzed by measurement of endogenous β-glucuronidase activity. Data are presented as means + SD of three independent experiments. Asterisks reveal significance among groups analyzed by two-way ANOVA and Tukey post-test (*p < 0.05, **p < 0.01, *** p < 0.001, **** p < 0.0001).

Leukocytes adhesion is a crucial step preceding transmigration. Therefore, the role of epithelial ADAM17 on THP-1 cells adhesion during infection with *P. aeruginosa* (4 h, MOI 5) was investigated.

Epithelial cells infection with *P. aeruginosa* massively reduced THP-1 cell adhesion in comparison to the non-infected scramble control while, ADAM17 knockdown or pharmacological inhibition restored THP-1 adhesion (Figure 4.22 A and B).

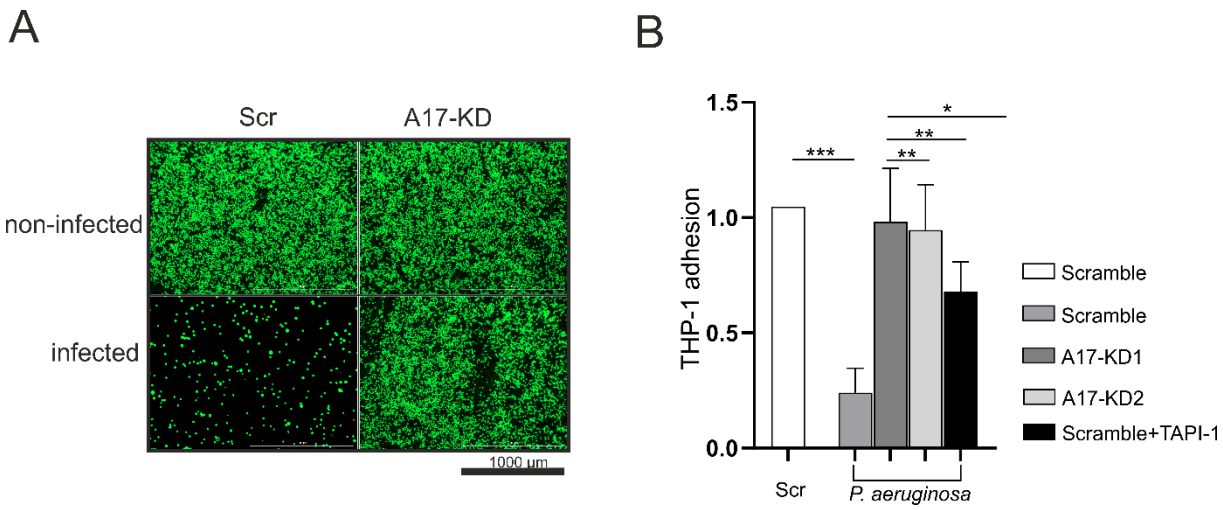

Figure 4. 22: *P. aeruginosa* induces THP-1 adhesion mediated by ADAM17.
(A-B) A549 cells were transduced with lentiviral particles for delivery of shRNA-carrying vectors for gene silencing of ADAM17 (A17-KD1 and A17-KD2). An unspecific shRNA (scramble) served as control. The cells were grown until forming a monolayer and incubated with 0.1% DMSO or 10 µM TAPI-1 for 30 min followed by infection with *P. aeruginosa* a (4 h, MOI 5). Subsequently, 5×10^5 of Calcein-AM labeled THP-1 cells were added to the A549 monolayer, the plate was centrifuged, washed 3 times with warm PBS and the fluorescence of the adhered cells was measured. Data are presented as means + SD of three independent experiments. Asterisks reveal significance among groups analyzed by one-way ANOVA and Tukey post-test (*p < 0.05, **p < 0.01, *** p < 0.001).

Thus, it seems feasible that the increase in THP-1 cell transepithelial migration during ADAM17 inhibition might be caused by an increase in THP-1 cell adhesion to epithelial cells. To test whether the increase in THP-1 adhesion to epithelial cells might be due to differences in epithelial cell survival, A549 cell survival was investigated during *P. aeruginosa* infection (4 h, MOI 5) and Exotoxin A stimulation (4 h, 100 ng/ml), respectively.

Live cell imaging revealed a strong increase in A549 cell death mediated by infection with *P. aeruginosa*, indicated by an increase in green cells and a decrease in red cells (Figure 4.23 A, B, C). Interestingly, pharmacological inhibition of ADAM17 by TAPI-1 significantly improved cell survival over time (Figure 4.23 A, B, C). However, neither Exotoxin A nor concomitant inhibition of ADAM17 by TAPI-1 had a significant effect on cell survival (Figure 4.23 D, E, F). In conclusion, in addition to cleavage of junctional and adhesion molecules, cell survival improvement due to inhibition of ADAM17 may explain the increase in THP-1 cells adhesion and transepithelial migration.

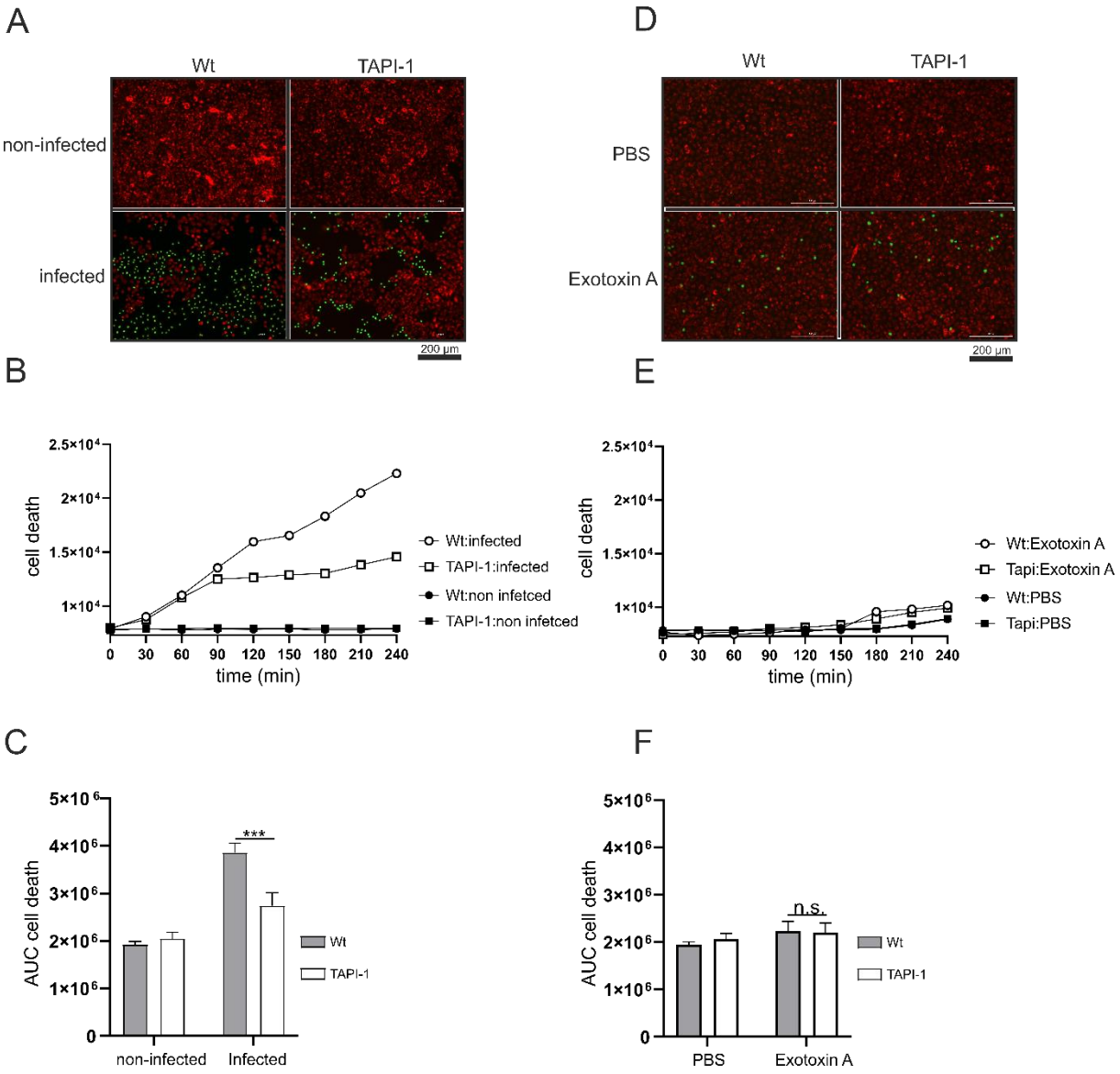

Figure 4. 23: ADAM17 inhibition promotes A549 cells survival during *P. aeruginosa* infection.
(A-F) A549 cells were grown in standard medium, stained with NucRed™ Live 647 for 15 min, pre-incubated with 0.1% DMSO or 10 µM TAPI-1 for 30 min, followed by (A,B,C) infection with *P. aeruginosa* (4 h, MOI 5) or (D,E,F) stimulation with Exotoxin A (4 h, 100 ng/ml) in the presence of SYTOX™ green. The fluorescence of SYTOX™ green and NucRed™ Live 647 was analyzed every 30 min. Data are shown as (A,D) representative images, (B,E) SYTOX™ green florescence over time and (C,F) area under the curve of SYTOX™ green of three independent experiments. Asterisks reveal significance among groups analyzed by two-way ANOVA and Tukey post-test (*** $p < 0.001$, n.s. not significant).

4.3 Functional implication of leukocytic ADAM10 and ADAM17 in *P. aeruginosa* mediated infection *in vitro* and *in vivo*

4.3.1 Exosomal release of ADAM10 and ADAM17 may drive disease severity during lung infection

Signaling, proteins and enzymes are all potential contents that can be transported by exosomes. TNF-α, ACE2 and ADAM17 have been shown to play a detrimental effect during COVID-19 infection (Hirayama et al., 2017; Jocher et al., 2022). Therefore, the activity of ADAM10 and ADAM17 released on exosomes during different stages of COVID-19 infection (mild symptoms and severe symptoms required ICU admission) was investigated. Exosomal activity of both ADAM10 and ADAM17 was significantly increased during COVID-19 infection (Figure 4.24 A and B, activity over time C and D). Interestingly, ADAM17 exosomal activity was significantly increased with increased disease severity (Figure 4.24 B and D), comparing hostitalized patients with milder symptoms and patients requiring intensive care.

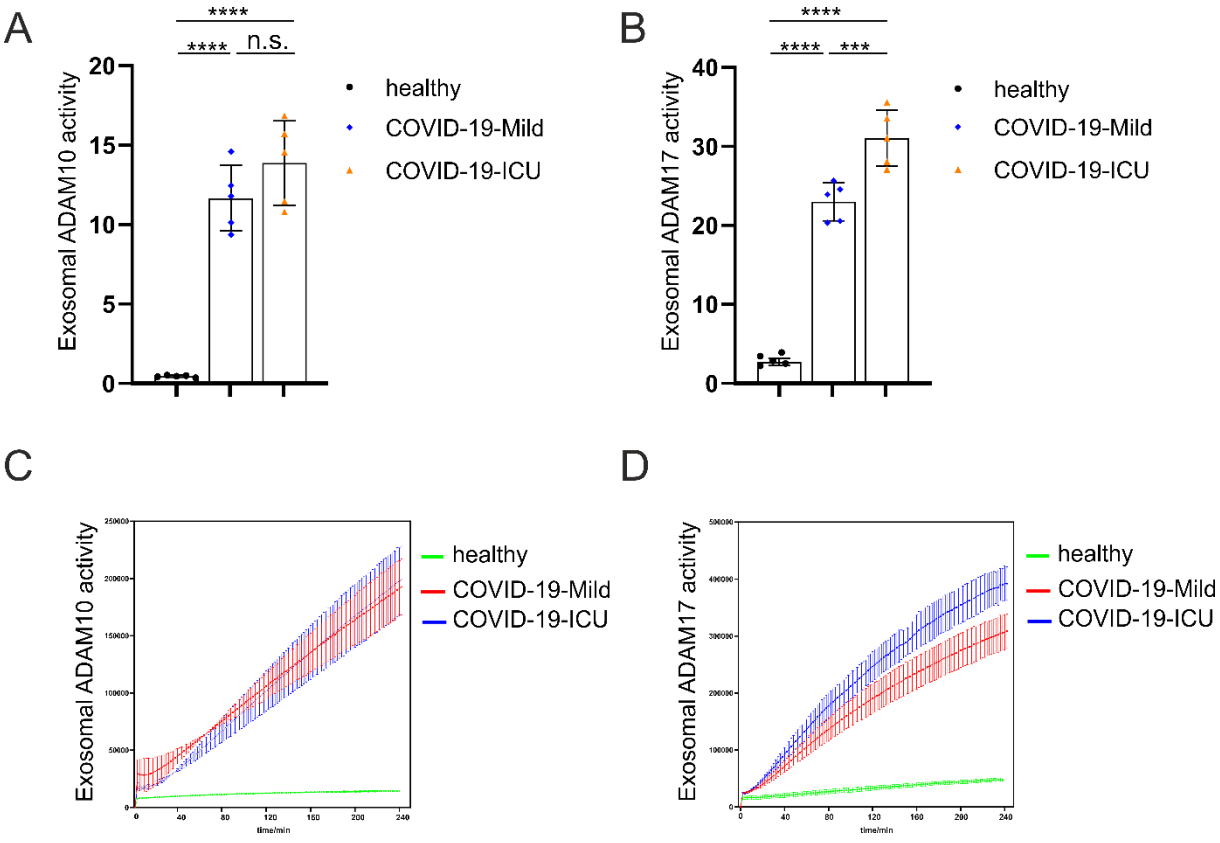

Figure 4. 24: ADAM10 and ADAM17 exosomal activity during COVID-19 infection
(A-D) The serum of healthy volunteers or COVID-19 patients were diluted in HBSS and assigned for different centrifugation steps. The extracellular vesicles (100,000xg) were collected by sterile PBS and loaded to a sucrose gradient comprising layers to be separated according to the density. The pellet was resuspended in DMEM medium (phenol red free) for FRET based activity measurements for ADAM10 and ADAM17. Data are presented as means +/- SD of the slope of the activity (A-B) or the activity over time (C-D) of five donors per group. Asterisks reveal significance among groups analyzed by one-way ANOVA and Tukey post-test (**** $p < 0.0001$).

To examine if this increase in the exosomal activity holds true for general hospital pneumonia or specific for viral/COVID-19 infection, sera of bacterial pneumonia patients were analyzed. The activity of both ADAM10 and ADAM17 were significantly increased on the circulating exosomes in comparison to healthy volunteers (Figure 4.25 A and B, activity over time C and D).

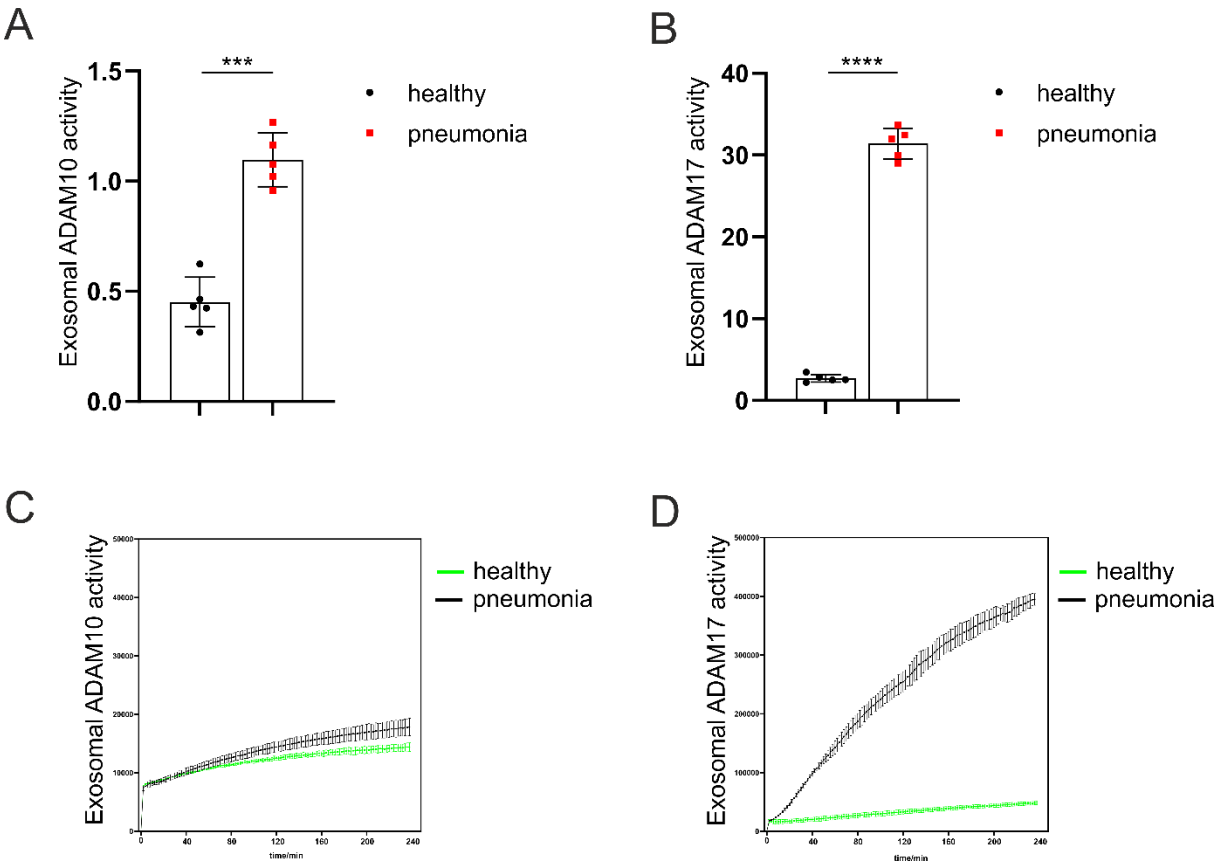

Figure 4. 25: ADAM10 and ADAM17 exosomal activity during pneumonia infection
(A-D) The serum of healthy volunteers or pneumonia patients were diluted in HBSS and assigned for different centrifugation steps. The extracellular vesicles (100,000xg) were collected by sterile PBS and loaded to a sucrose gradient comprising layers to be separated according to the density. The pellet was resuspended in DMEM medium (phenol red free) for FRET based activity measurements for ADAM10 and ADAM17. Data are presented as means +/- SD of the slope of the activity (A-B) or the activity over time (C-D) of five donors per group. Asterisks reveal significance among groups analyzed by one-way ANOVA and Tukey post-test (*** $p < 0.001$, **** $p < 0.0001$).

The collaboration of the lung epithelium and leukocytes builds the first line defense against the invading pathogens. As shown earlier in this thesis, active ADAM10 but not ADAM17 was released on exosomes upon infection of lung epithelial cells with *P. aeruginosa* (Aljohmani et al., 2022a; Aljohmani et al., 2022b). In order to investigate the potential source of exosomal activity of ADAM10 and ADAM17 in the serum of pneumonia patients, the expression and maturation of ADAM10 and ADAM17 in human neutrophils and THP-1 cells during infection with *P. aeruginosa* (2 h, MOI 5) were analyzed. In both cell types, a cellular increase of ADAM10 and decrease of ADAM17 was observed (Figure 4.26 A-D).

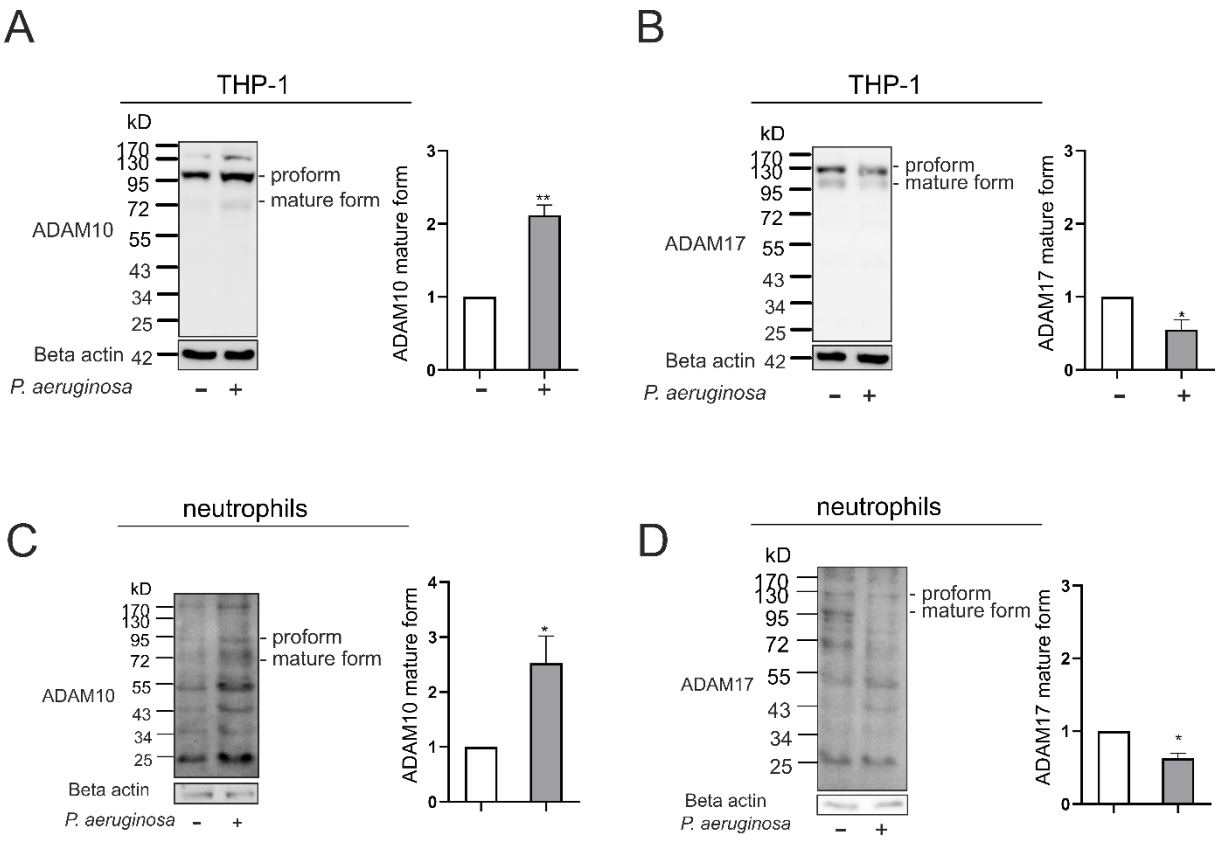

Figure 4. 26: Regulation of ADAM10 and ADM17 in human neutrophils and THP-1 cells during infection with *P. aeruginosa.*
(A-D) Human neutrophils or THP-1 cells were infected with *P. aeruginosa* (2 h, MOI 5). ADAM10 (A,C) or ADAM17 (B,D) expression and maturation were analyzed in the cell lyse by Western blot using an antibody against the C-terminal domain. Beta actin served as loading control. Band intensity was quantified by densitometry relative to non-infected cells. Quantitative data are presented as means + SD of three independent experiments. Asterisks reveal significance difference relative to the control analyzed using two tailed two samples t-test (* $p < 0.05$, ** $p < 0.01$).

Interestingly, infection with *P. aeruginosa* strongly increased the release of ADAM10 in exosomes derived from these cells, while it was absent in the non-infected control (Figure 4.27 A and B). ADAM17 expression in exosomes was increased up to 1.5-fold in the infected cells (Figure 4.27 C-F).

Next, we investigated the exosomal release of ADAM10 and ADAM17 at early time point of infection in a murine pneumonia model using mice lacking ADAM10 or ADAM17 in all hematopoietic cells (Vav-Adam10-/- mice or Vav-Adam17-/- mice). Pneumonia was induced by intranasal instillation of *P. aeruginosa* (10^5 CFU) for 12 h. Infection with *P. aeruginosa* increased ADAM10 but not ADAM17 activity on exosomes derived from serum of wildtype (littermate) mice compared to non-infected mice (Figure 4.28 A and B). The increase in ADAM10 exosomal activity due to infection was significantly reduced in Vav-Adam10$^{-/-}$ mice (figure 4.28 A). Interestingly, despite the lack of changes in ADAM17 activity during infection, Vav-Adam17$^{-/-}$ mice showed a decrease in basal ADAM17 activity on exosomes compared to littermate mice (Figure 4.28 B).

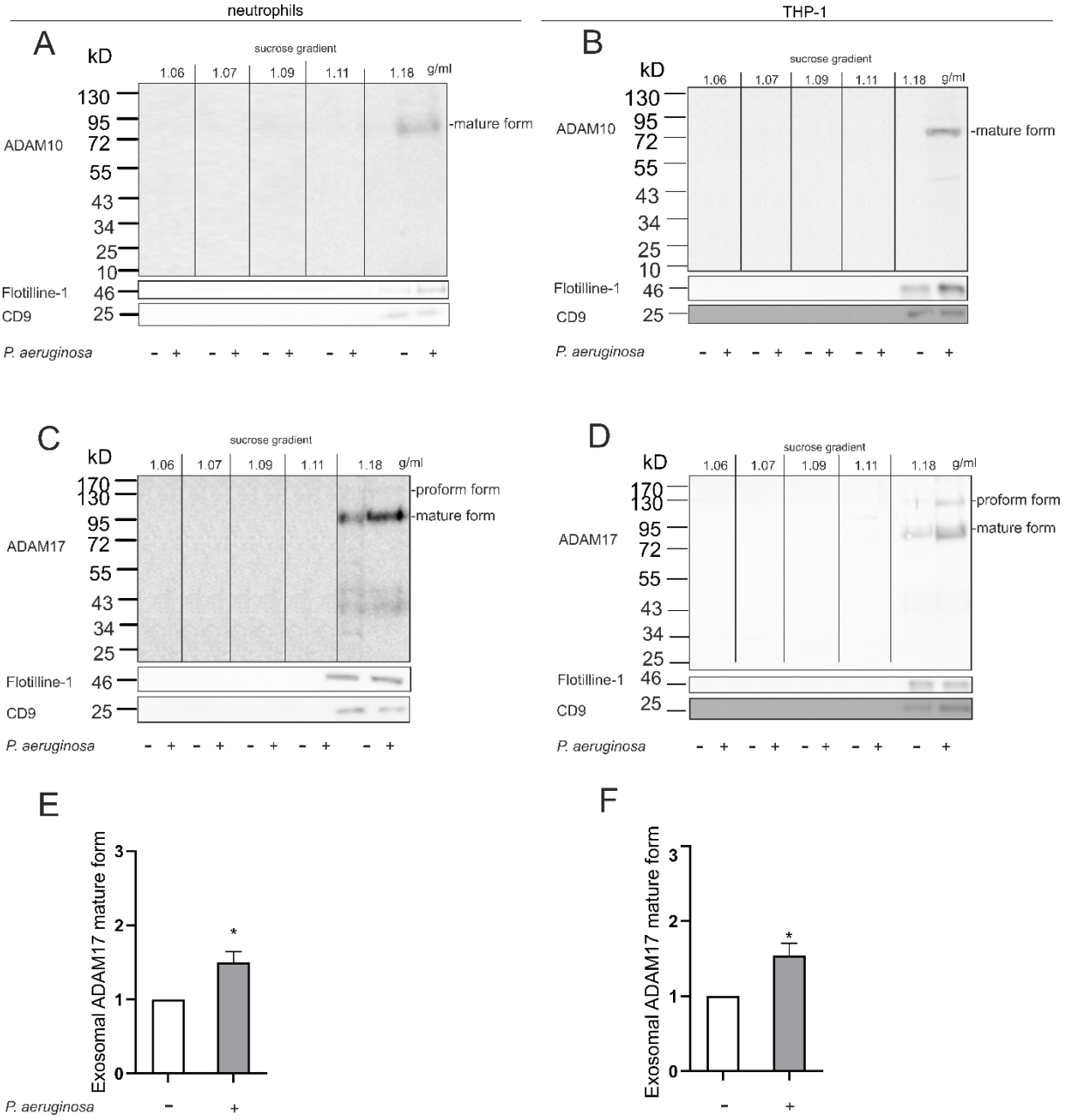

Figure 4. 27: *P. aeruginosa* induces release of ADAM10 and ADAM17 in exosomes derived from human neutrophils and THP-1 cells.

2×10^7 of human neutrophils or THP-1 cells were infected with *P. aeruginosa* (2 h, MOI 5). Subsequently, the cells were lysed and the medium was assigned for different centrifugation steps. The extracellular vesicles (100,000xg) were collected by sterile PBS and loaded to a sucrose gradient comprising layers to be separated according to the density. The pellet was resuspended in SDS buffer for Western blot analysis. The expression of ADAM10 (C-terminal domain), ADAM17 (C-terminal domain), Flottilin-1 and CD9 in each layer were analyzed by Western blot. Representative blots of three independent experiments are shown. Band intensity was quantified by densitometry relative to non-infected cells. Quantitative data are presented as means + SD of three independent experiments. Asterisks reveal significance difference relative to the control analyzed using two tailed two samples t-test (* $p < 0.05$).

The activity of ADAM10 and ADAM17 on exosomes was also displayed on the protein levels indicated by an increase in ADAM10 maturation in infected littermate compared to knockout mice, and a decrease in ADAM17 maturation in knockout mice comparing to littermate infected and non-infected mice (Figure 4.28 C and D). Thus, a high percentage of the exosomal activity of ADAM10 and ADAM17 seems to be derived from leukocytes.

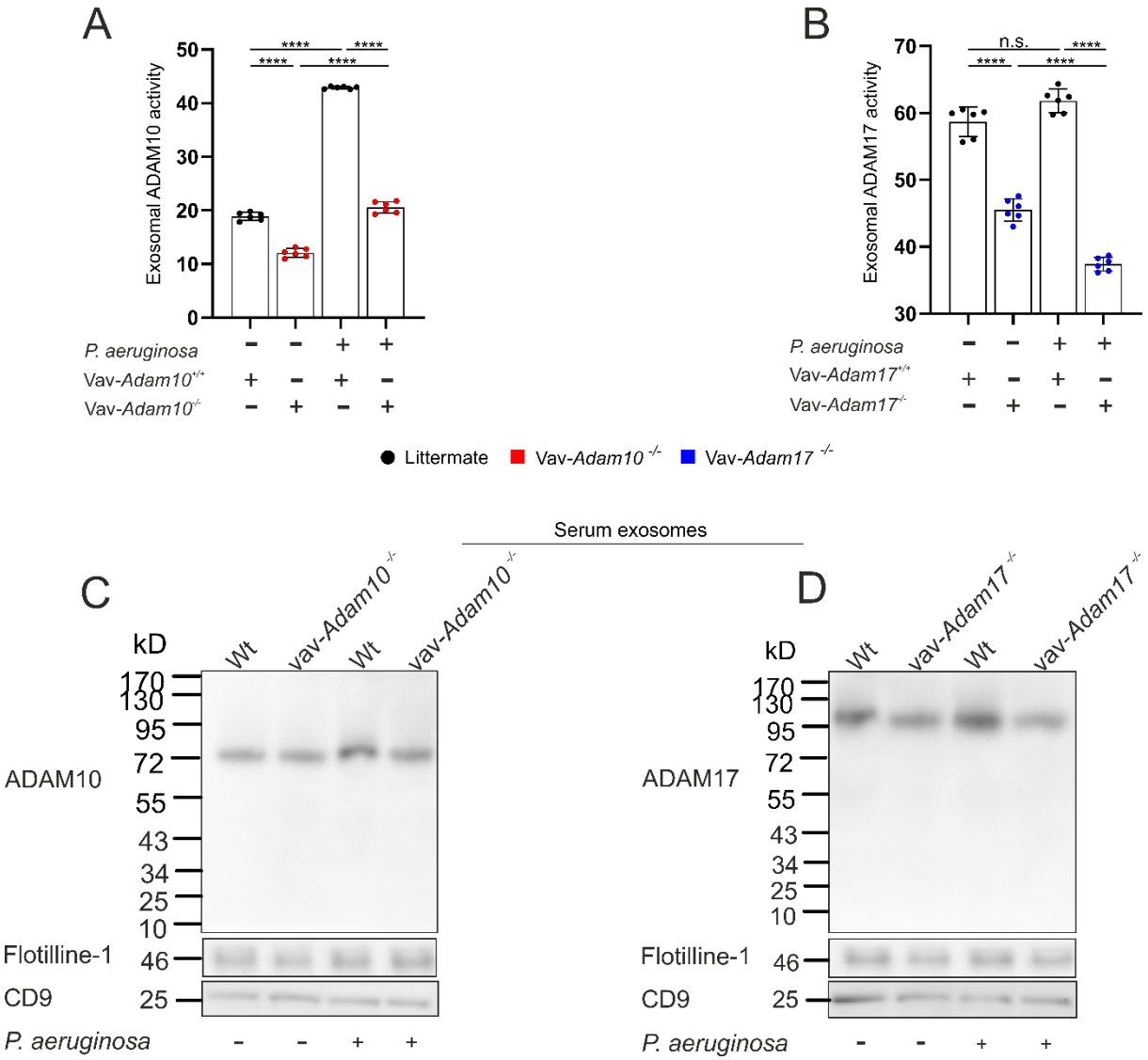

Figure 4. 28: ADAM10 and ADAM17 exosomal activity in the serum of murine model of *P. aeruginosa*-induced pneumonia
Littermates, Vav-*Adam10*$^{-/-}$ or Vav-*Adam17*$^{-/-}$ mice were infected with 10^5 CFU of *P. aeruginosa* (PA103) or PBS as control by intranasal instillation for 12 h. The serum of littermates, Vav-*Adam10*$^{-/-}$ or Vav-*Adam17*$^{-/-}$ mice was diluted in HBSS and assigned for different centrifugation steps. The extracellular vesicles (100,000xg) were collected by sterile PBS and loaded to a sucrose gradient comprising layers to be separated according to the density. The pellet was either resuspended in DMEM medium (phenol red free) for FRET based activity measurements for ADAM10 and ADAM17 (A-B) or resuspended in SDS buffer for Western blot analysis ©. (C) The expression of ADAM10 (antibody against the C-terminal domain), ADAM17 (antibody against the C-terminal domain), Flottilin-1 and CD9 in each layer were analyzed by Western blot. (A-B) Data are presented as means +/- SD of the slope of the activity of six mice per group or (C) representative blots of three independent experiments are shown. Asterisks reveal significance among groups analyzed by one-way ANOVA and Tukey post-test (**** $p < 0.0001$, n.s. not significant).

4.3.2 ADAM10 or ADAM17 in leukocytes regulate the severity of *P. aeruginosa* induced pneumonia

Vav-*Adam10*$^{-/-}$, Vav-*Adam17*$^{-/-}$ or littermate mice were further investigated to evaluate the effect of both proteases on the local and systemic inflammation. Both genotypes had no impact on basal phenotype as described previously (Pruessmeyer et al., 2014). M-CASS showed a significant decrease in pneumonia manifestations along with reduced hypothermia in Vav-*Adam10*$^{-/-}$ mice compared to infected littermates (figure 4.29 A). Interestingly, Vav-*Adam17*$^{-/-}$mice showed a significant increase in both parameters (Figure 4.29 B).

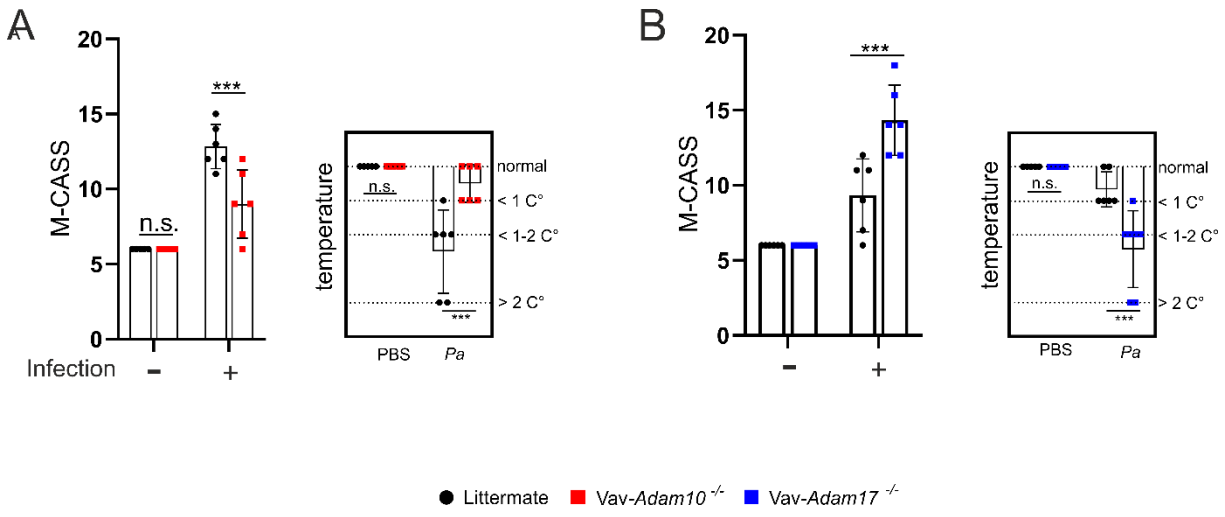

Figure 4. 29: Role of ADAM10 and ADAM17 in driving pneumonia severity
Littermates, Vav-*Adam10*$^{-/-}$ or Vav-*Adam17*$^{-/-}$ mice were infected with *P. aeruginosa* or PBS as a control by intranasal instillation for 12 h. (A-B) The severity of pneumonia and the development of fever were evaluated using GV-Solas scoring and M-CASS. Data are presented as means +/- SD of six mice per group. Asterisks reveal significance among groups analyzed by two-way ANOVA and Tukey post-test (***p < 0.001, n.s. not significant).

In correlation with reduced pneumonia manifestations, lung wet-dry-ratio and thickness of alveolar septa (indicators of lung edema development), as well as BAL protein (indicator of barrier disturbance) were significantly improved in Vav-*Adam10*$^{-/-}$ mice (figure 4.30 A, B and C). Again, Vav-*Adam17*$^{-/-}$ mice showed an increase in all parameters, which is in line with the increase in pneumonia severity (figure 4.30 A, B and C).

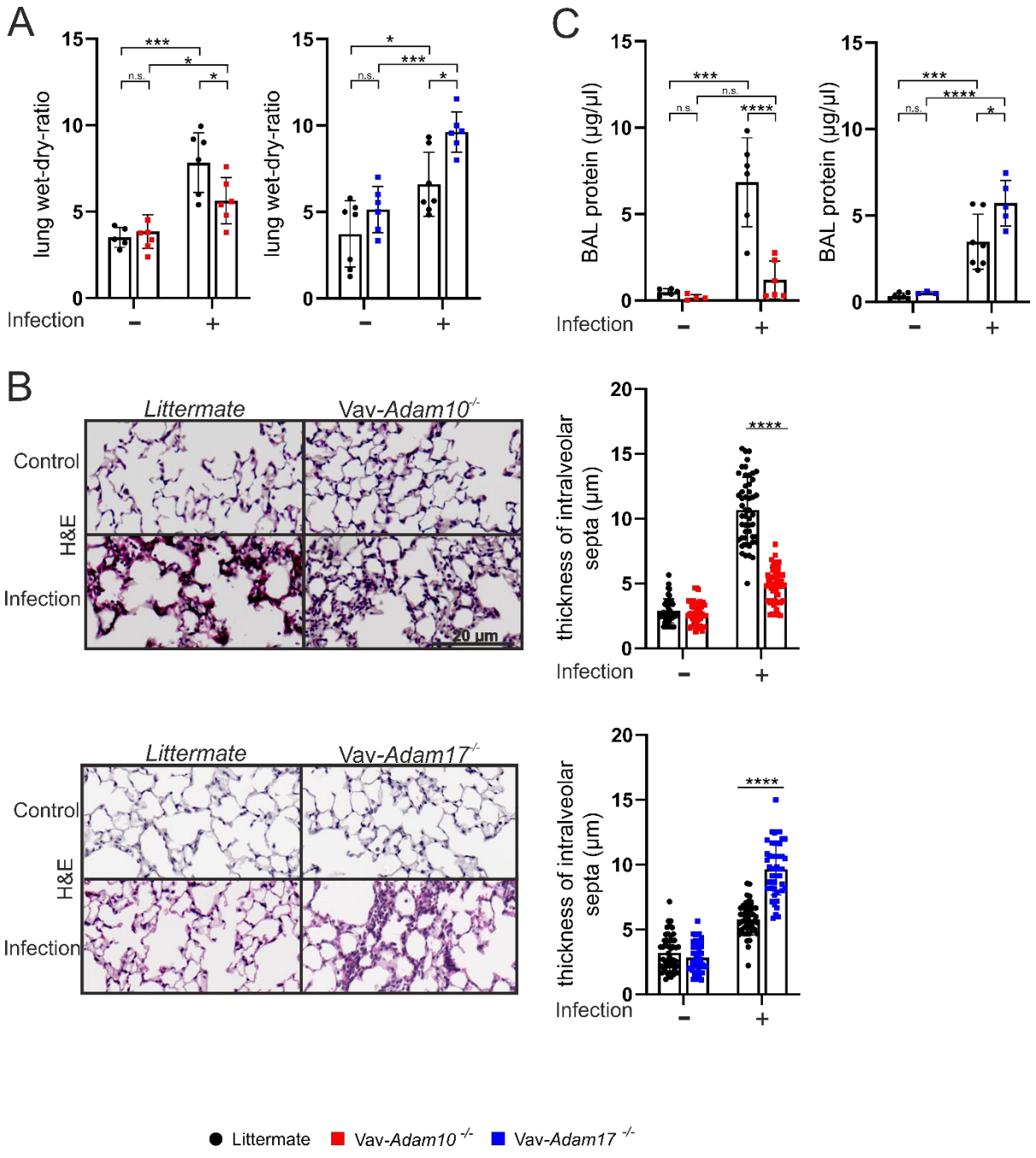

Figure 4. 30: Role of leukocytic ADAM10 and ADAM17 in barrier disruption during *P. aeruginosa*-induced pneumonia
Littermates, Vav-*Adam10*$^{-/-}$ or Vav-*Adam17*$^{-/-}$ mice were infected with *P. aeruginosa* or PBS as a control by intranasal instillation for 12 h. (A) Lung right auxiliary lob was used to determine wet-dry-ratio. (B) Lung left lob was embedded in paraffin, sliced into 5 µm sections and stained with hematoxylin-eosin to evaluate the thickness of interalveolar septa (thickness was evaluated in 10 random regions of interest for each section of each mouse, representative images are shown). (C) BAL protein content was quantified using BCA kit. Data are presented as means +/- SD of six mice per group. Asterisks reveal significance among groups analyzed by two-way ANOVA and Tukey post-test (*p < 0.05, ***p < 0.001, ****p < 0.0001, n.s. not significant).

Leukocyte recruitment to the site of infection is an important step for bacterial clearance, however, overshooting inflammation can result in permeant tissue damage. Flow cytometry analysis of BAL leukocyte content indicated reduced monocyte recruitment and similar neutrophil and macrophage count

in Vav-*Adam10*$^{-/-}$ mice in comparison to infected littermates (Figure 4.31 A). However, infection of Vav-*Adam17*$^{-/-}$mice showed a significant decrease in all cell types compared to littermates (Figure 4.31 B).

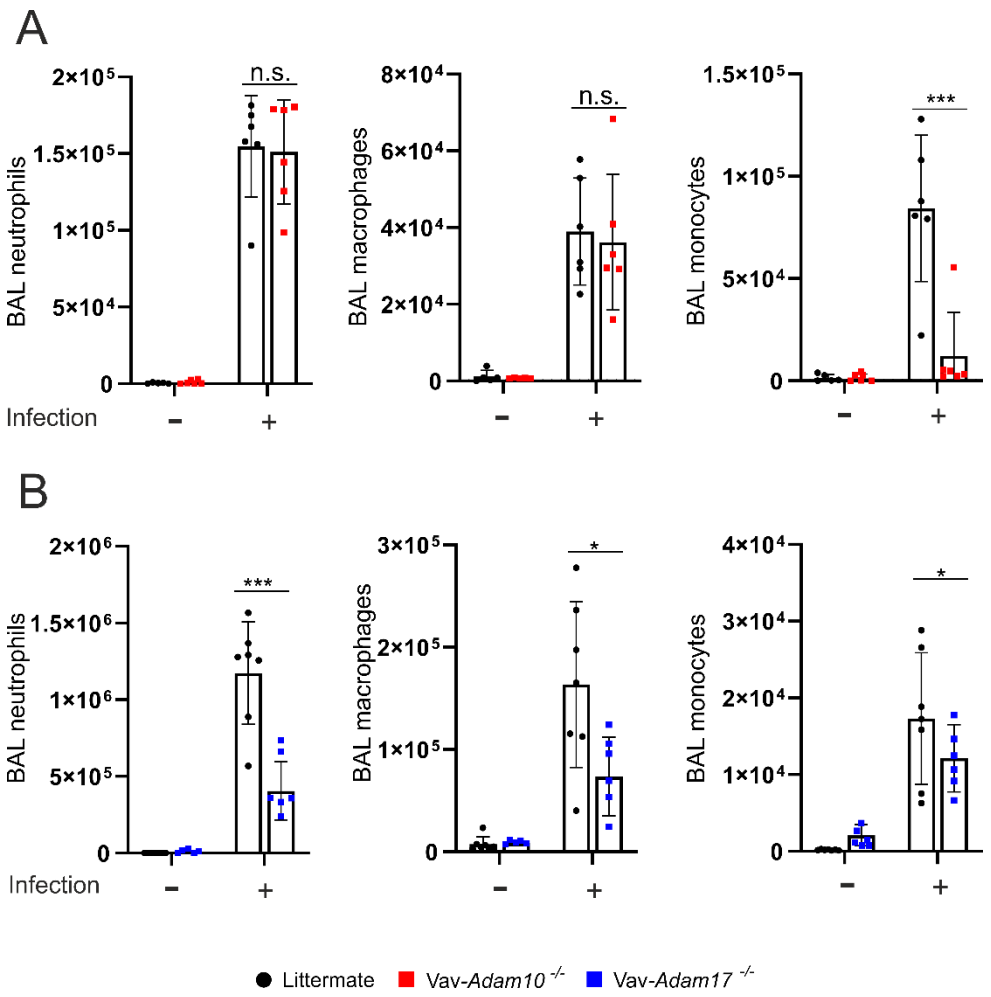

Figure 4. 31: Role of leukocytic ADAM10 and ADAM17 in leukocytes recruitment to alveolar space during *P. aeruginosa*-induced pneumonia
(A-B) Littermates, Vav-*Adam10*$^{-/-}$ or Vav-*Adam17*$^{-/-}$ mice were infected with *P. aeruginosa* or PBS as a control by intranasal instillation for 12 h. Cells of BAL were stained with FITC-conjugated monoclonal anti-mouse CD11b, eFluor450-conjugated monoclonal anti-mouse CD11c, PerCP-Cy5.5-conjugated monoclonal anti-mouse CD45, APC-conjugated monoclonal anti-mouse Ly6G and PE-Cy7-conjugated monoclonal anti-mouse F4/80 to evaluate the content of neutrophils, macrophages, and monocytes by flow cytometry. Data are presented as means +/- SD of six mice per group. Asterisks reveal significance among groups analyzed by two-way ANOVA and Tukey post-test (*p < 0.05, ***p < 0.001, n.s. not significant).

Despite the decrease in the monocyte content and similar numbers of neutrophils and macrophages in Vav-*Adam10*$^{-/-}$ mice, there was a significant decrease in the pro-inflammatory cytokines TNF-α, CXCL1, and IL-6 (Figure 4.32 A) upon infection. Vav-*Adam17*$^{-/-}$mice showed a significant decrease in TNF-α levels and similar CXCL1 and IL-6 levels (figure 4.32 B). In general, no basic differences in non-infected cells were observed.

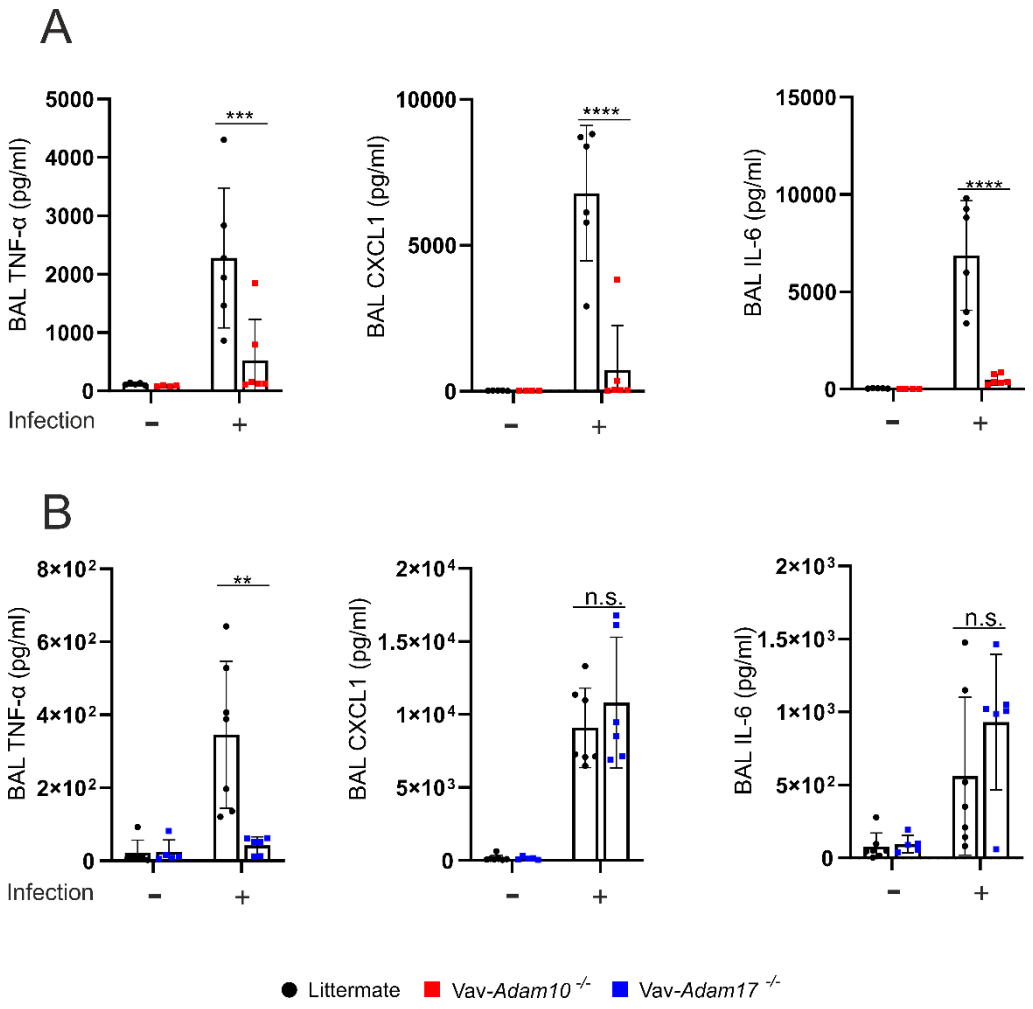

Figure 4. 32: Role of leukocytic ADAM10 and ADAM17 in alveolar cytokines release during *P. aeruginosa*-induced pneumonia
(A-B) Littermates, Vav-*Adam10*$^{-/-}$ or Vav-*Adam17*$^{-/-}$ mice were infected with *P. aeruginosa* or PBS as a control by intranasal instillation for 12 h. BAL was centrifuged at 16,000xg for 15 min and 4 °C, and the supernatant was used to analyze the BAL content of mTNF-α, mCXCL1 (KC) and mIL-6 using commercial ELISA kits following the manufacturers' protocol. Data are presented as means +/- SD of six mice per group. Asterisks reveal significance among groups analyzed by two-way ANOVA and Tukey post-test (**p < 0.01, ***p < 0.001, ****p < 0.0001, n.s. not significant).

Trafficking of leukocytes from blood, across the endothelium, to the site of infection is a key step regulating the inflammatory process. Flow cytometric analysis of blood cell samples showed a significant increase in neutrophils, monocytes and macrophages in both Vav-*Adam10*$^{-/-}$ and Vav-*Adam17*$^{-/-}$mice compared to infected littermates (Figure 4.33 A and B).

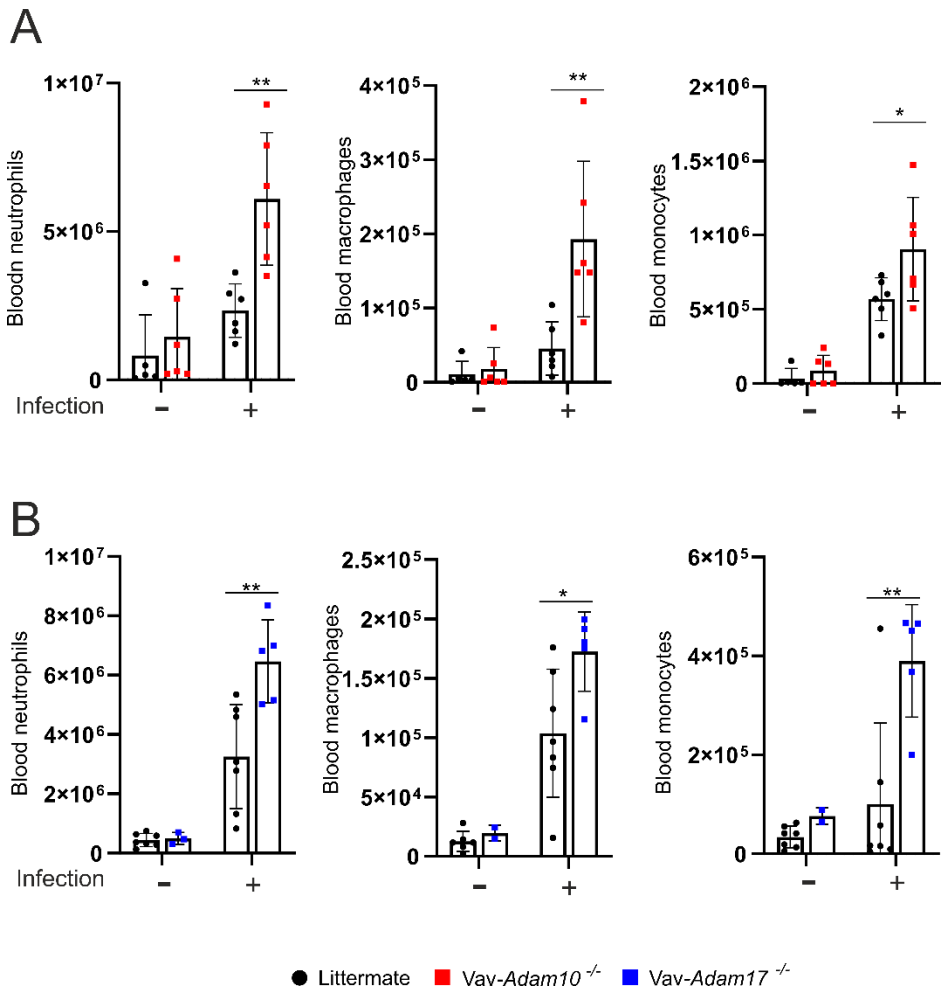

Figure 4. 33: Role of leukocytic ADAM10 and ADAM17 in leukocytes recruitment during *P. aeruginosa*-induced pneumonia

(A-B) Littermates, Vav-*Adam10*$^{-/-}$ or Vav-*Adam17*$^{-/-}$ mice were infected with *P. aeruginosa* or PBS as a control by intranasal instillation for 12 h. Blood was stained with FITC-conjugated monoclonal anti-mouse CD11b, eFluor450-conjugated monoclonal anti-mouse CD11c, PerCP-Cy5.5-conjugated monoclonal anti-mouse CD45, APC-conjugated monoclonal anti-mouse Ly6G and PE-Cy7-conjugated monoclonal anti-mouse F4/80 to evaluate the content of neutrophils, macrophages, and monocytes by flow cytometry. Data are presented as means +/- SD six mice per group. Asterisks reveal significance among groups analyzed by two-way ANOVA and Tukey post-test (*p < 0.05, **p < 0.01).

The leukocytosis observed in both Vav-*Adam10*$^{-/-}$ and Vav-*Adam17*$^{-/-}$mice was correlated with an increase in the systemic clearance of *P. aeruginosa* observed by a significant decrease in blood CFU (Figure 4.34 A and B).

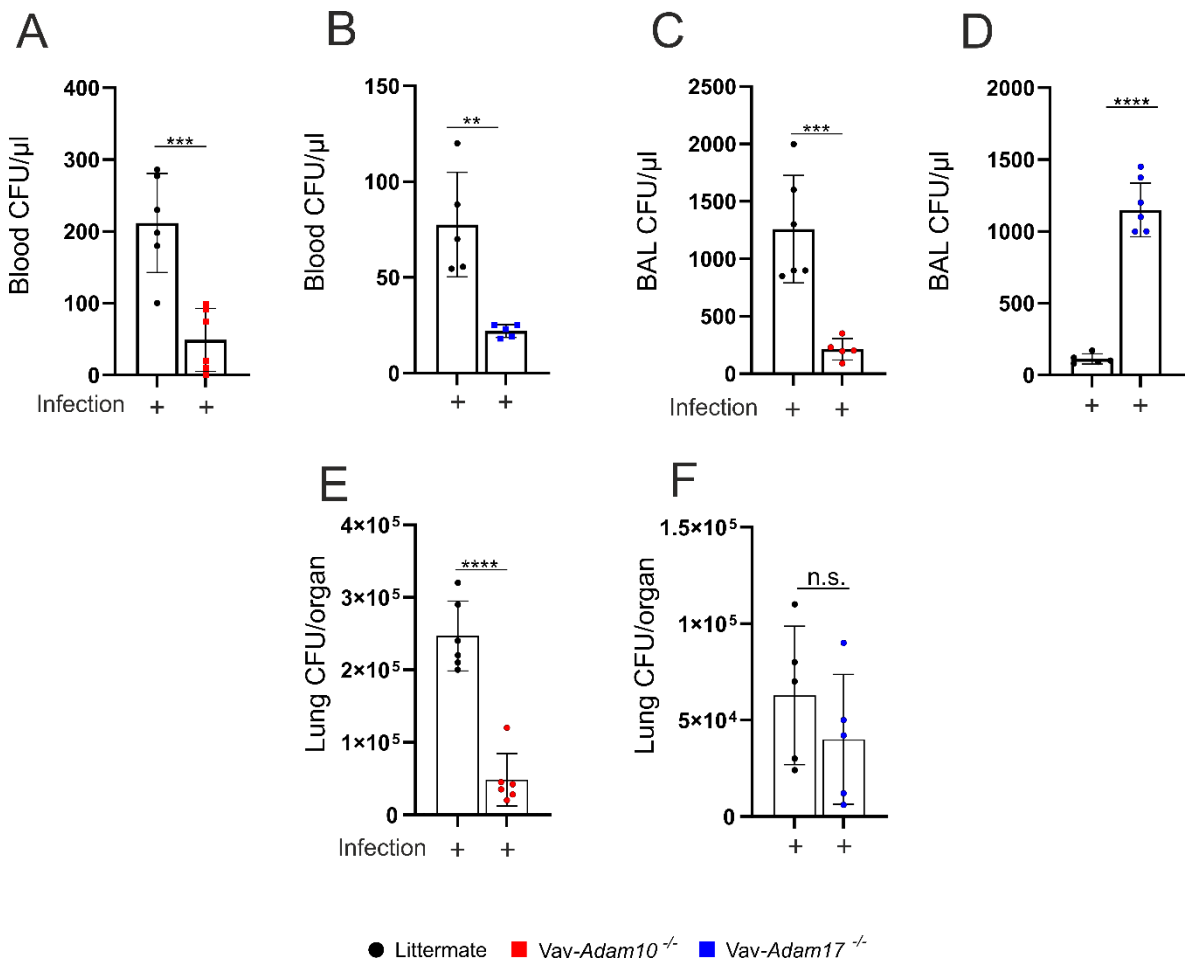

Figure 4. 34: Role of leukocytic ADAM10 and ADAM17 in bacteria clearance during *P. aeruginosa*-induced pneumonia
littermates, Vav-*Adam10*$^{-/-}$ or Vav-*Adam17*$^{-/-}$ mice were infected with *P. aeruginosa* or PBS as a control by intranasal instillation for 12 h. (A-B) Citrated blood, (C-D) BAL fluid or (E-F) lung tissues were serially diluted in sterile PBS, streaked out on LB agar plates and incubated overnight at 37°C. Counted CFUs were multiplied by the dilution factor and adjusted to the number per organ. Data are presented as means +/- SD of six mice per group. Asterisks reveal significance among groups analyzed by one-way ANOVA and Tukey post-test (*p < 0.05, **p < 0.01, ***p < 0.001, n.s. not significant).

4.3.3 ADAM10 changes neutrophil and monocyte properties regulating bacterial clearance in an auto-and paracrine/cell-intrinsic manner

Pneumonia severity was decreased and increased in Vav-*Adam10*$^{-/-}$ and Vav-*Adam17*$^{-/-}$mice, respectively (Figure 4.30 A and B). Reduced leukocyte recruitment to the alveolar space in Vav-*Adam17*$^{-/-}$mice led to a local increase in *P. aeruginosa* CFU (Figure 4.34 D) which may explain the increase in pneumonia manifestation. On the other hand, despite equal neutrophil and macrophage numbers compared to the littermate mice, Vav-*Adam10*$^{-/-}$ mice showed higher *P. aeruginosa* clearance in BAL and in the lung tissue, which was in line with decreased pneumonia manifestations (figure 4.34 C and E). To investigate the underlying mechanisms in more detail, the role of ADAM10 and ADAM17 on phagocytosis as well as cell survival was investigated using human primary neutrophils and THP-1 cells. Inhibition of ADAM10 using GI254023X (as pharmacological inhibitor) significantly enhanced

the phagocytosis efficiency for GFP-labeled *P. aeruginosa* (2 h, MOI 5) in both cell types (Figure 4.35 A). Interestingly, this was associated with a significant increase in the survival of both cell types (Figure 4.35 B). However, inhibition of ADAM17 using TAPI-1 had no effect on neither phagocytosis nor cell survival (Figure 4.35 A and B).

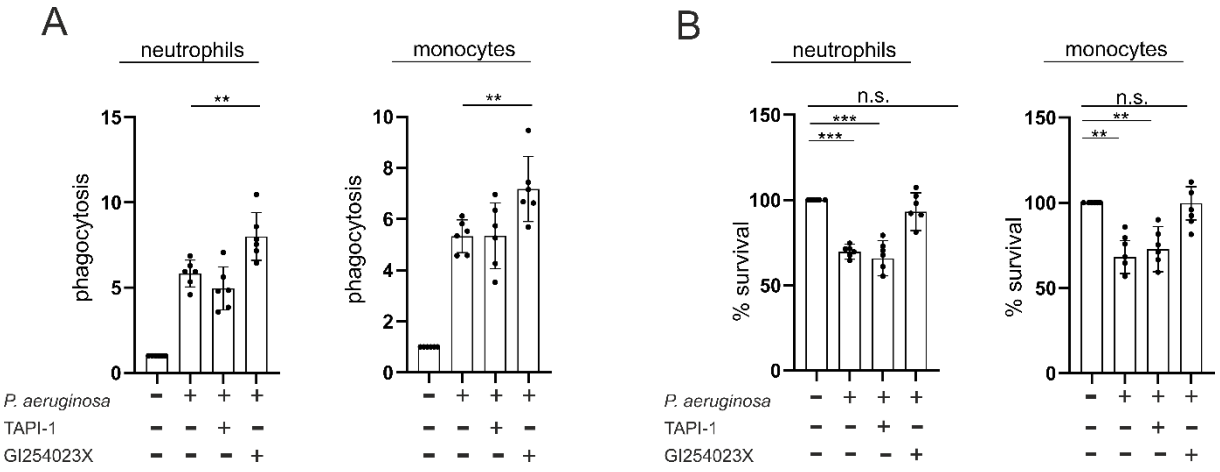

Figure 4. 35: Role of ADAM10 and ADAM17 in human neutrophils and THP-1 cells phagocytosis and survival during *P. aeruginosa* infection
(A-B) Human neutrophils or THP-1 cells were pre-incubated with 0.1% DMSO, 10 µM GI254023X or 10 µM TAPI-1 for 30 min and infected with GFP-labelled *P. aeruginosa* (2 h, MOI 5). The GFP signals of the non-phagocytosed *P. aeruginosa* were quenched by Trypan blue. (A) The phagocytosis of *P. aeruginosa* was analyzed by measuring the median of the GFP signal intensity relative to the signal of the non-infected cells by flow cytometry. (B) Cellular survival was analyzed by measuring the median of the APC signal intensity of Trypan blue relative to the signal of the non-infected cells by flow cytometry. Quantitative data are presented as means +/- SD of six independent experiments. Asterisks reveal significant differences relative to the control analyzed using one sample t-test (**p < 0.01, ***p < 0.001, n.s. not significant).

Neutrophils are considered to have a major impact on the pool of ROS in the blood. ROS induced oxidative stress can increase the disease severity, contributing to several cell death pathways and further effecting the bacterial killing capacity (Villalpando-Rodriguez, Gibson, 2021). As expected, infection led to an increase in ROS production in comparison to non-infected cells (Figure 4.36 A). Fitting with improved cell survival, inhibition of ADAM10 significantly decreased ROS production in both cell types infected with *P. aeruginosa* (2 h, MOI 5) compared to infected cells without inhibitor treatment (Figure 4.36 A). Interestingly, ADAM17 inhibition resulted in an increase in ROS production (figure 4.36 A). To evaluate the effect of the difference in cell survival and ROS generation on the bacterial killing capacity, both cell types were infected with *P. aeruginosa* (2 h, MOI 5) and the CFU number of live bacteria was counted. Only Inhibition of ADAM10 improved *P. aeruginosa* killing capacity, which is corelated with the improvement of the phagocytosis process, whereas inhibition of ADAM17 did not display any difference (Figure 4.36 B).

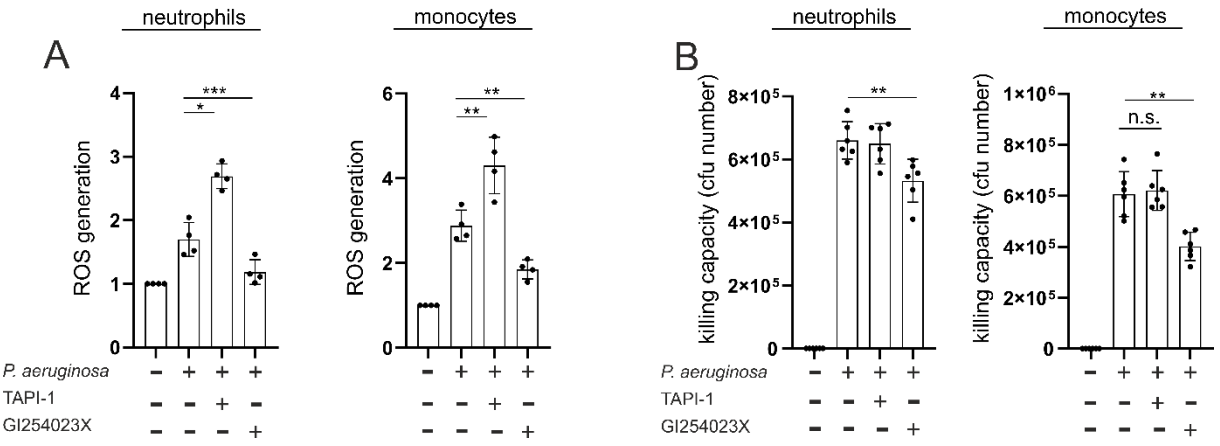

Figure 4. 36: Role of ADAM10 and ADAM17 in human neutrophils and THP-1 cells ROS generation and bacteria-killing capacity during *P. aeruginosa* infection
Human neutrophils or THP-1 cells were pre-incubated with 0.1% DMSO, 10 µM GI254023X or 10 µM TAPI-1 for 30 min and (A) stained with ROS dye for 30 min followed by infection with *P. aeruginosa* (2 h, MOI 5) or (B) infection with GFP-labelled *P. aeruginosa* (2 h, MOI 5). The GFP signals of the non-phagocytosed *P. aeruginosa* were quenched by Trypan blue. (A) The generation of ROS was evaluated by detecting the fluorescence signals after subtraction of the background at an excitation/emission of 520/605 nm. (B) Infected cells were resuspended in PBS and streaked out on agar plates, and the live bacteria were counted after overnight incubation at 37C°. Quantitative data are presented as means +/- SD of six independent experiments. Asterisks reveal significant differences relative to the control analyzed using one sample t-test (*p < 0.05, **p < 0.01, ***p < 0.001, n.s. not significant).

Oxidative stress has been shown to activate p38 and Src kinase signaling pathways (Brill et al., 2009; Giannoni et al., 2005; Kulisz et al., 2002). Furthermore, this activation was dependent on proteases activity (Brill et al., 2009). Therefore, we investigated the involvement of both kinases on the mentioned functional properties. Pharmacological inhibition of p38 by SB203580 or Src kinase by PP2 had no impact on the phagocytosis process or cell survival of both human neutrophils or THP-1 cells (figure 4.37 A and B). In contrast, inhibition of Src kinase significantly reduced ROS generation (Figure 4.37 C). To further investigate whether *P. aeruginosa* infection contributed to p38 signaling, the phosphorylation of p38 during infection with *P. aeruginosa* (2 h, MOI 5) in the presence or absence of ADAM10 or ADAM17 inhibitors was investigated. However, neither *P. aeruginosa* infection nor ADAM10 or ADAM17 inhibition had any impact on p38 phosphorylation in both cell types (figure 4.37 D).

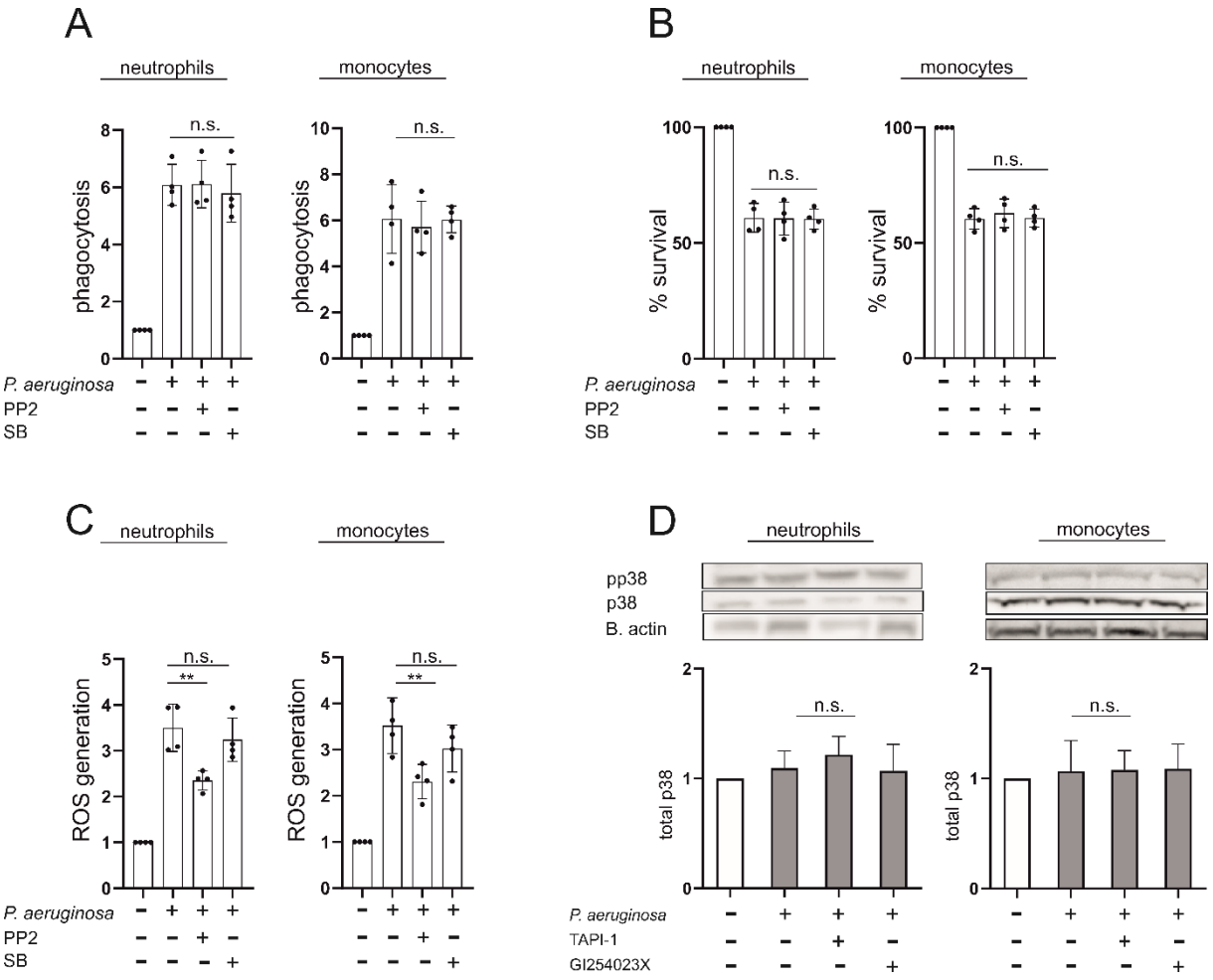

Figure 4. 37: Role of p38 and Src kinase signaling in human neutrophils and THP-1 cells on ROS generation and bacteria killing capacity during *P. aeruginosa* infection
(A-C) Human neutrophils or THP-1 cells were pre-incubated with 0.1% DMSO, 10 µM PP2 or 10 µM SB for 30 min and (A-B) infected with GFP-labelled *P. aeruginosa* (2 h, MOI 5) or (C) stained with ROS dye for 30 min followed by infection with *P. aeruginosa* (2 h, MOI 5). (A-B) The GFP signals of the non-phagocytosed *P. aeruginosa* were quenched by Trypan blue. (A) The phagocytosis of *P. aeruginosa* was analyzed by measuring the median of GFP signal relative to the signal of the non-infected cells by flow cytometry. (B) Cellular survival was analyzed by measuring the median of APC signal intensity of Trypan blue relative to the signal of the non-infected cells by flow cytometry. (C) The generation of ROS was evaluated by detecting the fluorescence signals after subtraction of the background at an excitation/emission: 520/605 nm. (D) Human neutrophils or THP-1 cells were pre-incubated with 0.1% DMSO, 10 µM GI254023X or 10 µM TAPI-1 for 30 min and infected with *P. aeruginosa* (2 h, MOI 5). p38 and pp38 expression was analyzed in the cell lysate by Western blot using an antibody against the phosphorylated and non-phosphorylated form of p38. Representative blots of independent experiments are shown. Quantitative data are presented as means +/- SD of (A-C) four or (D) three independent experiments. Asterisks reveal significance difference relative to the control analyzed using one sample t-test (** $p < 0.01$, n.s. not significant).

Beside the catalytic activity mediated by the metalloproteinase domain, ADAM proteases compose several domains, including but not limited to the disintegrin domain, that participates in a variety of cell-intrinsic functions. Thus, media transfer experiments were performed to investigate whether the observed effects on phagocytosis or ROS generation were due to the release of soluble ectodomains or based in cell-intrinsic functions. Human neutrophils and THP-1 cells were infected with *P. aeruginosa* (2 h, MOI 5), respectively, in the absence or presence of ADAM10 or ADAM17 inhibition. Subsequently, the soluble factors released from these cells were directly added to GI254023X or TAPI-1 pre-incubated cells, followed by evaluation of phagocytosis capacity and ROS production,

respectively. ADAM10 or ADAM17 inhibition had no effect on the phagocytosis capacity (figure 4.38 A) and was dependent on the soluble factors transferred. However, the effects on ROS generation (decrease by ADAM10 inhibition, increase by ADAM17 inhibition) remained the same (figure 4.38 B). Thus, ADAM10 seems to regulate the antimicrobial capacity of neutrophils and monocytes in an autocrine/paracrine (phagocytosis and survival) and cell-intrinsic (ROS production) manner, respectively.

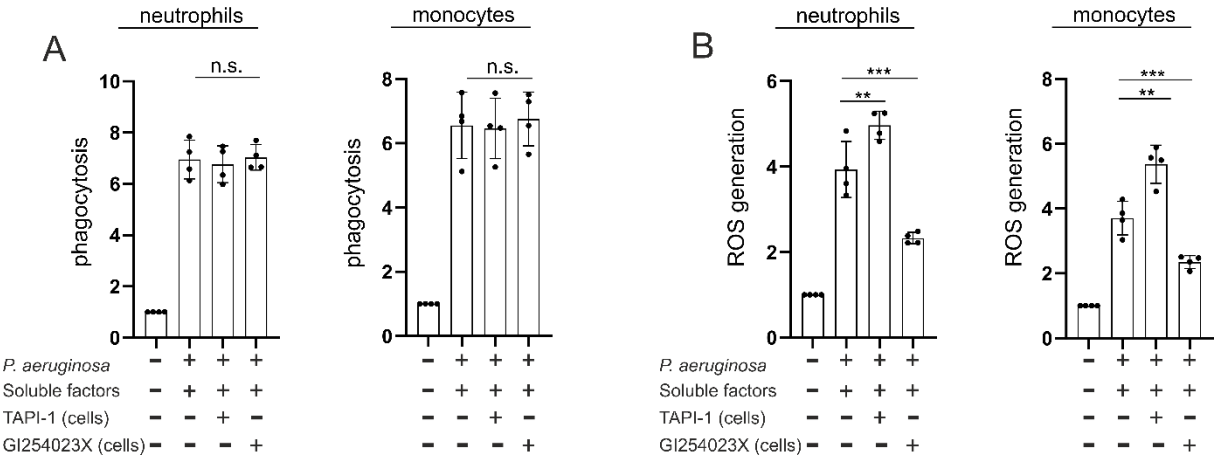

Figure 4. 38: Autocrine/paracrine and cell-intrinsic function of ADAM10 and ADAM17 in phagocytosis and ROS generation during *P. aeruginosa* infection
(A-B) Human neutrophils or THP-1 cells were (A) infected with GFP-labelled *P. aeruginosa* (2 h, MOI 5) or (B) stained with ROS dye for 30 min followed by infection with *P. aeruginosa* (2 h, MOI 5). The soluble factors released from these cells were directly added to 0.1% DMSO, 10 µM GI254023X or 10 µM TAPI-1 pre-incubated cells and infected again with the respective *P. aeruginosa* for 2 h. (A) The GFP signals of the non-phagocytosed *P. aeruginosa* were quenched by Trypan blue. The phagocytosis of *P. aeruginosa* was analyzed by measuring the median of GFP signal relative to the signal of the non-infected cells by flow cytometry. (B) The generation of ROS was evaluated by detecting the fluorescence signals after subtraction of the background at an excitation/emission: 520/605 nm. Quantitative data are presented as means +/- SD of four independent experiments. Asterisks reveal significance difference relative to the control analyzed using one sample t-test (** $p < 0.01$, *** $p < 0.001$, n.s. not significant).

4.3.4 ADAM10-deficiency shapes the local immune response to an anti-inflammatory phenotype

As mentioned earlier, ADAM10 and ADAM17 inhibition decreased and increased, respectively, the ROS generation during infection with *P. aeruginosa* in human neutrophils and THP-1 cells. As MPO considers one of the tissues damaging ROS, the MPO level in the alveolar space of Vav-*Adam10*$^{-/-}$ and Vav-*Adam17*$^{-/-}$ mice infected with *P. aeruginosa* was analyzed. Despite the equal number of neutrophils and macrophages in BAL of Vav-*Adam10*$^{-/-}$ mice, MPO level was significantly decreased in infected mice compared to littermates (figure 4.39 A). In line with the increased ROS production in neutrophils and THP-1 cells infected with *P. aeruginosa*, infected Vav-*Adam17*$^{-/-}$ mice showed a significant increase in MPO level in comparison to littermate mice (figure 4.39 B).

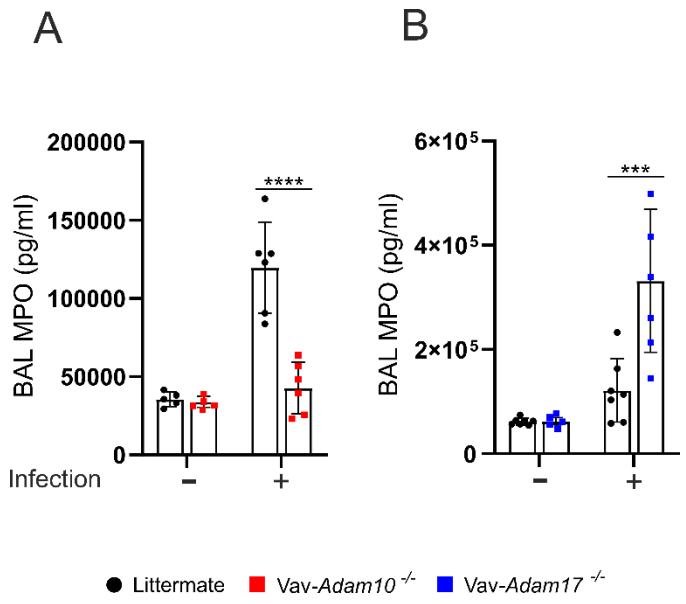

Figure 4. 39: Role of leukocytic ADAM10 and ADAM17 in alveolar MPO activity during *P. aeruginosa*-induced pneumonia
littermates, Vav-*Adam10*$^{-/-}$ or Vav-*Adam17*$^{-/-}$ mice were infected with *P. aeruginosa* or PBS as control by intranasal instillation for 12 h. (A-B) BAL was centrifuged at 16,000xg for 15 min and 4 °C, and the supernatant was used to analyze the BAL content of MPO using commercial ELISA kits following the manufacturers' protocol. Data are presented as means +/- SD of six mice per group. Asterisks reveal significance among groups analyzed by two-way ANOVA and Tukey post-test (*** $p < 0.001$, **** $p < 0.0001$, n.s. not significant).

Polarization of macrophages has been described to shape their phenotype and function, and consequently, the inflammatory response (Yunna et al., 2020). Therefore, macrophage polarization in the lung tissue of littermates, Vav-*Adam10*$^{-/-}$ and Vav-*Adam17*$^{-/-}$mice infected with *P. aeruginosa* in comparison to the control-treated mice was investigated by immunohistochemistry. As observed for alveolar macrophage numbers, lung tissues of infected Vav-*Adam10*$^{-/-}$ mice showed similar numbers of CD68^{+}(general macrophages), and CD86^{+} (M1) macrophages compared to infected littermates (Figure 4.40 A and B). Interestingly, CD163^{+} (M2) macrophages were significantly increased in Vav-*Adam10*$^{-/-}$ mice (figure 4.40 C). In contrast, CD68^{+}, CD86^{+} or CD163^{+} macrophages were similar in Vav-*Adam17*$^{-/-}$mice (figure 4.40 D-F). In general, no basic phenotypes based on the genotype were observed.

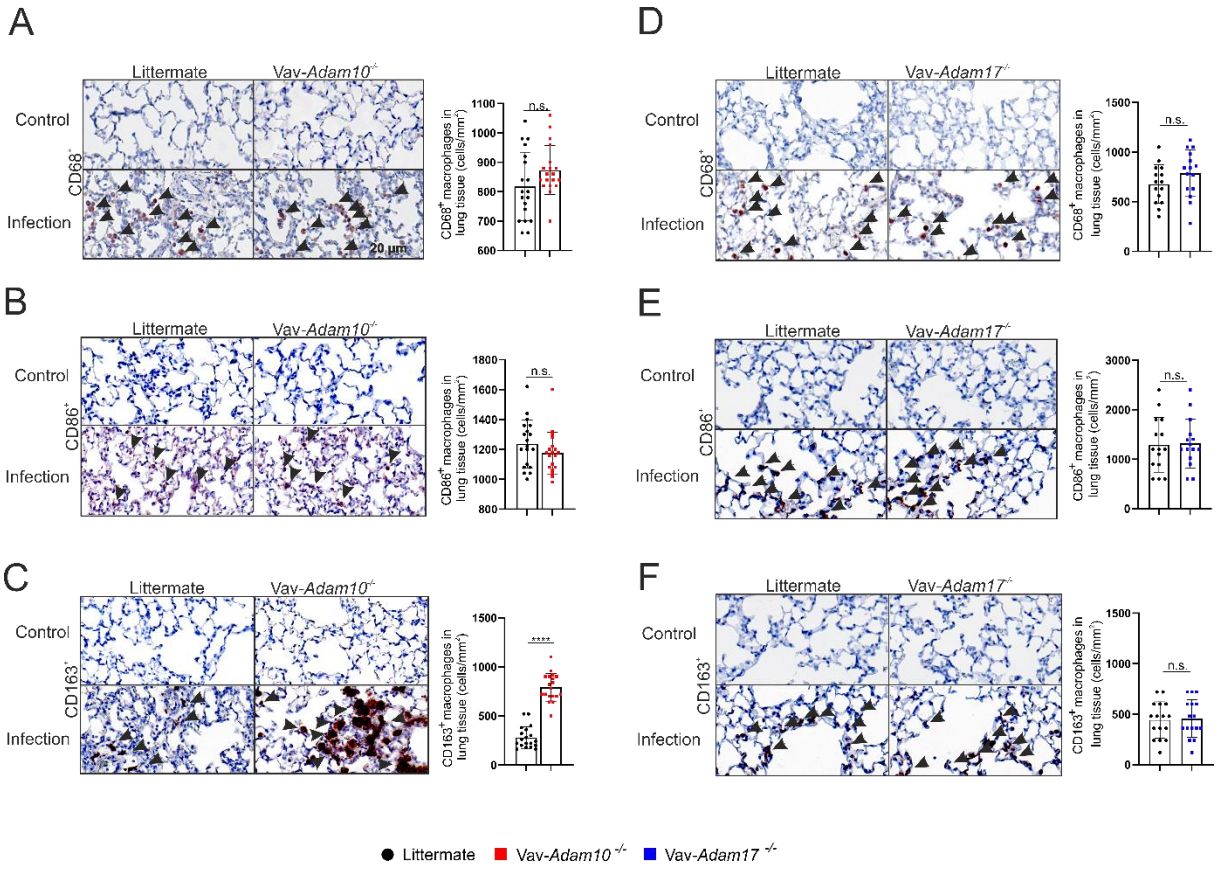

Figure 4. 40: ADAM-dependent macrophage polarization during *P. aeruginosa*-induced pneumonia
(A-F) Littermates, Vav-*Adam10*$^{-/-}$ or Vav-*Adam17*$^{-/-}$ mice were infected with *P. aeruginosa* or PBS as a control by intranasal instillation for 12 h. (A-F) Lung left lobs were embedded in paraffin, sliced into 5 µm sections and stained with antibodies against CD68 (general macrophages), CD86 (M1) or CD163 (M2). General macrophages, M1 and M2 macrophages were counted manually and blindly in each section. Data are presented as means +/- SD of macrophages number per mm^2 of six mice per group. Representative images are shown. Asterisks reveal significance among groups analyzed by one-way ANOVA and Tukey post-test (****p < 0.0001, n.s. not significant).

5 Discussion

5.1 Functional implication of ADAM10 and ADAM17 in *P. aeruginosa* mediated epithelial cells infection *in vitro*

In the present study it was observed that ADAM10 and ADAM17 display a pathogen and toxin dependent effect during the inflammatory response. During *P. aeruginosa* infection or Exotoxin A stimulation, ADAM10 and ADAM17 modulated several key inflammatory manifestations, including leukocyte transepithelial migration, total and paracellular protein permeability as well as epithelial tissue regeneration and survival. Further, the pathogen-dependent maturation and activation of both proteases was mainly mediated by the toxins released by *P. aeruginosa*. In Addition, *P. aeruginosa* induced an exocytic release of active ADAM10 but not ADAM17 in EVs like exosomes mediating shedding activity at a distinct site *in trans* position. These findings add evidences that ADAM10 and ADAM17 may be promising targets for the development of novel anti-infective treatment strategies.

Lung pneumonia caused by invading pathogens and their released toxins can result in ARDS and sepsis. The secreted toxins from Gram-negative or Gram-positive bacteria represent a sophisticated weapon predisposing to several molecular malfunctions (Kumar et al., 2019). The proteolytic activity of ADAM10 and ADAM17 has been shown to regulate sterile inflammation both *in vitro* and *in vivo*. Studies have shown that ADAM10 cleaves TLR4 and the receptor for advanced glycation end products (RAGE), suggesting an activation by cell wall components (Raucci et al., 2008; Yang et al., 2017). The role of ADAM10 during lung inflammation was highlighted through the discovery that it serves as a receptor for the pore-forming α-hemolysin toxin produced by *S. aureus* (Wilke, Bubeck Wardenburg, 2010). In addition, the shedding of the TNF-receptor 1 by ADAM17 is the initiating event of TNFα-induced necroptosis in endothelial cells, which promotes tumor cell extravasation and metastasis formation (Bolik et al., 2022). The toxin stimulated the expression of ADAM10 in pulmonary epithelial cells, eventually leading to bacterial invasion and death in mice models of α-hemolysin induced lung inflammation (Inoshima et al., 2011). In addition, lung endothelial ADAM17 regulated the inflammatory response during LPS-induced acute lung injury (Dreymueller et al., 2012a). Despite the vital role of ADAM10 and ADAM17 proteolytic activity in sterile inflammation, the regulation and clinical impact in epithelial cells during lung infections remain poorly understood.

S. pneumoniae, a Gram-positive bacterium, did not affect ADAM10 or ADAM17 expression or activity. In contrast, exposure to the Gram-negative bacterium *P. aeruginosa* led to a significant increase in ADAM10 and ADAM17 activity and related pathogenic processes, such as cleavage of E-cadherin and JAM-A as endogenous substrate as well as betacellulin and TGF-α as exogenous substrate, respectively. As bacterial inactivation aims to suppress bacterial growth and preserves the integrity (Smelt, Brul, 2014), the results suggest that the activation of epithelial ADAM10 and ADAM17 in response to *P. aeruginosa*, is primarily driven by the secretion of toxins and can occur independently of the interaction

with pattern recognition receptors. *P. aeruginosa* has been observed to display an elevated influx of calcium following the infection (Tran Van Nhieu et al., 2018), which is thought to be the result of the presence of the pore-forming toxin Exolysin A. The pore-forming ability of Exolysin A promotes calcium entry to the host cell which leads to ADAM10 release from the ER (Huber, 2022). In contrast, Exotoxin A is a potent ADP-ribosyltransferase that can modify and inhibit protein biosynthesis by inactivating eEF2 on the ribosomes (Zdanovsky et al., 1993). This leads to a reduction in protein synthesis and a subsequent decrease in the overall growth and survival of the cell (Michalska, Wolf, 2015). Despite the fact that the pore-forming property of Exotoxin A has not been proven yet, calcium imaging experiment showed an increase in intracellular calcium during stimulation with Exotoxin A. Moreover, it was shown that the increased calcium levels in the cytoplasm were due to calcium influx rather than a release from the intercellular storage, such as the ER. In line with this finding, Exotoxin A has been shown to block calcium efflux from ER through the interaction with the α-subunit of sec-61 (Schauble et al., 2014). Exotoxin A gains entry into cells through endocytosis by the interaction cognate receptor, CD91 (Kounnas et al., 1992). Once bound to the receptor, Exotoxin A is internalized into the cell via either clathrin-coated pits or the lipid-sorting pathway (Michalska, Wolf, 2015). This process may result in alterations of the membrane fluidity and reorganization of membrane microdomains, such as lipid rafts, and the activation of G protein-coupled receptors (GPCR), which may then activate calcium ion channels. However, in-depth investigations are needed to test the hypothesis that Exotoxin A-mediated activation of ADAM proteases is at least in parts through GPCR-activation.

ADAM17 activation takes place via a kinase-mediated mechanism, specifically through the involvement of Protein kinase C (PKC) and Mitogen-activated protein kinase (MAPK) signaling pathways, with calcium influx playing a less significant role (Le Gall et al., 2009). ExoS, ExoT, and ExoA are known to exhibit ADP-ribosyltransferase activity, with ExoS and ExoT additionally containing a RhoGTPase activating domain on their N-terminus (Barbieri, 2000; Goehring et al., 1999). ADAM17 activation has been observed to depend on the redox state, which could be altered through the generation of reactive oxygen species involving GTPases (Wang et al., 2009; Willems et al., 2010). This suggests that the induction of ROS production could potentially be a mechanism of ADAM17 activation during *P. aeruginosa* infection. However, the current understanding of these aspects is speculative, and further studies are warranted to provide more conclusive evidence. In addition, the inhibition of ADAM17 was found to significantly increase the cell survival of lung epithelial cells during *P. aeruginosa* infection, thereby preserving the integrity of the epithelial barrier. This finding aligns with previous findings that demonstrated the pivotal role of ADAM17 in regulating cell survival. For example, it has been shown that the shedding of the TNF-receptor 1 by ADAM17 is the initiating event of TNFα-induced necroptosis in endothelial cells, which promotes tumor cell extravasation and metastasis formation (Bolik et al., 2022).

The interplay between the tight and adherence junction molecules helps to maintain the structural integrity of the cell and contributes to the regulation of various physiological processes, including cell migration and differentiation (Shen et al., 2011). Thus, the proteolytic cleavage of these molecules can result in the loss of intercellular adhesion, leading to the disruption of tight and adherence junctions and a subsequent increase in cell permeability (Frank, Hostetter, 2007; Yuksel et al., 2021). E-cadherin, a transmembrane glycoprotein that plays a key role in intercellular adhesion, is a well-known substrate of ADAM10 (Izaguirre et al., 2010; Maretzky et al., 2005). In studies of α-hemolysin, ADAM10 has been found to play an important role in the activation of the NLRP3 (nucleotide-binding domain, leucine-rich–containing family, pyrin domain–containing-3) inflammasome (Ezekwe et al., 2016). Inhibition of ADAM10 showed to mitigate the upregulation of MMP2 and MMP9 expression in cases of traumatic brain injury (Appel et al., 2021). Moreover, the ADAM10-TIMP-1 (tissue inhibitor of metalloproteinases) complex is responsible for the binding and processing of pro-MMP9, further highlighting the importance of ADAM10 in wound repair processes (Li et al., 2017). Thus, the improvement of wound repair observed in this thesis through inhibition of ADAM10 and concomitant stimulation with Exotoxin A can likely be attributed to the reduction of the earlier mentioned downstream effects. On the other hand, the reduction in wound closure resulting from the pharmacological inhibition of ADAM10, both in general and after stimulation with Exotoxin A (the inhibition only during the migration phase), is likely a consequence of the decreased ability to cleave E-cadherin. JAM-A as substrate of ADAM17 is a multifunctional cell surface protein modulating many cellular functions, including migration, polarity, paracellular permeability and proliferation. Despite that the role of JAM-A in tissue cell migration is a topic of debate and discussion in the scientific community, some studies have shown that reducing the levels of JAM-A in keratinocytes leads to an increase in cell proliferation and wound closure (Wang et al., 2018). In this thesis, Exotoxin A stimulation impaired epithelial cells wound closure and regeneration, while co-inhibition of ADAM17 improved epithelial migration and regeneration. The ability of Exotoxin A to alter epithelial integrity and impede repair processes supports this observation (Heggers et al., 1992). It has been demonstrated that an increase in full-length JAM-A is correlated with a decrease in soluble JAM-A (Severson, Parkos, 2009). The latter form of JAM-A not only impedes tissue cell migration but also contributes to the transmigration of leukocytes (Koenen et al., 2009). Thus, the improved wound closure due to ADAM17 inhibition could be attributed to the inhibition of JAM-A cleavage. The general disturbance of wound repair in response to infection with the bacterium *P. aeruginosa* is regulated, in part, through the ERK/p38 signaling pathways (Muller et al., 2009) and the generation of reactive oxygen species. Additionally, an imbalanced ratio of pro- and activated forms of matrix metalloproteinases, such as MMP2 and MMP9, contributes to the impaired wound repair.

The disruption of barrier integrity is a critical aspect in the development of a range of pathological conditions (Carlier et al., 2021). The breakdown of barriers, such as the epithelial layer, increases the permeability of proteins, as observed in this study and others (Azghani, 1996), and creates avenues for

the systemic invasion of pathogens, as well as the reverse migration of immune cells, such as alveolar macrophages and leukocytes, into the inflamed lung (Brune et al., 2015). In the present study, gene silencing and inhibiting ADAM10 or ADAM17 decreased and increased the transepithelial migration of monocytic cells during *P. aeruginosa* infection, respectively. The increased transmigration mediated by ADAM17 inhibition is facilitated by the increased adhesion of these cells to the epithelial layer, which is an early milestone event in the transmigration process. Infection with *P. aeruginosa* strains with intact pilli leads to the upregulation of integrins and adhesion molecules, such as ICAM-1, which are essential for the adhesion of leukocytes to the inflamed tissue and the subsequent transmigration across the epithelial layer and at the same time they are within the substrate spectrum of ADAM17 (Gravelle et al., 2010; Qin et al., 1996). This could explain the stronger induction of transepithelial migration that occurs during infection with *P. aeruginosa* comparing to Exotoxin A. The strain used in this thesis, PA103, produces high amounts of Exotoxin A and shows a cytotoxic phenotype dependent on ExoU (Hirakata et al., 2000). Furthermore, other virulence factors and secretion systems, such as LasB, pyocyanin, and T3SS, may also contribute to changes in epithelial integrity. The synergistic impact of different exotoxins is further amplified by the higher induction of ADAM10 and ADAM17 activity seen during infection with *P. aeruginosa* compared to stimulation with Exotoxin A alone.

The role of ADAM10 and ADAM17 in cellular communication and signaling is complex and still not fully understood. ADAM10 has been shown to be present in exosomes, which are small vesicles that are released by cells and play a critical role in cellular communication and signaling (Scharfenberg et al., 2020; Stoeck et al., 2006; Tosetti et al., 2018). Despite some evidence suggesting that ADAM10 can be proteolytically cleaved (by other proteases) and released as a soluble ectodomain, there have only been a few studies that have proposed cleavage to occur *in trans*, or on a different cell surface (Althoff et al., 2000). In addition, ADAM17 may not only function in its cell-associated form but may also be released as a soluble ectodomain by the action of other proteases like ADAM8 (Scharfenberg et al., 2020). This has been observed in breast cancer cells, where the rapid release of the ectodomain led to the formation of a cell-associated remnant form (Scharfenberg et al., 2020). In the present study, a significant portion of the measured ADAM10 activity was found to be released on exosomes. The results clearly showed that the ADAM10 on exosomes is proteolytically active and capable of cleaving substrates on other cells. Although it is not possible to exclude the possibility that the exosomes first fuse with the plasma membrane and then mediate cleavage *in cis*, the limited rate time of uptake (max. 2 h in our study) (Franzen et al., 2014) suggests that the cleavage is triggered by *P. aeruginosa* infection and occurs primarily *in trans* via exosomal ADAM10. In contrast to these observations, no degradation or remnant forms of ADAM17 were observed, nor was there any evidence of release on exosomes, indicating that epithelial ADAM17 functions in a cell-associated manner during *P. aeruginosa* infection. Exosomes play a role in cellular communication and signaling in the human body (Welton et al., 2010), and their stability in the bloodstream makes them well-suited for transporting products between cells and tissues (Boukouris, Mathivanan, 2015; Zeringer et al., 2015). The release of exosomes upon local

infection in the lung, triggered by *P. aeruginosa*, has the potential to result in systemic effects, including the spread of inflammatory and pro-inflammatory mediators or the transport of proteases to other tissues, where they can mediate proteolytic activity (Rahn, Becker-Pauly, 2022). The release of ADAM10 on exosomes in response to *P. aeruginosa* infection has the potential to play an important role in the development of systemic inflammation in patients suffering from *P. aeruginosa*-induced pneumonia. This mechanism of pathogenesis could be a key factor in causing widespread inflammation in the body, making it imperative to understand its underlying mechanisms. To verify this hypothesis, it is important to conduct translational studies that isolate exosomes from patient serum samples with microbiologically characterized infections. This will provide valuable insights into using of exosomal ADAM10 as a predictive marker in *P. aeruginosa* infection.

As antimicrobial and multi-drug resistance becomes more widespread, there is a growing need for developing novel anti-infective agents that target either inter-bacterial communication or the interaction between bacterial toxins and their host membrane partners (Krueger, Brown, 2019; Liu et al., 2020; Otto, 2020). This study has demonstrated that the regulation of ADAM10 and ADAM17 is largely dependent on the released toxins, rather than the bacterial particles themselves, as evidenced by the use of heat-inactivated bacteria. This finding is consistent with prior reports on the release of cytokines and cytokine receptors following exposure to *P. aeruginosa* LPS and flagellin infections (Gomez et al., 2005; Raoust et al., 2009). Despite the strong functional effects of Exotoxin A stimulation living *P. aeruginosa* possessed a higher activation capacity in comparison to heat-inactivated bactieria. In addition to the T2SS-derived ExoA, the bacteria secrete virulence factors such as ExoS, ExoT, ExoY, and elastase through the T3SS system. These virulence factors play an essential role in the regulation of lung barrier integrity. It was also demonstrated that the absence of ExoS and ExoT resulted in ExoU being the primary cytotoxin responsible for lung epithelial cell death. The production of ExoU has been linked to rapid and severe lung injury and is frequently associated with the most severe pathological outcomes in both experimental animal models and clinical patients (Hauser, 2009; Juan et al., 2017). ExoY has been found to be highly prevalent in clinically isolated strains of *P. aeruginosa*, and its role as a key edema factor has been well established. The impact of this toxin on critically ill patients with *P. aeruginosa* lung infection is significant, with a marked contribution to end-organ dysfunction (Feltman et al., 2001; Morrow et al., 2017). This indicates that the cytotoxic effect of *P. aeruginosa* is a multifactorial process that involves several virulence factors working in a coordinated manner. Indeed, the investigations in this thesis revealed that the effect of Exotoxin A on epithelial cell survival was negligible, in contrast to the impact of *P. aeruginosa* infection. Thus, it is highly probable that the activation of ADAM10 or ADAM17 is influenced by a variety of toxins released by *P. aeruginosa* during infection.

5.2 Functional implication of ADAM10 and ADAM17 in *P. aeruginosa* mediated leukocyte cells infection *in vitro* and *in vivo*

In the present study, a release of ADAM10 and ADAM17 in exosomes to the serum was observed for viral and bacterial pneumonia patients, which correlated with the disease severity. In addition, leukocytes could be identified as key contributors to the release of ADAM10 and ADAM17 on exosomes, possibly shaping the systemic immune response during pneumonia. Moreover, this study has uncovered new insights into the mechanisms governing the inflammatory response within the microenvironment of the lung, highlighting the contrasting roles played by leukocytic ADAM10 and ADAM17. ADAM10 seems to be a key orchestrator of pro-inflammatory signaling promoting M1 polarization, increasing the production of ROS, releasing cytokines, and inducing tissue damage. In contrast, ADAM17 appears to play a critical role in regulating the intensity of the initial immune response, serving to maintain a necessary and protective level of inflammation and ROS production. As such, the balance and activity of ADAM10 and ADAM17 may hold critical implications for the progression and outcome of a diverse range of diseases that impact multiple organs and systems.

Several studies have demonstrated that a deficiency of ADAM10 on leukocytes can impede their recruitment and reduce edema formation in models of sterile lung inflammation (Pruessmeyer et al., 2014). Additionally, this deficiency has been associated with improved survival rates during *S. aureus*-induced pneumonia. Notably, this survival benefit was observed despite the absence of alterations in bacterial clearance or protein leakage but rather was linked to decreased release of the pro-inflammatory cytokine IL-1beta (Becker et al., 2014). In contrast to the mentioned studies, in the present study no changes in the number of recruited cells in Vav-*Adam10*$^{-/-}$ mic, but increased bacterial clearance and reduced protein leakage were observed. These results suggest that tissue damage is reduced in these mice, indicating a potential protective effect of ADAM10 deficiency in leukocytes. Leukocytes lacking ADAM17 exhibited increased neutrophil accumulation during peritonitis due to impaired L-selectin cleavage (Long et al., 2012). This finding is consistent with the current observations during *P. aeruginosa*-induced pneumonia, where ADAM17 deficiency is associated with increased neutrophil accumulation in the blood.

Furthermore, the activation of ADAM proteases occured in a pathogen and toxin-dependent manner (Aljohmani et al., 2022a; Aljohmani et al., 2022b). *S. aureus* and *P. aeruginosa* are two types of bacteria with different characteristics. *S. aureus* is a Gram-positive bacterium with a thick peptidoglycan cell wall, while *P. aeruginosa* is a Gram-negative bacterium with a thinner peptidoglycan layer and an additional outer membrane containing LPS (Lichtenberg et al., 2022). These differences in cell surface composition can have significant implications for how these bacteria interact with their environment, including how they are recognized and cleared by the immune system. *S. aureus* α-hemolysin used ADAM10 as a pore-forming receptor (Wilke, Bubeck Wardenburg, 2010), whereas *P. aeruginosa*-Exotoxin A induced a strong calcium influx activating ADAM10 (Aljohmani et al., 2022b). Taken

together, the distinct cell surface composition and toxin repertoire may help to explain the differential activation and relevance of ADAM proteases in the clearance of these bacteria (Seifert et al., 2020).

Adequate clearance of bacterial infection is dependent on the number of phagocytes recruited to the site of infection, as well as their ability to survive (Li et al., 2002). These factors, in turn, affect the total number of leukocytes and their efficiency in clearing the infection. Indeed, ADAM10 deficiency can improved the clearance capacity of leukocytes. This was due to an increase in both the phagocytosis capacity and survival of phagocytes, resulting in a higher number of active and functional leukocytes that are able to effectively eliminate bacterial pathogens. A murine model of polymicrobial sepsis revealed a beneficial impact of ADAM17 inhibition in reducing disease severity (Mishra et al., 2016). In contrast, in this thesis, deficiency of ADAM17 resulted in a deleterious increase in bacterial burden and exacerbated disease progression, as evidenced by the notable M-CASS and GV-Solas scoring. The observed detrimental effects may, in part, be attributed to the compromised ability of immune cells to cross the endothelium, as evidenced by the reduced diapedesis. ROS production is tightly regulated in the body under normal physiological conditions, and it is typically maintained in a state of equilibrium, which is essential for achieving a state of redox homeostasis (Herb, Schramm, 2021). However, when this equilibrium is disrupted, either by an increase in ROS production or a decrease in scavenging capacity, it can result in a state of oxidative stress that can have serious consequences such as alveolar damage or thrombosis (Laforge et al., 2020). Based on the recent findings, it appears that inhibiting ADAM17 can lead to an increase in the cellular production of ROS. This increase in ROS generation could also potentially explain the observed tissue damage and severity in vav-*Adam17*$^{-/-}$ mice.

Several studies have employed various models to explore different aspects of infection and the potential formation of sepsis. For instance, the *P. aeruginosa* model that was used in this thesis focused on the development of lung infection and pneumonia. In contrast, a cecum ligation and puncture model was employed to simulate sepsis as a systemic disease caused by Gram-positive bacteria. As the disease progresses, there is a shift in the bacterial composition from Gram-negative and anaerobic to aerobic bacteria (Hyde et al., 1990). Indeed, this shift from local to systemic disease in patients with manifested pneumonia might be reflected at the exosomal level. This thesis has revealed an intriguing correlation between the severity of pneumonia and the activity of ADAM10 and ADAM17 on exosomes. The exosomal activity of ADAM10 was increased in early murine pneumonia. However, in manifested pneumonia (pneumonia in hospitalized patients), the exosomal activity of ADAM17 became more dominant. The shift from active ADAM10 to ADAM17 at the exosomal level likely reflects a change in the cellular processes that occur as the disease progresses from a more localized to a more systemic inflammatory response.

COVID-19 pandemic has further emphasized the importance of exosomes in triggering the adaptive immune response and inducing multi-organ failure. In addition, studies have shown that the SARS-CoV-2 virus, which causes COVID-19, can exploit the exosomal pathway to evade the immune system and

spread throughout the body (Gurunathan et al., 2021; Pesce et al., 2021). Proteolytic active exosomes have the ability to induce proteolysis in *trans*, potentially affecting distinct organ sites through paracrine/endocrine signaling (Aljohmani et al., 2022b). Moreover, the circulating substrate angiotensin-converting enzyme 2 has been identified as a predictor of mortality in hospitalized COVID-19 patients (Fagyas et al., 2022). Given these findings, exosomal ADAM proteases could contribute to the pathogenesis of COVID-19. Indeed, a general increase of ADAM10 activity and a severity dependent increase of ADAM17 on the exosomes of COVID-19 patients was observed. Thus, the ability of proteolytic active ADAMs on exosomes to induce proteolysis in *trans* raises the possibility that ADAM proteases may regulate the progression of COVID-19 and the development of multi-organ failure. Given the potential importance of ADAM proteases in the context of infectious lung diseases, it is important to conduct further translational, preclinical, and clinical studies to evaluate their diagnostic, prognostic, and therapeutic value. Specifically, these studies should focus on assessing how ADAM proteases affect the immune response in infected lungs as well as how they impact the use of exosomes as cargo systems for drug delivery. Overall, by conducting these investigations, we can gain a more comprehensive understanding of the potential applications of ADAM proteases in the prevention, diagnosis, and treatment of infectious lung diseases. This knowledge can help guide the development of new therapies and ultimately improve outcomes for patients affected by these conditions.

6 References

1. Abel S, Hundhausen C, Mentlein R, Schulte A, Berkhout TA, Broadway N, Hartmann D, Sedlacek R, Dietrich S, Muetze B, Schuster B, Kallen KJ, Saftig P, Rose-John S, Ludwig A (2004) The transmembrane CXC-chemokine ligand 16 is induced by IFN-gamma and TNF-alpha and shed by the activity of the disintegrin-like metalloproteinase ADAM10. J Immunol 172:6362-6372
2. Adams DH, Lloyd AR (1997) Chemokines: leucocyte recruitment and activation cytokines. Lancet 349:490-495
3. Aderem A, Underhill DM (1999) Mechanisms of phagocytosis in macrophages. Annu Rev Immunol 17:593-623
4. Aderem A (2003) Phagocytosis and the inflammatory response. J Infect Dis 187 Suppl 2:S340-345
5. Al-Nedawi K, Meehan B, Kerbel RS, Allison AC, Rak J (2009) Endothelial expression of autocrine VEGF upon the uptake of tumor-derived microvesicles containing oncogenic EGFR. Proc Natl Acad Sci U S A 106:3794-3799
6. Aliberti S, Dela Cruz CS, Amati F, Sotgiu G, Restrepo MI (2021) Community-acquired pneumonia. Lancet 398:906-919
7. Aljohmani A, Yildiz D (2020) A Disintegrin and Metalloproteinase-Control Elements in Infectious Diseases. Front Cardiovasc Med 7:608281
8. Aljohmani A, Andres NN, Yildiz D (2022a) Pseudomonas aeruginosa Alters Critical Lung Epithelial Cell Functions through Activation of ADAM17. Cells 11
9. Aljohmani A, Opitz B, Bischoff M, Yildiz D (2022b) Pseudomonas aeruginosa Triggered Exosomal Release of ADAM10 Mediates Proteolytic Cleavage in Trans. Int J Mol Sci 23
10. Althoff K, Reddy P, Voltz N, Rose-John S, Mullberg J (2000) Shedding of interleukin-6 receptor and tumor necrosis factor alpha. Contribution of the stalk sequence to the cleavage pattern of transmembrane proteins. Eur J Biochem 267:2624-2631
11. Andersson ER, Sandberg R, Lendahl U (2011) Notch signaling: simplicity in design, versatility in function. Development 138:3593-3612
12. Andreini C, Banci L, Bertini I, Elmi S, Rosato A (2005) Comparative analysis of the ADAM and ADAMTS families. J Proteome Res 4:881-888
13. Andrzejewski MG, Koelsch A, Kogel T, Dreymueller D, Schwarz N, Ludwig A (2010) Distinct role of the intracellular C-terminus for subcellular expression, shedding and function of the murine transmembrane chemokine CX3CL1. Biochem Biophys Res Commun 395:178-184
14. Appel D, Hummel R, Weidemeier M, Endres K, Golz C, Schafer MKE (2021) Pharmacologic Inhibition of ADAM10 Attenuates Brain Tissue Loss, Axonal Injury and Pro-inflammatory Gene Expression Following Traumatic Brain Injury in Mice. Front Cell Dev Biol 9:661462
15. Azghani AO, Gray LD, Johnson AR (1993) A bacterial protease perturbs the paracellular barrier function of transporting epithelial monolayers in culture. Infect Immun 61:2681-2686
16. Azghani AO (1996) Pseudomonas aeruginosa and epithelial permeability: role of virulence factors elastase and exotoxin A. Am J Respir Cell Mol Biol 15:132-140
17. Barbieri JT (2000) Pseudomonas aeruginosa exoenzyme S, a bifunctional type-III secreted cytotoxin. Int J Med Microbiol 290:381-387
18. Barbieri JT, Sun J (2004) Pseudomonas aeruginosa ExoS and ExoT. Rev Physiol Biochem Pharmacol 152:79-92
19. Barnes PJ (2003) Cytokine-directed therapies for the treatment of chronic airway diseases. Cytokine Growth Factor Rev 14:511-522
20. Basbaum C, Li D, Gensch E, Gallup M, Lemjabbar H (2002) Mechanisms by which gram-positive bacteria and tobacco smoke stimulate mucin induction through the epidermal growth factor receptor (EGFR). Novartis Found Symp 248:171-176; discussion 176-180, 277-182

21. Becker RE, Berube BJ, Sampedro GR, DeDent AC, Bubeck Wardenburg J (2014) Tissue-specific patterning of host innate immune responses by Staphylococcus aureus alpha-toxin. J Innate Immun 6:619-631
22. Blobel CP (2005) ADAMs: key components in EGFR signalling and development. Nat Rev Mol Cell Biol 6:32-43
23. Bolik J, Krause F, Stevanovic M, Gandrass M, Thomsen I, Schacht SS, Rieser E, Muller M, Schumacher N, Fritsch J, Wichert R, Galun E, Bergmann J, Roder C, Schafmayer C, Egberts JH, Becker-Pauly C, Saftig P, Lucius R, Schneider-Brachert W, Barikbin R, Adam D, Voss M, Hitzl W, Kruger A, Strilic B, Sagi I, Walczak H, Rose-John S, Schmidt-Arras D (2022) Inhibition of ADAM17 impairs endothelial cell necroptosis and blocks metastasis. J Exp Med 219
24. Boukouris S, Mathivanan S (2015) Exosomes in bodily fluids are a highly stable resource of disease biomarkers. Proteomics Clin Appl 9:358-367
25. Brill A, Chauhan AK, Canault M, Walsh MT, Bergmeier W, Wagner DD (2009) Oxidative stress activates ADAM17/TACE and induces its target receptor shedding in platelets in a p38-dependent fashion. Cardiovasc Res 84:137-144
26. Brune K, Frank J, Schwingshackl A, Finigan J, Sidhaye VK (2015) Pulmonary epithelial barrier function: some new players and mechanisms. Am J Physiol Lung Cell Mol Physiol 308:L731-745
27. Cappenberg A, Margraf A, Thomas K, Bardel B, McCreedy DA, Van Marck V, Mellmann A, Lowell CA, Zarbock A (2019) L-selectin shedding affects bacterial clearance in the lung: a new regulatory pathway for integrin outside-in signaling. Blood 134:1445-1457
28. Cardiff RD, Miller CH, Munn RJ (2014) Manual hematoxylin and eosin staining of mouse tissue sections. Cold Spring Harb Protoc 2014:655-658
29. Carlier FM, de Fays C, Pilette C (2021) Epithelial Barrier Dysfunction in Chronic Respiratory Diseases. Front Physiol 12:691227
30. Cendra MDM, Torrents E (2021) Pseudomonas aeruginosa biofilms and their partners in crime. Biotechnol Adv 49:107734
31. Cesaro A, Abakar-Mahamat A, Brest P, Lassalle S, Selva E, Filippi J, Hebuterne X, Hugot JP, Doglio A, Galland F, Naquet P, Vouret-Craviari V, Mograbi B, Hofman PM (2009) Differential expression and regulation of ADAM17 and TIMP3 in acute inflamed intestinal epithelia. Am J Physiol Gastrointest Liver Physiol 296:G1332-1343
32. Chang JH, Kwon HY (2007) Expression of 14-3-3delta, cdc2 and cyclin B proteins related to exotoxin A-induced apoptosis in HeLa S3 cells. Int Immunopharmacol 7:1185-1191
33. Chen L, Deng H, Cui H, Fang J, Zuo Z, Deng J, Li Y, Wang X, Zhao L (2018) Inflammatory responses and inflammation-associated diseases in organs. Oncotarget 9:7204-7218
34. Clayton A, Turkes A, Dewitt S, Steadman R, Mason MD, Hallett MB (2004) Adhesion and signaling by B cell-derived exosomes: the role of integrins. FASEB J 18:977-979
35. Conrad C, Yildiz D, Cleary SJ, Margraf A, Cook L, Schlomann U, Panaretou B, Bowser JL, Karmouty-Quintana H, Li J, Berg NK, Martin SC, Aljohmani A, Moussavi-Harami SF, Wang KM, Tian JJ, Magnen M, Valet C, Qiu L, Singer JP, Eltzschig HK, Group CAS, Bertrams W, Herold S, Suttorp N, Schmeck B, Ball ZT, Zarbock A, Looney MR, Bartsch JW (2022) ADAM8 signaling drives neutrophil migration and ARDS severity. JCI Insight 7
36. Corcoran C, Rani S, O'Brien K, O'Neill A, Prencipe M, Sheikh R, Webb G, McDermott R, Watson W, Crown J, O'Driscoll L (2012) Docetaxel-resistance in prostate cancer: evaluating associated phenotypic changes and potential for resistance transfer via exosomes. PLoS One 7:e50999
37. Cott C, Thuenauer R, Landi A, Kuhn K, Juillot S, Imberty A, Madl J, Eierhoff T, Romer W (2016) Pseudomonas aeruginosa lectin LecB inhibits tissue repair processes by triggering beta-catenin degradation. Biochim Biophys Acta 1863:1106-1118
38. Coulthard MG, Morgan M, Woodruff TM, Arumugam TV, Taylor SM, Carpenter TC, Lackmann M, Boyd AW (2012) Eph/Ephrin signaling in injury and inflammation. Am J Pathol 181:1493-1503
39. Cross AS, Sadoff JC, Iglewski BH, Sokol PA (1980) Evidence for the role of toxin A in the pathogenesis of infection with Pseudomonas aeruginosa in humans. J Infect Dis 142:538-546

40. De Oliveira DMP, Forde BM, Kidd TJ, Harris PNA, Schembri MA, Beatson SA, Paterson DL, Walker MJ (2020) Antimicrobial Resistance in ESKAPE Pathogens. Clin Microbiol Rev 33
41. DeBerge MP, Ely KH, Cheng GS, Enelow RI (2013) ADAM17-mediated processing of TNF-alpha expressed by antiviral effector CD8+ T cells is required for severe T-cell-mediated lung injury. PLoS One 8:e79340
42. DeBerge MP, Ely KH, Wright PF, Thorp EB, Enelow RI (2015) Shedding of TNF receptor 2 by effector CD8(+) T cells by ADAM17 is important for regulating TNF-alpha availability during influenza infection. J Leukoc Biol 98:423-434
43. Deuss M, Reiss K, Hartmann D (2008) Part-time alpha-secretases: the functional biology of ADAM 9, 10 and 17. Curr Alzheimer Res 5:187-201
44. Dolnik O, Volchkova V, Garten W, Carbonnelle C, Becker S, Kahnt J, Stroher U, Klenk HD, Volchkov V (2004) Ectodomain shedding of the glycoprotein GP of Ebola virus. EMBO J 23:2175-2184
45. Dreymueller D, Martin C, Kogel T, Pruessmeyer J, Hess FM, Horiuchi K, Uhlig S, Ludwig A (2012a) Lung endothelial ADAM17 regulates the acute inflammatory response to lipopolysaccharide. EMBO Mol Med 4:412-423
46. Dreymueller D, Pruessmeyer J, Groth E, Ludwig A (2012b) The role of ADAM-mediated shedding in vascular biology. Eur J Cell Biol 91:472-485
47. Dreymueller D, Uhlig S, Ludwig A (2015) ADAM-family metalloproteinases in lung inflammation: potential therapeutic targets. Am J Physiol Lung Cell Mol Physiol 308:L325-343
48. Dreymueller D, Ludwig A (2017) Considerations on inhibition approaches for proinflammatory functions of ADAM proteases. Platelets 28:354-361
49. Dupre-Crochet S, Erard M, Nubetae O (2013) ROS production in phagocytes: why, when, and where? J Leukoc Biol 94:657-670
50. Edwards DR, Handsley MM, Pennington CJ (2008) The ADAM metalloproteinases. Mol Aspects Med 29:258-289
51. Etzerodt A, Maniecki MB, Moller K, Moller HJ, Moestrup SK (2010) Tumor necrosis factor alpha-converting enzyme (TACE/ADAM17) mediates ectodomain shedding of the scavenger receptor CD163. J Leukoc Biol 88:1201-1205
52. Ewan VC, Witham MD, Kiernan M, Simpson AJ (2017) Hospital-acquired pneumonia surveillance-an unmet need. Lancet Respir Med 5:771-772
53. Ezekwe EA, Jr., Weng C, Duncan JA (2016) ADAM10 Cell Surface Expression but Not Activity Is Critical for Staphylococcus aureus alpha-Hemolysin-Mediated Activation of the NLRP3 Inflammasome in Human Monocytes. Toxins (Basel) 8:95
54. Fabbri M, Paone A, Calore F, Galli R, Gaudio E, Santhanam R, Lovat F, Fadda P, Mao C, Nuovo GJ, Zanesi N, Crawford M, Ozer GH, Wernicke D, Alder H, Caligiuri MA, Nana-Sinkam P, Perrotti D, Croce CM (2012) MicroRNAs bind to Toll-like receptors to induce prometastatic inflammatory response. Proc Natl Acad Sci U S A 109:E2110-2116
55. Fagyas M, Fejes Z, Suto R, Nagy Z, Szekely B, Pocsi M, Ivady G, Biro E, Beko G, Nagy A, Kerekes G, Szentkereszty Z, Papp Z, Toth A, Kappelmayer J, Nagy B, Jr. (2022) Circulating ACE2 activity predicts mortality and disease severity in hospitalized COVID-19 patients. Int J Infect Dis 115:8-16
56. Fang SB, Zhang HY, Meng XC, Wang C, He BX, Peng YQ, Xu ZB, Fan XL, Wu ZJ, Wu ZC, Zheng SG, Fu QL (2020) Small extracellular vesicles derived from human MSCs prevent allergic airway inflammation via immunomodulation on pulmonary macrophages. Cell Death Dis 11:409
57. Faure E, Mear JB, Faure K, Normand S, Couturier-Maillard A, Grandjean T, Balloy V, Ryffel B, Dessein R, Chignard M, Uyttenhove C, Guery B, Gosset P, Chamaillard M, Kipnis E (2014) Pseudomonas aeruginosa type-3 secretion system dampens host defense by exploiting the NLRC4-coupled inflammasome. Am J Respir Crit Care Med 189:799-811
58. Feltman H, Schulert G, Khan S, Jain M, Peterson L, Hauser AR (2001) Prevalence of type III secretion genes in clinical and environmental isolates of Pseudomonas aeruginosa. Microbiology (Reading) 147:2659-2669

59. Feuillet V, Medjane S, Mondor I, Demaria O, Pagni PP, Galan JE, Flavell RA, Alexopoulou L (2006) Involvement of Toll-like receptor 5 in the recognition of flagellated bacteria. Proc Natl Acad Sci U S A 103:12487-12492
60. Filloux A (2011) Protein Secretion Systems in Pseudomonas aeruginosa: An Essay on Diversity, Evolution, and Function. Front Microbiol 2:155
61. Finigan JH, Faress JA, Wilkinson E, Mishra RS, Nethery DE, Wyler D, Shatat M, Ware LB, Matthay MA, Mason R, Silver RF, Kern JA (2011) Neuregulin-1-human epidermal receptor-2 signaling is a central regulator of pulmonary epithelial permeability and acute lung injury. J Biol Chem 286:10660-10670
62. Fioranelli M, Roccia MG, Flavin D, Cota L (2021) Regulation of Inflammatory Reaction in Health and Disease. Int J Mol Sci 22
63. Folgueras AR, Pendas AM, Sanchez LM, Lopez-Otin C (2004) Matrix metalloproteinases in cancer: from new functions to improved inhibition strategies. Int J Dev Biol 48:411-424
64. Frank CF, Hostetter MK (2007) Cleavage of E-cadherin: a mechanism for disruption of the intestinal epithelial barrier by Candida albicans. Transl Res 149:211-222
65. Franzen CA, Simms PE, Van Huis AF, Foreman KE, Kuo PC, Gupta GN (2014) Characterization of uptake and internalization of exosomes by bladder cancer cells. Biomed Res Int 2014:619829
66. Garton KJ, Gough PJ, Blobel CP, Murphy G, Greaves DR, Dempsey PJ, Raines EW (2001) Tumor necrosis factor-alpha-converting enzyme (ADAM17) mediates the cleavage and shedding of fractalkine (CX3CL1). J Biol Chem 276:37993-38001
67. Garton KJ, Gough PJ, Philalay J, Wille PT, Blobel CP, Whitehead RH, Dempsey PJ, Raines EW (2003) Stimulated shedding of vascular cell adhesion molecule 1 (VCAM-1) is mediated by tumor necrosis factor-alpha-converting enzyme (ADAM 17). J Biol Chem 278:37459-37464
68. Giannoni E, Buricchi F, Raugei G, Ramponi G, Chiarugi P (2005) Intracellular reactive oxygen species activate Src tyrosine kinase during cell adhesion and anchorage-dependent cell growth. Mol Cell Biol 25:6391-6403
69. Giebeler N, Zigrino P (2016) A Disintegrin and Metalloprotease (ADAM): Historical Overview of Their Functions. Toxins (Basel) 8:122
70. Goehring UM, Schmidt G, Pederson KJ, Aktories K, Barbieri JT (1999) The N-terminal domain of Pseudomonas aeruginosa exoenzyme S is a GTPase-activating protein for Rho GTPases. J Biol Chem 274:36369-36372
71. Gomez MI, Sokol SH, Muir AB, Soong G, Bastien J, Prince AS (2005) Bacterial induction of TNF-alpha converting enzyme expression and IL-6 receptor alpha shedding regulates airway inflammatory signaling. J Immunol 175:1930-1936
72. Gordon DL, Rice JL (1988) Opsonin-dependent and independent surface phagocytosis of S. aureus proceeds independently of complement and complement receptors. Immunology 64:709-714
73. Gordon S (2016) Phagocytosis: An Immunobiologic Process. Immunity 44:463-475
74. Gough PJ, Garton KJ, Wille PT, Rychlewski M, Dempsey PJ, Raines EW (2004) A disintegrin and metalloproteinase 10-mediated cleavage and shedding regulates the cell surface expression of CXC chemokine ligand 16. J Immunol 172:3678-3685
75. Gravelle S, Barnes R, Hawdon N, Shewchuk L, Eibl J, Lam JS, Ulanova M (2010) Up-regulation of integrin expression in lung adenocarcinoma cells caused by bacterial infection: in vitro study. Innate Immun 16:14-26
76. Grotzinger J, Lorenzen I, Dusterhoft S (2017) Molecular insights into the multilayered regulation of ADAM17: The role of the extracellular region. Biochim Biophys Acta Mol Cell Res 1864:2088-2095
77. Gulati A, Kaur D, Krishna Prasad GVR, Mukhopadhaya A (2018) PRR Function of Innate Immune Receptors in Recognition of Bacteria or Bacterial Ligands. Adv Exp Med Biol 1112:255-280
78. Gurunathan S, Kang MH, Kim JH (2021) Diverse Effects of Exosomes on COVID-19: A Perspective of Progress From Transmission to Therapeutic Developments. Front Immunol 12:716407

79. Hakulinen J, Keski-Oja J (2006) ADAM10-mediated release of complement membrane cofactor protein during apoptosis of epithelial cells. J Biol Chem 281:21369-21376
80. Hannoodee S, Nasuruddin DN (2022). Acute Inflammatory Response. In StatPearls (Treasure Island (FL)).
81. Hardy KS, Tessmer MH, Frank DW, Audia JP (2021) Perspectives on the Pseudomonas aeruginosa Type III Secretion System Effector ExoU and Its Subversion of the Host Innate Immune Response to Infection. Toxins (Basel) 13
82. Hauser AR (2009) The type III secretion system of Pseudomonas aeruginosa: infection by injection. Nat Rev Microbiol 7:654-665
83. Heggers JP, Haydon S, Ko F, Hayward PG, Carp S, Robson MC (1992) Pseudomonas aeruginosa exotoxin A: its role in retardation of wound healing: the 1992 Lindberg Award. J Burn Care Rehabil 13:512-518
84. Herb M, Schramm M (2021) Functions of ROS in Macrophages and Antimicrobial Immunity. Antioxidants (Basel) 10
85. Hirakata Y, Finlay BB, Simpson DA, Kohno S, Kamihira S, Speert DP (2000) Penetration of clinical isolates of Pseudomonas aeruginosa through MDCK epithelial cell monolayers. J Infect Dis 181:765-769
86. Hirayama A, Awano S, Seta Y, Ansai T (2017) ADAM17 regulates TNF-alpha expression upon lipopolysaccharide stimulation in oral keratinocytes. Biomed Res 38:157-165
87. Hooper NM, Karran EH, Turner AJ (1997) Membrane protein secretases. Biochem J 321 (Pt 2):265-279
88. Hordijk PL (2016) Recent insights into endothelial control of leukocyte extravasation. Cell Mol Life Sci 73:1591-1608
89. Horiuchi K, Kimura T, Miyamoto T, Takaishi H, Okada Y, Toyama Y, Blobel CP (2007) Cutting edge: TNF-alpha-converting enzyme (TACE/ADAM17) inactivation in mouse myeloid cells prevents lethality from endotoxin shock. J Immunol 179:2686-2689
90. Hougaard S, Loechel F, Xu X, Tajima R, Albrechtsen R, Wewer UM (2000) Trafficking of human ADAM 12-L: retention in the trans-Golgi network. Biochem Biophys Res Commun 275:261-267
91. Hu J, Van den Steen PE, Sang QX, Opdenakker G (2007) Matrix metalloproteinase inhibitors as therapy for inflammatory and vascular diseases. Nat Rev Drug Discov 6:480-498
92. Huber P (2022) ExlA: A New Contributor to Pseudomonas aeruginosa Virulence. Front Cell Infect Microbiol 12:929150
93. Huet O, Ramsey D, Miljavec S, Jenney A, Aubron C, Aprico A, Stefanovic N, Balkau B, Head GA, de Haan JB, Chin-Dusting JP (2013) Ensuring animal welfare while meeting scientific aims using a murine pneumonia model of septic shock. Shock 39:488-494
94. Hundhausen C, Misztela D, Berkhout TA, Broadway N, Saftig P, Reiss K, Hartmann D, Fahrenholz F, Postina R, Matthews V, Kallen KJ, Rose-John S, Ludwig A (2003) The disintegrin-like metalloproteinase ADAM10 is involved in constitutive cleavage of CX3CL1 (fractalkine) and regulates CX3CL1-mediated cell-cell adhesion. Blood 102:1186-1195
95. Hyde SR, Stith RD, McCallum RE (1990) Mortality and bacteriology of sepsis following cecal ligation and puncture in aged mice. Infect Immun 58:619-624
96. Inoshima I, Inoshima N, Wilke GA, Powers ME, Frank KM, Wang Y, Bubeck Wardenburg J (2011) A Staphylococcus aureus pore-forming toxin subverts the activity of ADAM10 to cause lethal infection in mice. Nat Med 17:1310-1314
97. Inoshima N, Wang Y, Bubeck Wardenburg J (2012) Genetic requirement for ADAM10 in severe Staphylococcus aureus skin infection. J Invest Dermatol 132:1513-1516
98. Inoue A, Ishiguro J, Kitamura H, Arima N, Okutani M, Shuto A, Higashiyama S, Ohwada T, Arai H, Makide K, Aoki J (2012) TGFalpha shedding assay: an accurate and versatile method for detecting GPCR activation. Nat Methods 9:1021-1029
99. Izaguirre MF, Larrea D, Adur JF, Diaz-Zamboni JE, Vicente NB, Galetto CD, Casco VH (2010) Role of E-cadherin in epithelial architecture maintenance. Cell Commun Adhes 17:1-12
100. Jain S, Self WH, Wunderink RG, Team CES (2015) Community-Acquired Pneumonia Requiring Hospitalization. N Engl J Med 373:2382

101. Janeway CA, Jr. (1989) Approaching the asymptote? Evolution and revolution in immunology. Cold Spring Harb Symp Quant Biol 54 Pt 1:1-13
102. Jaumouille V, Grinstein S (2011) Receptor mobility, the cytoskeleton, and particle binding during phagocytosis. Curr Opin Cell Biol 23:22-29
103. Jocher G, Grass V, Tschirner SK, Riepler L, Breimann S, Kaya T, Oelsner M, Hamad MS, Hofmann LI, Blobel CP, Schmidt-Weber CB, Gokce O, Jakwerth CA, Trimpert J, Kimpel J, Pichlmair A, Lichtenthaler SF (2022) ADAM10 and ADAM17 promote SARS-CoV-2 cell entry and spike protein-mediated lung cell fusion. EMBO Rep 23:e54305
104. Jorissen E, Prox J, Bernreuther C, Weber S, Schwanbeck R, Serneels L, Snellinx A, Craessaerts K, Thathiah A, Tesseur I, Bartsch U, Weskamp G, Blobel CP, Glatzel M, De Strooper B, Saftig P (2010) The disintegrin/metalloproteinase ADAM10 is essential for the establishment of the brain cortex. J Neurosci 30:4833-4844
105. Jouault A, Saliba AM, Touqui L (2022) Modulation of the immune response by the Pseudomonas aeruginosa type-III secretion system. Front Cell Infect Microbiol 12:1064010
106. Juan C, Pena C, Oliver A (2017) Host and Pathogen Biomarkers for Severe Pseudomonas aeruginosa Infections. J Infect Dis 215:S44-S51
107. Kahlert C, Kalluri R (2013) Exosomes in tumor microenvironment influence cancer progression and metastasis. J Mol Med (Berl) 91:431-437
108. Kalluri R, LeBleu VS (2020) The biology, function, and biomedical applications of exosomes. Science 367
109. Kawaguchi M, Mitsuhashi Y, Kondo S (2005) Overexpression of tumour necrosis factor-alpha-converting enzyme in psoriasis. Br J Dermatol 152:915-919
110. Kneidl J, Loffler B, Erat MC, Kalinka J, Peters G, Roth J, Barczyk K (2012) Soluble CD163 promotes recognition, phagocytosis and killing of Staphylococcus aureus via binding of specific fibronectin peptides. Cell Microbiol 14:914-936
111. Ko SY, Lin SC, Wong YK, Liu CJ, Chang KW, Liu TY (2007) Increase of disintergin metalloprotease 10 (ADAM10) expression in oral squamous cell carcinoma. Cancer Lett 245:33-43
112. Koenen RR, Pruessmeyer J, Soehnlein O, Fraemohs L, Zernecke A, Schwarz N, Reiss K, Sarabi A, Lindbom L, Hackeng TM, Weber C, Ludwig A (2009) Regulated release and functional modulation of junctional adhesion molecule A by disintegrin metalloproteinases. Blood 113:4799-4809
113. Koff JL, Shao MX, Ueki IF, Nadel JA (2008) Multiple TLRs activate EGFR via a signaling cascade to produce innate immune responses in airway epithelium. Am J Physiol Lung Cell Mol Physiol 294:L1068-1075
114. Kohutek ZA, diPierro CG, Redpath GT, Hussaini IM (2009) ADAM-10-mediated N-cadherin cleavage is protein kinase C-alpha dependent and promotes glioblastoma cell migration. J Neurosci 29:4605-4615
115. Kopan R, Ilagan MX (2009) The canonical Notch signaling pathway: unfolding the activation mechanism. Cell 137:216-233
116. Kounnas MZ, Morris RE, Thompson MR, FitzGerald DJ, Strickland DK, Saelinger CB (1992) The alpha 2-macroglobulin receptor/low density lipoprotein receptor-related protein binds and internalizes Pseudomonas exotoxin A. J Biol Chem 267:12420-12423
117. Krueger E, Brown AC (2019) Inhibition of bacterial toxin recognition of membrane components as an anti-virulence strategy. J Biol Eng 13:4
118. Kuba K, Imai Y, Rao S, Gao H, Guo F, Guan B, Huan Y, Yang P, Zhang Y, Deng W, Bao L, Zhang B, Liu G, Wang Z, Chappell M, Liu Y, Zheng D, Leibbrandt A, Wada T, Slutsky AS, Liu D, Qin C, Jiang C, Penninger JM (2005) A crucial role of angiotensin converting enzyme 2 (ACE2) in SARS coronavirus-induced lung injury. Nat Med 11:875-879
119. Kulisz A, Chen N, Chandel NS, Shao Z, Schumacker PT (2002) Mitochondrial ROS initiate phosphorylation of p38 MAP kinase during hypoxia in cardiomyocytes. Am J Physiol Lung Cell Mol Physiol 282:L1324-1329
120. Kumar H, Kawai T, Akira S (2011) Pathogen recognition by the innate immune system. Int Rev Immunol 30:16-34

121. Kumar R, Feltrup TM, Kukreja RV, Patel KB, Cai S, Singh BR (2019) Evolutionary Features in the Structure and Function of Bacterial Toxins. Toxins (Basel) 11
122. Kumar V (2022) Toll-Like Receptors in Adaptive Immunity. Handb Exp Pharmacol 276:95-131
123. Kuwahara I, Lillehoj EP, Koga T, Isohama Y, Miyata T, Kim KC (2007) The signaling pathway involved in neutrophil elastase stimulated MUC1 transcription. Am J Respir Cell Mol Biol 37:691-698
124. Laforge M, Elbim C, Frere C, Hemadi M, Massaad C, Nuss P, Benoliel JJ, Becker C (2020) Tissue damage from neutrophil-induced oxidative stress in COVID-19. Nat Rev Immunol 20:515-516
125. Lannes-Costa PS, de Oliveira JSS, da Silva Santos G, Nagao PE (2021) A current review of pathogenicity determinants of Streptococcus sp. J Appl Microbiol 131:1600-1620
126. Le Gall SM, Bobe P, Reiss K, Horiuchi K, Niu XD, Lundell D, Gibb DR, Conrad D, Saftig P, Blobel CP (2009) ADAMs 10 and 17 represent differentially regulated components of a general shedding machinery for membrane proteins such as transforming growth factor alpha, L-selectin, and tumor necrosis factor alpha. Mol Biol Cell 20:1785-1794
127. Lecuyer H, Virion Z, Barnier JP, Matczak S, Bourdoulous S, Bianchini E, Saller F, Borgel D, Nassif X, Coureuil M (2018) An ADAM-10 dependent EPCR shedding links meningococcal interaction with endothelial cells to purpura fulminans. PLoS Pathog 14:e1006981
128. Lee HJ, Woo Y, Hahn TW, Jung YM, Jung YJ (2020) Formation and Maturation of the Phagosome: A Key Mechanism in Innate Immunity against Intracellular Bacterial Infection. Microorganisms 8
129. Leick M, Azcutia V, Newton G, Luscinskas FW (2014) Leukocyte recruitment in inflammation: basic concepts and new mechanistic insights based on new models and microscopic imaging technologies. Cell Tissue Res 355:647-656
130. Levi M (2010) The coagulant response in sepsis and inflammation. Hamostaseologie 30:10-12, 14-16
131. Li KL, Huang HY, Ren H, Yang XL (2022) Role of exosomes in the pathogenesis of inflammation in Parkinson's disease. Neural Regen Res 17:1898-1906
132. Li QC, Liang Y, Su ZB (2019) Prophylactic treatment with MSC-derived exosomes attenuates traumatic acute lung injury in rats. Am J Physiol Lung Cell Mol Physiol 316:L1107-L1117
133. Li Y, Karlin A, Loike JD, Silverstein SC (2002) A critical concentration of neutrophils is required for effective bacterial killing in suspension. Proc Natl Acad Sci U S A 99:8289-8294
134. Li Z, Takino T, Endo Y, Sato H (2017) Activation of MMP-9 by membrane type-1 MMP/MMP-2 axis stimulates tumor metastasis. Cancer Sci 108:347-353
135. Lichtenberg M, Jakobsen TH, Kuhl M, Kolpen M, Jensen PO, Bjarnsholt T (2022) The structure-function relationship of Pseudomonas aeruginosa in infections and its influence on the microenvironment. FEMS Microbiol Rev 46
136. Lichtenthaler SF (2011) alpha-secretase in Alzheimer's disease: molecular identity, regulation and therapeutic potential. J Neurochem 116:10-21
137. Liu PC, Liu X, Li Y, Covington M, Wynn R, Huber R, Hillman M, Yang G, Ellis D, Marando C, Katiyar K, Bradley J, Abremski K, Stow M, Rupar M, Zhuo J, Li YL, Lin Q, Burns D, Xu M, Zhang C, Qian DQ, He C, Sharief V, Weng L, Agrios C, Shi E, Metcalf B, Newton R, Friedman S, Yao W, Scherle P, Hollis G, Burn TC (2006) Identification of ADAM10 as a major source of HER2 ectodomain sheddase activity in HER2 overexpressing breast cancer cells. Cancer Biol Ther 5:657-664
138. Liu PV (1974) Extracellular toxins of Pseudomonas aeruginosa. J Infect Dis 130 Suppl:S94-99
139. Liu Y, Liu Y, Du Z, Zhang L, Chen J, Shen Z, Liu Q, Qin J, Lv H, Wang H, He L, Liu J, Huang Q, Sun Y, Otto M, Li M (2020) Skin microbiota analysis-inspired development of novel anti-infectives. Microbiome 8:85
140. Long C, Hosseinkhani MR, Wang Y, Sriramarao P, Walcheck B (2012) ADAM17 activation in circulating neutrophils following bacterial challenge impairs their recruitment. J Leukoc Biol 92:667-672
141. Long ME, Mallampalli RK, Horowitz JC (2022) Pathogenesis of pneumonia and acute lung injury. Clin Sci (Lond) 136:747-769

142. Ludwig A, Hundhausen C, Lambert MH, Broadway N, Andrews RC, Bickett DM, Leesnitzer MA, Becherer JD (2005) Metalloproteinase inhibitors for the disintegrin-like metalloproteinases ADAM10 and ADAM17 that differentially block constitutive and phorbol ester-inducible shedding of cell surface molecules. Comb Chem High Throughput Screen 8:161-171
143. Lum L, Reid MS, Blobel CP (1998) Intracellular maturation of the mouse metalloprotease disintegrin MDC15. J Biol Chem 273:26236-26247
144. Luyt CE, Hekimian G, Koulenti D, Chastre J (2018) Microbial cause of ICU-acquired pneumonia: hospital-acquired pneumonia versus ventilator-associated pneumonia. Curr Opin Crit Care 24:332-338
145. Maretzky T, Reiss K, Ludwig A, Buchholz J, Scholz F, Proksch E, de Strooper B, Hartmann D, Saftig P (2005) ADAM10 mediates E-cadherin shedding and regulates epithelial cell-cell adhesion, migration, and beta-catenin translocation. Proc Natl Acad Sci U S A 102:9182-9187
146. Maretzky T, Scholz F, Koten B, Proksch E, Saftig P, Reiss K (2008) ADAM10-mediated E-cadherin release is regulated by proinflammatory cytokines and modulates keratinocyte cohesion in eczematous dermatitis. J Invest Dermatol 128:1737-1746
147. Mathieu M, Martin-Jaular L, Lavieu G, Thery C (2019) Specificities of secretion and uptake of exosomes and other extracellular vesicles for cell-to-cell communication. Nat Cell Biol 21:9-17
148. Medzhitov R (2001) Toll-like receptors and innate immunity. Nat Rev Immunol 1:135-145
149. Medzhitov R (2008) Origin and physiological roles of inflammation. Nature 454:428-435
150. Medzhitov R (2010) Inflammation 2010: new adventures of an old flame. Cell 140:771-776
151. Michalska M, Wolf P (2015) Pseudomonas Exotoxin A: optimized by evolution for effective killing. Front Microbiol 6:963
152. Mishra HK, Johnson TJ, Seelig DM, Walcheck B (2016) Targeting ADAM17 in leukocytes increases neutrophil recruitment and reduces bacterial spread during polymicrobial sepsis. J Leukoc Biol 100:999-1004
153. Mittal M, Siddiqui MR, Tran K, Reddy SP, Malik AB (2014) Reactive oxygen species in inflammation and tissue injury. Antioxid Redox Signal 20:1126-1167
154. Mogensen TH (2009) Pathogen recognition and inflammatory signaling in innate immune defenses. Clin Microbiol Rev 22:240-273, Table of Contents
155. Morrow KA, Frank DW, Balczon R, Stevens T (2017) The Pseudomonas aeruginosa Exoenzyme Y: A Promiscuous Nucleotidyl Cyclase Edema Factor and Virulence Determinant. Handb Exp Pharmacol 238:67-85
156. Moss ML, Minond D (2017) Recent Advances in ADAM17 Research: A Promising Target for Cancer and Inflammation. Mediators Inflamm 2017:9673537
157. Muller M, Li Z, Maitz PK (2009) Pseudomonas pyocyanin inhibits wound repair by inducing premature cellular senescence: role for p38 mitogen-activated protein kinase. Burns 35:500-508
158. Muller WA (2003) Leukocyte-endothelial-cell interactions in leukocyte transmigration and the inflammatory response. Trends Immunol 24:327-334
159. Muller WA (2011) Mechanisms of leukocyte transendothelial migration. Annu Rev Pathol 6:323-344
160. Muller WA (2013) Getting leukocytes to the site of inflammation. Vet Pathol 50:7-22
161. Nakanaga T, Nadel JA, Ueki IF, Koff JL, Shao MX (2007) Regulation of interleukin-8 via an airway epithelial signaling cascade. Am J Physiol Lung Cell Mol Physiol 292:L1289-1296
162. Nazarenko I, Rana S, Baumann A, McAlear J, Hellwig A, Trendelenburg M, Lochnit G, Preissner KT, Zoller M (2010) Cell surface tetraspanin Tspan8 contributes to molecular pathways of exosome-induced endothelial cell activation. Cancer Res 70:1668-1678
163. Nimmerjahn F, Ravetch JV (2011) FcgammaRs in health and disease. Curr Top Microbiol Immunol 350:105-125
164. Nourshargh S, Krombach F, Dejana E (2006) The role of JAM-A and PECAM-1 in modulating leukocyte infiltration in inflamed and ischemic tissues. J Leukoc Biol 80:714-718
165. Otto M (2020) Staphylococci in the human microbiome: the role of host and interbacterial interactions. Curr Opin Microbiol 53:71-77

166. Paland N, Bohme L, Gurumurthy RK, Maurer A, Szczepek AJ, Rudel T (2008) Reduced display of tumor necrosis factor receptor I at the host cell surface supports infection with Chlamydia trachomatis. J Biol Chem 283:6438-6448
167. Pauwels AM, Trost M, Beyaert R, Hoffmann E (2017) Patterns, Receptors, and Signals: Regulation of Phagosome Maturation. Trends Immunol 38:407-422
168. Peinado H, Aleckovic M, Lavotshkin S, Matei I, Costa-Silva B, Moreno-Bueno G, Hergueta-Redondo M, Williams C, Garcia-Santos G, Ghajar C, Nitadori-Hoshino A, Hoffman C, Badal K, Garcia BA, Callahan MK, Yuan J, Martins VR, Skog J, Kaplan RN, Brady MS, Wolchok JD, Chapman PB, Kang Y, Bromberg J, Lyden D (2012) Melanoma exosomes educate bone marrow progenitor cells toward a pro-metastatic phenotype through MET. Nat Med 18:883-891
169. Pesce E, Manfrini N, Cordiglieri C, Santi S, Bandera A, Gobbini A, Gruarin P, Favalli A, Bombaci M, Cuomo A, Collino F, Cricri G, Ungaro R, Lombardi A, Mangioni D, Muscatello A, Aliberti S, Blasi F, Gori A, Abrignani S, De Francesco R, Biffo S, Grifantini R (2021) Exosomes Recovered From the Plasma of COVID-19 Patients Expose SARS-CoV-2 Spike-Derived Fragments and Contribute to the Adaptive Immune Response. Front Immunol 12:785941
170. Peschon JJ, Slack JL, Reddy P, Stocking KL, Sunnarborg SW, Lee DC, Russell WE, Castner BJ, Johnson RS, Fitzner JN, Boyce RW, Nelson N, Kozlosky CJ, Wolfson MF, Rauch CT, Cerretti DP, Paxton RJ, March CJ, Black RA (1998) An essential role for ectodomain shedding in mammalian development. Science 282:1281-1284
171. Powers ME, Kim HK, Wang Y, Bubeck Wardenburg J (2012) ADAM10 mediates vascular injury induced by Staphylococcus aureus alpha-hemolysin. J Infect Dis 206:352-356
172. Pruessmeyer J, Ludwig A (2009) The good, the bad and the ugly substrates for ADAM10 and ADAM17 in brain pathology, inflammation and cancer. Semin Cell Dev Biol 20:164-174
173. Pruessmeyer J, Martin C, Hess FM, Schwarz N, Schmidt S, Kogel T, Hoettecke N, Schmidt B, Sechi A, Uhlig S, Ludwig A (2010) A disintegrin and metalloproteinase 17 (ADAM17) mediates inflammation-induced shedding of syndecan-1 and -4 by lung epithelial cells. J Biol Chem 285:555-564
174. Pruessmeyer J, Hess FM, Alert H, Groth E, Pasqualon T, Schwarz N, Nyamoya S, Kollert J, van der Vorst E, Donners M, Martin C, Uhlig S, Saftig P, Dreymueller D, Ludwig A (2014) Leukocytes require ADAM10 but not ADAM17 for their migration and inflammatory recruitment into the alveolar space. Blood 123:4077-4088
175. Qin L, Quinlan WM, Doyle NA, Graham L, Sligh JE, Takei F, Beaudet AL, Doerschuk CM (1996) The roles of CD11/CD18 and ICAM-1 in acute Pseudomonas aeruginosa-induced pneumonia in mice. J Immunol 157:5016-5021
176. Rabiei P, Mohabatkar H, Behbahani M (2019) Studying the effects of several heat-inactivated bacteria on colon and breast cancer cells. Mol Biol Res Commun 8:91-98
177. Rahn S, Becker-Pauly C (2022) Meprin and ADAM proteases as triggers of systemic inflammation in sepsis. FEBS Lett 596:534-556
178. Ramirez JA, Wiemken TL, Peyrani P, Arnold FW, Kelley R, Mattingly WA, Nakamatsu R, Pena S, Guinn BE, Furmanek SP, Persaud AK, Raghuram A, Fernandez F, Beavin L, Bosson R, Fernandez-Botran R, Cavallazzi R, Bordon J, Valdivieso C, Schulte J, Carrico RM, University of Louisville Pneumonia Study G (2017) Adults Hospitalized With Pneumonia in the United States: Incidence, Epidemiology, and Mortality. Clin Infect Dis 65:1806-1812
179. Rana S, Yue S, Stadel D, Zoller M (2012) Toward tailored exosomes: the exosomal tetraspanin web contributes to target cell selection. Int J Biochem Cell Biol 44:1574-1584
180. Raoust E, Balloy V, Garcia-Verdugo I, Touqui L, Ramphal R, Chignard M (2009) Pseudomonas aeruginosa LPS or flagellin are sufficient to activate TLR-dependent signaling in murine alveolar macrophages and airway epithelial cells. PLoS One 4:e7259
181. Raposo G, Nijman HW, Stoorvogel W, Liejendekker R, Harding CV, Melief CJ, Geuze HJ (1996) B lymphocytes secrete antigen-presenting vesicles. J Exp Med 183:1161-1172
182. Raucci A, Cugusi S, Antonelli A, Barabino SM, Monti L, Bierhaus A, Reiss K, Saftig P, Bianchi ME (2008) A soluble form of the receptor for advanced glycation endproducts (RAGE) is produced

by proteolytic cleavage of the membrane-bound form by the sheddase a disintegrin and metalloprotease 10 (ADAM10). FASEB J 22:3716-3727

183. Reboud E, Bouillot S, Patot S, Beganton B, Attree I, Huber P (2017) Pseudomonas aeruginosa ExlA and Serratia marcescens ShlA trigger cadherin cleavage by promoting calcium influx and ADAM10 activation. PLoS Pathog 13:e1006579
184. Reiss K, Maretzky T, Ludwig A, Tousseyn T, de Strooper B, Hartmann D, Saftig P (2005) ADAM10 cleavage of N-cadherin and regulation of cell-cell adhesion and beta-catenin nuclear signalling. EMBO J 24:742-752
185. Rio C, Buxbaum JD, Peschon JJ, Corfas G (2000) Tumor necrosis factor-alpha-converting enzyme is required for cleavage of erbB4/HER4. J Biol Chem 275:10379-10387
186. Robinson JM (2008) Reactive oxygen species in phagocytic leukocytes. Histochem Cell Biol 130:281-297
187. Roghani M, Becherer JD, Moss ML, Atherton RE, Erdjument-Bromage H, Arribas J, Blackburn RK, Weskamp G, Tempst P, Blobel CP (1999) Metalloprotease-disintegrin MDC9: intracellular maturation and catalytic activity. J Biol Chem 274:3531-3540
188. Rosales C, Uribe-Querol E (2017) Phagocytosis: A Fundamental Process in Immunity. Biomed Res Int 2017:9042851
189. Rossi E, La Rosa R, Bartell JA, Marvig RL, Haagensen JAJ, Sommer LM, Molin S, Johansen HK (2021) Pseudomonas aeruginosa adaptation and evolution in patients with cystic fibrosis. Nat Rev Microbiol 19:331-342
190. Sahin U, Weskamp G, Kelly K, Zhou HM, Higashiyama S, Peschon J, Hartmann D, Saftig P, Blobel CP (2004) Distinct roles for ADAM10 and ADAM17 in ectodomain shedding of six EGFR ligands. J Cell Biol 164:769-779
191. Scharfenberg F, Helbig A, Sammel M, Benzel J, Schlomann U, Peters F, Wichert R, Bettendorff M, Schmidt-Arras D, Rose-John S, Moali C, Lichtenthaler SF, Pietrzik CU, Bartsch JW, Tholey A, Becker-Pauly C (2020) Degradome of soluble ADAM10 and ADAM17 metalloproteases. Cell Mol Life Sci 77:331-350
192. Schauble N, Cavalie A, Zimmermann R, Jung M (2014) Interaction of Pseudomonas aeruginosa Exotoxin A with the human Sec61 complex suppresses passive calcium efflux from the endoplasmic reticulum. Channels (Austin) 8:76-83
193. Scheller J, Chalaris A, Garbers C, Rose-John S (2011) ADAM17: a molecular switch to control inflammation and tissue regeneration. Trends Immunol 32:380-387
194. Schirrmeister W, Gnad T, Wex T, Higashiyama S, Wolke C, Naumann M, Lendeckel U (2009) Ectodomain shedding of E-cadherin and c-Met is induced by Helicobacter pylori infection. Exp Cell Res 315:3500-3508
195. Schlondorff J, Blobel CP (1999) Metalloprotease-disintegrins: modular proteins capable of promoting cell-cell interactions and triggering signals by protein-ectodomain shedding. J Cell Sci 112 (Pt 21):3603-3617
196. Schneeberger EE, Lynch RD (2004) The tight junction: a multifunctional complex. Am J Physiol Cell Physiol 286:C1213-1228
197. Schultz MJ, Rijneveld AW, Florquin S, Speelman P, SJH VAND, T VDP (2001) Impairment of host defence by exotoxin A in Pseudomonas aeruginosa pneumonia in mice. J Med Microbiol 50:822-827
198. Schulz B, Pruessmeyer J, Maretzky T, Ludwig A, Blobel CP, Saftig P, Reiss K (2008) ADAM10 regulates endothelial permeability and T-Cell transmigration by proteolysis of vascular endothelial cadherin. Circ Res 102:1192-1201
199. Seals DF, Courtneidge SA (2003) The ADAMs family of metalloproteases: multidomain proteins with multiple functions. Genes Dev 17:7-30
200. Seegar TC, Blacklow SC (2019) Domain integration of ADAM family proteins: Emerging themes from structural studies. Exp Biol Med (Maywood) 244:1510-1519
201. Seifert A, Wozniak J, Dusterhoft S, Kasparek P, Sedlacek R, Dreschers S, Orlikowsky TW, Yildiz D, Ludwig A (2020) The iRhom2/ADAM17 Axis Attenuates Bacterial Uptake by Phagocytes in a Cell Autonomous Manner. Int J Mol Sci 21

202. Severson EA, Parkos CA (2009) Structural determinants of Junctional Adhesion Molecule A (JAM-A) function and mechanisms of intracellular signaling. Curr Opin Cell Biol 21:701-707
203. Shen L, Weber CR, Raleigh DR, Yu D, Turner JR (2011) Tight junction pore and leak pathways: a dynamic duo. Annu Rev Physiol 73:283-309
204. Sherwood ER, Toliver-Kinsky T (2004) Mechanisms of the inflammatory response. Best Pract Res Clin Anaesthesiol 18:385-405
205. Shiau JW, Tang TK, Shih YL, Tai C, Sung YY, Huang JL, Yang HL (2000) Mice immunized with DNA encoding a modified Pseudomonas aeruginosa exotoxin A develop protective immunity against exotoxin intoxication. Vaccine 19:1106-1112
206. Shimaoka T, Nakayama T, Kume N, Takahashi S, Yamaguchi J, Minami M, Hayashida K, Kita T, Ohsumi J, Yoshie O, Yonehara S (2003) Cutting edge: SR-PSOX/CXC chemokine ligand 16 mediates bacterial phagocytosis by APCs through its chemokine domain. J Immunol 171:1647-1651
207. Simpson RJ, Lim JW, Moritz RL, Mathivanan S (2009) Exosomes: proteomic insights and diagnostic potential. Expert Rev Proteomics 6:267-283
208. Siraki AG (2021) The many roles of myeloperoxidase: From inflammation and immunity to biomarkers, drug metabolism and drug discovery. Redox Biol 46:102109
209. Smelt JP, Brul S (2014) Thermal inactivation of microorganisms. Crit Rev Food Sci Nutr 54:1371-1385
210. Smith TM, Jr., Tharakan A, Martin RK (2020) Targeting ADAM10 in Cancer and Autoimmunity. Front Immunol 11:499
211. Stoeck A, Keller S, Riedle S, Sanderson MP, Runz S, Le Naour F, Gutwein P, Ludwig A, Rubinstein E, Altevogt P (2006) A role for exosomes in the constitutive and stimulus-induced ectodomain cleavage of L1 and CD44. Biochem J 393:609-618
212. Stone AL, Kroeger M, Sang QX (1999) Structure-function analysis of the ADAM family of disintegrin-like and metalloproteinase-containing proteins (review). J Protein Chem 18:447-465
213. Suh JH, Joo HS, Hong EB, Lee HJ, Lee JM (2021) Therapeutic Application of Exosomes in Inflammatory Diseases. Int J Mol Sci 22
214. Tjelle TE, Lovdal T, Berg T (2000) Phagosome dynamics and function. Bioessays 22:255-263
215. Tosello V, Ferrando AA (2013) The NOTCH signaling pathway: role in the pathogenesis of T-cell acute lymphoblastic leukemia and implication for therapy. Ther Adv Hematol 4:199-210
216. Tosetti F, Vene R, Camodeca C, Nuti E, Rossello A, D'Arrigo C, Galante D, Ferrari N, Poggi A, Zocchi MR (2018) Specific ADAM10 inhibitors localize in exosome-like vesicles released by Hodgkin lymphoma and stromal cells and prevent sheddase activity carried to bystander cells. Oncoimmunology 7:e1421889
217. Tran Van Nhieu G, Dupont G, Combettes L (2018) Ca(2+) signals triggered by bacterial pathogens and microdomains. Biochim Biophys Acta Mol Cell Res 1865:1838-1845
218. Tricker E, Cheng G (2008) With a little help from my friends: modulation of phagocytosis through TLR activation. Cell Res 18:711-712
219. Tsukita S, Furuse M, Itoh M (2001) Multifunctional strands in tight junctions. Nat Rev Mol Cell Biol 2:285-293
220. Uribe-Querol E, Rosales C (2020) Phagocytosis: Our Current Understanding of a Universal Biological Process. Front Immunol 11:1066
221. Valadi H, Ekstrom K, Bossios A, Sjostrand M, Lee JJ, Lotvall JO (2007) Exosome-mediated transfer of mRNAs and microRNAs is a novel mechanism of genetic exchange between cells. Nat Cell Biol 9:654-659
222. Van Itallie CM, Anderson JM (2004) The molecular physiology of tight junction pores. Physiology (Bethesda) 19:331-338
223. Vidal M, Sainte-Marie J, Philippot JR, Bienvenue A (1989) Asymmetric distribution of phospholipids in the membrane of vesicles released during in vitro maturation of guinea pig reticulocytes: evidence precluding a role for "aminophospholipid translocase". J Cell Physiol 140:455-462

224. Vijay K (2018) Toll-like receptors in immunity and inflammatory diseases: Past, present, and future. Int Immunopharmacol 59:391-412
225. Vikstrom E, Bui L, Konradsson P, Magnusson KE (2009) The junctional integrity of epithelial cells is modulated by Pseudomonas aeruginosa quorum sensing molecule through phosphorylation-dependent mechanisms. Exp Cell Res 315:313-326
226. Villalpando-Rodriguez GE, Gibson SB (2021) Reactive Oxygen Species (ROS) Regulates Different Types of Cell Death by Acting as a Rheostat. Oxid Med Cell Longev 2021:9912436
227. Wagener BM, Hu R, Wu S, Pittet JF, Ding Q, Che P (2021) The Role of Pseudomonas aeruginosa Virulence Factors in Cytoskeletal Dysregulation and Lung Barrier Dysfunction. Toxins (Basel) 13
228. Wang Y, Herrera AH, Li Y, Belani KK, Walcheck B (2009) Regulation of mature ADAM17 by redox agents for L-selectin shedding. J Immunol 182:2449-2457
229. Wang Y, Zheng J, Han Y, Zhang Y, Su L, Hu D, Fu X (2018) JAM-A knockdown accelerates the proliferation and migration of human keratinocytes, and improves wound healing in rats via FAK/Erk signaling. Cell Death Dis 9:848
230. Ware LB, Matthay MA (2000) The acute respiratory distress syndrome. N Engl J Med 342:1334-1349
231. Welton JL, Khanna S, Giles PJ, Brennan P, Brewis IA, Staffurth J, Mason MD, Clayton A (2010) Proteomics analysis of bladder cancer exosomes. Mol Cell Proteomics 9:1324-1338
232. Wetzel S, Seipold L, Saftig P (2017) The metalloproteinase ADAM10: A useful therapeutic target? Biochim Biophys Acta Mol Cell Res 1864:2071-2081
233. Wilke GA, Bubeck Wardenburg J (2010) Role of a disintegrin and metalloprotease 10 in Staphylococcus aureus alpha-hemolysin-mediated cellular injury. Proc Natl Acad Sci U S A 107:13473-13478
234. Willems SH, Tape CJ, Stanley PL, Taylor NA, Mills IG, Neal DE, McCafferty J, Murphy G (2010) Thiol isomerases negatively regulate the cellular shedding activity of ADAM17. Biochem J 428:439-450
235. Wood SJ, Goldufsky JW, Seu MY, Dorafshar AH, Shafikhani SH (2023) Pseudomonas aeruginosa Cytotoxins: Mechanisms of Cytotoxicity and Impact on Inflammatory Responses. Cells 12
236. Yang WS, Kim JJ, Han NJ, Lee EK, Park SK (2017) 1,25-Dihydroxyvitamin D3 Attenuates the Effects of Lipopolysaccharide by Causing ADAM10-Dependent Ectodomain Shedding of Toll-Like Receptor 4. Cell Physiol Biochem 41:2104-2116
237. Yuksel H, Ocalan M, Yilmaz O (2021) E-Cadherin: An Important Functional Molecule at Respiratory Barrier Between Defence and Dysfunction. Front Physiol 12:720227
238. Yunna C, Mengru H, Lei W, Weidong C (2020) Macrophage M1/M2 polarization. Eur J Pharmacol 877:173090
239. Zdanovsky AG, Chiron M, Pastan I, FitzGerald DJ (1993) Mechanism of action of Pseudomonas exotoxin. Identification of a rate-limiting step. J Biol Chem 268:21791-21799
240. Zeringer E, Barta T, Li M, Vlassov AV (2015) Strategies for isolation of exosomes. Cold Spring Harb Protoc 2015:319-323
241. Zunke F, Rose-John S (2017) The shedding protease ADAM17: Physiology and pathophysiology. Biochim Biophys Acta Mol Cell Res 1864:2059-2070

7 Appendix

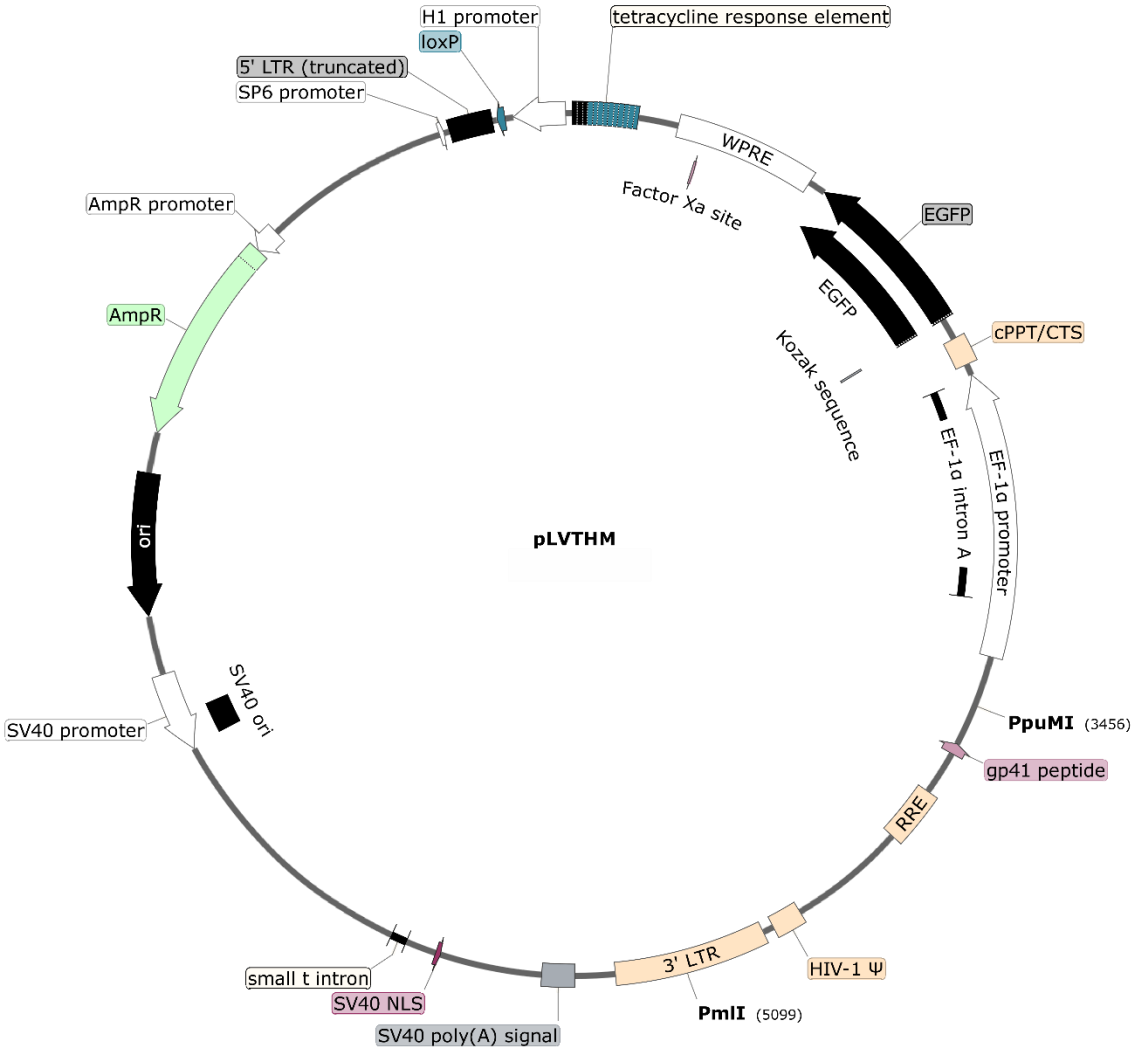

Figure 7. 1: Vector map of pLVTHM
The pLVTHM vector is used for the expression of the targeting shRNA or the unspecific shRNA (scr).

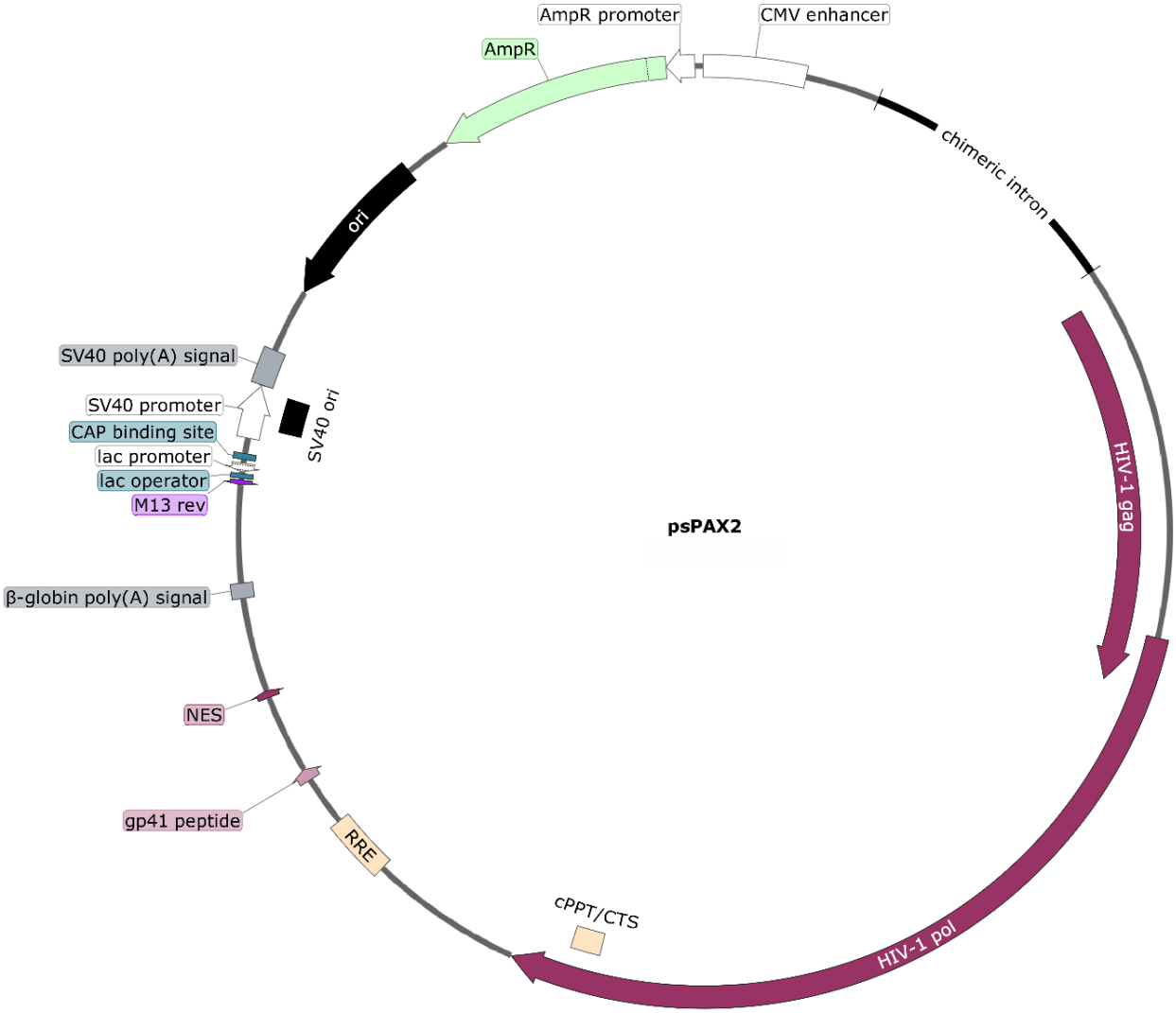

Figure 7. 2: Vector map of psPAX2
The psPAX2 vector is viral packaging vector, encodes the HIV gene gag-pol and additional auxiliary proteins

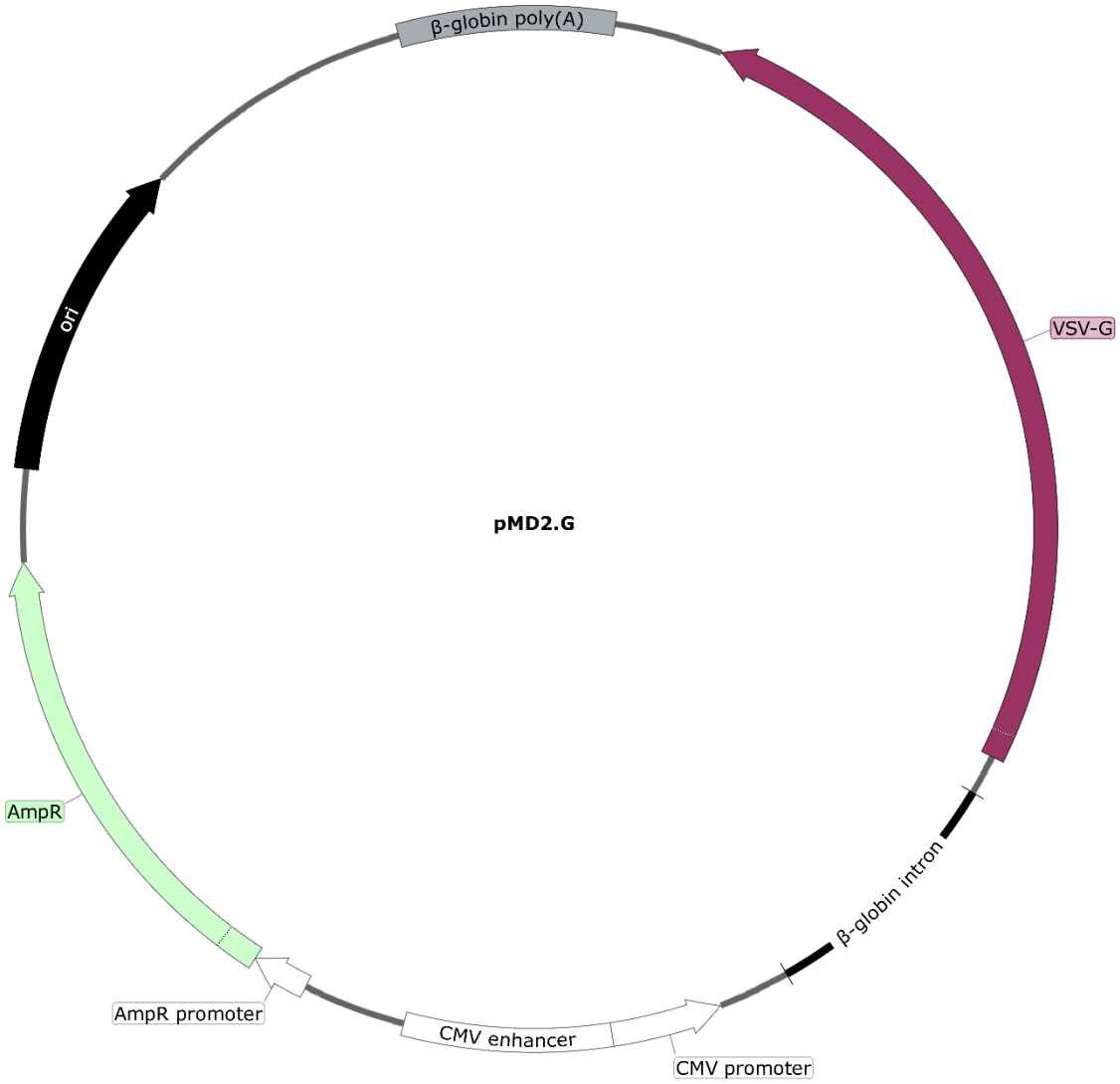

Figure 7. 3: Vector map of pMD2.G
The pMD2.G vector Contains the information for the surface protein vsv-G, which is responsible for the infection of mammalian cells of different species.

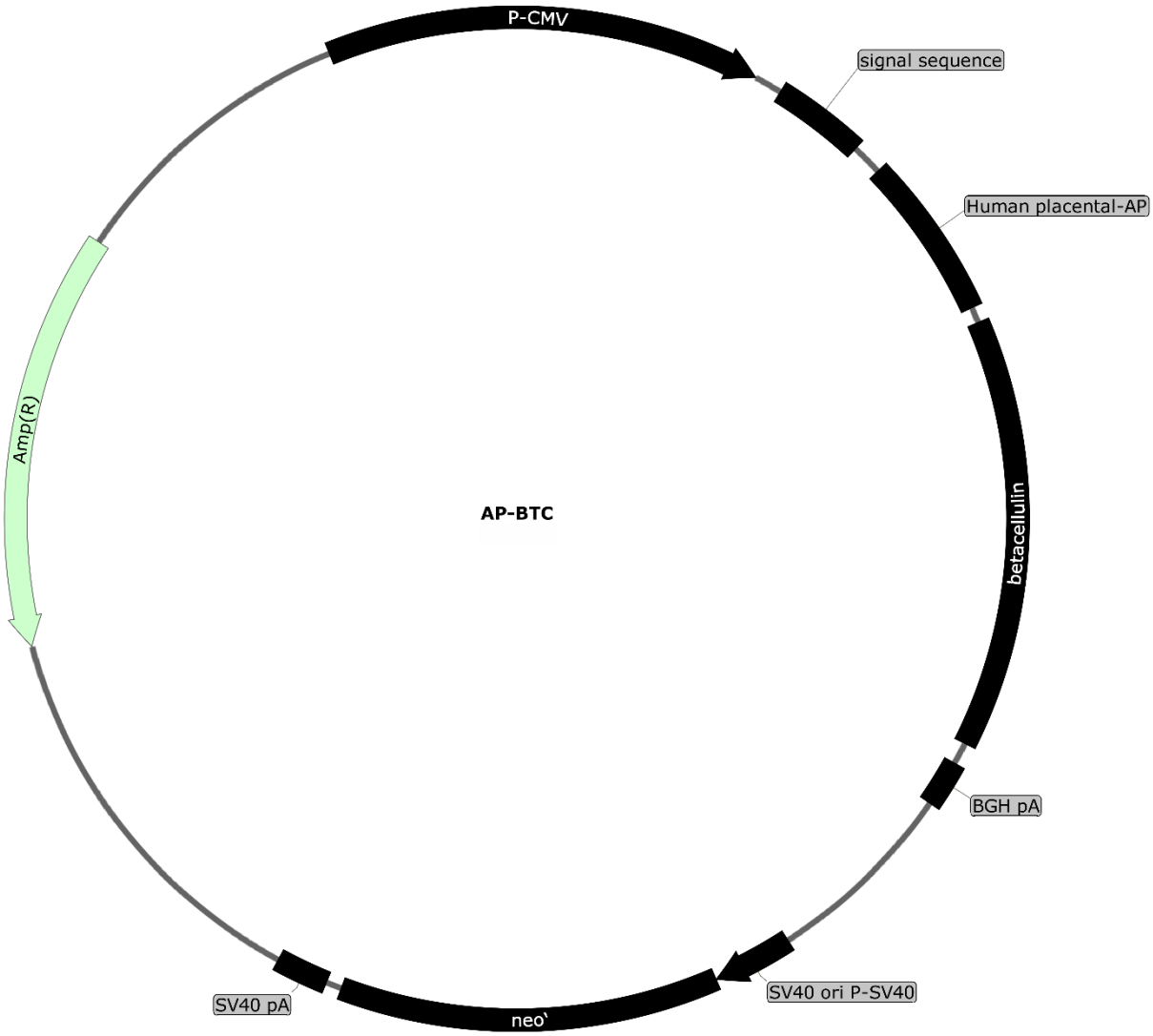

Figure 7. 4: Vector map of AP-BTC
The AP-BTC vector contains Rc/CMV backbone constructed with human placental alkaline tagged with human betacellulin

Figure 7. 5: Vector map of AP-TGF-α
The AP-BTC vector contains Rc/CMV backbone constructed with human placental alkaline tagged with human TGF-α

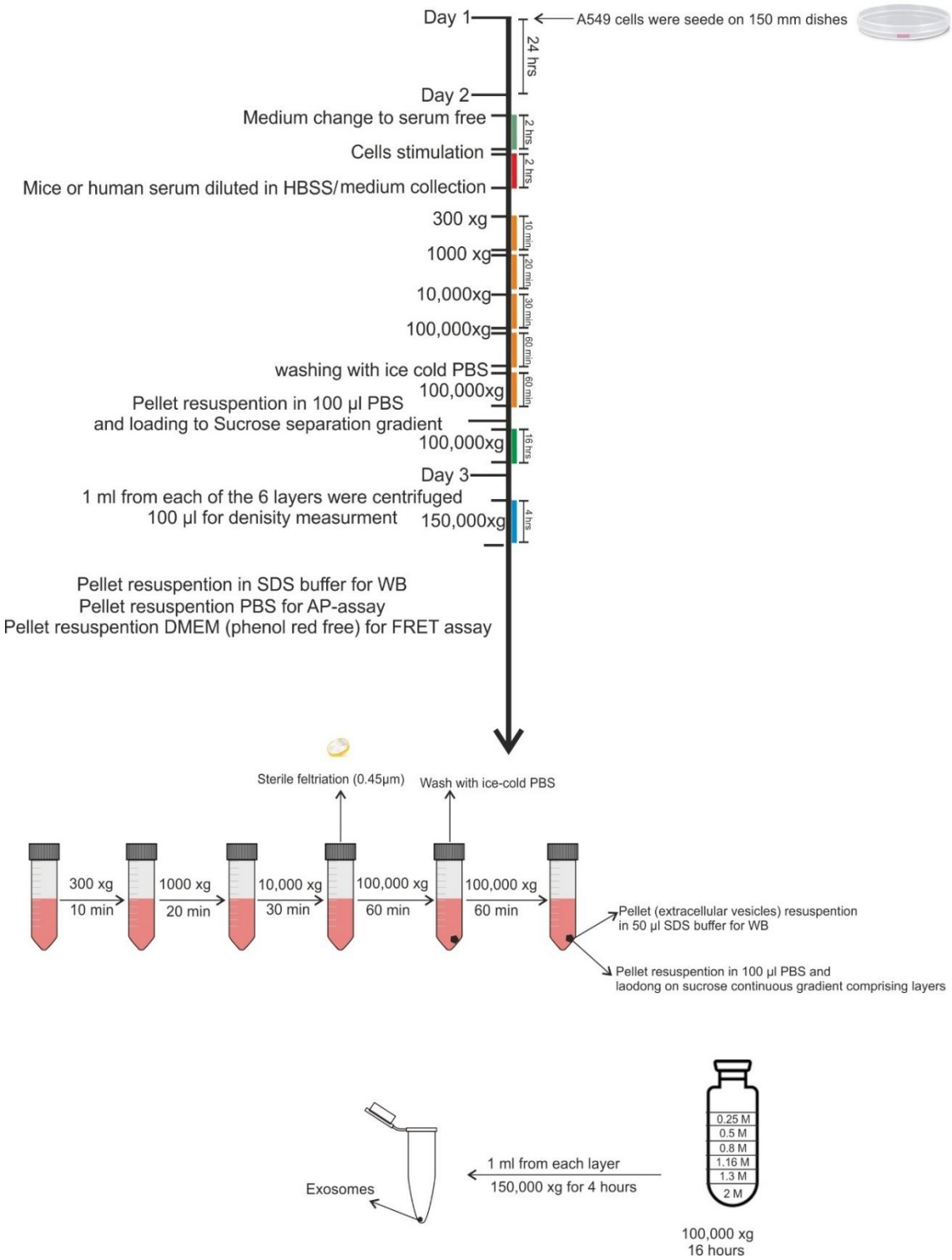

Figure 7. 6: Method description for exosomes preparation.
A549 cells, THP-1 cells or human neutrophils were cultured in serum free medium and assigned for exosome preparation as described in 3.2.1.4

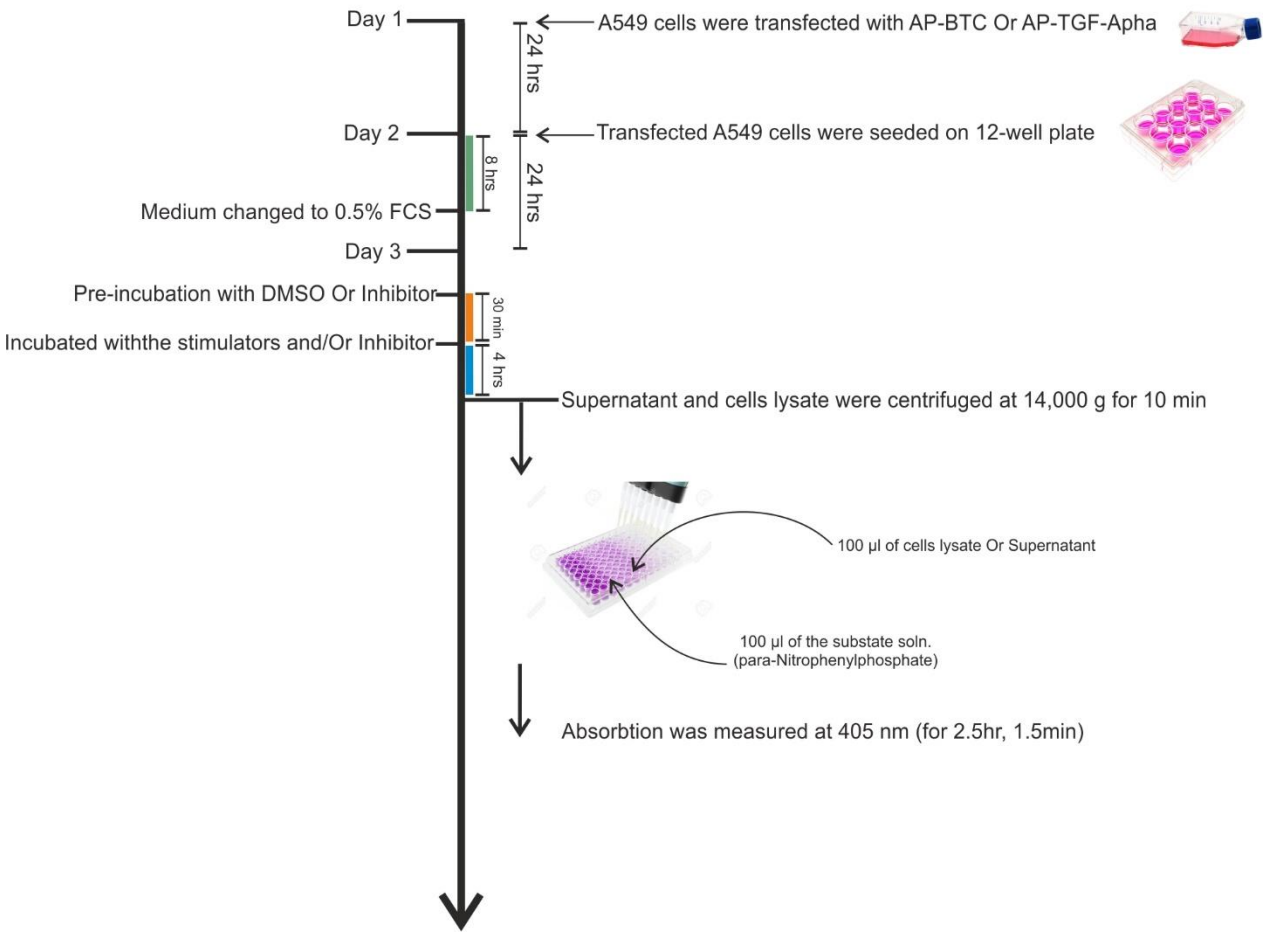

Figure 7. 7: Method description for AP activity assay
A549 cells were transfected with plasmid encoding either betacellulin or TGF-α tagged with alkaline phosphatase on the N-terminal domain and assigned for AP activity assay as described in 3.2.4.1

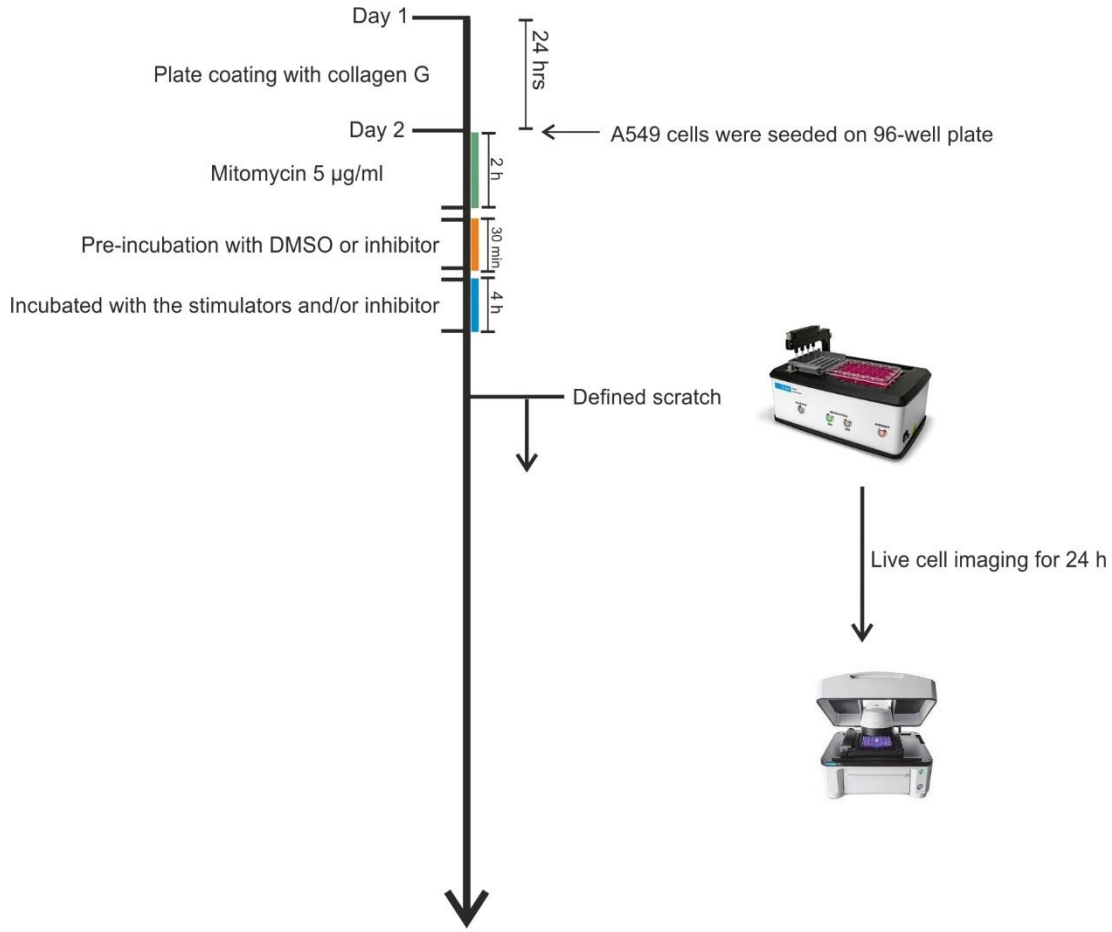

Figure 7. 8: Method description for epithelial wound closure assay
96-well plates were coated with collagen G for 2 h, and 2×10^4 of A549 cells were seeded and grown in DMEM (+10 % FCS) for 48-72 h until the formation of a uniform monolayer and assigned for wound healing assay as described in 3.2.4.4

8 Acknowledgement

First and foremost, I am grateful to my supervisor Prof. Daniela Yildiz for her uncountable advices, continuous support, and patience during my PhD study. I would also like to thank Prof. Markus Bischoff for all his assistance.

Special thanks to Helmholtz Institute for Pharmaceutical Research Saarland (HIPS) for funding this work and for the organization team Prof. Claus-Michael Lehr, Prof. Markus Meyer, Dr. Brigitta Loretz, Dr. Sascha Manier and Jacqueline Rehne.

I want to thank all the members of our lovely lab, Maria Rieseweber, Nina Schnellbach, Guillermo Gharzia, Mariana Guedes and Clarissa Neumann, for providing a lovely family environment and continuous help and support.

Special thanks to my friends Julia Jaffal, Sofia Maragkou, Amer Khalifa, Mohd Henia, Houssein Salah and Yasser Medlej who made this journey smooth and joyful.

Last but not least, I would like to express my lovely gratitude to my parents, sister and brothers for their tremendous understanding and encouragement throughout this journey.

9 Publications

Original papers

1- Mayyas FA, **Aljohmani AI**, Alzoubi KH (2020) The Impact of Spironolactone on Markers of Myocardial Oxidative Status, Inflammation and Remodeling in Hyperthyroid Rats. Curr Mol Pharmacol 13:206-215

2- **Aljohmani A**, Opitz B, Bischoff M, Yildiz D (2022b) Pseudomonas aeruginosa triggered exosomal release of ADAM10 mediates proteolytic cleavage in trans. Int J Mol Sci 23

3- Conrad C, Yildiz D, Cleary SJ, Margraf A, Cook L, Schlomann U, Panaretou B, Bowser JL, Karmouty-Quintana H, Li J, Berg NK, Martin SC, **Aljohmani A**, Moussavi-Harami SF, Wang KM, Tian JJ, Magnen M, Valet C, Qiu L, Singer JP, Eltzschig HK, Group CAS, Bertrams W, Herold S, Suttorp N, Schmeck B, Ball ZT, Zarbock A, Looney MR, Bartsch JW (2022) ADAM8 signaling drives neutrophil migration and ARDS severity. JCI Insight 7

4- **Aljohmani A**, Andres NN, Yildiz D (2022a) Pseudomonas aeruginosa alters critical lung epithelial cell functions through activation of ADAM17. Cells 11

5- Ahmad-Mansour N, Elhawy MI, Huc-Brandt S, Youssouf N, Patzold L, Martin M, Abdel-Wadood N, **Aljohmani A**, Morsli M, Krasteva-Christ G, Becker SL, Yildiz D, Lavigne JP, Gannoun-Zaki L, Bischoff M, Molle V (2022) Characterization of the Secreted Acid Phosphatase SapS Reveals a Novel Virulence Factor of Staphylococcus aureus That Contributes to Survival and Virulence in Mice. Int J Mol Sci 23

Review papers

1- **Aljohmani A**, Yildiz D (2020) A Disintegrin and Metalloproteinase-Control Elements in Infectious Diseases. Front Cardiovasc Med 7:608281

Under revision

1- **Aljohmani A**, Herr C, Witzenrath M, Pätzold L, Bischoff M, Wartenberg P, Boehm U, Laschke M, Hannig M, Lehr CM, Bals R, Yildiz D. Leukocytic ADAM10 and ADAM17 are essential control elements of disease severity and systemic outcome in bacterial and viral pneumonia. (**Under revision**).

2- Kuhn T*, **Aljohmani A***, Zielke L, Frank N, Mehanny M, Hoppstädter J, Kiemer A, Yildiz D*, Fuhrmann G*. A cell-free, biomimetic hydrogel based on probiotic membrane vesicles ameliorates wound healing. (*first/senior authors) Journal of Controlled Release – Revision submitted.

3- **Aljohmani A***, Heinze H*, Gharzia FG, Reda B, Becker S, Bischoff M, Hannig M, Yildiz D. Extracellular release of ADAM proteases orchestrates periodontal disease severity. (*first authors equal contribution)

10 Resume

The curriculum vitae was removed from the electronic version of the doctoral thesis for reasons of data protection

Tag der Promotion: 30.04.2024

Dekan: Prof. Dr. Michael D. Menger

Berichterstatter: Jun.-Prof. Dr. Daniela Yildiz

Prof. Dr. Dr. Sören Becker

Prof. Dr. Thomas Reinheckel